2038-5625

Italian Journal of Agrometeorology

Rivista Italiana di Agrometeorologia

n. 1 – 2021

Poste Italiane spa - Tassa pagata - Piego di libro
Aut. n. 072/DCB/FI1/VF del 31.03.2005

FIRENZE UNIVERSITY PRESS

Cover photo by Graziano Lampa

Italian Journal of Agrometeorology

n. 1 - 2021

Firenze University Press

The ***Italian Journal of Agrometeorology*** (***IJAm - Rivista Italiana di Agrometeorologia***) is the official periodical of the Italian Association of Agrometeorology (AIAM) and aims to publish original scientific contributions in English on agrometerology, as a science that studies the interactions of hydrological and meteorological factors with the agricultural and forest ecosystems, and with agriculture in its broadest sense (including livestock and fisheries).

SUBSCRIPTION INFORMATION
IJAm articles are freely available online, but print editions are available to paying subscribers. Subscription rates are in Eur and are applicable worldwide.
Annual Subscription: € 50,00 Single Issue: € 25,00

CONTACT INFORMATION
Please contact ordini@fupress.com, if you have any questions about your subscription or if you would like to place an order for the print edition. Information on payment methods will be provided after your initial correspondence.

Published by
Firenze University Press – University of Florence, Italy
Via Cittadella, 7 - 50144 Florence - Italy
http://www.fupress.com/ijam

Italian Journal of Agrometeorology
Rivista Italiana di Agrometeorologia

Firenze University Press
www.fupress.com/ijam

OPEN ACCESS

Citation: A. Farashi, Z. Karimian (2021) Predicting the potential habitat of Russian-Olive (*Elaeagnus angustifolia*) in urban landscapes. *Italian Journal of Agrometeorology* (1): 3-19. doi: 10.36253/ijam-1071

Received: September 5, 2020

Accepted: November 14, 2020

Published: August 9, 2021

Data Availability Statement: All relevant data are within the paper and its Supporting Information files.

Competing Interests: The Author(s) declare(s) no conflict of interest.

Funding: This study was funded by the Vice-Presidency for Science and Technology of Iran (grant number 96002787).

Author contributions statement: All authors contributed to the study conception and design. Material preparation, data collection and analysis were performed by Azita Farashi and Zahra Karimian. The first draft of the manuscript was written by Azita Farashi and all authors commented on previous versions of the manuscript. All authors read and approved the final manuscript.

Predicting the potential habitat of Russian-Olive (*Elaeagnus angustifolia*) in urban landscapes

Azita Farashi[1], Zahra Karimian[2]

[1] *Department of Environmental Sciences, Faculty of Natural Resource and Environment, Ferdowsi University of Mashhad, Mashhad, Iran*
[2] *Department of Ornamental Plants, Research Center for Plant Sciences, Ferdowsi University of Mashhad, Iran*
E-mail: farashi@um.ac.ir; zkarimianf@gmail.com

Abstract. Russian-olive *(Elaeagnus angustifolia)* is a species native to southern Europe and central and eastern Asia. This species plays an important role in urban landscape design because of its rapid growth, resistance in harsh climates and tolerance to human-caused pressure. Understanding its potential dispersal and restricting parameters are the first steps toward the sustainable use of this species. Here, we used Species Distribution Models to predict the potential distribution of Russian-olive in Iran climate and estimate the possible limiting factors for its spread. Our results highlighted the importance of environmental variables including climatic factors, soil, and lithology in the distribution of this species throughout the country. According to these results, suitable habitats for Russian-olive are located in the north of Iran along the Alborz and Koppeh-Dagh mountain ranges. Therefore, the suitable habitats for this species are limited to only nine percent of the country. A habitat suitability map can be used to evaluate future developments in urban areas and predict the dispersal range of Russian-olive in Iran. Our results show that Russian-olive can be used to create new green spaces in urban climates in the northern regions of Iran.

Keywords: climate, green space, ornamental tree, SDM, urban areas.

INTRODUCTION

The Middle East and North Africa are home to five percent of Earth's human population. However, only one percent of the global freshwater resources is located in Middle Eastern and North African countries (Djuma et al. 2016). As a result, water scarcity looms large across the region (Al-Ansari and Knutsson 2011; Al-Ansari et al. 2014; Abbas et al. 2018). To complicate the problem even further, population growth and political tensions threaten the sustainability of existing water resources in the Middle East and North Africa (Djuma et al. 2016).

Consequently, making use of different water sources and enhancing the resilience of water supply is crucial to meet the needs of the increasing urban population (Bichai et al. 2015). The environmental damage associated with urban devel-

opment has drawn attention to the need for green spaces in cities, which will lead to increased water use (Zhang et al. 2017). Green spaces are among the indicators of sustainable urban development. When planning for urban green spaces, numerous elements, such as economic, political, social, and cultural factors, along with management and planning considerations need to be taken into account (Haq 2011). Conservation of biological resources and maintaining soil and water quality are among the services provided by urban green spaces (Haq 2011, 2015). Many studies indicate that plant particularly trees can improve the urban microclimate and influence thermal comfort in various ways including shading, controlling the humidity, wind break, pollutant absorption and produce oxygen (Abreu- Harbich et al. 2015; Thoma et al. 2016; Afshar et al., 2018).

In arid regions such as the Middle East, design of urban green spaces is one of the main challenges facing city planners and urban architects. One solution to address this challenge is the use of native plant species which are adapted to the dry conditions of the region (Katz and Shafroth 2003; Kiseleva and Chindyaeva 2011).

The first step in utilizing native species is identification of their habitat requirements. Species distribution models (SDMs) trace their origin to the 1970s and have remained a common tool for ecologists throughout the following decades (e.g., Guisan and Zimmermann 2000; Guisan and Thuiller 2005; Rooper et al. 2016). In the time since their conception, several SDM algorithms have been developed, as discussed by Elith and Leathwick (2009) and Farashi and Alizadeh-Noughani (2018). These algorithms distinguish the major variables that determine a species' suitable habitat and show how predictor variables impact response variables. Furthermore, SDM algorithms enable researchers to see species' potential distribution (Liang and Stohlgren, 2011; Liang et al. 2017). Through modifications, these algorithms have been optimized for use in fields such as biogeography, ecology, evolution, and species conservation and management (Mikolajczak et al., 2015; Hannah et al., 2015). SDMs have also been used to assess the potential distribution of plant species (e.g., Kumar and Stohlgren 2009; Hemsing and Bryn 2012; Zhang et al., 2013; Guida et al. 2014; Hu et al. 2018). In the present study, we have used SDMs to predict the spatial distribution of Russian-olive (*Elaeagnus angustifolia*), a native plant species in Iran. Iran is a Middle Eastern country located on Earth's arid belt with upwards 60% of the country's area having an arid or semi-arid climate. In areas that receive little precipitation and experience severe fluctuations from year to year, agriculture is often limited by water availability (Modarres and da Silva 2007).

Russian-olive is native to Eurasia that occurs on coasts, in riparian areas, along watercourses, in other relatively moist habitats and also in many arid and semiarid regions of the world (Klich, 2000; Peterson et al., 2003). Soil salinity (low to medium concentrations), pH and water supply and moisture (low) are important environmental factors in Russian-olive habitat (Carman, 1982; Zitzer and Dawson, 1992; Reynolds and Cooper, 2010; Dubovyk et al., 2016). Russian-olive is resistant to drought (+46 °C) and frost (-46 °C) (Stratu et al., 2016; Akbolat et al., 2008). This tree is an ecologically valuable plant that are adapted to a variety of harsh conditions such as cold, drought, and salinity or alkalinity of soil (Asadiar et al. 2013; Zhang et al. 2018). The species endures through water scarcity by using groundwater (Katz and Shafroth 2003). Along with its desirable ecological characteristics, Russian-olive possess aesthetic values such as its beautiful oval crown, arching branches, silver leaves and shiny dark red fruits. Therefore *E. angustifolia* is particularly suitable for urban landscapes in arid regions such as Iran. This tree can be used to create sustainable green spaces in urban climates of Iran.

MATERIALS AND METHODS

Study area and species

Iran is located in Western Asia between 24˚-40˚ N and 44˚-64˚ E. Due to its habitat diversity and phytogeographic variety, Iran hosts rich biodiversity. Over 8,000 species of plants are found in Iran, of which 1,810 are endemic (Ghahraman and Attar 2000; Willis 2001). Russian-olive is a deciduous tree, sometimes with a shrubby habit, in the family Elaeagnaceae (Saboonchian et al. 2014). This species naturally grows in central and eastern Asia and southern Europe. Russian-olive grows quickly, reaching a maximum height of 10 m and maximum trunk diameter of 30 cm. Trees usually bear fruit after 5-6 years (Katz and Shafroth 2003).

Species distribution models

SDMs were developed in Biomod2 package (Thuiller et al. 2009, 2014) in R version 3.1.25 (R Core Team 2014). 10 different algorithms were used to study the species (Tab. 1). The algorithms can be categorized as: regression, machine learning, classification and enveloping algorithms. Regression-based algorithms include generalized linear models (GLMs) and generalized additive models (GAMs) which generate linear and non-linear equations between presence data and environmental variables, respectively. Machine learning algorithms include artificial neural networks (ANN), boosted regression trees, (BRT), multivariate adaptive regression splines (MARS), maximum

Table 1. The SDM algorithms in biomod[2] used in this study.

SDM	Variable	Type	Reference	TSS
ANN	Artificial neural networks	P/A	Lek and Guégan (1999)	0.71
BRT	Boosted regression trees	P/A	Elith et al. (2008)	0.71
CART	Classification and regression trees	P/A	Vayssières et al. (2000)	0.60
FDA	Flexible discriminant analysis	P/A	Hastie et al. (1994)	0.72
GAM	Generalized additive models	P/A	Guisan et al. (2002)	0.60
GLM	Generalized linear models	P/A	Guisan et al. (2002)	0.70
MaxEnt	Maximum entropy	P/B	Phillips et al. (2006)	0.80
MARS	Multivariate adaptive regression splines	P/A	Friedman (1991)	0.61
RF	Random forest	P/A	Breiman (2001)	0.65
SRE	Surface range envelope	P/B	Busby (1991)	0.65
Ensemble	-	-	Araújo and New (2007)	0.85

P: Presence; A: Absence; B: Background.

entropy (MaxEnt), and random forest (RF). Machine learning algorithms directly generate the environmental space using input data. Classification algorithms such as classification and regression trees (CART) and flexible discriminate analyses (FDA) successively divide data into homogenous partitions. Surface range envelope (SRE), the only enveloping method used in this study, investigates environmental conditions at the points of occurrence and uses the results to find similar areas (Merow et al. 2014).

Variable importance was calculated by a permutation procedure used in biomod, which is independent of the modelling technique. Once the models were trained (i.e., calibrated), a standard prediction was made. Then, one of the variables was randomized and a new prediction was made. The correlation score between the new prediction and the standard prediction was calculated and gave an estimation of the variable importance in the models (Thuiller et al., 2009).

Models were evaluated using the True Skill Statistic (TSS). TSS is the sum of sensitivity and specificity minus 1, and does not depend on prevalence (Allouche et al. 2006; Fielding and Bell 1997). TSS was used to create an ensemble-forecasting framework, as per Araújo and New (2007). All models contributed to the ensemble model. However, those with better performance, as indicated by TSS, were given more weight (Thuiller et al. 2009). A threshold value was defined by maximizing training sensitivity and specificity in order to create a binary (presence/absence) map from outputs of the algorithms (Liu et al. 2005; Liu et al. 2011). Sensitivity and specificity are statistical index of the performance of a binary classification analysis. Sensitivity calculate the proportion of actual presences which are correctly predicted as such, while specificity calculate the proportion of pseudoabsences which are predicted as absences. By maximizing the sum of sensitivity and specificity, the associated threshold corresponds to the point on the ROC curve (i.e. sensitivity against 1-specificity) whose tangent slope is equal to 1 (Kaivanto 2008; Jiguet et al. 2011). The approach was selected to calculate the threshold for presence/absence predictions in biomod2 (Liu et al. 2005).

Presence data and environmental variables

Occurrence records and distribution of the species were obtained from herbariums of Ferdowsi University of Mashhad, Tehran University, and University of Birjand. Flora Iranica (Rechinger, 1963-2015) and Flora of Iran (Assadi et al. 1988-2017). Herbaria data were obtained from field samplings between 2009 and 2019. The coordinates of all the occurrence points were recorded using a hand-held multichannel Global Positioning System (GPS) receiver with a positional accuracy of ±5 m. The spatially correlated presence points were removed using spatial autocorrelation and Moran's I test. The number of presence points was 83 (Fig. 1).

Topographic, geographic, edaphic, and climatic variables were used as input for the algorithms. Topographic variables were obtained from the national cartographic center of Iran (NCC) at 1-km spatial resolution. Geological survey and mineral exploration of Iran (GSI) provided the geographic data at 1-km spatial resolution. Edaphic variables were accessed from the agricultural research, education and extension organization of Iran (AREEO) at 1-km spatial resolution.

Mean elevation and mean slope for all raster cells in a 1-km radius were the two topographic variables used in modeling. Geographic and edaphic variables included soil orders and lithology, respectively. An initial set of 20

Table 2. Environmental predictors and their relative contributions to ensemble model of *E. angustifolia*.

Environmental variables	Mean +SD	Relative contribution (%)
Climatic variables		
Mean Diurnal Range[1] (°C)	38.01±3.08	4.0
Temperature Seasonality[2]	8162.63±995.89	0.3
Mean Temperature of Warmest Quarter (°C)	27.26±4.49	22.3
Mean Temperature of Coldest Quarter (°C)	6.39±5.87	1.0
Annual Precipitation (mm)	208.13±140.89	0.1
Precipitation of Wettest Quarter (mm)	111.34±64.48	0.4
Precipitation of Driest Quarter (mm)	5.86±13.09	1.1
Annual solar radiation (kJ m^{-2} day^{-1})	10743.56±1906.88	10.2
Topographic variables		
Altitude (m)	1251.24±686.64	0.2
Slope (degree)	6.20±7.93	0.6
Geographic variable		
Lithology	557 classes	50.2
Edaphic variable		
Soil order	20 classes	8.5

[1] Mean of monthly (max temp - min temp).

[2] Standard deviation × 100.

climatic variables, including precipitation, temperature, and solar radiation were obtained from the Worldclim database (http://www.worldclim.org). Climatic variables were used at a resolution of 30" (~ 1km). The correlation between all pairs of variables was tested. If -0.7 > r > +0.7, one of the two variables was excluded from the input data. The correlation tests reduced the number of variables to 12, which were subsequently used to model habitat suitability (Tab. 2).

RESULTS

All ten models showed a relatively good performance predicting the distribution of Russian-olive (Tab. 1). The results of modeling evaluation based on the TSS values showed that the combination of models performed relatively better than each individual model. Moreover, a model evaluation test showed that ensemble model performed better than other distribution models. The distribution map obtained from the ensemble model has been presented in Fig. 1. Our results showed that most of the suitable habitats for Russian-olive are located in the north of Iran. Only 9.5 percent of the country was suitable to grow this species (Fig. 1).

Suitable habitats based for each province have been presented in a separate map (Fig. 2). North Khorasan had the highest, and Ilam and Bushehr had the lowest proportion of suitable habitats among all provinces (Fig. 2). The

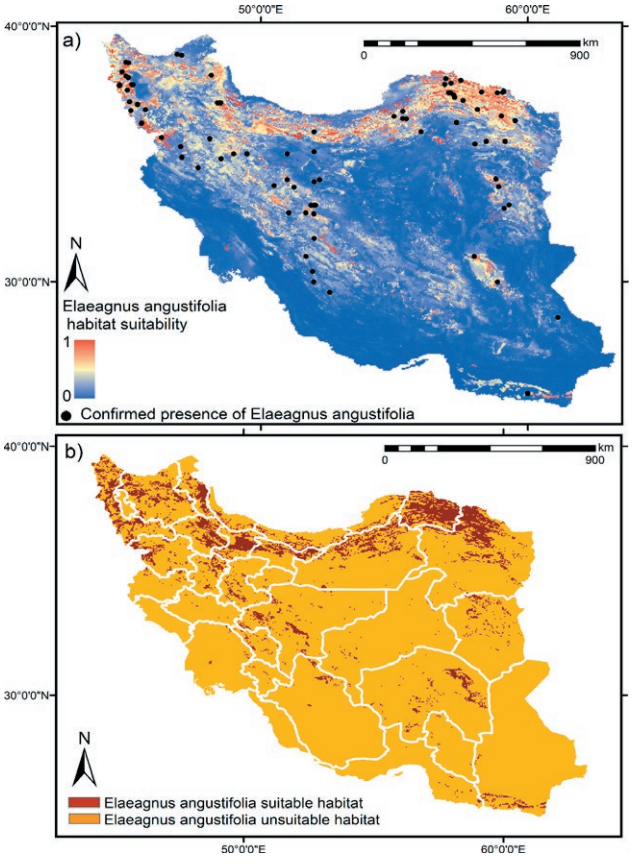

Fig. 1. Habitat suitability of *E. angustifolia* and its suitable habitats in Iran using ensemble model (a: continuous map, b: categorical map).

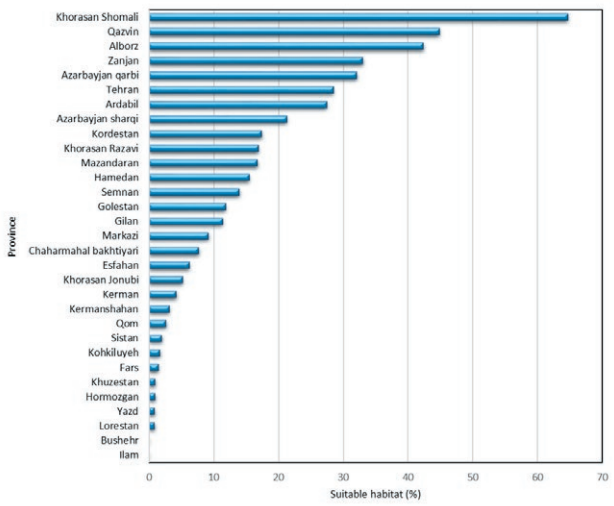

Fig. 2. Suitable habitats of *E. angustifolia* in each province.

relative importance of environmental variables changed based on different models. According to ensemble model, the most important environmental variables to predict habitat suitability for this species were lithology (50% of the contribution), mean temperature of the warmest quarter (22% of the contribution), annual solar radiation (10% of the contribution) and soil order (8% of the contribution) (Tab. 2).

Response curves for the four dominant environmental factors are shown in Fig. 3. There are unimodal relationships between habitat suitability and annual solar radiation. Peak presence probability was observed at 8150 kJ m^{-2} day^{-1}. The relationship between the habitat suitability values and mean temperature of the warmest quarter was best described by an exponential decay with the peak response at 5-7 °C. The results also demonstrated that any increase in mean temperature of the warmest quarter and

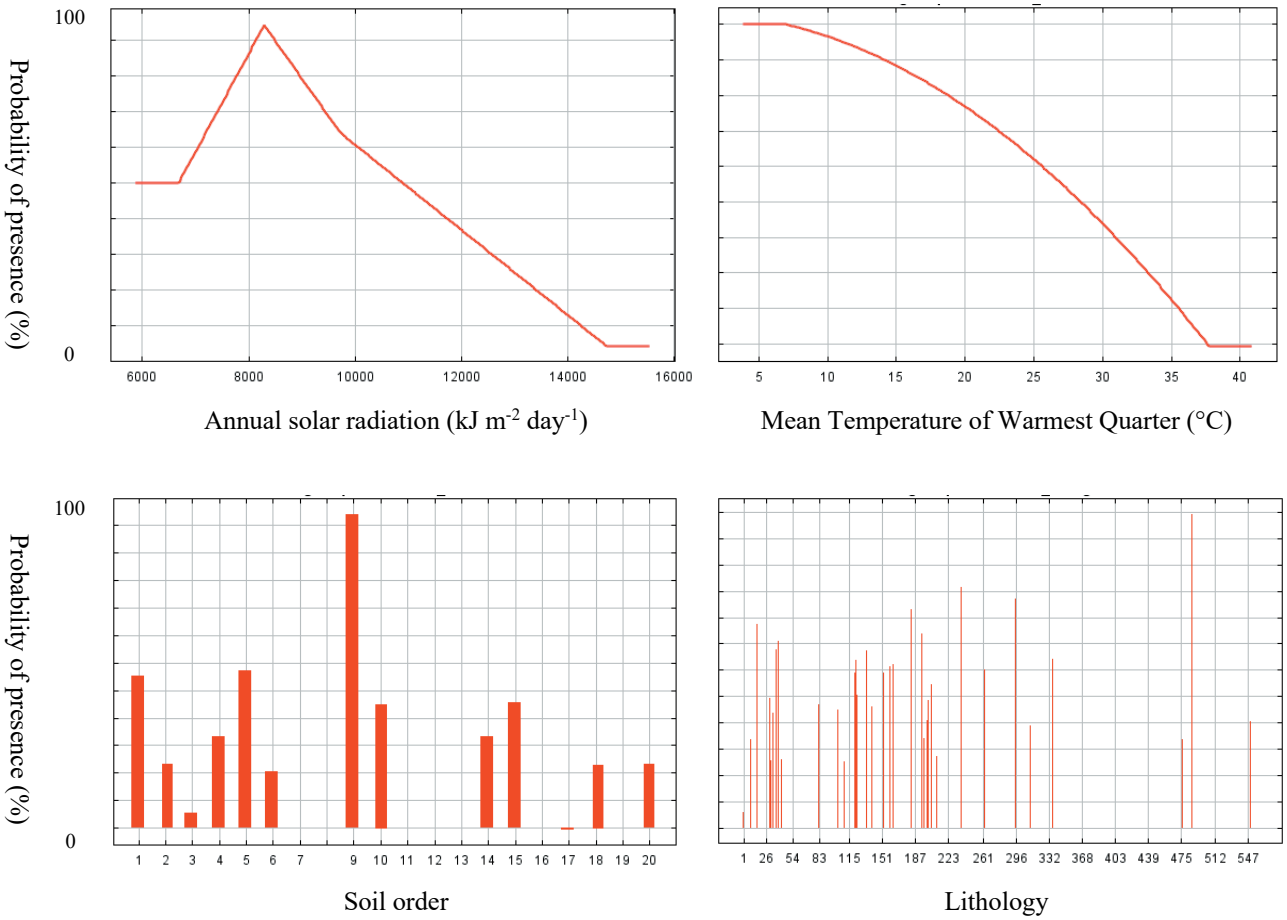

Fig. 3. Response curves of environmental variables for *E. angustifolia* (see soil order and lithology legend in supplementary file, Class 9 in soil order: rocky lands, Class 488 in lithology: high-level piedmont fan and valley terrace deposits).

annual solar radiation led to a decrease in habitat suitability for Russian-olive.

The relationship between the habitat suitability values with soil order and lithology showed that this species could grow in different soil and rock classes. However, the highest presence probability is observed in rocky lands and high-level piedmont fan and valley terrace deposits (Fig. 3).

DISCUSSION

Iran is a large country, containing a variety of climates. While the northern regions have a temperate climate, southern regions are dry and frequently experience droughts and water scarcity (Abbaspour et al., 2009; Bannayan et al., 2010). Our results show the prominent role of mean temperature of warmest quarter, annual solar radiation, lithology, and soil order in creating a suitable habitat for Russian-olive. The contribution of other variables was not considerable. Previous studies have shown that Russian-olive is capable of growing under both flooded and drought conditions in its native range (Asadiar, et al., 2013, Stannard et al., 2002) as well as its introduced range (Katz and Shafroth, 2003; Reynolds and Cooper, 2010). *E. angustifolia*'s extensive root network allows it to utilize moisture stored in deep soil or groundwater (Cui et al., 2015; Dubovyk et al., 2016). Owing to insufficient hydro-geological data, we could not use these variables in our study. Nevertheless, we recommend including them in future studies when they become available for Iran.

Our findings also reveal the importance of environmental variables such as soil (soil orders) and lithology in determining suitable habitats for Russian-olive, which supports the findings of previous studies (Zitzer and Dawson, 1992; Carman and Brotherson, 1982; Khamzina et al., 2009; Collette and Pither, 2015). The results demonstrate how Russian-olive can survive only under certain climatic conditions but can continue to grow on a number of soil orders and lithological formations (Lesica and Miles 2001; Katz and Shafroth, 2003; Reynolds and Cooper 2010; Collette and Pither, 2015). This makes Russian-olive a good candidate for shelterbelts in different regions (Olson and Knopf 1986; Pearce et al., 2009).

Roughly 9% of Iran is suitable habitat for Russian-olive, stretching along the Alborz and Koppeh-Dagh mountain ranges (Fig. 1). The Alborz and Koppeh-Dagh are comparable with temperate European mountain ranges such as the Alps in terms of endemism (Tribsch and Schonswetter 2003; Noroozi et al. 2008, 2018). Iranian provinces vary regarding habitat suitability for Russian-olive. All provinces, with the exception of Ilam and Bushehr (in the west and south of Iran, respectively), contained suitable habitats for Russian-olive. North Khorasan (64.7%), Qazvin (44.8%), and Alborz (42.4%) had the highest proportion of suitable habitats for Russian-olive. Suitability maps can inform future urban development and predict the future range of Russian-olive.

Therefore, it is suggested to protect the critical habitats of Russian-olive and use this species in urban green spaces. Russian-olive is not a demanding species and can survive for 50-80 years in different conditions. *E. angustifolia* is used to as a soil stabilizer, a hedge plant, and a fragrant ornamental. Due to its characteristics, Russian-olive is used in shelterbelts and urban landscapes (Kolesnikov, 1974; Kiseleva and Chindyaeva, 2011).

Russian-olive can become invasive (Reynolds and Cooper, 2010; Collette and Pither, 2015). After its introduction as an ornamental plant, Russian-olive became invasive in the US and Canada in the early 20th century (Katz and Shafroth 2003). The species negatively affected riparian forests and, as a result, was declared a noxious species in Colorado and New Mexico (Katz and Shafroth 2003; Collette and Pither, 2015). Introduction of this species to areas outside its native range should be done with caution. However, such considerations are not needed when planting Russian-olives in its native range since the species will not disrupt the natural processes of its native ecosystems (Strauss et al., 2006; Marsh-Matthews et al., 2011; Zhang et al., 2018). Moreover, native species can be advantageous to the local economy. As a result, we recommend the use of Russian-olive in urban landscapes in northern Iran.

A common assumption among SDMs is that species can only establish in areas that are ecologically similar to their native range (Kearney 2006). However, a species niche might change (Broennimann et al., 2007). As a result, the output of SDM algorithms is an approximation of species' niche in new environments. The differences in bioclimatic conditions between native areas and those we are making predictions for might lead to an underestimation of actual suitable areas. Thus, more accurate predictions can only be made by taking into account both biotic and abiotic variables and their interactions. These studies can be further improved through comparisons with areas under invasion by alien invasive species. In the meantime, the mere presence of suitable habitats for a species should not encourage managers to use the species before more extensive investigations are performed. However, the efficiency of SDMs is affected by several parameters (Allouche et al. 2008) such as the characteristics of environmental data (e.g. type, variance data; Aguirre-Gutiérrez et al. 2013), characteristics of species data (e.g. geographical accuracy, sample size, field survey constraints, or auto-correlation structure; Huettmann and Diamond 2006), species ecology (e.g. distribution range, abundance,

niche limits of species; Saupe et al., 2012), computer power (i.e. too many cells may be too demanding on computer resources), model (e.g. presence only/presence-absence; Aguirre and Gutiérrez et al., 2013), and spatial resolution (Farashi and Naderi 2017). Despite their shortcomings, SDMs can still help us grasp the biological history of a species distribution (Silva Rocha et al., 2015). Further investigation is needed to study niche shift, distinguish the most influential variables, and pinpoint the role of other factors in determining distribution of the species.

ACKNOWLEDGMENT

This work was supported by Iran National Science Foundation [grant number 96002787].

REFERENCES

Abbas N, Wasimi S, Al-Ansari N, Sultana N 2018 Water resources problems of Iraq: Climate change adaptation and mitigation. Journal of Environmental Hydrology 26.

Abbaspour KC, Faramarzi M, Ghasemi SS, Yang H 2009 Assessing the impact of climate change on water resources in Iran. Water resources research 45(10).

Abreu-Harbich LV, Labaki LC, Matzarakis A 2015 Effect of tree planting design and tree species on human thermal comfort in the tropics. Landscape and Urban Planning 138: 99–109.

Aguirre-Gutiérrez, J., Carvalheiro, L. G., Polce, C., van Loon, E. E., Raes, N., Reemer, M., & Biesmeijer, J. C. (2013). Fit-for-purpose: species distribution model performance depends on evaluation criteria–Dutch hoverflies as a case study. PloS one, 8(5), e63708..

Akbolat D, Ertekin C, Menges HO, Guzel E, Ekinci K 2008 Physical and Nutritional Properties of Oleaster (*Elaeagnus angustifolia* L.) Growing in Turkey. Asian Journal of Chemistry 20(3): 2358-2366 Al-Ansari N, Abdellatif M, Zakaria S, Knutsson S, Mustafa Y 2014 Future Prospects for Macro Rainwater Harvesting (RWH) technique in north east Iraq. Journal of Water Resource and Protection 6(5): 403-420.

Al-Ansari N, Knutsson S 2011 Toward prudent management of water resources in Iraq. Journal of Advanced Science and Engineering Research (1): 53-67.

Allouche O, Tsoar A, Kadmon R 2006 Assessing the accuracy of species distribution models: prevalence, kappa and the true skill statistic (TSS). Journal of applied ecology 43(6): 1223-1232.

Allouche, O., Steinitz, O., Rotem, D., Rosenfeld, A., & Kadmon, R. (2008). Incorporating distance constraints into species distribution models. Journal of Applied Ecology, 45(2), 599-609..

Araújo, M.B. New, M 2007 Ensemble forecasting of species distributions. Trends in Ecology Evolution 22: 42–47.

Asadiar LS, Rahmani F, Siami A 2013 Assessment of genetic diversity in the Russian olive (*Elaeagnus angustifolia*) based on ISSR genetic markers. Revista Ciência Agronômica 44(2): 310-316.

Assadi M, Maassoumi AA, Khatamsaz M, Mozaffarian V. (Eds.) 1988–2017 Flora of Iran vols. 1–76 Research Institute of Forests and Rangelands Publications, Tehran .

Bannayan M, Sanjani S, Alizadeh A, Lotfabadi SS, Mohamadian A 2010 Association between climate indices, aridity index, and rainfed crop yield in northeast of Iran. Field Crops Research 118 (2): 105-114.

Bichai F, Ryan H, Fitzgerald C, Williams K, Abdelmoteleb A, Brotchie R, Komatsu R 2015 Understanding the role of alternative water supply in an urban water security strategy: An analytical framework for decision-making. Urban Water Journal 12(3): 175-189.

Broennimann O, Treier, UA, Müller-Schärer H, Thuiller W, Peterson AT, Guisan A 2007 Evidence of climatic niche shift during biological invasion. Ecology letters 10(8): 701-709.

Carman JG, Brotherson JD 1982. Comparisons of sites infested and not infested with saltcedar (*Tamarix pentandra*) and Russian olive (*Elaeagnus angustifolia*). Weed Science 30(4): 360-364.

Collette LK, Pither J 2015 Russian-olive (*Elaeagnus angustifolia*) biology and ecology and its potential to invade northern North American riparian ecosystems. Invasive Plant Science and Management 8(1): 1-14.

Cui Y, Ma J, Sun W, Sun J, Duan Z 2015 A preliminary study of water use strategy of desert plants in Dunhuang, China. Journal of Arid Land 7(1): 73-81.

Djuma H, Bruggeman, A, Eliades M Lange, M A 2016 Non-conventional water resources research in semi-arid countries of the Middle East. Desalination and Water Treatment 57(5): 2290-2303.

Dubovyk O, Menz G, Khamzina A 2016 Land suitability assessment for afforestation with *Elaeagnus angustifolia* L. In degraded agricultural areas of the lower amudarya river basin. Land Degradation Development 27(8): 1831-1839.

Elith J, Leathwick JR 2009 Species distribution models: ecological explanation and prediction across space and time. Annual review of ecology, evolution, and systematics 40: 677-697.

Farashi A, Alizadeh-Noughani M 2018 Effects of models and spatial resolutions on the species distribution

model performance. Modeling Earth Systems and Environment 4(1): 263-268.

Farashi, A., & Naderi, M. (2017). Predicting invasion risk of raccoon Procyon lotor in Iran using environmental niche models. Landscape and Ecological Engineering, 13(2), 229-236..

Fielding AH, Bell JF 1997 A review of methods for the assessment of prediction errors in conservation presence/absence models. Environmental conservation 24(1): 38-49.

Ghahraman A, Attar F 2001 Biodiversity of plant species in Iran. Published by Tehran University, 1, pp. 1210.

Guida RJ, Abella SR, Smith Jr WJ, Stephen H, Roberts CL 2014 Climatic change and desert vegetation distribution: Assessing thirty years of change in southern Nevada's Mojave Desert. The Professional Geographer 66(2): 311-322.

Guisan A, Thuiller W 2005 Predicting species distribution: offering more than simple habitat models. Ecology letters 8(9): 993-1009.

Guisan A, Zimmermann NE 2000 Predictive habitat distribution models in ecology. Ecological modelling 135(2): 147-186.

Hannah L, Midgley G, Davies I, Davies F, Ries L, Thuiller W, Stoms D 2015 BioMove-Improvement and Parameterization of a Hybrid Model for the Assessment of Climate Change impacts on the Vegetation of California.

Haq SMA 2011 Urban green spaces and an integrative approach to sustainable environment. Journal of environmental protection 2(05): 601.

Haq SMA 2015 Urban green spaces and an integrative approach to sustainable environment. Urban Ecology: Strategies for Green Infrastructure and Land Use; Etingoff, K., Ed, 147-16.

Hemsing L, Bryn A 2012 Three methods for modelling potential natural vegetation (PNV) compared: A methodological case study from south-central Norway. Norsk Geografisk Tidsskrift-Norwegian. Journal of Geography 66(1): 11-29.

Hu Z, Guo K, Jin S Pan H 2018 The influence of climatic changes on distribution pattern of six typical *Kobresia* species in Tibetan Plateau based on MaxEnt model and geographic information system. Theoretical and Applied Climatology 1-16.

Huettmann, F., & Diamond, A. W. (2006). Large-scale effects on the spatial distribution of seabirds in the Northwest Atlantic. Landscape Ecology, 21(7), 1089-1108.

Jiguet, F., Barbet-Massin, M., & Chevallier, D. (2011). Predictive distribution models applied to satellite tracks: modelling the western African winter range of European migrant Black Storks Ciconia nigra. Journal of Ornithology, 152(1), 111-118..

Kaivanto, K. (2008). Maximization of the sum of sensitivity and specificity as a diagnostic cutpoint criterion. Journal of clinical epidemiology, 61, 516-518..

Karimi Afshar N, Karimian Z, Doostan R, Habibi Nokhandan M 2018 influence of planting designs on winter thermal comfort in an urban park. Journal of Environmental Engineering and Landscape Management 26(3): (232-240).

Katz GL, Shafroth PB 2003 Biology, ecology and management of *Elaeagnus angustifolia* L. (Russian olive) in western North America. Wetlands 23(4): 763-777.

Kearney M 2006 Habitat, environment and niche: what are we modelling? *Oikos* 115(1), 186-191.

Khamzina A, Lamers JP, Vlek PL 2009 Nitrogen fixation by *Elaeagnus angustifolia* in the reclamation of degraded croplands of Central Asia. Tree physiology 29(6): 799-808.

Kiseleva TI, Chindyaeva LN 2011 Biology of oleaster (*Elaeagnus angustifolia* L.) at the northeastern limit of its range. Contemporary Problems of Ecology 4(2): 218-222.

Klich MG 2000 Leaf variations in *Elaeagnus angustifolia* related to environmental heterogeneity. Environmental and Experimental Botany 44: 171–183.

Kolesnikov AI 1974 *Dekorativnaya dendrologiya* [Decorative dendrology]. Moscow: Lesnaya promyshlennost'[in Russian].

Kumar S, Stohlgren TJ. 2009 Maxent modeling for predicting suitable habitat for threatened and endangered tree *Canacomyrica monticola* in New Caledonia. Journal of Ecology and the Natural Environment 1(4): 94-98.

Lesica P, Miles S 2001 Natural history and invasion of Russian olive along eastern Montana rivers. *Western North American Naturalist*, 1-10.

Liang CT, Stohlgren TJ. 2011. Habitat suitability of patch types: A case study of the Yosemite toad. Frontiers of Earth Science, 5: 217-228.

Liang CT, Grasso RL, Nelson-Paul JJ, Vincent KE, Lind AJ 2017 Fine-Scale Habitat Characteristics Related to Occupancy of the Yosemite Toad, *Anaxyrus canorus*. Copeia 105(1): 120-127.

Liu C, Berry PM, Dawson TP, Pearson, RG 2005 Selecting thresholds of occurrence in the prediction of species distributions. Ecography, 28(3): 385-393..

Liu C, White M, Newell G 2011 Measuring and comparing the accuracy of species distribution models with presence–absence data. Ecography 34(2), 232-243.

Marsh-Matthews E, Matthews WJ, Franssen NR 2011 Can a highly invasive species re-invade its native community? The paradox of the red shiner. Biological Invasions 13(12): 2911-2924.

Merow C, Smith M., Edwards Jr TC, Guisan A, McMahon SM, Normand S, Elith J 2014 What do we gain

from simplicity versus complexity in species distribution models? Ecography 37(12): 1267-1281.

Mikolajczak A, Maréchal D, Sanz T, Isenmann M, Thierion V, Luque S 2015 Modelling spatial distributions of alpine vegetation: A graph theory approach to delineate ecologically-consistent species assemblages. Ecological informatics 30: 196-202.

Modarres R, da Silva VDPR 2007 Rainfall trends in arid and semi-arid regions of Iran. Journal of arid environments 70(2): 344-355.

Noroozi J, Akhani H, Breckle SW 2008 Biodiversity and phytogeography of the alpine flora of Iran. Biodiversity and Conservation 17(3): 493-521.

Noroozi J, Talebi A, Doostmohammadi M, Rumpf SB, Linder HP, Schneeweiss GM 2018 Hotspots within a global biodiversity hotspot-areas of endemism are associated with high mountain ranges. Scientific reports 8.

Olson T E, Knopf FL 1986 Naturalization of Russian-olive in the western United States. Western Journal of Applied Forestry 1(3): 65-69.

Pearce CM, Smith DG, VanDevender TR, Espinosa-Garcia F., Harper-Lore BL, Hubbard T 2009 Rivers as conduits for long-distance dispersal of introduced weeds: example of Russian olive (*Elaeagnus angustifolia*) in the northern Great Plains of North America. Invasive Plants on the Move: Controlling Them in North America 410-427.

Peterson AT, Papes M, Kluz DA 2003 Predicting the potential invasive distributions of four alien plant species in North America. Weed Science 51(6): 863-868.

Rechinger KH, (ed.) 1963–2015 Flora Iranica, vols. 1–181. Akademische Druck- u. Verlagsanstalt, Graz; vol. 175. Akademische Verlagsgesellschaft, Salzburg; vols. 176–181. Verlag des Naturhistorischen Museums, Wien.

Reynolds LV, Cooper DJ 2010 Environmental tolerance of an invasive riparian tree and its potential for continued spread in the southwestern US. Journal of Vegetation Science 21(4): 733-743.

Rooper CN, Sigler MF, Goddard P, Malecha P, Towler R, Williams K, Zimmermann M 2016 Validation and improvement of species distribution models for structure-forming invertebrates in the eastern Bering Sea with an independent survey. Marine Ecology Progress Series 551: 117-130.

Saboonchian F, Jamei R, Sarghein SH 2014 Phenolic and flavonoid content of *Elaeagnus angustifolia* L. (leaf and flower). Avicenna journal of phytomedicine 4(4): 231.

Saupe, E. E., Barve, V., Myers, C. E., Soberón, J., Barve, N., Hensz, C. M., ... & Lira-Noriega, A. (2012). Variation in niche and distribution model performance: the need for a priori assessment of key causal factors. Ecological Modelling, 237, 11-22..

Silva Rocha I, Salvi D, Sillero N, Mateo JA, Carretero MA 2015 Snakes on the Balearic Islands: an invasion tale with implications for native biodiversity conservation. PloS one 10(4): e0121026.

Stannard M, Ogle D, Holzworth L, Scianna J, Suleaf E 2002 History, biology, ecology, suppression of Russian olive (*Elaeagnus angustifolia* L.). Boise, ID: USDA-NRCS 1-14.

Stratu A, Costică N, Costică M 2016 Wooden species in the urban green areas and their role in improving the quality of the environment. PESD 10(2): 173-184.

Strauss S., Webb CO, Salamin N 2006 Exotic taxa less related to native species are more invasive. Proceedings of the National Academy of Sciences 103(15): 5841-5845.

Thoma JK, Couttsa AM, Broadbenta AM, Tapper NJ 2016 The influence of increasing tree cover on mean radiant temperature across a mixed development suburb in Adelaide, Australia, Urban Forestry & Urban Greening 20: 233–242.

Thuiller W, Georges D, Engler R 2014 biomod2: Ensemble platform for species distribution modeling. 3:1-64.

Thuiller W., Lafourcade B., Engler R., Araújo M.B. 2009. BIOMOD–a platform for ensemble forecasting of species distributions. *Ecography* 32(3): 369-373. .

Tribsch A, Schönswetter P 2003 Patterns of endemism and comparative phylogeography confirm palaeoenvironmental evidence for Pleistocene refugia in the Eastern Alps. Taxon 52(3): 477-497.

Willis AJ 2001 Endangered plants in Iran. New phytologist 149(2): 165-165.

Zhang X, Li G, Du S 2018 Simulating the potential distribution of *Elaeagnus angustifolia* L. based on climatic constraints in China. Ecological Engineering 113: 27-34.

Zhang X, Mi F, Lu N, Yan N, Kuglerova L, Yuan S, Ma OZ 2017 Green space water use and its impact on water resources in the capital region of China. Physics and Chemistry of the Earth, Parts A/B/C 101: 185-194.

Zhang ZD, Zang RG, Convertino M 2013 Predicting the distribution of potential natural vegetation based on species functional groups in fragmented and species-rich forests. Plant Ecology and Evolution 146(3): 261-271.

Zitzer SF, Dawson JO 1992 Soil properties and actinorhizal vegetation influence nodulation of *Alnus glutinosa* and *Elaeagnus angustifolia* by Frankia. Plant and Soil 140(2): 197-204.

Lithology legend

ID	Geo unit	Description
1	Ewf	Flysch with exotic blocks of Eocene limestone, Cretaceous limestone and ophiolitic components
2	gb	Gabbro
3	gb	Layered and isotropic gabbro
4	gsch	Glaucophane schist
5	h	Contact metamorphic rocks: two mica Hornfels; cordierite Hornfels; andalusite-sillimanite Hornfels and locally metamorphosed carbonate rocks
6	hz	Harzburgite
7	Island	Unknown
8	Ja.bv	Andesitic and basaltic volcanic rocks
9	Ja.bvt	Andesitic to basaltic volcanic tuff
10	Jav	Andesitic volcanic
11	Javs	Andesitic volcano sediment
12	Javt	Andesitic volcanic tuff
13	Jbash	Shale with intercalations of sandstone
14	Jbd	Dark grey, well-bedded, oolitic, ammonitiferous limestone, sandstone and shale
15	Jbg	Pale-green silty shale and sandstone
16	Jbv	Basaltic volcanic
17	am	Amphibolite
18	ba	Basalt and basaltic andesite pillow lavas
19	Cag	Grey thick-bedded to massive limestone and dolomite
20	Cb	Alternation of dolomite, limestone and verigated shale
21	Cd	Dolomite, quartzarenite, shale and limestone containing Trilobite
22	Cg	Limestone, shale, dolomite and gypsum
23	Cl	Dark red medium-grained arkosic to subarkosic sandstone and micaseous siltstone
24	Cm	Dark grey to black fossiliferous limestone with subordinate black shale
25	COm	Dolomite platy and flaggy limestone containing trilobite; sandstone and shale
26	Cs	Light olive-green shale with intercalations of quartzarenite and fossiliferous limestone
27	Cz	Dark red, micaceous siltstone and fine-grained sandstone
28	Czl	Undifferentiated unit, composed of dark red micaceous siltstone and sandstone
29	D2met	Alternation of marble, micaschist, amphibolite and quartzite
30	db	Diabase
31	Db	Grey and black, partly nodular limestone with intercalations of calcareous shale
32	Db-sh	Undifferentiated limestone, shale and marl
33	DC2met	Mica schist, green schist, graphite schist, and minor marble
34	DCkh	Yellowish, thin to thick-bedded, fossiliferous argillaceous limestone, dark grey limestone, greenish marl and shale, locally including gypsum
35	DCsh	Alternation of shale, marl and limestone
36	di-gb	Gabbro to diorite, diorite and trondhjemite
37	Dp	Light red to white, thick bedded quartzarenite with dolomite intercalations and gypsum
38	Ds	Black and grey dolomite
39	Dsb	Dolomite, limestone and shale
40	Dsh	Alternation of shale, marl and fossiliferous limestone, clay with intercalations of quartz arenite
41	du	Dunite
42	E	Undivided Eocene rocks
43	E1-2f	Lower-Middle Eocene flysch-sandstone, shale volcanoclastic sandstone, coarse grained siliceous sandstone minor limestone and pebble conglomerate
44	E1c	Pale-red, polygenic conglomerate and sandstone
45	E1f	Silty shale, sandstone, marl, sandy limestone, limestone and conglomerate
46	E1l	Nummulitic limestone
47	E1m	Marl, gypsiferous marl and limestone
48	E1s	Sandstone, conglomerate, marl and sandy limestone
49	E2-3f	Sandstone, calcareous sandstone and limestone
50	E2c	Conglomerate and sandstone
51	E2f	Sandstone, calcareous sandstone and limestone
52	E2l	Nummulitic limestone
53	E2m	Pale red marl, gypsiferous marl and limestone
54	E2mg	Gypsiferous marl
55	E2s	Sandstone, marl and limestone
56	E2sht	Tuffaceous shale and tuff
57	E3c	Conglomerate and sandstone
58	E3f	Sandstone-shale sequence with siltstone, mudstone, limestone and conglomerate
59	E3m	Marl, sandstone and limestone
60	E3sm	Sandstone and marl
61	Ea.bv	Andesitic and basaltic volcanic
62	Ea.bvs	Andesitic to basaltic volcano sediment
63	Ea.bvt	Andesitic to basaltic volcanic tuff
64	Eabvb	Andesitic to basaltic volcano breccia
65	Easv	Andesitic subvolcanic
66	Eat	Andesitic tuff
67	Eav	Unknown
68	Eav	Andesitic volcanic
69	Eavb	Andesitic volcano breccia
70	Eavs	Andesitic volcano sediment
71	Eavt	Andesitic volcanic tuff
72	Ebt	Basaltic tuff
73	Ebv	Basaltic volcanic rocks
74	Ebvs	Basaltic volcano sediment
75	Ebvt	Basaltic volcanic tuff
76	Ed.asv	Dacitic to andesitic subvolcanic rocks
77	Ed.at	Dacitic to Andesitic tuff
78	Ed.avb	Dacitic to Andesitic volcano breccia
79	Ed.avs	Dacitic to Andesitic volcano sediment
80	Edav	Dacitic to Andesitic volcanic

ID	Geo unit	Description
81	Edavt	Dacitic andesitic volcanic tuff
82	Edi	Diorite
83	Edsv	Rhyolitic to rhyodacitic subvolcanic
84	Edt	Rhyolitic to rhyodacitic tuff
85	Edv	Rhyolitic to rhyodacitic volcanic
86	Edvb	Rhyolitic to rhyodacitic volcano breccia
87	Edvs	Rhyolitic to rhyodacitic volcano sediment
88	Edvt	Rhyolitic to rhyodacitic volcanic tuff
89	Ef	Eocene flysch in general, composed of shale, marl, sandstone, conglomerate and limestone
90	Efv	Silty shale, marl, thin-bedded limestone, tuffaceous sandstone and basaltic volcanic rocks
91	Egb	Gabbro
92	Egr	Granite
93	Egr-di	Granite to diorite
94	Eja	Grey and brown weathered, massive dolomite, low weathered thin to medium -beded dolomite and massive, feature forming, buff dolomitic limestone
95	Ek	Well bedded green tuff and tuffaceous shale
96	Ek.a	Calcareous shale with subordinate tuff
97	Ekgy	Gypsum
98	Ekh	Olive-green shale and sandstone
99	Ekn	Tine-bedded argillaceous limestone and calcareous shale
100	Eksh	Greenish-black shale, partly tuffaceous with intercalations of tuff
101	Ekv1	Early-Eocene, sandstone, siltstone and shale with nummulitic limestone intercalation
102	Ekv2	Middle-Eocene, lower part composed of sandstone, siltstone and shale
103	Ekv3	Middle-Eocene, upper part composed of sandstone, siltstone shale and marl with limestone intercalation
104	EMas-sb	Undivided Asmari and Shahbazan Formation
105	EOa-bv	Andesitic to basaltic volcanic
106	EOas-ja	Undivided Asmari and Jahrum Formation, regardless to the disconformity separates them
107	EOasv	Eocene-Oligocene andesitic subvolcanic
108	EOav	Eocene-Oligocene andesitic lava flows
109	EObv	Eocene-Oligocene basaltic lava flows
110	EOd	Eocene-Oligocene diorite
111	EOd-av	Dacitic to Andesitic volcanic
112	EOdsv	Eocene-Oligocene rhyolitic to rhyodacitic subvolcanic
113	EOdv	Rhyolitic to rhyodacitic volcanic rocks
114	EOf	Rytmically bedded sandstone and shale with volcanoclastic sandstone, minor limestone and tuff
115	EOgr	Eocene-Oligocene granite and granodiorite
116	EOgr-d	Eocene-Oligocene granite to diorite
117	EOgy	Gypsum
118	EOsa	Salt dome
119	EOsc	Sandstone, siltstone, shale and conglomerate
120	EOt	Ignembrite and tuff
121	Eph	Phyllite
122	Esl	Red shale and pelagic limestone
123	Eslv	Red shale, pelagic limestone and amigdaloidal basic volcanic rocks
124	Jch	Dark grey argillaceous limestone and marl
125	Jd	Well-bedded to thin-bedded, greenish-grey argillaceous limestone with intercalations of calcareous shale
126	Jd.avs	Dacitic to Andesitic volcano sediment
127	Jdav	Jurassic dacite to andesite lava flows
128	Jdt	Rhyolitic to rhyodacitic tuff
129	Jdvt	Rhyolitic to rhyodacitic volcanic tuff
130	Je	Massive, light-grey reef limestone
131	Jel	Reefal limestone
132	Jf	Flysch turbidites sandstone, shale, conglomerate, volcanic rocks and limestone; this unit transgresivly overlies the metamorphic rocks
133	Jh	Alternation of sandstone and sandy to argillaceous shale with intercalations of coal and carbonaceous shale
134	Jk	Conglomerate, sandstone and shale with plantremains and coal seams
135	JKav	Andesitic flows and their associated pyroclastics with or without intercalations of limestone
136	JKbl	Grey, thick-bedded, oolitic, fetid limestone
137	Jkc	Honogenous, well rounded quartzos conglomerate
138	JKdi	Diorite
139	JKkgp	Undivided Khami Group, consist of massive thin-bedded limestone comprising the following formations: Surmeh, Hith Anhydrite, Fahlian, Gadvan and Dariyan
140	JKkgp-bgp	Jurassic to Cretaceous undivided sedimentary rocks including Khami and Bagestan Groups
141	JKl	Crystalized limestone and calc- schist
142	Jks	Alternation of sandstone and shale
143	JKsj	Pale red argillaceous limestone, marl, gypsiferous marl, sandstone and conglomerate
144	Jl	Light grey, thin-bedded to massive limestone
145	Jmz	Grey thick-bedded limestone and dolomite
146	Jph	Phyllite, slate and meta-sandstone (Hamadan Phyllites)
147	Jq	Sandstone, shale, thin-bedded limestone and calcareous shale
148	Jr	Red manganiferous chert
149	Js	Shale with intercalations of conglomerate, sandstone, radiolarite, limestone and volcanic
150	Jsc	Conglomerate
151	Jshl.s	Sandy to silty gluconitic limestone and calcareous limestone
152	Jsm	Thick-bedded to massive dolomitic limestone, thin-bedded argillaceous limestone and marl
153	Jss	Sandstone
154	JUavs	Andesitic volcano sediment
155	JUavt	Andesitic volcanic Tuff

ID	Geo unit	Description
156	Jub	Sandstone, siltstone, Pectinid limestone, marl, gypsum
157	Juc	White, quartzous conglomerate
158	Judi	Upper Jurassic diorite
159	JUdv	Rhyolitic to rhyodacitic volcanic
160	Jugn	Granite gneiss normally with augen structure
161	Jugr	Upper Jurassic granite including Shir Kuh Granite and Shah Kuh Granite
162	Jugr	Upper Jurassic granite including Shir Kuh Granite and Shahkuh Granite
163	Jugr-di	Upper Jurassic granite to diorite intrusive
164	Jugy	Gypsum
165	Jumb	Late Jurassic marble and mamorized limestone
166	Jupl	Pectinid limestone and marl
167	Jurb	Sandstone, siltstone, and fine-grained conglomerate
168	Jus	Red sandstone and siltstone
169	K	Cretaceous rocks
170	K1-2lm	Albian-Cenomanian marl and argillaceous limestone
171	K1a.bv	Andesitic and basaltic volcanic rocks
172	K1avt	Andesitic volcanic tuff
173	K1bl	Grey, thick-bedded to massive oolitic limestone
174	K1bv	Early-Cretaceous basaltic lava flows
175	K1bvt	Basaltic volcanic tuff
176	K1c	Red conglomerate and sandstone
177	K1l	Massive to thick-bedded orbitolina limestone
178	K1m	Limestone, argillaceous limestone; tile red sandstone and gypsiferous marl
179	K2a.bv	Andesitic and basaltic volcanic rocks
180	K2asv	Andesitic subvolcanic
181	K2av	Andesitic volcanic
182	K2bv	Basaltic volcanic
183	K2c	Conglomerate and sandstone
184	K2d.asv	Dacitic to andesitic subvolcanic rocks
185	K2d.av	Dacitic to Andesitic volcanic
186	K2di	Diorite
187	K2gb	Gabbro
188	K2gr	Granite
189	K2l	Hyporite bearing limestone
190	K2l,m,s	Limestone, marl and sandstone
191	K2l1	Hyporite bearing limestone
192	K2l2	Thick-bedded to massive limestone
193	K2lm	Pale-red marl, gypsiferous marl and limestone
194	K2m,l	Marl, shale and detritic limestone
195	K2shm	Shale calcareous shale and sandstone with intercalations of limestone
196	Ka.bv	Andesitic to basaltic volcanic
197	Kab	Blue-grey marl and shale
198	M1f	Rhytmically bedded sandstone, calcareous sandstone, mudstone, gypsiferous mudstone and shale
199	M2-3s	Sandstone, siltstone, conglomerate, shale, mudstone and shell beds
200	M2gm	Gypsiferous and calcareous marl, marlstone and mudstone with interbedded siltstone and sandstone (Gushi Marl and part of Sabz unit)
201	M3ms	Marl and marlstone, locally gypsiferous and sandstone with interbedded shale and marl
202	Ma.bv	Andesitic-basaltic volcanic rocks
203	Mat	Andesitic tuff
204	Mav	Miocene andesitic lava flows locally basalt
205	mb	Marble
206	Mbv	Basaltic volcanic rocks
207	Mc	Red conglomerate and sandstone
208	Mcs	Red conglomerate, sandstone, siltstone and mudstone
209	Md.av	Dacitic to andesitic subvolcanic rocks
210	Mdt	Rhyolitic to rhyodacitic tuff
211	Mgr	Granite
212	Mgs	Anhydrite, salt, grey and red marl alternating with anhydrite, argillaceous limestone and limestone
213	Mm,s,l	Marl, calcareous sandstone, sandy limestone and minor conglomerate
214	Mmn	Unknown
215	Mmn	Low weathering gray marls alternating with bands of more resistant shelly limestone
216	Mms	Alternations of marl, silty clay shale, sandstone and dolomitic limestone
217	MPa.bv	Andesitic to basaltic volcanic
218	MPa.bvt	Andesitic to basaltic volcanic tuff
219	MPasv	Andesitic subvolcanic
220	MPd.av	Dacitic to andesitic volcanic
221	MPLav	Andesitic volcanic
222	MPlc	Polymictic conglomerate, sandstone and mudstone
223	MPLdvt	Rhyolitic to rhyodacitic volcanic tuff
224	MPlfgp	FARS GROUP comprising the following formation Gachsaran, Mishan and Aghajari,
225	MPls	sandstone with siltstone, mudstone and minor conglomerate
226	Ms	Sandstone siltstone with minor conglomerate
227	Msc	Varigated gypsiferous clay shale; conglomerate and sandstone
228	MuPlaj	Brown to grey, calcareous, feature-forming sandstone and low weathering, gypsum- veined, red marl and siltstone
229	Mur	Red marl, gypsiferous marl, sandstone and conglomerate
230	Murc	Red conglomerate and sandstone
231	Murgy	Gypsum
232	Murm	Light-red to brown marl and gypsiferous marl with sandstone intercalations
233	Murmg	Gypsiferous marl
234	Mursh	Varigated shale, gypsiferous marl and sandstone
235	Mv	Volcanic in general
236	Mvs	Tuff interbedded with sandstone and siltstone
237	Oa.bv	Andesitic to basaltic volcanic

ID	Geo unit	Description
238	Oa.bvs	Andesitic to basaltic volcano sediment
239	Oasv	Andesitic subvolcanic
240	Oat	Andesitic tuff
241	Oav	Oligocene andesitic lava flows
242	Oavt	Andesitic volcanic tuff
243	Obv	Basaltic Volcanic
244	Oc	Polimictic conglomerate, sandstone and siltstone
245	Od.asv	Dacitic to andesitic subvolcanic rocks
246	Od.av	Dacitic to andesitic volcanic
247	Odi	Diorite
248	Odi-gb	Diorite to gabbro
249	Odsv	Rhyolitic to rhyodacitic subvolcanic
250	Odv	Rhyolitic to rhyodacitic volcanic
251	Odvb	Rhyolitic to rhyodacitic volcano breccia
252	Odvs	Rhyolitic to rhyodacitic volcano sediment
253	Odvt	Rhyolitic to rhyodacitic volcanic tuff
254	Ogb	Gabbro
255	Ogr	Granite
256	Ogr-di	Granite to diorite
257	Ogrsv	Granite subvolcanic
258	Olav	Rhyolitic to rhyodacitic volcanic rocks
259	Olc,s	Conglomerate and sandstone
260	Olgr	Oligocene granite and granodiorite
261	Olgy	Gypsum
262	Olm,s,c	Red and green silty, gypsiferous marl, sandstone and gypsum
263	om1	Tectonized association of peridotites, gabbro, diorite, trondhjemite, diabase and basic volcanic
264	om2	Tectonized association of pelagic limestone, radiolarian chert, radiolarian shale with basic volcanic and intrusive rocks of ophiolitic rocks
265	om3	Pelagic limestone, radiolarian chert and shale in association with basalt and basaltic andesite pillow lava
266	OMa.bv	Andesite and andesitic lava flow
267	OMap	Andesitic pyroclastic rocks
268	OMas	Cream to brown-weathering, feature-forming, well-jointed limestone with intercalations of shale
269	OMat	Andesitic tuff
270	OMav	Andesitic volcanic
271	OMavs	Andesitic volcano sediment
272	OMbt	Basaltic tuff
273	OMbv	Basalt and subvolcanic
274	OMbvb	Basaltic volcano breccia
275	OMbvs	Basaltic volcano sediment
276	OMc	Basal conglomerate and sandstone
277	OMd.at	Dacitic Andesitic tuff
278	OMd.av	Dacitic Andesitic volcanic
279	OMdi	Diorite
280	OMdi-gb	Diorite to gabbro
281	OMdsv	Rhyolitic to rhyodacitic subvolcanic
282	OMdv	Rhyolite and rhyodacite
283	OMdvs	Rhyolitic to rhyodacitic volcano sediment
284	OMdvt	Rhyolitic to rhyodacitic volcanic tuff
285	OMf	Rhytmically bedded sandstone and shale, with minor siltstone and mudstone
286	OMgb	Oligo-Miocene gabbro and microgabbro
287	OMgr	Oligo-Miocene granite and granodiorite
288	OMgr-di	Granite to diorite
289	OMl	Unknown
290	OMq	Limestone, marl, gypsiferous marl, sandymarl and sandstone
291	OMql	Massive to thick-bedded reefal limestone
292	OMqm	Marl with intercalations of limestone
293	OMr	Red, grey, and green silty marls interbedded with subordinate silty limestone and minor sandstone ribs
294	OMrb	Red Beds composed of red conglomerate, sandstone, marl, gypsiferous marl and gypsum
295	OMssh	Yellow-green shale and sandstone locally with limestone intercalation
296	OMz1	Alternation of varigated siltyclay shale with sandstone
297	OMz2	Massive to thick bedded tuffaceous sandstone and varigated shale
298	OMz3	Alternation of sandstone with siltstone and claystone
299	OPLavs	Andesitic volcano sediment
300	OS	Undifferentiated Ordivician and Silurian rocks
301	P34	Unknown
302	P	Undifferentiated Permian rocks
303	PAav	Andesitic volcanic
304	PAbv	Basaltic volcanic
305	PAbvt	Basaltic volcanic Tuff
306	PAdv	Rhyolitic to rhyodacitic volcanic
307	PAEa.bv	Andesitic to basaltic volcanic
308	PAEa.bvt	Andesitic to basaltic volcanic tuff
309	PAEav	Andesitic volcanic
310	PAEavb	Andesitic volcano breccia
311	PAEavs	Andesitic volcano sediment
312	PAEavt	Andesitic volcanic tuff
313	PAEbvs	Basaltic volcano sediment
314	PAgr	Granite
315	PAgr-di	Granite to diorite
316	pC-C	Late proterozoic-early Cambrian undifferentialed rocks
317	pC-Cd	Recrystalised dolomite and fetid limestone; violet-red micaceous sandstone and siltstone; gypsum
318	pC-Ch	Rock salt, gypsum & blocks of contorted masses of sedimentary material such as black laminated fetid limestone, brown cherty dolomite, red sandstone & varigated shale in association with igneous rocks such as diabase, basalt, rhyolite and trachyte
319	pC-Cs	Thick dolomite and limestone unit, portly cherty with thick shale intercalations
320	pCa.bv	Andesite and basalt
321	pCam	Amphibolite

ID	Geo unit	Description
322	pCav	Andesitic volcanic
323	pCbr	Dolomite and sandstone
324	pCdi	Precambrian diorite
325	pCdv	Rhyolitic to rhyodacitic volcanic
326	pCgn	Gneiss, granite gneiss and locally including migmatite
327	pCgr	Precambrian granite to granodiorite
328	pCgr-di	Granite to diorite
329	pCk	Dull green grey slaty shales with subordinate intercalation of quartzitic sandstone
330	pCmb	Marble
331	pCmt1	Medium-grade, regional metamorphic rocks
332	pCmt2	Low-grade, regional metamorphic rocks
333	pCph	Phyllite
334	pCr	Dolomite and limestone, partly cherty; redish sandy shale and sandstone, volcanic rocks and tuffs
335	pCrr	Acidic volcanic rocks
336	pd	Peridotite including harzburgite, dunite, lerzolite and websterite
337	Pd	Red sandstone and shale with subordinate sandy limestone
338	pd1	Ulttrabasic rocks
339	Pda	Limestone, dolomite, dolomitic limestone and thick layers of anhydrite in alternation with dolomite in middle part
340	Peasv	Andesitic subvolcanic
341	Pec	Conglomerate and sandstone
342	PeEck	Limestone, marl and gysiferous marl
343	PeEck-kh	Undifferentiated unit, including limestone, marl shale and sandstone
344	PeEf	Flysch turbidite, sandstone and calcareous mudstone
345	PeEm	Marl and gypsiferous marl locally gypsiferous mudstone
346	PeEpd	Blue and purple shale and marl interbedded with the argillaceous limestone
347	PeEph	Phyllite
348	PeEps-ck	Undifferentiated unit, including conglomerate, sandstone, limestone and marl
349	PeEs	Arkosic to subarkosic sandstone
350	PeEsa	Pale red marl, marlstone, limestone, gypsum and dolomite
351	PeEsh	Shale and calcareous shale
352	PeEtz	Grey and brown, medium-bedded to massive fossiliferous limestone
353	PeEz	Reef-type limestone and gypsiferous marl
354	Pel	Medium to thick-bedded limestone
355	Pem	Marl, gypsiferous marl and limestone
356	Pems	Mudstone calcareous shale, limestone and minor sandstone
357	Peps	Red well consolidated conglomerate, sandstone and mudstone
358	Pes	Sandstone, calcareous shale and mudstone
359	Pgf	Polygenic conglomerate, red sandstone and sandy mudstone
360	Pgkc	Light-red coarse grained, polygenic conglomerate with sandstone intercalations
361	pgr	Plagiogranite
362	Pj	Massive to thick-bedded, dark-grey, partly reef type limestone and a thick yellow dolomite band in the upper part
363	Pla.bv	Andesitic to basaltic volcanic
364	Plasv	Pliocene andesitic subvolcanic
365	Plat	Andesitic tuff
366	Plav	Andesitic lavas with minor basaltic andesite, tuff and breccias interbedded with volcanoclastic sandstone and boulder conglomerate (Bazman Volcanism)
367	Plbk	Alternating hard of consolidated, massive, feature forming conglomerate and low -weathering cross -bedded sandstone
368	Plbv	Basaltic lava flows
369	Plc	Polymictic conglomerate and sandstone
370	Plc	Polymictic conglomerate and sandstone
371	Pld.asv	Dacitic to andesitic subvolcanic rocks
372	Pld.at	Dacitic andesitic tuff
373	Pld.av	Dacitic andesitic volcanic
374	Pld.avs	Dacitic andesitic volcano sediment
375	Pldsv	Pliocene rhyolitic to rhyodacitic subvolcanic
376	Pldt	Rhyolitic to rhyodacitic tuff
377	Pldv	Rhyolitic to rhyodacitic volcanic
378	Pldvt	Rhyolitic to rhyodacitic volcanic tuff
379	Plgr	Granite
380	Plgr-di	Granite to diorite
381	Plmb1	Pyroclastics and claystone with vertebrate fauna remains
382	Plmb2	Ash flows and associated rocks
383	Plmb3	Ash flows and associated pyroclastic rocks, conglomerate, sandstone and shale
384	Plms	Marl, shale, sandstone and conglomerate
385	PlQabv	Andesite, andesitic basalt and olivine basalt
386	PlQap	Silty clay, sand, gravel and volcanic ash
387	PlQav	Andesitic volcanic
388	PlQavs	Andesitic volcanic in association with sedimentary rocks
389	PlQbv	Basaltic volcanic
390	PlQc	Fluvial conglomerate, Piedmont conglomerate and sandstone.
391	PlQd.avt	Dacitic andesitic volcanic tuff
392	PlQdv	Rhyolitic to rhyodacitic volcanic
393	PlQlu	Unfolded, poorly consolidated, yellowish silt, sand and gravel
394	PlQm	Lacustrine terraces fine grained deposits and lake sediments
395	PlQms	Poorly cemented, unindurated sandstone and mudstone
396	Pmb	Marble

ID	Geo unit	Description
397	Pml	Slightly metamorphosed fossiliferous (Fusulinid) limestone, locally crystaline limestone
398	Pn	Dark grey limestone and shale
399	Pr	Dark grey medium-bedded to massive limestone
400	Psch1	Metamorphosed turbidite including phyllite, crystaline limestone calc-schist
401	Psch2	Metamorphosed turbidite in associated with met ultrabasic and basic rock
402	PTR	Undifferentiated Permo-Triassic sedimentary rocks
403	px	Pyroxenite
404	Pz	Undifferentiated lower Paleozoic rocks
405	Pz1a.bv	Andesitic basaltic volcanic
406	Pz1av	Andesitic volcanic
407	Pz1di	Lower Paleozoic diorite
408	Pz1gn	Gneiss and anatectic granite
409	Qft1	High level piedmont fan and valley terrace deposits
410	TRml	Meta- limestone, meta-quartzarenite, phyllite and meta- volcanic
411	Pz2	Undifferentiated Upper Paleozoic rocks
412	PZ2a.bv	Andesitic basaltic volcanic
413	PZ2asv	Andesitic subvolcanic
414	PZ2bv	Basaltic volcanic
415	PZ2bvt	Basaltic volcanic tuff
416	PZ2gr	Granite
417	Pzkb	Undifferentiated basic schist pelitic schist, psammitic schist, calc-silicate rocks, amphibolite, recrystalized limestone, marble and phyllite
418	Qabv	Andesite to basaltic volcanic
419	Qabvs	Andesitic to basaltic volcano sediment
420	Qal	Stream channel, braided channel and flood plain deposits
421	Qasv	Andesitic subvolcanic
422	Qat	Andesitic tuff
423	Qav	Andesitic volcanic Basaltic volcanic
424	Qavs	Andesitic volcano sediment
425	Qba	Silty clay, sandy tuff and fresh water limestone
426	Qbv	Olivine basalt and basalt related to Bazman Volcanism and partly related to Taftan Volcanism
427	Qbvs	Basaltic volcano sediment
428	Qcf	Clay flat
429	Qcsm	Clay salt marsh
430	Qcu	Cultivated area
431	Qdi	Diorite
432	Qdt	Rhyolitic to rhyodacitic tuff
433	Pz1gr	Lower Paleozoic granite, including Zarigan granite and Narigan granite
434	Pz1mt	Gneiss, anatectic granite, amphibolite, kyanite, staurolite schist, quartzite and minor marble
435	Qft1	High level piedmont fan and valley terrace deposits
436	Qft1	High level piedmont fan and valley terrace deposits
437	Qft2	Low level piedmont fan and valley terrace deposits
438	Qft2	Low level piedmont fan and valley terrace deposits
439	Qft2	Low level piedmont fan and valley terrace deposits
440	Qft2	Low level piedmont fan and valley terrace deposits
441	Qft2	Low level piedmont fan and valley terrace deposits
442	Qft2	Low level piedmont fan and valley terrace deposits
443	Qft2	Low level piedmont fan and valley terrace deposits
444	Qft2	Low level piedmont fan and valley terrace deposits
445	Qft2	Low level piedmont fan and valley terrace deposits
446	Qft2	Low level piedmont fan and valley terrace deposits
447	Qft2	Low level piedmont fan and valley terrace deposits
448	Qgb	Gabbro
449	Qgr	Granite
450	Qitd	Intertidal deposits
451	Qm	Swamp and marsh
452	Qmt	Undifferentiated marine terraces
453	QPLavt	Andesitic volcanic tuff
454	QPLdasv	Dacitic to andesitic subvolcanic rocks
455	Qs	Sand dunes and sand sheet
456	Qs,d	Unconsolidated wind-blown sand deposit including sand dunes
457	Qsf	Salt flat
458	Qsl	Salt Lake
459	Qsw	Swamp
460	Qtr	Teravertine
461	Qvc	Coarse grained fanglomerate composed of volcaniclastic materials locally with intercalation of lava flows
462	sea	Unknown
463	sm1	Sedimentary melange-sheared and boudined sediments with no recognizable stratigraphy containing tectonic blocks of Cretaceous to Eocene age
464	sm2	Sedimentary melange-sheard and boudined sediments with norecognisable stratigraphy, containing tectonic blocks of Cretaseous to Miocene age
465	Sn	Greenish grey, shale, sandstone, sandylime, coral limestone and dolomite
466	sp	Spilitic rocks locally with pillow structure
467	sp1	Spilite spilitic andesite and diabasic tuff
468	spr	Sub-marine, vesicular basalt, locally with pillow structure in association with radiolarian chert
469	sr	Serpentinite
470	tm	Tectonic melange-association of ophiolitic components, pelagic limestone, radiolarian chert and shale with or without Eocene sedimentary rocks
471	TRa.bv	Triassic, andesitic and basaltic volcanic
472	TRav	Andesitic Volcanic
473	TRavt	Andesitic volcanic tuff
474	TRba	Red to light green conglomerate and microconglomerate with intercalations of sandstone and shale
475	TRbv	Basaltic volcanic
476	TRdl	Crystaline limestone and dolomite

ID	Geo unit	Description
477	TRe	thick bedded grey oolitic limestone; thin-platy, yellow to pinkish shaly limestone with worm tracks and well to thick-bedded dolomite and dolomitic limestone
478	TRe1	Thin bedded, yellow to pinkish argillaceous limestone with worm tracks
479	TRe2	Thick bedded dolomite
480	TRJa.bv	Andesitic to Basaltic Volcanic
481	TRJlr	Grey, thin to thick bedded, partly cherty, neritic limestone intercalation of radiolarian shale and chert
482	TRJs	Dark grey shale and sandstone
483	TRJvm	Meta-volcanic, phyllites, slate and meta- limestone
484	TRkk-nz	Thin to medium-bedded, dark grey dolomite; thin-bedded dolomite, greenish shale and thin-bedded argillaceous limestone
485	TRKubl	Kuh Bistoon limestone
486	TRKurl	Purple and red thin-bedded radiolarian chert with intercalations of neritic and pelagic limestone
487	TRmi	Shale and sandstone with coal seams
488	Qft1	High level piedmont fan and valley terrace deposits
489	TRn	Sandstone, quartz arenite, shale and fossiliferous limestone
490	TRn1	Grey green shale, siltstone and feldspathic sandstone underlain by pisolitic iron laterite horison
491	TRn2	Shale, Heterastridum bearing limestone and reddish-brown sandstone
492	TRn3	Shale interbedded with thin sandstone beds
493	TRn4	Black limestone, shale and sandstone
494	TRn5	Shale, siltstone, sandstone and thin sandy limestone with thin coal seams
495	TRqa	Red to brown shale, sandstone and conglomerate
496	TRs	Calcareous red shale
497	TRsh	Well-bedded, dense, yellow dolomite
498	TRsi	Tuffaceous sandstone, tuffaceous shale with intercalations of limestone, marl and conglomerate
499	TRuJm	Transitional zone composed of phyllite with intercalations of crystalized limestone and acidic volcanic horizons
500	Kad	White-cream Inoceramus bearing cherty and glauconitic argillaceous limestone
501	Kad-ab	Undifferentiated unit including argillaceous limestone, marl and shale
502	Kat	Olive green glauconitic sandstone and shale
503	Kav	Andesitic volcanic
504	Kavt	Andesitic volcanic tuff
505	Kbgp	Undivided Bangestan Group, mainly limestone and shale, Albian to Companian, comprising the following formations: Kazhdumi, Sarvak, Surgah and Ilam
506	Kbsh	Dark grey slightly phyllitized shale with intercalations of sandstone and limestone
507	Kbv	Basaltic volcanic
508	Kbvt	Basaltic volcanic tuff
509	Kd.av	Dacitic to Andesitic volcanic
510	Kda-fa	Grey to brown, partly oolitic, massive limestone; limestone in alternation with marl and thick-bedded to massive orbitolina bearing limestone
511	Kdi	Diorite
512	Kdzsh	Marl, shale, sandstone and limestone
513	KEpd-gu	Grey and brown, medium-bedded to massive fossiliferous limestone
514	Kfsh	Dark grey argillaceous shale
515	Kgb	Gabbro
516	Kgr	Granite
517	Kgu	Bluish grey marl and shale with subordinate thin-bedded argillaceous -limestone
518	Kk	Buff, thick-bedded limestone, marlstone and marl
519	Kkz	Grey to dark grey bituminous shale with intercations of limestone
520	Kl	Lower Cretaceous undifferentiated rocks
521	Klav	Andesitic volcanic rocks
522	Klsm	Marl, shale, sandy limestone and sandy dolomite
523	Klsol	Grey thick-bedded to massive orbitolina limestone
524	Knl	Massive grey to black limestone
525	Kns	Red sandstone and conglomeratic sandstone
526	Knsh	Dark green calcareous shale
527	Knz	Gloconitic sandstone
528	KPAavs	Andesitic Volcano sediment
529	KPeam	Dark olive-brown, low weathered siltstone and sandstone with local development of chert conglomerates and shelly limestone
530	KPedu	Undifferentiated limestone, basic to intermediate lava and pillow lava, metavolcanic, phyllite, schist, sediments, metasediments with minor tuff and intrusive rocks
531	KPef	Thinly bedded sandstone and shale with siltstone, mudstone limestone and conglomerate
532	KPefv	Crystal tuff, tuffaceous sandstone, recrystalized limestone and sandy limestone, red chert and pillow lava
533	KPegr	Late Cretaceous-Early Paleocene granite
534	KPegr-di	Late Cretaceous-Early Paleocene granite to diorite intrusive rocks
535	KPeph	Phyllite
536	KPvs	Volcanic and volcanoclastic rocks including tuff, basalt, minor conglomerate and slamp breccia
537	Ksm,l	Marl and calcareous shale with intercalations of limestone
538	Ksn	Grey to block shale and thin layers of siltstone and sandstone
539	Ksr	Ammonite bearing shale with interaction of orbitolin limestone
540	Ksv	Grey, thick-bedded to massive limestone with thin marl intercalations in upper part
541	Ktb	Massive, shelly, cliff-forming partly anhydritic limestone

ID	Geo unit	Description
542	Ktl	Thin to medium bedded argillaceous limestone and thick bedded to massive, grey orbitolina bearing limestone
543	Ktr	Grey oolitic and bioclastic orbitolina limestone
544	Ktzl	Thick bedded to massive, white to pinkish orbitolina bearing limestone
545	Ku	Upper cretaceous, undifferentiated rocks
546	Kuabv	Late-Cretaceous andesitic and basaltic lava flows
547	Kuavs	Andesitic Volcano sedimentary
548	Kuf	Unknown
549	Kuf	Flysch type sediments including shale, sandstone, limestone and conglomerate
550	Kufsh	Mudstone, shale and sandstone
551	Kuft	Flysch turbidites
552	Kufv	Flysch-volcanic rocks
553	Kugr	Granite and granodiorite
554	Kugr-di	Granite to Diorite
555	Kupl	Globotrunca limestone
556	Kur	Radiolarian chert and shale
557	Kurl	Undifferentiated pelagic limestone and radiolarian chert
558	Kus	Flysch turbidite sandstone with interbed calcareous mudstone and shale
559	Kussh	Dark grey shale
560	Kussh	Dark grey shale
561	l	Massive, recrystalized limestone with minor phyllite and schist
562	L.E-Oa.bv	Andesitic to basaltic volcanic
563	L.E-Oa.bvt	Andesitic to basaltic volcanic tuff
564	L.E-Oav	Andesitic volcanic
565	L.E-Obv	Basaltic volcanic
566	L.E-Od.at	Dacitic to andesitic tuff
567	L.E-Od.av	Dacitic to andesitic volcanic
568	L.E-Od.avb	Dacitic to andesitic volcano breccia
569	L.E-Od.avt	Dacitic to andesitic volcanic tuff
570	L.E-Odi	Diorite
571	L.E-Odsv	Late Eocene-Early Oligocene rhyolitic to rhyodacitic subvolcanic rocks
572	L.E-Odv	Rhyolitic to rhyodacitic volcanic
573	L.E-Of	Feldespatoidal intrusive rock
574	L.E-Ogr	Late Eocene-Early Oligocene granite
575	Lake	Unknown
576	lv	Listvinite
577	M1-2f	Thickly bedded sandstone with interbedded siltstone and shale
578	M1-2m	Shale, gypsiferous shale, gypsiferous mudstone and silty shale with minor sandstone and limestone

Soil order legend

ID	Soil order
1	Inceptisols/Vertisols
2	Inceptisols
3	Entisols/Inceptisols
4	Entisols/Aridisols
5	Aridisols
6	Rock outcrops/ Inceptisols
7	Rock outcrops/Entisols
8	Playa
9	Rocky lands
10	Kalut
11	Dune lands
12	Marsh
13	Coastal sands
14	Bad lands
15	Mollisols
16	Water body
17	Urban
18	Salt plug
19	Salt flats
20	Alfisols

Italian Journal of Agrometeorology
Rivista Italiana di Agrometeorologia

Firenze University Press
www.fupress.com/ijam

OPEN ACCESS

Citation: S. Weine Paulino Chaves, R. Duarte Coelho, J. de Oliveira Costa, S. André Tapparo (2021) Micrometeorological modeling and water consumption of tabasco pepper cultivated under greenhouse conditions. *Italian Journal of Agrometeorology* (1): 21-36. doi: 10.36253/ijam-1221

Received: February 14, 2021

Accepted: May 26, 2021

Published: August 9, 2021

Data Availability Statement: All relevant data are within the paper and its Supporting Information files.

Competing Interests: The Author(s) declare(s) no conflict of interest.

Micrometeorological modeling and water consumption of tabasco pepper cultivated under greenhouse conditions

Sérgio Weine Paulino Chaves[1], Rubens Duarte Coelho[2], Jéfferson de Oliveira Costa[2,*], Sergio André Tapparo[3]

[1] *Federal Rural University of the Semi-Arid/UFERSA, Department of Environmental and Technological Sciences, Francisco Mota, 572, 59625-900, Mossoró, RN, Brazil*
[2] *University of São Paulo/USP-ESALQ, Department of Biosystems Engineering, C.P. 09, 13418-900 Piracicaba, SP, Brazil*
[3] *Federal Institute of Mato Grosso do Sul/IFMS, Campus Ponta Porã, highway BR-463, km 14, 79909-000, Ponta Porã, MS, Brazil*
*Corresponding author. E-mail address: costajo@alumni.usp.br

Abstract. Micrometeorological variables of tabasco pepper cultivated under greenhouse and drip irrigated conditions have not been presented to date in literature, especially the water consumption of these plants, in terms of crop evapotranspiration (ET_c) and crop coefficient (K_c). The determination of these variables is extremely important for the application of the correct amount of water to irrigated crops in these environments because PM FAO (56) standard methodology was idealized for outdoor environments. The objective of this work was to develop models of estimation of micrometeorological variables in greenhouse conditions and to determine the water demand, in terms of evapotranspiration (ET) and K_c, of the pepper (*Capsicum frutescens* L.), cv. Tabasco McIlhenny, drip irrigated using drainage lysimeters. The research was carried out in an experimental area located at the University of Sao Paulo (USP) in Piracicaba, SP, Brazil. The following micrometeorological variables were monitored: air temperature, air relative humidity (digital thermohygrometer) and evaporation (mini-pan) (EMT). Drainage lysimeters were used to obtain the ET_c and the reference evapotranspiration (ET_o) was estimated outside the greenhouse by the Penman Monteith (ET_oPM), Hargreaves and Samani (ET_oHS) methods and the class "A" pan method (ECA). It was concluded that the total value of mini-pan evaporation (EMT) inside the greenhouse was practically equal to ET_oPM, 5% lower than ET_oHS and 31% higher than ECA in the outdoor environment. ET values ranged from 0.28 to 2.42 mm day^{-1} and total crop ET was 446.43 mm. The K_c values for the first pepper production cycle were: 0.17 in the initial phase, 0.76 in the flowering and fruiting phase and 0.39 in the harvest phase, for the second production cycle, the value of K_c was 0.50 at the harvest phase.

Keywords: *Capsicum frutescens* L, evapotranspiration, lysimetry, micro irrigation.

1. INTRODUCTION

Changes in micrometeorological variables as air temperature, relative humidity, radiation and evapotranspiration for crops under plastic-covered

environments have been studied in several locations in Brazil (Andrade Júnior et al., 2011; Costa et al., 2015; Chavaria et al., 2009) and the world (Kittas and Bartzanas, 2007; Meiri et al., 2011; AbdelGhany and Helal, 2011; Giménez et al., 2013; Qiu et al., 2015), either for research as well as commercial purposes, where the methodology FAO (56) ET_oPM standard that is recommended for outdoor use requires some adaptations to be used under greenhouse conditions.

Allen et al. (1998) suggested that for the reference evapotranspiration calculation (ET_o) under greenhouse conditions, the wind speed at two meters height should be set at 0.5 m s^{-1}, because according to the same authors, this improves the accuracy of estimates in very low wind speed conditions, however, do not present any experiments that support this practical suggestion.

Studies show that the ratio between crop evapotranspiration (ET_c) in greenhouse and ET_o in outdoor environment can also cause a variation in the estimate of crop coefficient (K_c). In the greenhouse, in general, the ET_o is lower, around 60 to 80% of that found in outdoor environments (Farias et al., 1994; Orgaz et al., 2005; Qiu et al., 2011).

In the specific case of *Capsicum* species, which have a growing cycle of 120 to 150 days and consume between 600 and 1250 mm of water, depending on climatic conditions and the variety planted, the average K_c is 0.40 immediately after transplantation, 0.95 to 1.10 during the period of full coverage and, for green peppers, 0.80 to 0.90 at harvest (Doorenbos and Kassam, 2000).

Chaves et al. (2005) and Miranda et al. (2006) studied the water demand of the tabasco pepper (*Capsicum frutescens* L.) under field conditions in the semi-arid climate region (Northeast Brazil) and observed a total evapotranspiration of 1083 mm of water for one cycle of 135 days, based on sprinkler irrigation and using three drainage lysimeters to determine water consumption. The average water consumption during crop cycle was 7.4 mm day^{-1}.

Meanwhile, Miranda et al. (2006) under similar conditions, observed that pepper plants consumed an average of 888 mm for a 300-day cycle with drip irrigation system and using a weighing lysimeter to determine water consumption. They obtained ET_c values for tabasco pepper, which ranged from 1.0 to 5.6 mm day^{-1}. However, studies on the water consumption of pepper crop under greenhouse conditions are still unavailable in literature.

Commercial tabasco pepper planted at outdoor conditions, usually suffer from bird attack who really appreciate the fruit flavor, in this way, they must be kept at a certain distance from the plantation to avoid damages; the must friendly way of doing this is the pepper cultivation under greenhouse conditions. Traditionally, family farmers are the main producers of tabasco pepper, thus the use of low-cost equipment to control irrigation as the class A mini-pan must be emphasized in research and extension purposes.

This work is based on the hypothesis that micrometeorological variables under greenhouse conditions can be estimated by regression equations created from data collected at a suitably open weather station near these greenhouses. In addition, the use of drainage lysimeters to determine the ET_c of pepper under greenhouse may be a precise way of obtaining K_c and assist in determining the correct amount of water for pepper irrigation in these environments.

In this context, the objective of this work was to develop equations for estimation of micrometeorological elements under greenhouse conditions and to determine the water demand, in terms of evapotranspiration and K_c, of the pepper (*Capsicum frutescens* L.) cv. Tabasco McIlhenny, drip irrigated and cultivated under greenhouse using drainage lysimeters.

2. MATERIAL AND METHODS

2.1. Location and characterization of the experimental area

The work was conducted in an experimental area of the Biosystems Engineering Department (ESALQ), University of São Paulo (USP), located in Piracicaba, State of São Paulo (22º42'30" S, 47º38'00" W; elevation of 546 m), southeastern Brazil. The local climate, according to the Köppen classification, is Cwa type (Alvares et al., 2013), dry winter and warmer month temperature greater than 22°C, average temperature 21.6°C, average relative humidity of 73% and annual precipitation of 1280 mm.

The experiment was carried out in a greenhouse composed of two twinned spans (with galvanized metal structure), arc cover (with high density transparent polyethylene diffuser film, 150 microns). The greenhouse had the following dimensions: 14 m wide, 22 m long, central height 4.0 m and ceiling height 2.5 m (consisting of four front windows at the ends). The closed sides with protective screen (50% shade) and 20 cm reinforced concrete skirting board (Fig. 1A). Inside the greenhouse, 112 vases of 500 L were distributed in rows. The fiber cement vases had the following dimensions: 0.92 m wide, 1.08 m long and 0.65 m high (Fig. 1B). At the bottom of the vase was placed a 5 cm thick layer of gravel, covered by a geotextile blanket. A 25 mm diameter PVC drain was also installed, drilled and covered at the bottom by the geotextile blanket and buried vertically in the ground. The geographic coordinates of the greenhouse are: 22º42'39" S lat., 47º37'45" W long. and elevation of 546 m.

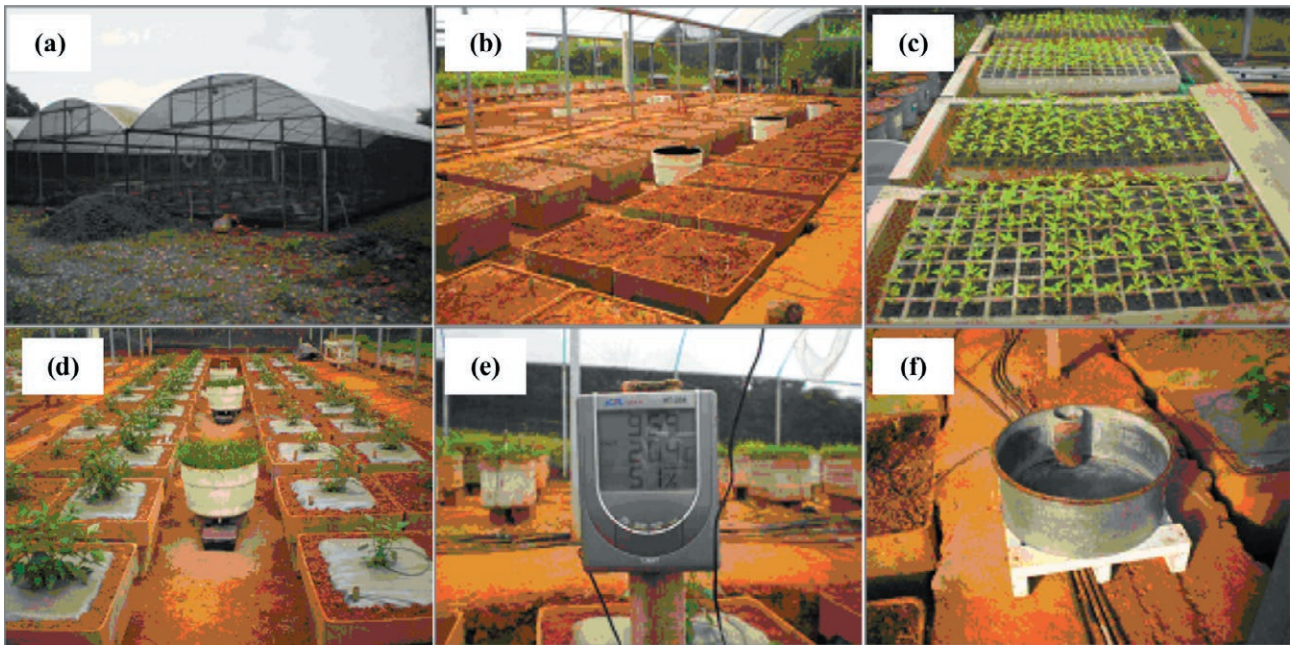

Fig. 1. Images of the experimental area and equipment used for monitoring meteorological variables. External view of the greenhouse used in the experiment (A); Internal view of the greenhouse with the distribution of the vases used for planting the crop (B); Trays used for sowing (C); Internal view of the greenhouse after planting the seedlings and view of the drainage lysimeters in the center (D); Digital thermo-hygrometer used (E); Mini-pan used in the experiment (F).

Making a general comparison with the average external field conditions and agricultural practices adopted in Brazil, we can say that in general the cultivation is done in home gardens for domestic consumption and in commercial gardens that supply the local markets. The spacing used is 1.2 to 1.5 m between rows, by 0.6 m between plants, in general. Productivity is around 15 Mg ha^{-1} (Chaves et al., 2005). They are grown in regions with variable rainfall from 600 to 1200 mm and an average temperature of 25°C.

2.2. Planting and conduction the crop

The genetic material used was pepper (*Capsicum frutescens* L.) cv. tabasco. Sowing was performed in 128 cell trays (Fig. 1C) and at 57 days after sowing (DAS) the seedlings were transplanted to the greenhouse. The spatial arrangement used for greenhouse planting was in double rows, with a spacing of 2.58 x 0.92 m (between rows) and 1.57 m (between plants), with one seedling per vase (Fig. 1D), resulting in a population of 3636 plants ha^{-1}. The vases received a mulching and the plants were conducted with two pruning plants, resulting in sixteen branches: the first at 7 days after transplanting (DAT), leaving the plant with two pairs of leaves; and the second at 62 DAT, leaving the plant with four branches and two pairs of leaves per branch. The peppers were harvested from 185 to 350 DAT, when they reached the characteristic color of the cultivar.

Planting fertilization was performed based on the chemical analysis of the soil, according to Raij et al. (1996), applying the following products: monoammonium phosphate, simple superphosphate, potassium chloride, zinc sulfate and boric acid. In conducting the crop, fertigation was performed based on nutrient concentrations recommended for hydroponic cultivation of peppers. Fertilizers applied via fertigation were ammonium nitrate, calcium nitrate, monoammonium phosphate, monopotassium phosphate, potassium chloride (white), potassium sulfate, potassium nitrate and magnesium sulfate.

Phytosanitary treatments were performed periodically throughout the crop cycle, starting at 15 DAT, at intervals of 15 to 20 days, respecting the deficiencies of the products. Manual weeding was carried out, so that the plants were always free from competitors. The irrigation system was based on one dripper per plant. Each dripper was connected to a 4 microtube discharge divider with dripper piles, evenly positioned in each vase. Irrigation depths were applied as a function of total irrigation need (NTI) and soil cover. The NTI was calculated daily from the ET_c estimate using drainage lysimeters installed inside the greenhouse (Fig. 1D).

For the analysis of the performance of the irrigation system, data were collected by means of flow uniformity tests in all drippers. The parameters used to evaluate the uniformity of the irrigation system used were the Christiansen Uniformity Coefficient - CUC, the Emission Uniformity - EU, also known as the Distribution Uniformity Coefficient - CUD and the Application Efficiency - Ea. On average, a water application efficiency of 91% was obtained based on the evaluation of the irrigation system.

2.3. Monitoring of weather variables

The meteorological variables monitored during the experiment were: air temperature, relative humidity and evaporation. To obtain temperature and humidity values, a digital thermohygrometer was installed inside the greenhouse at 2 m height (Fig. 1E). The equipment stored in the memory the daily maximum and minimum measurements, after the readings, between 8 and 9 am, the daily averages of temperature and humidity were calculated. Evaporation values of the mini-pan were obtained daily, between 8 and 9 am, by means of a micrometer screw, accurate to 0.02 mm, and a mini-pan that had 0.60 m in diameter and 0.25 m high and was installed 5 m from the end of the greenhouse on a wooden platform to prevent the pan from contacting the ground and to allow air circulation (Fig. 1F).

The values of the maximum, average and minimum temperatures, and the humidity obtained in the ESALQ/USP automatic weather station were correlated by simple linear regression (RLS) for the autumn, winter, spring and summer seasons, with their values elements obtained inside the greenhouse. In this case, the temperature data were collected by sensors installed at 2 m height and protected against direct solar radiation. The collection height is the same as the sensors installed inside the greenhouse because the vases that received the plants were positioned in an excavated way in the soil, so that the edge of the vase coincided with the soil surface.

Evaporation values of the mini-pan inside the greenhouse were correlated, also by RLS, for the intervals of 1, 3, 5 and 7 days, with the ET_o values in the outdoor environment. Thus, we analyzed the possibility of using external data to estimate data inside the greenhouse.

2.4. Determination of crop water requirement

The ET_c was obtained for each phase of crop development, corresponding to the difference between the volume of water placed on the lysimeter and the drained volume (liters), divided by the area (m^2) equivalent to the crop spacing.

The ET_c estimate began at 20 DAT, when it was verified that the water storage in the lysimeters were in equilibrium. For the estimation of ET_o outside the greenhouse, the methods of Penman Monteith (ET_oPM), Hargreaves and Samani (ET_oHS) and the class "A" pan (ECA), were used, according to Equations 1, 2 and 3, respectively. The calculations were performed based on the weather data of the ESALQ/USP automatic station, collected from June 2007 to April 2008, thus 330 days in total. The ESALQ/USP meteorological station is located on the premises of Biosystems Engineering Department (LEB). The geographical coordinates of the post are as follows: 22º42'30" S lat., 47º38'00" W long. and elevation of 546 meters. The post consists of a conventional station and an automatic station, which performs meteorological observations every 15 minutes. The automatic station started in 1997 and regularly records data on precipitation, temperature, air humidity, solar radiation, radiation balance, evapotranspiration, speed and wind direction.

$$ET_0PM = \frac{0{,}408s(R_n-G)+\frac{\gamma 900U_2(e_s-e_a)}{T+273}}{s+\gamma(1+0{,}34U_2)} \quad (1)$$

where ET_oPM is the reference evapotranspiration, Penman-Monteith (PM) (mm day^{-1}), Rn is the total daily net radiation (MJ m^{-2} day^{-1}), G is the soil heat flux (MJ m^{-2} day^{-1}), γ is the psychrometric constant (kPa $ºC^{-1}$), T is the mean air temperature (°C), U_2 is the wind speed at 2 m high (m s^{-1}), es is the vapor saturation pressure (kPa), ea is the vapor partial pressure (kPa) and s is the slope of the vapor pressure curve at air temperature (kPa $ºC^{-1}$).

$$ET_o\ HS=0.0023\ Qo\ (Tmax-\ Tmin)^{0.5}\ (T+17.8) \quad (2)$$

where ET_oHS is the reference evapotranspiration, Hargreaves-Samani (HS) (mm day^{-1}), Qo is the extraterrestrial global solar radiation (mm day^{-1}), T_{MAX} is the maximum air temperature (°C), T_{MIN} is the minimum air temperature (ºC) and T is the average air temperature (ºC).

$$ET_o\ ECA=Kp\ ECA \quad (3)$$

where ET_oECA is the reference evapotranspiration, class "A" pan (ECA) (mm day^{-1}), Kp is the coefficient class "A" pan (dimensionless), according to Equation 4, and ECA is the evaporation class "A" pan (mm day^{-1}).

$$Kp=0.482+0.024\ Ln(B)-0.000376\ U+\ 0.0045\ RH \quad (4)$$

where B is the surround (m), U is the wind speed (km day^{-1}) and RH is the average daily relative humidity (%).

Table 1. Development stages of the pepper crop adapted for the experiment in question.

Phases	Phase I	Phase II	Phase III	Phase IV	Phase V	Phase VI	Phase VII
Periods (days)	0 - 96	97 - 166	167 - 186	187 - 225	226 - 245	246 - 267	268 - 350
Years	---------- 2007 ----------				---------- 2008 ----------		
Months	May to August	September to November	November	December to January	January	February	February to April

With the results obtained from ET_c and ET_o, the K_c was calculated according to Equation 5 for the different stages of development throughout phenological cycle, by the ratio between ET_c and ET_o.

$$Kc = \frac{ETc}{ETo} \quad (5)$$

In the ET_c and K_c analyzes, the different developmental stages were adapted, according to Allen et al. (1998), and divided into seven phases: Phase I: Initial, from the time of transplantation to the point where the crop reaches approximately 20% of its development; Phase II: development-flowering, beginning at the end of phase I and ending at a point immediately before flowering-fruiting, which corresponds to a range of 70 to 80% of vegetation cover; Phase III: flowering-fruiting period; Phase IV: flowering-fruiting-harvest period from the end of phase III to the harvest. Phase V: end of first production cycle, harvest period; Phase VI: flowering-fruiting period, begins at the end of phase V and ends at a point immediately before flowering-fruiting-harvesting of the second production cycle; Phase VII: flowering-fruiting-harvest period (Table 1).

3. RESULTS AND DISCUSSION

3.1. Air temperature variation and correlation

Fig. 2A, 2B and 2C illustrate, respectively, the variations in maximum (T_{MAX}), average (T_{MED}) and minimum (T_{MIN}) temperatures (observed and estimated) inside the greenhouse and outside during the pepper cycle, comprised between 23 DAT, initial phase, and 350 DAT, last harvest, within 327 days.

The average values of T_{MAX} observed inside the greenhouse and outdoors for the autumn, winter, spring and summer seasons were 40 and 27°C, 36 and 28 °C, 42 and 30°C and 44 and 30°C, respectively, representing a significant percentage difference of approximately 33, 22, 29 and 32%. For T_{MED}, the mean values were, respectively, 28 and 20°C, 25 and 20°C, 30 and 23°C and 32 and 23°C, with a difference of approximately 29, 20, 23 and 28%. Finally, T_{MIN}, which presented the respective average values of 16 and 15°C, 13 and 12 °C, 18 and 17°C and 20 and 19°C, representing a difference of approximately 1°C in both stations.

Vásquez et al. (2005), working in a greenhouse, in the same place, in the spring-summer season from 2001 to 2002, found average values of T_{MAX}, T_{MED} and T_{MIN} of 34, 25 and 18°C, respectively. Frizzone et al. (2005), also in the same place, in the summer of 2001, found average values of 35, 24 and 13°C, respectively, for T_{MAX}, T_{MED} and T_{MIN}.

From the beginning to the end of the cultivation cycle, in general, the average values of T_{MAX}, T_{MED} and T_{MIN} observed inside the greenhouse and outside were 41 and 29°C, 29 and 22°C and 17 and 16°C, respectively, representing a difference of 29, 24 and 6%. The ideal averages of T_{MAX} and T_{MIN} are, respectively, 35 and 18°C, and the optimal range of T_{MED} for the pepper development cycle is between 21 and 30°C (Mercado et al., 1997). Low temperatures slow the development of the plant, while high temperatures associated with low relative humidity lead to the autumn of flowers and fruits.

It was found that in 86% of the evaluated days, T_{MAX} exceeded the value of 35°C (Fig. 2A) and in 50% of those days it was below 18°C (Fig. 2C), these being the critical stages of flowering and fruiting and plant development. In only 4% of days, T_{MED} in the greenhouse was below 21°C, in 26% of the days evaluated it was above 30°C and in 70% it was within the optimal range (Fig. 2B), considered for the cycle crop development. A response to no stress condition came in the average pepper yield values obtained in the experiment, as shown in Table 2.

Therefore, given the temperature values and the behavior of the pepper throughout the cycle, it was observed that the optimal temperature range, between 21 and 30°C, predominated during the experimental phase. The average temperature seems to be the most important variable for the good development of the crop in greenhouse. Research carried out in the same experimental greenhouse and monitoring the environment temperature has achieved good results regarding the development of other crops such as coffee (Costa et al., 2018; Costa et al., 2019; Costa et al., 2020) and lawns

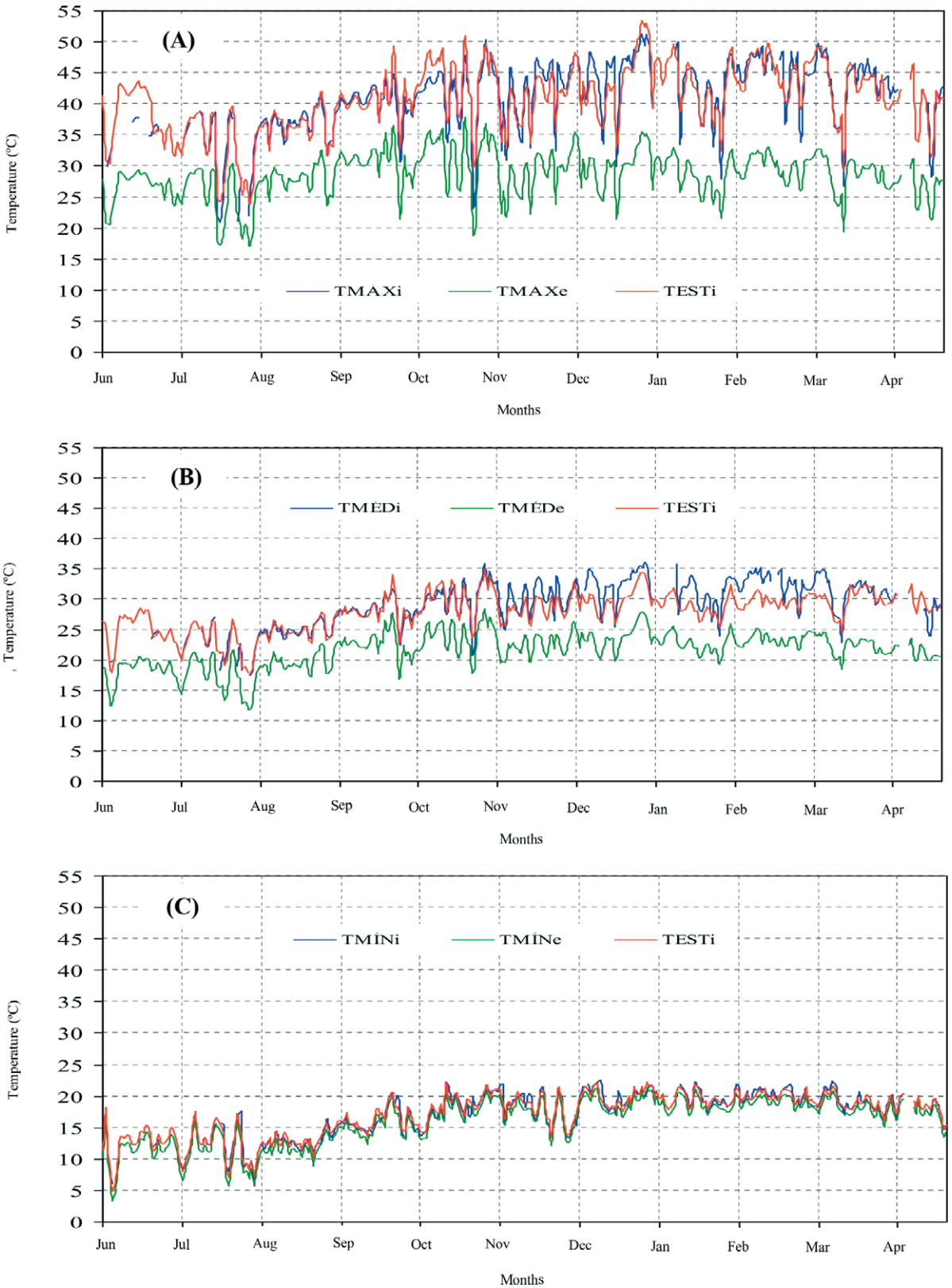

Fig. 2. Maximum (A), average (B) and minimum (C) temperature variation inside the greenhouse, outside and simulated outside during the experimental period.

Table 2. Average values pepper yield for the populations of 3636 ($PROD_1$) and 10000 plants ha^{-1} ($PROD_2$).

	$PROD_1$ (kg ha^{-1})	$PROD_2$ (kg ha^{-1})
Pepper yield*	9330.55	25272.73

* yield values were obtained per plant and extrapolated to values in kg ha^{-1} considering two plant populations.

(Tapparo et al., 2019), showing that the average temperature is the most important variable when compared to the extreme maximum and minimum values.

Fig. 3 shows the comparison between the temperatures obtained inside the greenhouse and outside during the pepper cycle, using RLS. The diagrams A, B, C and D correspond to the relationship between the T_{MAX} in the two environments and, respectively, the seasons of autumn, winter, spring and summer, just as, E, F, G and H correspond to the T_{MED} and I, J, L and M at T_{MIN}. Regardless of the determination coefficient (R^2) values, ranging from 0.65 to 0.95, all RLS equations were significant at 1% probability (**).

Comparing the obtained values of T_{MAX} inside the greenhouse and outside, it was found that the R^2 were 73, 91, 73 and 84% for the autumn, winter, spring and summer seasons (Fig. 3A, 3B, 3C and 3D), respectively, and therefore classified as good, excellent, good and very good. The R^2 values for T_{MED} were 90, 93, 66 and 67%, being classified as very good, excellent, and the last two regular for the respective seasons (Fig. 3E, 3F, 3G and 3H). For T_{MIN}, R^2 values were 89, 91, 87 and 84% for the respective seasons (Fig. 3I, 3J, 3L and 3M) and classified as very good, excellent and the last two very good.

Comparisons were also obtained between the temperatures collected inside the greenhouse and outside during the whole pepper cycle, which comprised between 23 DAT, initial phase, and 350 DAT, last harvest, in an interval of 327 days. The RLS equations, significant at 1% probability, were: $T_{MAXIN} = 1.315T_{MAXOUT} + 3.004$ (Equation 6); $T_{MEDIN} = 1.063T_{MEDOUT} + 4.777$ (Equation 7) and $T_{MININ} = 0.964\ T_{MINOUT} + 1.594$ (Equation 8) for T_{MAX}, T_{MED} and T_{MIN}, respectively. The values of R^2, referring to equations 6, 7 and 8, and their ratings were 0.713 (Good), 0.876 (Very good) and 0.943 (Excellent).

Therefore, given all the RLS equations, it can be said that they generally had a very good correlation. However, in order to have a better accuracy in the estimates of T_{MAX}, T_{MED} and T_{MIN} inside the greenhouse, the equations with the largest R^2 for each period should be used. It is advisable to estimate T_{MAX} throughout the year, the equations of autumn, winter, spring and summer. For T_{MED}, the autumn and winter equations, and Equation 7 in the spring-summer period. In the T_{MIN} estimate, only Equation 8.

3.2. Air relative humidity variation and correlation

Fig. 4A, 4B and 4C illustrate, respectively, the variations in the maximum (RH_{MAX}), average (RH_{MED}) and minimum (RH_{MIN}) relative humidity (observed and estimated) inside the greenhouse and outside during the pepper cycle, which comprised between 23 DAT, initial phase, and 350 DAT, last harvest, within 327 days.

The average values of RH_{MAX} observed inside the greenhouse and outdoors for the autumn, winter, spring and summer seasons were 85 and 100%, 81 and 99%, 81 and 99% and 85 and 100%, respectively, representing a percentage difference of approximately 15, 18, 18 and 15%. For RH_{MED}, the mean values were, respectively, 53 and 89%, 52 and 77%, 55 and 81% and 55 and 90%, with a significant difference of approximately 40, 32, 32 and 39%. Finally, RH_{MIN}, which presented the respective average values of 26 and 59%, 27 and 44%, 28 and 52% and 26 and 62%, representing a significant difference of approximately 56, 39, 46 and 58%.

Vasquez et al. (2005), working in a greenhouse, in the same place, in the spring-summer season from 2001 to 2002, found values of RH_{MAX}, RH_{MED} and RH_{MIN} of 90, 73 and 50%, respectively. Frizzone et al. (2005), also in the same place, in the summer of 2001, observed RH_{MED} of 76%.

From the beginning to the end of the cultivation cycle, in general, the average values of RH_{MAX}, RH_{MED} and RH_{MIN} observed inside the greenhouse and outside were 87 and 100%, 55 and 92% and 27 and 67%, respectively, a difference of 13, 40 and 60%. It was observed that the RH_{MAX}, RH_{MED} and RH_{MIN} measured in the outdoor environment was always higher than that measured inside the greenhouse and that there was a growing trend in the difference between the humidity obtained inside and outside the greenhouse. This growing trend shows that the greenhouse inside the RH_{MAX} approaches the one obtained in the outdoor environment, while the RH_{MIN} away.

Normally, relative humidity values approach each other in both environments and are sometimes lower inside the greenhouse (Montero et al., 1984; Farias et al., 1994; Rosenberg et al., 1989). However, such results were expected, since pepper cultivation was carried out in vases, so the area of influence of the wet soil area probably corresponded to a maximum of 36% of the cultivation spacing area, in the period of greatest water demand of the crop.

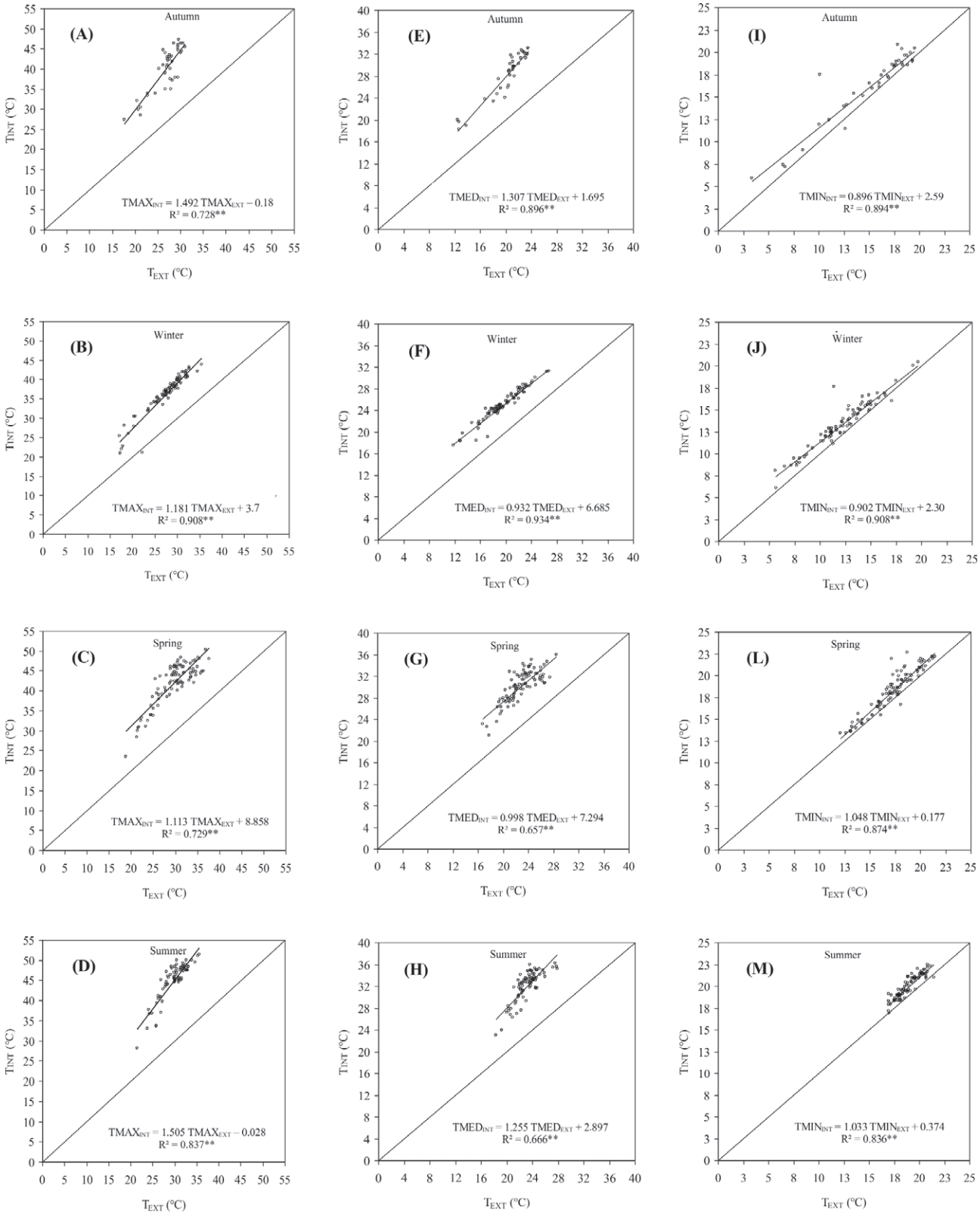

Fig. 3. Relationship between internal and external temperatures for maximum (A, B, C and D), average (E, F, G and H) and minimum (I, J, L and M) values, with the respective seasons of autumn, winter, spring and summer during the experimental period.

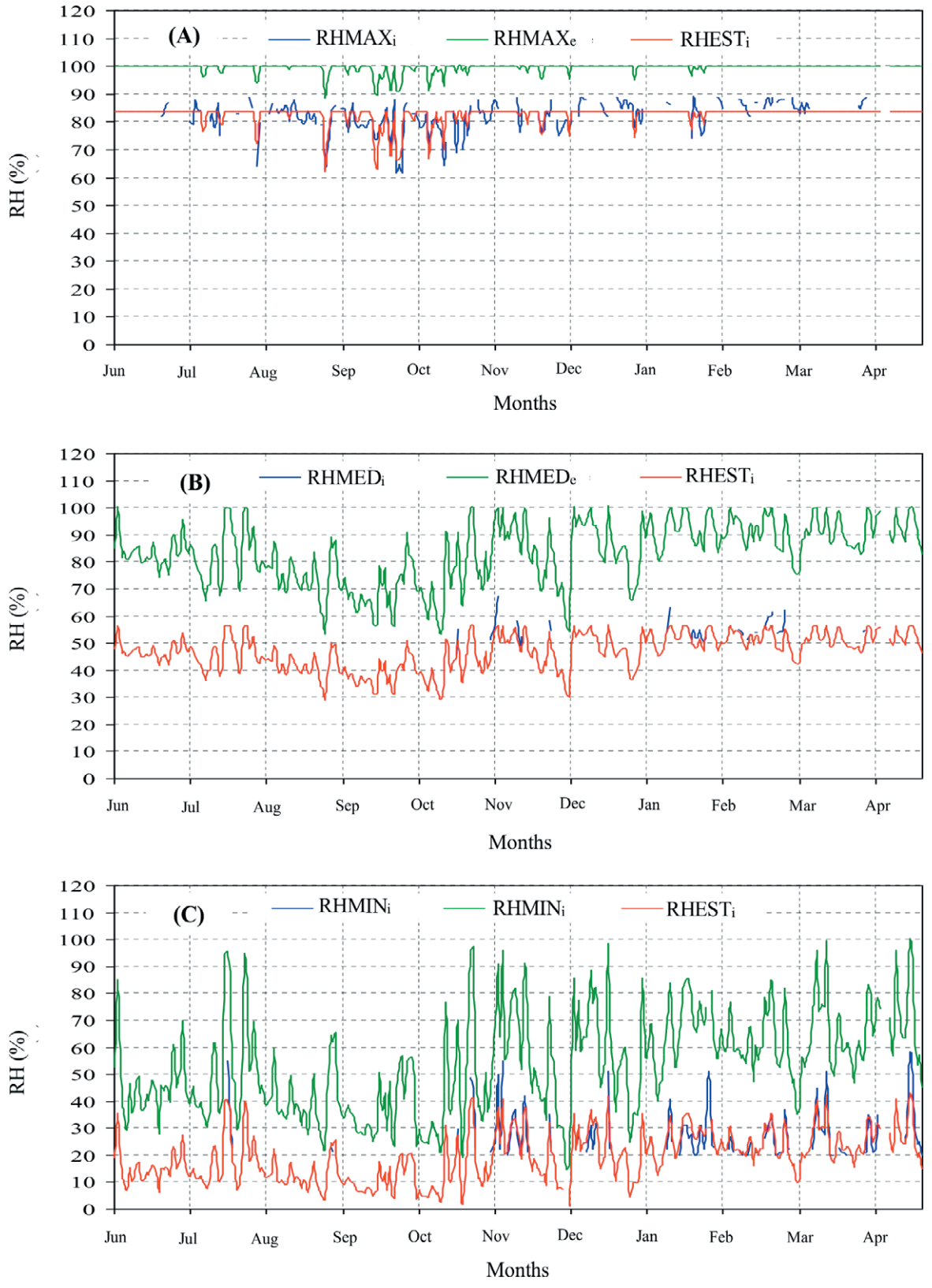

Fig. 4. Maximum (A), average (B) and minimum (C) relative humidity variation, inside the greenhouse, outside and simulated outside during the experimental period.

In addition, the management of drip irrigation also provides a smaller wet area. Therefore, it can be concluded that the greenhouse, the cultivation in vases and the management of drip irrigation were factors of change in the relative humidity inside the greenhouse. At no time during the pepper crop cycle, the relative humidity was above 95%, probably due to the crop condition.

During the experimental period, there was a failure in the humidity sensors of the station installed inside the greenhouse. When the relative humidity of the air is below 20% the sensor was unable to quantify and a considerable amount of data was lost.

Fig. 5A, 5B and 5C correspond to the relationship between RH_{MAX}, RH_{MED} and RH_{MIN} in both environments, respectively. Comparing the obtained values of RH_{MAX}, RH_{MED} and RH_{MIN} inside the greenhouse and outside environment, it is verified that the R^2 were 53% (Fig. 5A), 68% (Fig. 5B) and 69% (Fig. 5C), respectively, classified as bad and the last two regulars.

Regardless of the values of R^2, all RLS equations were significant at 1% probability (**). Therefore, given the RLS equations, it can be said that, in general, they had a regular correlation. However, in order to have a better accuracy of the relative humidity estimates inside the greenhouse, the RH_{MED} equation (Fig. 4B) should be used because it has the largest R^2 and represents the average condition of the environment.

3.3. Reference Evapotranspiration variation and correlation

During the conduction period of the pepper was monitored the variation of mini-pan evaporation (EMT), observed (ob) and estimated (e) inside the greenhouse, and the respective ET_o, estimated outside Penman-Monteith-PM (Fig. 6A), Hargreaves-Samani (HS) (Fig. 6B) and class "A" pan evaporation (ECA) (Fig. 6C) methods.

An important aspect refers to the EMTob inside the greenhouse (Fig. 6A, 6B and 6C), which covers only the interval from August to December, ie 140 days. The difference between 330 and 140 days is due to the discard of collected data that do not represent the reality of EMTob inside the greenhouse. This occurred from December, because of the shading of the mini-pan by the pepper plants. Also, it can be seen in Fig. 6C that there was a period without data recording, caused by a possible failure of operation of the class "A" evaporimeter of the weather station.

In April, June, July and August, the EMTe inside the greenhouse was higher than the estimated ET_oPM for the external environment, by 11, 2, 15 and 10%, respectively (Fig. 6A). The total ET_oPM values in these respective months were 54, 67, 60 and 90 mm, with means of 2.14, 2.25, 1.94 and 2.89 mm day^{-1}. For the months of September, October, November, December, January, February and March, EMTe corresponded, respectively, to 96, 95, 97, 95, 96, 100 and 98% of ET_oPM. From September to March, the monthly ET_oPM values were 111, 120, 106, 125, 96, 108 and 107 mm, respectively, with averages of 3.69, 3.88, 3.52, 4.03, 3.10, 3.71 and 3.45 mm day^{-1}. However, at the end of the pepper growing cycle, it was found that there was no difference between the values obtained from the EMTe inside the greenhouse (1042 mm) and the estimated ET_oPM in the outside environment (1045 mm).

Similar to the behavior observed in the EMTe in relation to ET_oPM (Fig. 6A), in April, June, July and August, the EMTe inside the greenhouse was higher than the estimated ET_oECA, for the outside environment, at 7, 16, 17 and 3%, respectively (Fig. 6C). The total ET_oECA values in these respective months were 67, 68, 68 and 91 mm, with averages of 2.69, 2.26, 2.20 and 2.94 mm day^{-1}.

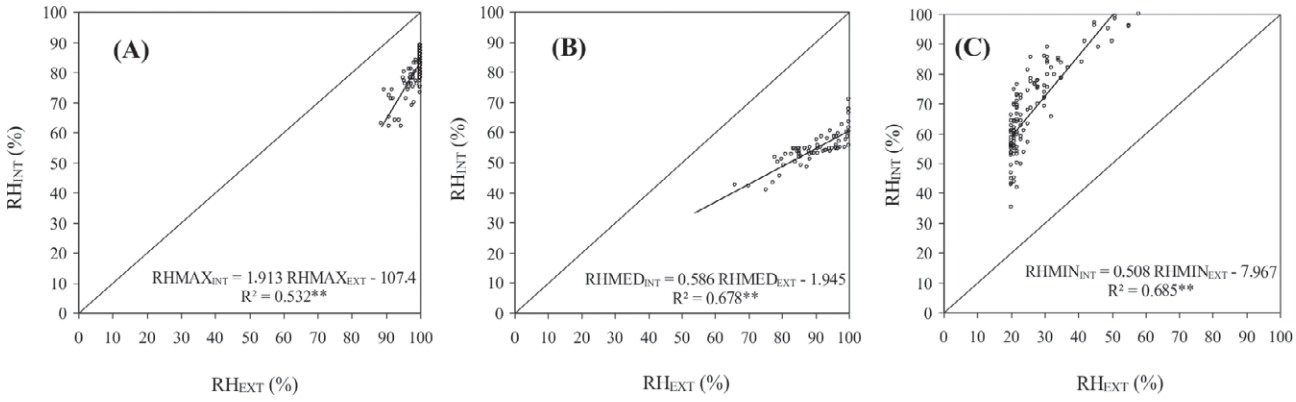

Fig. 5. Relationship between the relative humidity inside the greenhouse and the external environment, for the maximum (A), average (B) and minimum (C) values during the experimental period.

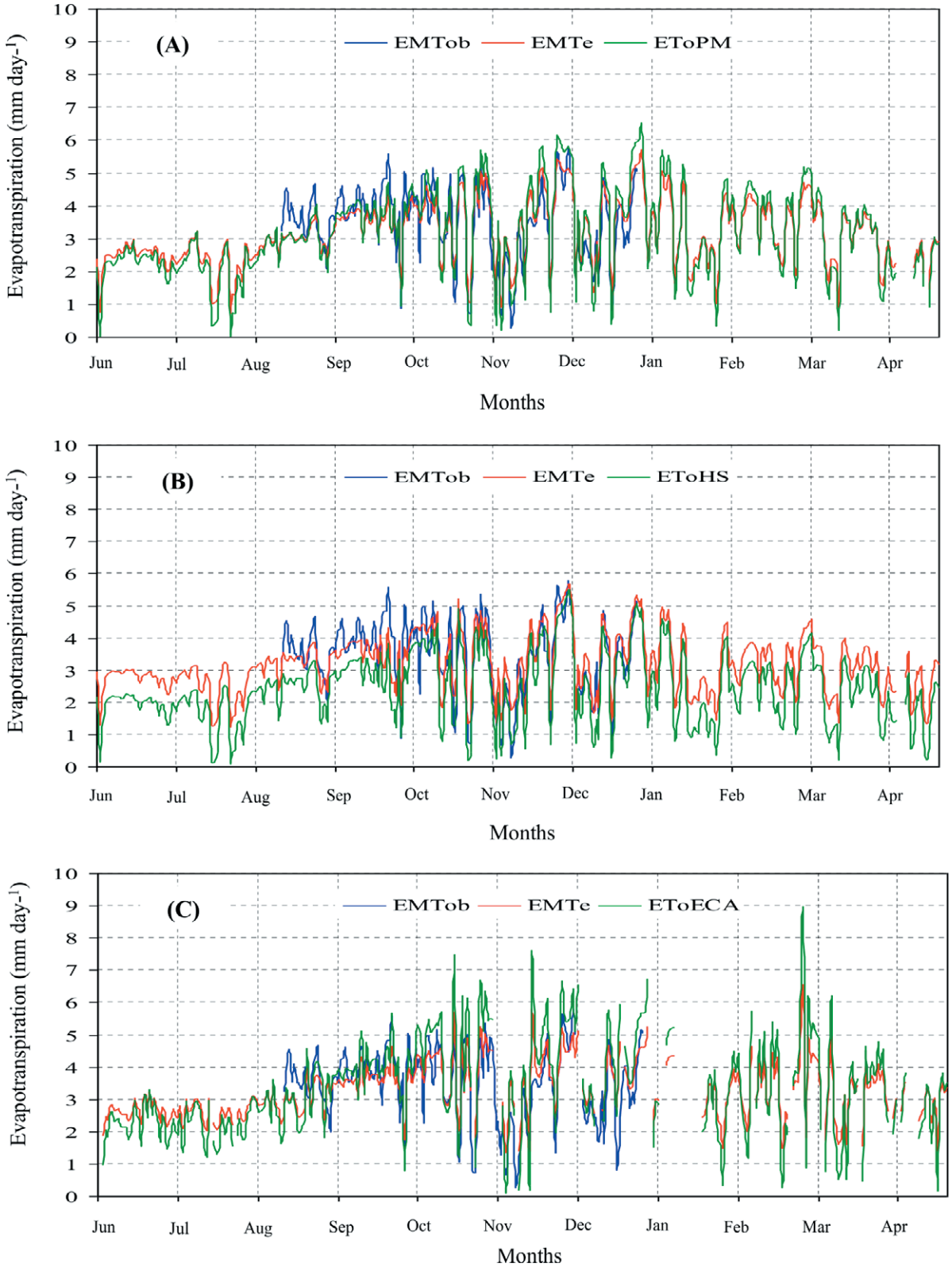

Fig. 6. Observed (ob), estimated (e) and mini-pan evaporation variation inside the greenhouse and respective reference evapotranspirations (ET_o) in the outside environment, estimated by Penman-Monteith-PM (A), Hargreaves-Samani-HS (B) and evaporation of the class "A" pan-ECA (C) during the experimental period.

For the months of September, October, November, December, January, February and March, EMTe corresponded, respectively, to 92, 87, 92, 88, 100, 94 and 97% of ET_oECA. From September to March, the monthly ET_oECA values were 117, 140, 117, 138, 97, 107 and 104 mm, respectively, with averages of 3.89, 4.52, 3.91, 4.45, 3.12, 3.70 and 3.34 mm day^{-1}. In general, at the end of the pepper crop cycle, the EMTe corresponded to 97% of ET_oECA, with respective values of 1080 and 1113 mm.

The EMTe inside the greenhouse was higher than the estimated PM and ECA evapotranspirations for the outside environment in April, June, July and August, and lower in September, October, November, December, January, February and March, respectively, autumn-winter and spring-summer seasons. According to several authors (Montero et al., 1984; Farias et al., 1994; Rosenberg et al., 1989), the partial opacity of the plastic film to solar radiation and the reduction of wind action are the main factors of evaporative demand of the sun, although the higher temperature and lower relative humidity inside the greenhouse compared to the outside environment may at times contribute to higher ET_o.

Thus, it can be said that, probably, in the conditions under which the experiment was performed, the effect of plastic film opacity on solar radiation and the reduction of wind action in the autumn-winter season was lower than in the spring-summer season, prevailing the influence of higher temperature and lower humidity on ET_o inside the greenhouse. In contrast, in the spring-summer season, the effect of plastic film opacity on solar radiation and the reduction of wind action was greater than in the autumn-winter season, highlighting the temperature and humidity variables. Even with the greater range of variation of high temperatures and low humidity between the interior of the greenhouse and the outside environment, in the spring-summer season, the ET_o inside the greenhouse was lower than that observed in the outside environment.

Comparing the results obtained from the EMTe inside the greenhouse with the estimated ET_oHS for the outside environment (Fig. 6B), it was found that in all months of data collection the EMTe was higher in 43, 56, 30, 24, 20, 27, 19, 36, 27, 28 and 51%, respectively, to ET_oHS. The corresponding monthly ET_oHS values were 58, 50, 77, 85, 97, 79, 98, 68, 76, 79 and 42 mm, with respective averages of 1.92, 1.60, 2.47, 2.83, 3.12, 2.63, 3.15, 2.19, 2.61, 2.55 and 1.69 mm day^{-1}. At the end of the pepper cultivation cycle, it was observed that the EMTe was 1049 mm and the ET_oHS 806 mm, representing a difference of 23%.

The HS method was developed for dry climate regions in California's semi-arid conditions (Hargreaves and Samani, 1982). In this context, the HS method may not be good for ET_o estimates in wet climate regions, with a tendency to underestimate the values (Fig. 7).

Fig. 8 shows the comparison between the EMT obtained inside the greenhouse and the ET_o outside during the pepper cycle by RLS. Diagrams A, B, C and D correspond to the relationship between EMT and ET_o estimated by PM, for the average intervals of 1, 3, 5 and 7 days, respectively, as well as, E, F, G and H correspond to the EMT and ET_o estimated by HS and, I, J, L and M to the EMT and ET_o estimated by the ECA. Regardless of the R^2 values, ranging from 0.55 to 0.81, all RLS equations were significant at 1% probability (**).

Comparing the values obtained from the EMT inside the greenhouse and from the ET_oPM outdoors, the R^2 was 72, 80, 69 and 65% for the average intervals of 1, 3, 5 and 7 days (Fig. 8A, 8B, 8C and 8D), respectively, and therefore classified as good, the first two, and regular, the last two. The R^2 values for the relationship between EMT and ET_oHS were 68, 81, 69 and 74%, being classified as fair, very good, fair and good for the respective average day intervals (Fig. 8E, 8F, 8G and 8H).

Regarding the relationship between EMT and ET_oECA, the R^2 values were 58, 57, 57 and 55% for the respective average day intervals (Fig. 8I, 8J, 8L and 8M) and all classified as regular. Therefore, given all the RLS equations, it can be said that, in general, they had a regular correlation. However, in order to have better accuracy of the EMT estimates for the average 1, 3, 5 and 7 day inter-

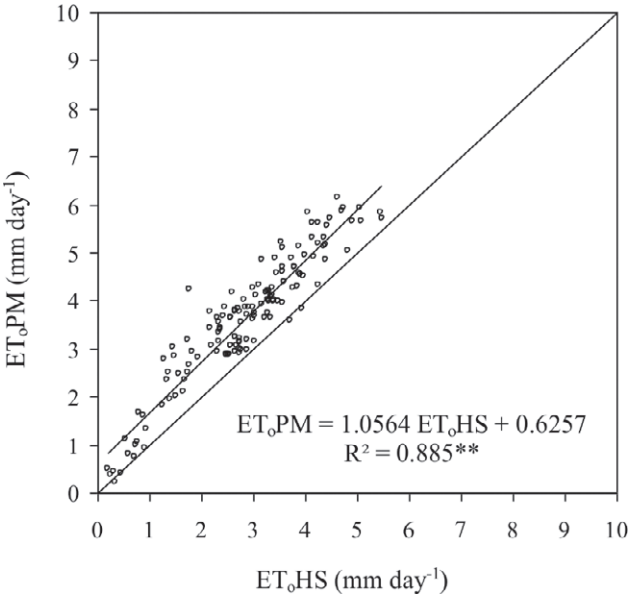

Fig. 7. Relationship between reference evapotranspirations (ET_o) in the outside environment, estimated by Penman-Monteith-PM and Hargreaves-Samani-HS, during the experimental period.

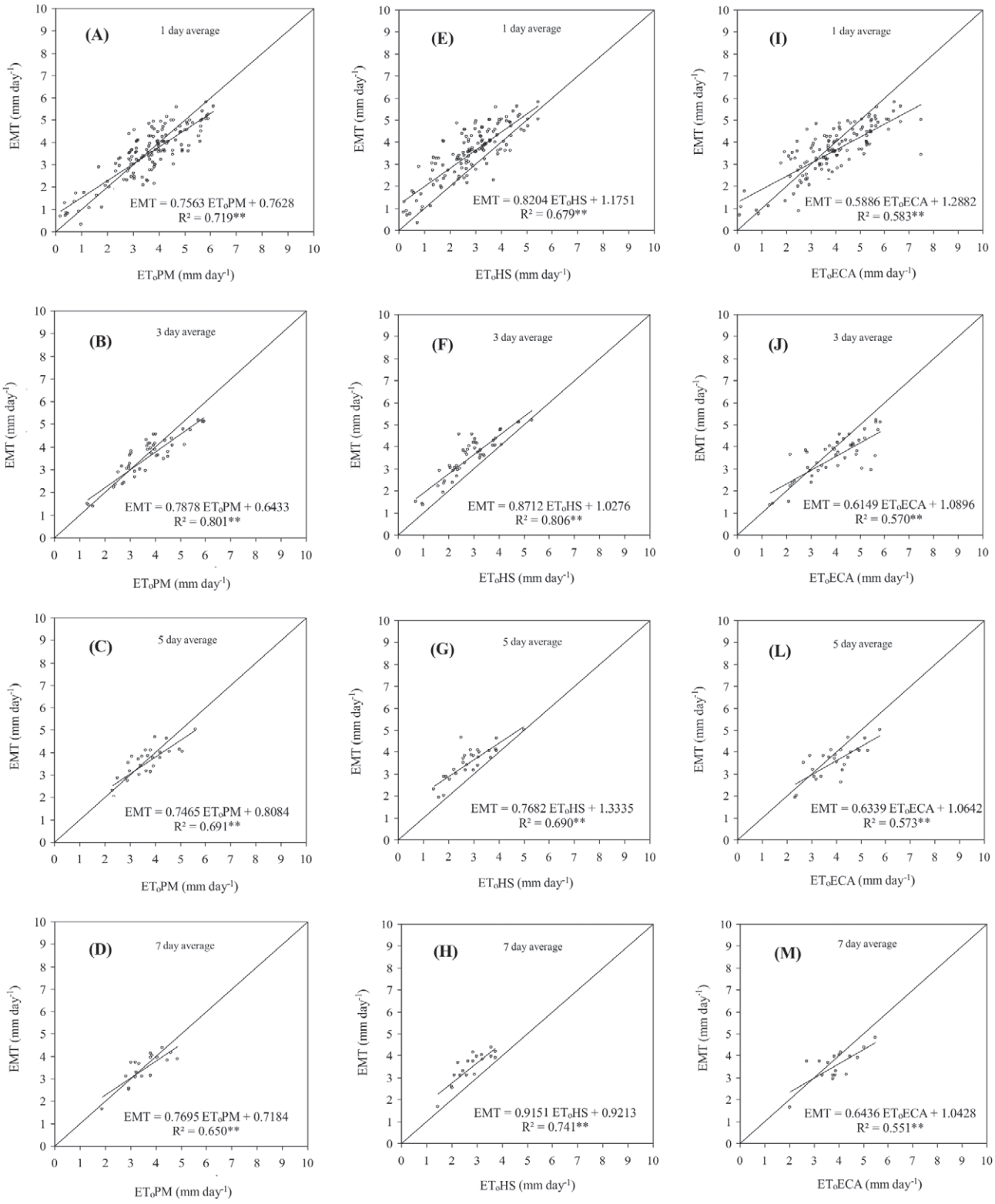

Fig. 8. Relationship between mini-pan evaporation (EMT) inside the greenhouse and reference evapotranspirations (ET_o) in the outside environment, estimated by Penman-Monteith-PM (A, B, C and D), Hargreaves-Samani-HS (E, F, G and H) and by evaporation of the class "A" pan-ECA (I, J, L and M), for the averages of 1, 3, 5 and 7 days, respectively, during the experimental period.

vals within the greenhouse, the equations with the largest R^2 should be used for each day interval (due to the irrigation management adopted by the irrigating), combined with the PM method, considered in the literature, the most appropriate for the estimation of ET_o. Therefore, it is advisable to estimate the EMT, for the average intervals of 1, 3, 5 and 7 days, the respective equations: EMT=0.7556 ET_oPM + 0.7628; EMT=0.7878 ET_oPM + 0.6433; EMT=0.7465 ET_oPM + 0.8084 and EMT=0.7695 ET_oPM + 0.7184, illustrated in Fig. 8A, 8B, 8C and 8D.

On the other hand, if it is difficult to estimate the ET_o in the outside environment, mainly due to unavailability of some meteorological data, necessary in the most complex methods, it is recommended, based on the correlations, to use the mini-pan to obtain the evaporative demand, inside the greenhouse, and thus properly manage irrigation. Angelocci et al. (2002) state that the choice of the ET_o estimation method requires criteria, which depend on factors such as the availability of meteorological data, the required time scale and the climatic conditions for which the methods were developed. For Farias et al. (1994), the use of the mini-pan inside the greenhouse, which is much smaller than the class "A" evaporimeter, seems more advisable because it occupies a smaller area and contributes less to raise the relative humidity of the environment, besides having lower cost and to be more practical.

3.4. Evapotranspiration and crop coefficient

During the conduction period, the ET_c, as shown in Fig. 9, was monitored. The ET_c values ranged from 0.28 to 2.42 mm day^{-1}. On average, the maximum ET_c occurred between 163 and 181 DAT, period comprised by the first flowering peak and fruit development. Miranda et al. (2006) found values that ranged from 1.0 to 5.6 mm day^{-1}, with maximum ET_c, between 80 and 135 DAT. Chaves et al. (2005), observed that on average, the maximum ET_c was 8.4 mm day^{-1} at 100 DAT.

In the harvesting period of the first pepper production cycle, between 181 and 256 DAT, the ET_c decreased considerably, reaching average values of 1.40 mm day^{-1} (Fig. 9). However, after the end of the first cycle, a second flowering and fruit development peak began, mean ET_c values increased rapidly from 1.40 to 1.81 mm day^{-1}, between 256 and 282 DAT. The maximum ET_c at the second peak occurred between 282 and 299 DAT. Subsequently, during the harvest period of the second production cycle, between 299 and 350 DAT, the ET_c decreased again, reaching average values of 1.20 mm day^{-1}.

In general, it can be seen that both the second flowering and fruit development peak and the harvest period

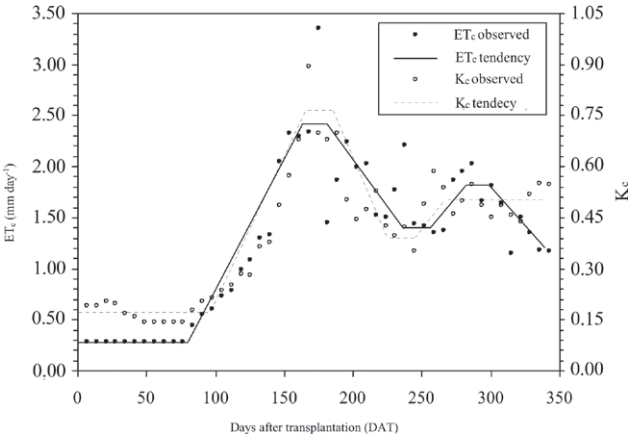

Fig. 9. Variation of crop evapotranspiration (ET_c) and crop coefficient (K_c) in pepper cultivation in greenhouse, as a function of the phenological phases of the crop and reference evapotranspiration (ET_o), estimated for the outside environment by the Penman-Monteith (PM) method.

of the second production cycle did not reach the same ET_c observed in the first production cycle. This behavior was also observed by Miranda et al. (2006). According to the authors, in the climatic conditions of the Northeast region of Brazil, the pepper presents two productive cycles.

The average ET_c during the conduction period of the pepper crop was 1.28 mm day^{-1} in a 350 days cycle. Miranda et al. (2006), obtained an average ET_c of 2.96 mm day^{-1} in a cycle of 350 days. While Chaves et al. (2005) found an average ET_c of 7.40 mm day^{-1} in 135 days. These differences in ET_c can probably be attributed to the location of the experiment (Southeast and Northeast Region of Brazil), climatic conditions (mainly solar radiation, temperature, relative humidity and wind speed), the conduction environment of the crop (in greenhouse), planting density (crop spacing), soil type, irrigation management (frequency or watering shift), irrigation system (drip and sprinkler), crop cycle length and the type of lysimeter (drainage and weighing) used to determine the water requirement of the crop.

Fig. 9 shows the variation of K_c pepper, by the relationship between ET_c and ET_o, as a function of the phenological phases of the crop and the ET_o, estimated for the outside environment by the method from Penman-Monteith (PM). Constant values of 0.17 were obtained in the initial phase (0 to 96 DAT), increasing values, on average 0.41, in the development-flowering phase (96 to 166 DAT), constant values of 0.76 in the flowering-fruiting (166 to 186 DAT), decreasing values, averaging 0.49, in the flowering-fruiting-harvesting phase (186 to 225 DAT), to constant values of 0.39 (225 to 245 DAT). This

period, between 0 and 245 DAT, was considered the first cycle of pepper production. However, the harvest period lasted until 283 DAT.

For the second pepper production cycle, between 245 and 350 DAT, it was observed that K_c values were slightly increasing, on average 0.45, in the final harvest phase of the first production cycle (245 to 283 DAT) and constant, with values of 0.50 in the flowering-fruiting-harvest phase (283 to 350 DAT). Miranda et al. (2006) found that the K_c values for the first cycle of pepper production were 0.30 (21 DAT), 1.22 (90 to 140 DAT) and 0.65 (165 DAT) for the second cycle yield 0.65 (165 to 180 DAT), 1.08 (200 to 230 DAT) and 0.60 (225 to 300 DAT). Chaves et al. (2005), observed constant values of 0.96 in the initial phase (0 and 25 DAT), increasing values, on average 1.13, in the development and flowering phase (25 to 75 DAT), again a trend of constant values of 1.29 in the fruiting phase (75 to 120) and finally decreasing values of 1.24 in the ripening and harvesting phase (120 to 135 DAT).

4. CONCLUSIONS

All simple linear regression equations for the air temperature variable generally had a very good correlation. For air humidity and evapotranspiration, in general, the equations presented a regular correlation.

In terms of water demand, the total evaporation value of the mini-pan inside the greenhouse was 1057 mm, in the outside environment, the reference evapotranspirations were 1045, 1113 and 806 mm, respectively, estimated by Penman-Monteith (ET_oPM), Hargreaves-Samani (ET_oHS) models and class "A" pan evaporation (ECA). In this condition, the evaporation mini-pan (EMT) was virtually equal to ET_oPM, 5% lower than ET_oHS and 31% higher than ECA.

During the conduction period of the pepper crop (May 2007 to April 2008), with a 350-day cycle, the evapotranspiration values ranged from 0.28 to 2.42 mm day^{-1}. The total evapotranspiration of the crop was 446.43 mm, with a water consumption of 1227.68 liters per plant.

The crop coefficient (K_c) values for the first pepper production cycle were: 0.17 in the initial phase of development (0 to 96 DAT), 0.76 in the flowering and fruiting phase (166 to 186 DAT) and 0.39. In the harvest phase (225 to 245 DAT), for the second production cycle, the K_c value was 0.50 (283 to 350 DAT).

Future research may consider our study in order to obtain more accurate K_c for pepper crop in field conditions. These prospects for improvement will depend on the control of climatic factors (mainly rains) in experiments outside the greenhouse and obtaining ET_o inside the greenhouse following the protocols that are recommended by the FAO bulletin.

ACKNOWLEDGEMENTS

This study was funded by three sources: a) *Coordenação de Aperfeiçoamento de Pessoal de Nível Superior - Brasil (CAPES)*, b) *Conselho Nacional de Desenvolvimento Científico e Tecnológico* (CNPq) and c) *Universidade de São Paulo (USP/ESALQ).*

REFERENCES

Abdel-Ghany, A.M. 2011. Solar energy conversions in the greenhouses. Sustainable Cities and Society 1: 219-226. https://doi.org/10.1016/j.scs.2011.08.002.

Allen, R.G., Jensen, M.E., Wright, J.L., Burman, R.D. 1989. Operational estimates of reference evapotranspiration. Agronomy journal 81: 650-662. https://doi.org/10.2134/agronj1989.00021962008100040019x.

Allen, R.G., Pereira, L.S., Raes, D., Smith, M. 1998. Crop evapotranspiration-Guidelines for computing crop water requirements-FAO Irrigation and drainage paper 56. FAO, Rome, 300: D05109.

Alvares, C.A., Stape, J.L., Sentelhas, P.C., Gonçalves, J.L.M., Sparovek, G. 2013. Köppen's climate classification map for Brazil. Meteorologische Zeitschrift 22: 711-728. http://dx.doi.org/10.1127/0941-2948/2013/0507.

Andrade Júnior, A.S.D., Damasceno, L.M., Dias, N.D.S., Gheyi, H.R., Guiselini, C. 2011. Climate variations in greenhouse cultivated with gerbera and relationship with external conditions. Engenharia Agrícola 31: 857-867. http://dx.doi.org/10.1590/S0100-69162011000500003.

Chavarria, G., Herter, F.G., Raseira, M.D.C.B., Rodrigues, A.C., Reisser, C., Silva, J.B.D. 2009. Mild temperatures on bud breaking dormancy in peaches. Ciência Rural 39: 2016-2021. http://dx.doi.org/10.1590/S0103-84782009000700010.

Chaves, S.W.P., Azevedo, B.M.de, Medeiros, J.F.D., Bezerra, F.M.L., Morais, N.B.de. 2005. Evapotranspiração e coeficiente de cultivo da pimenteira em lisímetro de drenagem. Revista Ciência Agronômica 36: 262-267.

Costa, J.de.O., Almeida, A.N.de, Coelho, R.D., Folegatti, M.V., José, J.V. 2015. Modelos de estimativa de elementos micrometeorológicos em ambiente protegido. Water Resources and Irrigation Management

4, 25-31. http://dx.doi.org/10.19149/2316-6886/wrim.v4n1-3p25-31.

Costa, J.de.O., Coelho, R.D., Barros, T.H.da.S., Fraga Junior, E.F., Fernandes, A.L.T. 2018. Physiological responses of coffee tree under different irrigation levels. Engenharia Agrícola, 38, 648-656. http://dx.doi.org/10.1590/1809-4430-eng.agric.v38n5p648-656/2018.

Costa, J.de.O., Coelho, R.D., Barros, T.H.da.S., Fraga Junior, E.F., Fernandes, A.L.T. 2019. Leaf area index and radiation extinction coefficient of a coffee canopy under variable drip irrigation levels. Acta Scientiarum. Agronomy, 41, 1-8. http://dx.doi.org/10.4025/actasciagron.v41i1.42703.

Costa, J.de.O., Coelho, R.D., Barros, T.H.da.S., Fraga Junior, E.F., Fernandes, A.L.T. 2020. Canopy thermal response to water deficit of coffee plants under drip irrigation. Irrigation and Drainage 69, 472-482. https://doi.org/10.1002/ird.2429.

Doorenbos, J.; Kassam, A.H. 2000. Efeito da água no rendimento das culturas. 2. ed. Trad. de H.R. Gheyi et al. Campina Grande: UFPB, 2000. 221p.

Farias, J.R.B., Bergamaschi, H., Martins, S.R. 1994. Evapotranspiração no interior de estufas plásticas. Revista Brasileira de Agrometeorologia 2: 17-22.

Frizzone, J.A., Cardoso, S.da.S., Rezende, R. 2005. Produtividade e qualidade de frutos de meloeiro cultivado em ambiente protegido com aplicação de dióxido de carbono e de potássio via água de irrigação. Acta Scientiarum. Agronomy 27: 707-717.

Giménez, C., Gallardo, M., Martínez-Gaitán, C., Stöckle, C.O., Thompson, R.B., Granados, M.R. 2013. VegSyst, a simulation model of daily crop growth, nitrogen uptake and evapotranspiration for pepper crops for use in an on-farm decision support system. Irrigation Science 31: 465-477. https://doi.org/10.1007/s00271-011-0312-2.

Hargreaves, G.H., Samani, Z.A. 1982. Estimating potential evapotranspiration. Journal of the irrigation and Drainage Division 108: 225-230.

Kittas, C., Bartzanas, T. 2007. Greenhouse microclimate and dehumidification effectiveness under different ventilator configurations. Building and Environment 42: 3774-3784. https://doi.org/10.1016/j.buildenv.2006.06.020.

Meiri, A., Naftaliev, B., Shmuel, D., Yechezkel, H., Communar, G., Friedman, S.P. 2011. Short-term watering-distance and symmetry effects on root and shoot growth of bell pepper plantlets. Agricultural water management 98: 1557-1568. https://doi.org/10.1016/j.agwat.2011.05.010.

Mercado, J.A., Mar Trigo, M., Reid, M.S., Valpuesta, V., Quesada, M.A. 1997. Effects of low temperature on pepper pollen morphology and fertility: evidence of cold induced exine alterations. Journal of Horticultural Science 72: 317-326. https://doi.org/10.1080/14620316.1997.11515518.

Miranda, F.D., Gondim, R.S., Costa, C.A.G. 2006. Evapotranspiration and crop coefficients for tabasco pepper (*Capsicum frutescens* L.). Agricultural Water Management 82: 237-246. https://doi.org/10.1016/j.agwat.2005.07.024.

Montero, J.I., Castilla, N., Ravé, E.G.de, Bretones, F. 1984. Climate under plastic in the almeria area. Greenhouse Construction and Covering Materials 170: 227-234. https://doi.org/10.17660/ActaHortic.1985.170.26.

Orgaz, F., Fernández, M.D., Bonachela, S., Gallardo, M., Fereres, E. 2005. Evapotranspiration of horticultural crops in an unheated plastic greenhouse. Agricultural water management 72: 81-96. https://doi.org/10.1016/j.agwat.2004.09.010.

Qiu, R., Du, T., Kang, S., Chen, R., Wu, L. 2015. Assessing the SIMDualKc model for estimating evapotranspiration of hot pepper grown in a solar greenhouse in Northwest China. Agricultural Systems 138: 1-9. https://doi.org/10.1016/j.agsy.2015.05.001.

Qiu, R., Kang, S., Li, F., Du, T., Tong, L., Wang, F., Li, S. 2011. Energy partitioning and evapotranspiration of hot pepper grown in greenhouse with furrow and drip irrigation methods. Scientia Horticulturae 129: 790-797. https://doi.org/10.1016/j.scienta.2011.06.012.

Raij, B. van. 1996. Recomendações de adubação e calagem para o Estado de São Paulo. Campinas: IAC.

Rosenberg, N.J., McKenney, M.S., Martin, P. 1989. Evapotranspiration in a greenhouse-warmed world: a review and a simulation. Agricultural and Forest Meteorology 47: 303-320. https://doi.org/10.1016/0168-1923(89)90102-0.

Tapparo, S.A., Coelho, R.D., Costa, J.de.O., Chaves, S.W.P. 2019. Growth and establishment of irrigated lawns under fixed management conditions. Scientia Horticulturae, 256, 108580. https://doi.org/10.1016/j.scienta.2019.108580.

Vásquez, M.A., Folegatti, M.V., Dias, N.D.S., Silva, C.R.da. 2005. Efeito do ambiente protegido cultivado com melão sobre os elementos meteorológicos e sua relação com as condições externas. Engenharia Agrícola 25: 137-143. http://dx.doi.org/10.1590/S0100-69162005000100015.

Italian Journal of Agrometeorology
Rivista Italiana di Agrometeorologia

Firenze University Press
www.fupress.com/ijam

OPEN ACCESS

Citation: G. Bagagiolo, D. Rabino, M. Biddoccu, G. Nigrelli, D. Cat Berro, L. Mercalli, F. Spanna, G. Capello, E. Cavallo (2021) Effects of inter-annual climate variability on grape harvest timing in rainfed hilly vineyards of Piedmont (NW Italy). *Italian Journal of Agrometeorology* (1): 37-49. doi: 10.36253/ijam-1083

Received: September 18, 2020

Accepted: June 19, 2021

Published: August 9, 2021

Data Availability Statement: All relevant data are within the paper and its Supporting Information files.

Competing Interests: The Author(s) declare(s) no conflict of interest.

Effects of inter-annual climate variability on grape harvest timing in rainfed hilly vineyards of Piedmont (NW Italy)

Giorgia Bagagiolo[1], Danilo Rabino[1], Marcella Biddoccu[1,*], Guido Nigrelli[2], Daniele Cat Berro[3], Luca Mercalli[3], Federico Spanna[4], Giorgio Capello[1], Eugenio Cavallo[1]

[1] *Istituto di Scienze e Tecnologie per l'Energia e la Mobilità Sostenibili (STEMS), Consiglio Nazionale delle Ricerche (CNR), Torino, Italy*
[2] *Istituto di Ricerca per la Protezione Idrogeologica (IRPI), Consiglio Nazionale delle Ricerche (CNR), Torino, Italy*
[3] *Società Meteorologica Italiana (SMI), Moncalieri (TO), Italy*
[4] *Regione Piemonte, Settore Fitosanitario e Servizi Tecnico Scientifici, Torino, Italy*
*Corresponding author. E-mail: marcella.biddoccu@cnr.it

Abstract. The current scenario of global warming impacts viticulture, influencing grape and wine quality. A study was carried out in the "Basso Monferrato" region, a rainfed hilly vine-growing area in NW Italy, to investigate the relationships between climate variables and grape harvest dates. The dates of harvest for some local wine grape varieties were recorded from 1962 to 2019 in the Vezzolano Experimental Farm and surrounding vineyards. Three series of climate data were investigated by means of trend analysis for temperature variables, Huglin index, and precipitation during the growing period. A significant trend was found for temperature variables (positive) and harvest dates (negative), indicating anticipation of harvest beginning from 11.6 to 34.2 days in the 58-years study period, depending on the variety. The influence of increasing temperature and Huglin index in anticipating the harvest period, particularly the harvest beginning, was also highly significant for all the considered varieties and vineyards in the Monferrato area. Implication under a climate warming scenario, the relevance of having available continuous and homogeneous datasets and possible future studies were also discussed.

Keywords: viticulture, climate change, agro meteorology, time series analysis, Italy.

1. INTRODUCTION

The *Global Warming of 1.5* °C IPCC special report (IPCC, 2018) clearly highlights and documents the numerous effects of the observed climate changes on natural and human activities. Not only an increase in temperature but a dramatic change in the frequency of extreme events, such as heatwaves, is also expected. In the last years, many studies investigated the sharp impacts of climate change on different agricultural sectors (Jones and Davis,

2000; Jones *et al.*, 2005; Jones, 2007; Moriondo and Bindi, 2007; Tomasi *et al.*, 2011; Ramos, 2017; Kociper *et al.*, 2019). Concerning viticulture, the climate effects significantly influence grape and wine quality (Mariani *et al.*, 2009). Grapevine (*Vitis vinifera L.*) growing is one of the most relevant agricultural sectors in Italy, with 708.000 ha, ranking at the third position in Europe for vineyard cultivation, after Spain and France (OIV, 2020). The Piedmont region (NW Italy) has a vineyard surface of 41.360 ha, almost totally devoted to wine production (ISTAT, 2020). In 2014 *The Vineyard Landscape of Piedmont: Langhe, Roero and Monferrato* was recognised as a UNESCO World Heritage Site for the outstanding landscapes and the importance of vine-growing and winemaking in the Region (UNESCO, 2020).

The study of climate evolution and its environmental, economic, and social effects need to be monitored through its variations over time through a historical series of meteorological data. This kind of data represents an essential resource for agro-meteorology to understand the current and predictive dynamics, address agronomical choices, and finally determine their qualitative and quantitative effects on agricultural production. The availability of long-lasting, complete and accurate data series is a fundamental added value to predict and react to climate variability. Inter-annual climate variability determines effects on the beginning and duration of phenological stages and, ultimately, on the grape harvest and yield (Jones and Davis, 2000). Grapevines have four primary developmental stages: (i) budbreak, (ii) flowering, (iii) veraison (beginning of maturation) and (iv) full ripeness (harvest). The time between these stages varies greatly with grape variety (Tomasi *et al.*, 2011), and it is mainly influenced by the air temperature of the growth period (Mullins *et al.*, 1992). Previous studies (Jones *et al.*, 2005; Ramos *et al.*, 2008) reported changes of 5-10 days for these stages per 1 °C of warming over the last 30–50 years averaged over several wine regions and varieties. In addition, the observed increase of warm days poses a threat to grape quality because it causes a situation of imbalance at maturity, concerning sugar content, acidity and phenolic and aromatic ripeness (Camps and Ramos, 2012).

Climate change brings warmer conditions, generally associated with shorter intervals between phenological stages and earlier harvest occurrence (Tomasi *et al.*, 2011). The grape harvest timing is closely related to the aptitude of the vine to yield and ripen fruit to the optimum levels (Jones and Davis, 2000). In the Italian region of Veneto (NE Italy), grape maturity dates have trended 19 days earlier over 45 years (1964–2009) for several varieties (Tomasi *et al.*, 2011), and similar trends for the harvest dates were observed across numerous other locations in Europe (Jones *et al.*, 2005) for many wine grape varieties. In the Spanish region of Penedès, an analysis of temperature and precipitation trends was correlated with the beginning and ending dates of grape harvest: the ripeness timing showed a continuous advance of between -0.7 and -1.1 days/year (Camps and Ramos, 2012). To our knowledge, no studies have been published correlating long-time climate and harvest data series in Piedmont region. It should be useful for examine the relationships between climate variables and the responses of grapevine in a context of climate change, with particular reference to the beginning and ending harvest dates.

The purpose of this work carried out in the Basso Monferrato, a rainfed hilly wine-growing area in Piedmont, is to investigate: (i) the existence of trends within long-time climate data series, considering the vine growing season, (ii) the existence of trends within harvest dates for some local wine grape varieties and (iii) the relationships between the considered climate variables and harvest parameters.

2. EXPERIMENTS

2.1. The study area

Since 1962, the Institute for Agricultural and Earthmoving Machines (IMAMOTER) of the Italian National Research Council (CNR) has been carrying out many studies about the environmental and agronomic management of sloping vineyards in the Monferrato area, particularly in the Vezzolano Experimental Farm (45°08'N, 7°96'E, 426 m a.s.l., located in the municipality of Albugnano and managed by IMAMOTER). The results presented in this paper originated from the agrometeorological monitoring activity and the information concerning the grape harvest in the Experimental Farm and the surrounding area over the period 1962-2019. Since October 2020, IMAMOTER has become part of the new Institute of Sciences and Technologies for Sustainable Energy and Mobility (STEMS).

The Vezzolano Experimental Farm is located in the northern part of the Monferrato area, namely in the "Basso Monferrato". It is extended on 27 hectares including many vineyards, mainly cultivated with Malvasia di Castelnuovo Don Bosco, Freisa and Barbera varieties. The climate is scharacterised by warm and relatively dry summer, rainy spring and autumn, and cold winter with snowfall events, corresponding to a transitional climate between pre-alpine and sublitoranean (ARPA, 2020). According to on-site meteorological data recorded in 1962-2019, the mean annual precipitation was 846 mm, mainly concentrated in May (109 mm), while the driest month was Janu-

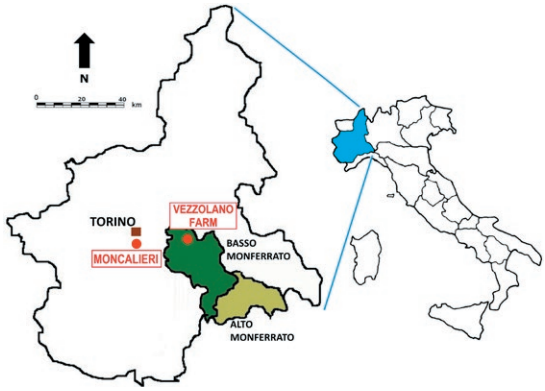

Fig. 1. Localization of the study site in Italy.

ary (43 mm). In the same period, the mean annual air temperature was 11.8 °C. The soil texture is silt loam (24% clay), and the soil is classified as *Typic Udorthent* (Soil Survey Staff, 2010; Nigrelli, 1998), derived from Miocene silty marls of the Tertiary Piedmontese Basin (Piana *et al.*, 2017). As typical in the Monferrato area, vineyards are arranged mainly with rows along contour lines ("girapoggio") or up-and-down the slope ("rittochino").

The Basso Monferrato has a long tradition of wine production, mainly dedicated to red wines, under the "Freisa d'Asti" DOC, the "Malvasia di Castelnuovo Don Bosco" DOC and the "Albugnano" DOC (Denomination of Controlled Origin) and the "Barbera d'Asti" DOCG (Denomination of Controlled and Guaranteed Origin), the highest designation of quality among Italian wines. The main grape varieties used for this purpose and cultivated in the area are Malvasia di Castelnuovo Don Bosco, Freisa, Bonarda, Barbera and Nebbiolo. The "Cantina Sociale del Freisa", a cooperative winery founded in 1953, is located in Castelnuovo Don Bosco village. In 1997 it was merged with the historic Wine Cellar of Barbera of San Damiano d'Asti in the "Cantina Sociale del Freisa - Terre dei Santi" winery, currently producing typical local wines from approximately 400 hectares of vineyards. Table 1 reports the cultivation surfaces and the yield related to "Cantina Sociale del Freisa – Terre dei Santi" in the two last years.

2.2. Climate data

In the present study, two long-lasting meteorological datasets related to Vezzolano site and to Moncalieri (near Torino) are considered to analyse inter-annual climatic variability.

The Vezzolano weather station is located in front of the farmhouse of Experimental Farm. The first station, operating since 1961 (Figure 2a) was composed by a mechanical thermo-hygrograph (Salmoiraghi, 1750 series), a pluviograph (SIAP Bologna), a totalising anemometer for wind run measuring (from 1971) and an evaporigraph, in addition to a solarimeter with graphic recorder (from 1981). The instruments were positioned in a wooden meteorological screen, about 1.3 m high from the concrete base. The devices were periodically calibrated, recording all the interventions and failures on monthly summaries of daily data. This station operated until 2006. The daily data (minimum, maximum and average temperature, average relative humidity and rainfall) were noted on the monthly meteorological agendas, indicating average and total decadal and monthly values.

Since March 2002, an automatic station was placed few meters apart from the mechanical one. It is equipped with sensors for measuring precipitation, temperature, relative humidity on an hourly basis and remote transmission systems of the data collected (Figure 2b). The station is part of the Piedmont Regional Agrometeorological Network (RAM), and its data are collected and made available to the public by the dedicated service of the Piedmont Region (Regione Piemonte, 2020).

In addition to the local data, the continuous datasets from the Moncalieri meteorological observatory are considered in this study. Long-term meteorological observations in Moncalieri – Collegio Carlo Alberto (Torino, 44°59'N, 7°41'E, 267 m a.s.l.) began in 1865 on the initiative of the Barnabite Catholic Priest and scientist Francesco Denza (Cat Berro *et al.*, 2015). The station is located within an urban area (Figure 3), atop of a historic building, as used in late 19th century, and the position of the instruments – even different from modern international

Table 1. Annual production of the "Cantina Sociale del Freisa – Terre dei Santi". For each cultivated grape varieties, total surfaces (ha) and total yield in grapes (t) are reported.

Year	Freisa		Malvasia di C. Don Bosco		Barbera		Bonarda		Nebbiolo	
	[ha]	[t]	[ha]	[t]	[ha]	[t]	[ha]	[t]	[ha]	[t]
2018	189	1453	47	400	45	316	17	123	17	125
2019	182	1060	46	275	42	222	18	67	17	98

Figure 2. Weather stations at the Vezzolano Experimental Farm: (a) the mechanical station that operated in the period 1961-2005 and, on the background, the Vezzolano Abbey (photo IMAMOTER, 11.03.2009) and (b) the automatic station placed near the older one in 2002 by the Regional Agrometeorological Network (RAM). Stations are placed in the in front of the farmhouse (photo IMAMOTER, 10.05.2008).

criteria – never changed to maintain the homogeneity of the time series. Since December 2001, an automatic weather station guarantees the continuity of measurements: temperature and relative humidity (in the Stevenson screen, as in the past), air pressure, precipitations, global solar radiation, wind speed and direction. Currently, Società Meteorologica Italiana (SMI) manages the station, collects and studies the recorded data. Data quality is regularly checked in collaboration with the leading Italian metrological institute (INRiM, Torino) within the framework of "MeteoMet" European project (https://www.meteomet.org/): instruments calibrations were carried out in 2012, 2016 and a new campaign is scheduled in 2021 (Bertiglia *et al.*, 2015). In 2018, World Meteorological Organization recognised Moncalieri observatory as "Centennial Observing Station" (WMO, 2020). The Moncalieri station is 23 km far from the Vezzolano Experimental Farm, but its series represent one of the most long-time, validated and homogeneous datasets in Piedmont and it can be considered as a reference for the surrounding area.

Figure 3. The tower of meteorological observatory in Moncalieri, managed by SMI (photo SMI, 11.04.2016).

Minimum and maximum daily temperature, and daily precipitation (Table 2) from the weather stations from the two locations (Vezzolano and Moncalieri) were used. For each year, from 1962 to 2019, temperature and precipitation variables were ssummarised for the growing season, considering three different time periods: from January to September (TMin_JS, TMax_JS, Prec_JS), from March to September (TMin_MS, TMax_MS, Prec_MS), and from April to September (TMin_AS, TMax_AS, Prec_MS). Consequently, the Huglin index was calculated for the same three periods (Hug_JS; Hug_MS, Hug_AS). According to results from previous studies carried out by Spanna and Lovisetto (2000) and by Lisa and Spanna (2003) in the Vezzolano Farm, in Piedmont vine areas when the Huglin bioclimatic heat index is calculated, as usual from April 1, it results in underestimation the real useful thermal contribution for the vine phenological development. Indeed, in March, but often already in February, many degree days useful for the phenological growth of the vine can be accumu-

Table 2. Weather stations considered in the study.

Station	Location	Altitude	timeline
Vezzolano (mechanical)	45°08'N, 7°96'E	426 m a.s.l.	1962÷2004
Vezzolano RAM	45°08'N, 7°96'E	426 m a.s.l.	2003÷2019
Moncalieri	44°59'N, 7°41'E	267 m a.s.l.	1960÷2019

lated, especially for the early varieties. Hence the choice to consider the January-September (JS) and March-September (MS) periods for the calculation of the Index. However, the calculation for the April-September (AS) period was also tested.

2.3. Grape harvest data

The data related to grape harvest timing were collected from the Vezzolano Experimental Farm of CNR-STEMS (former CNR-IMAMOTER), and from the "Cantina Sociale del Freisa – Terre dei Santi" on vineyards affiliated to the cellar in the surrounding area of the location of the weather station. The records of the harvest beginning data related to Vezzolano's vineyards cover the period from 1961 to 2019 for the Malvasia (BH_MAV), Freisa and Barbera (BH_FBV) varieties. The last two varieties are considered together as their harvest period usually is the same. The database of the "Cantina Sociale del Freisa – Terre dei Santi" of Castelnuovo Don Bosco covers the period 1958 to 2019 for the local varieties, with indication also of both the starting (BH_TS) and the ending day (EH_TS) of harvest operations.

2.4. Trend analysis

Trend analyses of the different climate variables (Tmin, Tmax, Prec, Hug for the three periods, January-September, March-September and April-September) and harvest parameters (beginning and end dates) were carried out. Trend analysis was implemented by linear regression when all conditions for parametric analysis were satisfied; otherwise, the non-parametric Mann-Kendall test (Kendall, 1975) and Sen's slope test (Sen, 1968) were carried out to determine the significance and slope of the trend, respectively. The time series were assessed for auto-correlation using the Durbin-Watson statistic. When the time series had autocorrelation, the modified Mann-Kendall test using prewhitening technique according to Hamed (2009) was applied. The interactions between climate and harvest parameter trends were also analysed. Linear regression between climate variables and harvest dates (beginning and end) was applied to identify the relationships between the different variables. Generalised least squares method was used in autocorrelation, and Kendall-Theil-Sen non-parametric regression was used when conditions for parametric linear regression were not satisfied. Statistical analyses were computed using R (R Core Team, 2020).

3. RESULTS

3.1. Characteristics and trends for climate and harvest dates of the study area

The mean values of the analysed climate variables for each considered growing period and any historical climate series, and mean values for the harvest dates are reported in Table 3. For the Vezzolano series, mean values of minimum temperature ranged from 8.5 °C to 12.6 °C and from 9.6 °C to 13.9 °C for the 1962-2004 and 2003-2019 periods, respectively, varying according to the considered growing period. The maximum temperature ranged from 18.2 °C to 22.8 °C and from 20.3 °C to 25.5 °C, for the first and second period of observation at Vezzolano, respectively. Observations at Moncalieri station across the 1960-2019 period revealed the minimum and maximum average temperature varying from 10.5 °C to 14.8 °C and 20.7 °C to 26.1 °C, respectively. The mean amount of precipitation, which showed high inter-annual variability, ranged from 402.2 mm to 656.9 mm across the three series while the Huglin index ranged from 1917.0 to 2590.2 degree-days per year. As expected, for those variables related to temperature, the mean values including in the computation the months of January and February (usually the coldest months in Italy's climate) resulted in being lower on average, 3.5 °C difference among minimum temperatures and 4.2 °C difference among maximum temperatures. Inversely, precipitation resulted lower when January and February were not computed (average difference of 115 mm).

For the Vezzolano site, mean values of minimum and maximum temperatures for the 2003-2019 series were about 1-2.5 °C higher than those recorded in the 1962-2004 series; this also resulted in more than 400 degree-days difference for Huglin index. Compared to the Vezzolano stations, Moncalieri station recorded higher temperatures (averagely 1.7 °C higher) and lower precipitations (averagely 108 mm lower).

Concerning the mean harvest dates, they differ from each other being referred to different grape varieties. Mean harvest beginning dates (BH) range between the 19th of September and the 2nd of October, while the mean ending date of harvest (EH) is the 15th of October. On average, the recorded dates vary across years in a range between 7 and 12 days.

Table 3. Mean annual values (±standard deviation) of each climate variable for the three data series and for each harvest variable.

	Variables[1]	Vezzolano 1962-2004	Vezzolano 2003-2019	Moncalieri 1960-2019
Climate	Tmin_JS (°C)	8.5 ±0.8	9.6 ±0.5	10.5 ±0.7
	Tmax_JS (°C)	18.2 ±1.1	20.3 ±0.8	20.7 ±1.3
	Prec_JS (mm)	640.3 ±198.5	656.9 ±163.6	517.8 ±156.3
	Hug_JS (°C-days)	1977.6 ±195.9	2417.1 ±146.4	2590.2 ±259.4
	Tmin_MS (°C)	11.1 ±0.8	12.4 ±0.5	13.4 ±0.7
	Tmax_MS (°C)	21.3 ±1.1	23.6 ±0.8	24.5 ±1.4
	Prec_MS (mm)	549.3 ±176.8	559.4 ±134.4	448.4 ±133.3
	Hug_MS (°C-days)	1967.6 ±193.4	2394.8 ±143.6	2577.4 ±252.0
	Tmin_AS (°C)	12.6 ±0.8	13.9±0.6	14.8 ±0.8
	Tmax_AS (°C)	22.8 ±1.2	25.5±0.8	26.1 ±1.4
	Prec_AS (mm)	489.5 ±180.8	489.4±108.9	402.2 ±124.5
	Hug_AS (°C-days)	1917.0 ±187.7	2310.0±132.3	2485.0 ±228.1
Harvest 1961-2019	BH_MAV (date±days)	27 September ±10 days		
	BH_FBV (date±days)	2 October ±7 days		
	BH_TS (date±days)	19 September ±12 days		
	EH_TS (date±days)	15 October ±8 days		

[1]Tmin_JS: mean annual minimum temperature from January to September (°C); Tmax_JS: mean annual maximum temperature from January to September (°C); Prec_JS: mean annual total precipitation from January to September (mm) Hug_JS: mean annual total value of Huglin's Heliothermal Index from January to September (°C-days). The suffix "MS" and "AS" indicate the same variables measured from March to September and from April to September. BH_MAV: mean harvest beginning date (date±days) for Malvasia (MAV); for Freisa-Barbera (FBV); for the "Cantina Sociale del Freisa – Terre dei Santi" (TS); EH_TS: mean harvest ending date (date±days) from the "Cantina Sociale del Freisa – Terre dei Santi".

The trends of historical time series were sanalysed to evaluate how climate variables have been changing within the last decades (Table 4). In general, results show significantly increasing trends with regard to temperature variables, namely minimum and maximum temperatures and Huglin index, especially for Moncalieri's series. Precipitation showed a relevant inter-annual variability, and no significant trends were observed for associated variables (Prec_JS, Prec_MS, Prec_AS) in any datasets.

In detail, concerning Vezzolano's 1962-2004 series, for all the considered periods of growing season (January to September, March to September and April to September) the Huglin index significantly increased over the period, ranging between 3.94 degree-days per year considering AS growing season and 4.96 degree-days per year when the month of March was computed in the growing season. In addition, for the MS growing season, a significant trend of 0.03 °C per year was also observed for minimum and maximum temperatures.

In Moncalieri's series, the positive trend identified for Tmin and Tmax was the same considering average values from January to September, from March to September and from April to September, showing a significant increase of 0.03 °C and 0.06 °C per year respectively. For the Huglin index the increasing trend observed in Moncalieri's series was particularly relevant. This variable demonstrated the higher significant average increase of 11.71 degree-days per year when computed from January to September.

For the Vezzolano series recorded from 2003 to 2019, only minimum temperature showed a significant increase of 0.04 °C per year.

The trends of the harvest dates (Table 5) were statistically significant for all the considered variables. They resulted in general anticipation for the beginning and the end of the harvest period. In particular, the maximum and the minimum change ratios were respectively -0.59 and -0.18 days per year, corresponding to the trends of the starting (BH_TS) and the ending (EH_TS) dates from the "Cantina Sociale del Freisa – Terre dei Santi" of Castelnuovo Don Bosco. Referring to a single variety and only to the Vezzolano farm, the starting date of harvest was anticipated by 3.7 and 2 days in ten years for Malvasia and Freisa-Barbera varieties, respectively.

3.2. Relationships between climate variability and grape harvest

The advance in the beginning and end of the harvest period was analysed in relation to different climatic vari-

Table 4. Temperature, precipitation and Huglin index trends for the three data series, significant at 95% level or higher (+ ≤ 0.050; * ≤ 0.010; ** ≤ 0.001; *** ≤ 0.0001). Numbers in brackets indicate values of R^2 or Kendall τ.

Variables[1]	Vezzolano 1962-2004	Vezzolano 2003-2019	Moncalieri 1960-2019
Tmin_JS (°C/year)	NS	0.04+ (0.21)	0.03*** (0.54)
Tmax_JS (°C/year)	0.03+ (0.09)	NS	0.06*** (0.62)
Prec_JS (mm/year)	NS	NS	NS
Hug_JS (°C-days/year)	4.43+ (0.08)	NS	11.71*** (0.62)
Tmin_MS (°C/year)	0.03** (0.15)	NS	0.03*** (0.60)
Tmax_MS (°C/year)	0.03+ (0.22)	NS	0.06*** (0.61)
Prec_MS (mm/year)	NS	NS	NS
Hug_MS (°C-days/year)	4.96* (0.10)	NS	11.39*** (0.63)
Tmin_AS (°C/year)	NS	NS	0.03*** (0.58)
Tmax_AS (°C/year)	NS	NS	0.06*** (0.56)
Prec_AS (mm/year)	NS	NS	NS
Hug_AS (°C-days/year)	3.94+ (0.19)	NS	9.97*** (0.58)

[1]Tmin_JS: mean variation per year of mean minimum temperature from January to September (°C/year); Tmax_JS: mean variation per year of mean maximum temperature from January to September (°C/year); Prec_JS: mean variation per year of total precipitation from January to September (mm/year) Hug_JS: mean variation per year of total value of Huglin's Heliothermal Index from January to September (°C-days/year). The suffix "MS" and "AS" indicate the same variables measured from March to September and from April to September.

Table 5. Harvest dates trends, significant at 95% level or higher (+ ≤ 0.050; * ≤ 0.010; ** ≤ 0.001; *** ≤ 0.0001).

Variables[1]	N	Slope
BH_MAV (days/year)	59	-0.37***
BH_FBV (days/year)	46	-0.20***
BH_TS (days/year)	59	-0.59***
EH_TS (days/year)	59	-0.18*

[1]BH_MAV: mean variation per year of harvest beginning date for Malvasia (days/year); BH_FBV: mean variation per year of harvest beginning date for Freisa-Barbera (days/year); BH_TS: mean variation per year of harvest beginning date from the "Cantina Sociale del Freisa – Terre dei Santi" (days/year); EH_TS: : mean variation per year of harvest ending date from the "Cantina Sociale del Freisa – Terre dei Santi" (days/year); N: number of years in each dataset.

ables that had shown significant trends. Almost all performed regression analysis resulted significant (P<0.05) or highly significant (P<0.0001). Table 6 reports the change ratios obtained in the regression analysis, estimating the average change in days of the harvest dates, in relation to temperature variables. In most of the sanalysed cases, the harvest date exhibited a negative correlation with the average minimum and maximum growing season temperature (Tmin_JS, Tmax_JS, Tmin_MS, Tmax_MS, Tmin_AS, Tmax_AS). According to the harvest date variables, all results for temperature variables showed significant variability in the absolute values of the change ratios, the considered growing season and the considered series. Concerning minimum temperatures, the starting date of harvest was anticipated from 5.32 days/°C for (BH_MAV for Tmin_MS) to 13.01 days/°C (BH_TS for Tmin_JS). Whereas, with regard to maximum temperatures, the starting date of harvest was anticipated from 1.62 days/°C for (BH_TS for Tmax_JS) to 7.46 days/°C (BH_TS for Tmax_MS). The change ratios for the minimum temperature for all the three series resulted in the highest (in absolute terms) with a very high significance level. For the average maximum temperature recorded at the Moncalieri observatory, the change ratios were similar considering January or March as starting month, ranging from -4.18 days/°C and -4.20 days/°C to -7.25 days/°C and -7.46 days/°C for the final (EH_TS) and starting (BH_TS) dates of harvest, respectively, for farms associated to the "Cantina Sociale del Freisa – Terre dei Santi" of Castelnuovo Don Bosco. The same values for AS period resulted slightly lower (about 1 °C).

A significant correlation was always found between the Huglin index and the harvest dates, in all cases with negative values ranging from -0.02 days/°C- days to -0.04 days/°C-days. Absolute values of the change ratios for the Huglin index were very similar among the three considered growing seasons.

4. DISCUSSION

Mean annual values of minimum and maximum temperature were lower for the Vezzolano long-term

Table 6. Relationship between harvest dates and climatic variables[1], significant at 95% level or higher (+ ≤ 0.050; * ≤ 0.010; ** ≤ 0.001; *** ≤ 0.0001).

Climate series	Independent Variable[1]	Change ratio			
		BH_MAV	BH_FBV	BH_TS	EH_TS
Vezzolano 1962-2004	Tmax_JS (days/°C)	-6.59***	-4.59***	-1.62***	-3.05**
	Hug_JS (days/°C-days)	-0.02***	-0.03***	-0.02***	-0.02***
	TMin_MS (days/°C)	-5.32***	-5.33**	-6.22***	-3.60**
	Tmax_MS (days/°C)	-6.62***	-4.69***	-2.45***	-3.46***
	Hug_MS (days/°C-days)	-0.03***	-0.03***	-0.02***	-0.02***
	Hug_AS (days/°C-days)	-0.02***	-0.03***	-0.02***	-0.02***
Vezzolano RAM 2003-2019	Tmin_JS (days/°C)	-11.80*	NS	-13.01***	-11.93**
Moncalieri 1961-2019	Tmin_JS (days/°C)	-9.35***	-6.89***	-6.50***	-6.19***
	Tmax_JS (days/°C)	-5.98***	-4.54***	-7.25***	-4.18***
	Hug_JS (days/°C-days)	-0.03***	-0.02***	-0.04***	-0.02***
	Tmin_MS (°C/year)	-9.18***	-6.90***	-11.48***	-6.80***
	Tmax_MS (°C/year)	-5.60***	-4.26***	-7.46***	-4.20***
	Hug_MS (days/°C-days)	-0.03***	-0.02***	-0.04***	-0.02***
	Tmin_AS (days/°C)	-8.36***	-6.20***	-11.31***	-5.68***
	Tmax_AS (days/°C)	-5.14***	-3.97***	-6.79***	-3.83***
	Hug_AS (days/°C-days)	-0.03***	-0.02***	-0.04***	-0.02***

[1] Tmin_JS: mean change ratio of harvest dates for each °C variation of minimum temperature from January to September (days/°C); Tmax_JS: mean change ratio of harvest dates for each °C variation of maximum temperature from January to September (days/°C); Hug_JS: mean change ratio of harvest dates for each °C-day variation of total value of Huglin's Heliothermal Index from January to September (°C-days). The suffix "MS" and "AS" indicate the same variables measured from March to September and from April to September. BH_MAV: mean variation per year of harvest beginning date in relation to temperature variables for Malvasia (MAV); for Freisa-Barbera (FBV); for the "Cantina Sociale del Freisa – Terre dei Santi" (TS); EH_TS: mean variation per year of harvest ending date in relation to temperature variables for the "Cantina Sociale del Freisa – Terre dei Santi".

(1962-2004) series than for the 2003-2019 period. Differences in average temperature can be partially ascribed to different sensors technology implemented in the RAM weather station. Nevertheless, the average annual temperature in Piedmont in the period 2000-2015 was higher than the reference 30-years (1971-2000) average temperature (ARPA, 2020); thus the most recent series likely reflects, to some extent, an increase of local temperature. Average temperatures measured at the Moncalieri observatory were the highest. The station's location at a lower altitude and in an urban context positively influences the measured temperature, especially maximum values in summer. The differences in measured temperatures are also reflected in the average values of the Huglin index. Mean precipitation was very similar for the two Vezzolano series. It was the lowest at Moncalieri station, due both to topographic reasons and to the station setup, with rain gauge placed at 26 meters from soil surface, likely resulting in underestimation of the precipitation amount due to the higher wind speed (Pollock *et al.*, 2018). The Vezzolano and Moncalieri series cover 42 and 59 years of weather observations, respectively, that were recorded homogeneously, and thus allow us to study relationships between climate data and harvest information collected over the same period. The analysis of the same relationships through a shorter and more recent series (Vezzolano 2003-2019), which corresponds to most of the datasets available in the region, highlighted the relevance of having available continuous and homogeneous datasets to carry out studies about the impact of climate temporal variability on crop growth and development.

The increase in mean maximum temperature (Tmax_JS and Tmax_MS) observed at Moncalieri over the whole period (1960-2019) is twice that of the trend obtained for the Vezzolano long-time series. This is particularly noteworthy since the difference between the two positive trends can be attributed to the inclusion in the Moncalieri series of the most recent 15 years, considering that in Piedmont the increasing trend of daily maximum temperature in the period 1981-2015 was 0.062 °C/year, while in the period 1958-2015 the

observed trend was 0.038 °C/year (ARPA, 2020). This result is also in agreement with the last IPCC assessment report (IPCC, 2014), highlighting that each of the last three decades has been successively warmer at the Earth's surface than any preceding decade since 1850. The increasing trend detected in the average temperature at the rural weather station of Vezzolano was not affected by urbanisation, thus can be ascribable entirely to the global warming trend.

The observed increasing trend of the Huglin index in the two long-term series (Vezzolano 1962-2004 and Moncalieri 1961-2019) was consistent with the temperatures increase. The relative mean annual values were generally in line with those observed in other Mediterranean viticultural areas. Indeed, in the Veneto region of Italy, the Huglin index for the 1964-2009 period averaged 2457 (Tomasi *et al.*, 2011), while in the Ribera del Duero area of Spain, for the period 2003-2013, a mean yearly Huglin index ranged from 1973 to 2328, varying according to the different considered sites (Ramos *et al.*, 2016). In addition, in their study, Ramos *et al.* (2016) observed a positive correlation of the Huglin index with sugar content and, at the same time, a negative correlation with the colour index and acidity levels, meaning the higher the Huglin index, the higher the maturity level of the grapes. In the present study two aspects resulted particularly relevant concerning the obtained values of Huglin index and associated classes of viticultural climate as defined by Tonietto and Carbonneau (2004). Firstly, differences among the three considered growing periods January-September, March-September and April -September were very marginal; therefore, the findings by Jones *et al.* (2010) supporting that, in a context of generally warmer temperatures, considering longer time span of growing season did not produce any meaningful differences in terms of viticultural climate classification were confirmed. Nevertheless, the trend of the Huglin index over a long-term period of observation showed a higher increase, from 12% to 26%, including March (+26% and +14%) or even February and January (+12% and +17%) in computation than the baseline method considering April-September, respectively at Vezzolano and Moncalieri. In particular, for the Vezzolano 1962-2004 series, the trends of the Huglin index for a larger time span of growing season indicate the contribution of late winter and early spring months in bringing forward conditions for vine's development.

Secondly, considering the site of Vezzolano, in 1962-2004 series, the Huglin index ranged 1917.0-1977.6 falling in the "temperate" class (1800 < HI < 2100), while 2003-2019 series the index ranged 2310.0-2417.1, falling in "warm-temperate" (2100 < HI < 2400) and "warm" (2400 < HI < 3000) class. The same situation was observed in a previous study (Laget *et al.*, 2008) carried out in the last decades in France where in some zones of the Hérault département, the Huglin index evolved with the result that some viticultural zones classified as "warm-temperate" between 1975 and 1996 were re-classified as "warm" between 1997 and 2005. As supported by some authors (Ramos *et al.*, 2016; earlier occurrences of phases and shorter phase duration in the future. The impact varies depending on the geo-localization of the studied region and its microclimate. The objective of this study is to further understand the impact of climate change on grapevine phenology by studying the role of varieties and microclimates through a regional assessment carried out in two future periods of time (2021–2050 and 2071–2099)(Alikadic *et al.*, 2019), the Huglin bioclimatic index is particularly interesting to follow in later season events, between veraison and harvest, being able to highlight ripening potentials of grapes. For this reason, future studies could investigate how the Huglin index evolve along with the growing stages of the vine in the study area and to what extent it can explain variation in the main phenological events under a climate warming scenario.

In the Vezzolano Experimental Farm the mean beginning harvest date varied according to grape variety (from 27 September to 2 October). The harvest beginning of farms affiliated to the "Cantina Sociale del Freisa – Terre dei Santi" was anticipated by at least 8 days, with greater inter-annual variability. The relevant variability of the beginning harvest dates, that ranged from 14 to 24 days was explained by the clear identification of a significant decreasing trend in all cases, from 11.6 to 34.22 days in 58 years (1961-2019), for harvesting Freisa-Barbera at Vezzolano and different varieties from vineyards affiliated to the "Cantina Sociale del Freisa – Terre dei Santi", respectively. Similar studies in other European countries led to comparable results, moving from the Mediterranean region towards more continental areas. In Spain, Camps and Ramos (2012) identified an advance of about 12 days, on average, as date of the beginning of harvest over the last 14 years of their study in the Penedès region. Studies in France reported advancing of the harvest between 18 and 21 days in the period from 1940 and 2000 (Ganichot, 2002) or by 2 weeks between 1972 and 2002 (Duchêne and Schneider, 2005). In Italy, Tomasi *et al.* (2011) detected that the beginning harvest dates were 19 days earlier over 1964–2009 for several varieties in Veneto. In eastern Austria, Koch *et al.* (2009) also showed a trend towards earlier harvest times between 1970–2007 with a 5-days advance every 10 years in Klosterneuburg, and an approximate

3-days advance every 10 years in the Vienna vineyard area. The anticipation of the harvest date in the long-term period could be affected by several factors, not only to climate-related ones, such as changes in the method for assessing the fruit ripening, or vineyard management. Nevertheless, the trend for harvest dates detected for the Monferrato areas appears comparable to evident trends already identified over different European regions and varieties. In addition, similar trends have been seen for other phenological phases by studies based on long-time climate series and also considering projections obtained from modelling. In Piedmont, long-term simulations performed over 60 years (1950-2009) with a crop growth model for Nebbiolo variety showed statistically significant variations of most of the model output variables (phenological stages, berry sugar content, LAI Maximum value, yield), with larger time trend slopes referring to the most recent 30-year period (1980–2009), thus confirming that ongoing climate change started influencing local vineyards since 1980 (Andreoli *et al.*, 2019). Based on crop model simulations over Europe for the period 2041-2070, Fraga *et al.* (2017) observed that mean phenological timings are projected to undergo significant advancements (e.g. budburst/harvest can be >1 month earlier), with implications also in the corresponding phenophase intervals.

The influence of inter-annual changes in temperature in anticipating the harvest period, particularly the harvest beginning, was significant for all the considered varieties and vineyards, in relation to the average temperature of the three series. The highest change ratios (absolute values) have been obtained for the 2003-2019 Vezzolano RAM series. The increase of the Huglin index showed a highly significant influence in determining anticipation of harvest, regardless of the considered growing season. Nevertheless, the significant trends identified for the Monferrato area confirm that temperature is the primary driver of grapevine phenology (Alikadic *et al.*, 2019), especially for harvest. Several studies show that the temperature rise is highly correlated to the earlier occurrence of phenological phases, affecting the final quality of products (Jones and Davis, 2000; Jones *et al.*, 2005; Dalla Marta *et al.*, 2010; Bock *et al.*, 2011). The timing of maturity directly relates to wine quality, since grape composition and subsequent wine quality are linked to growing season temperatures (Jones *et al.*, 2005; Jarvis *et al.*, 2017). Leolini *et al.* (2019), modelling the performance of Sangiovese grape variety in Tuscany, observed that a progressive increase of temperatures resulted in earlier phenological phases and an increasing trend of sugar content while, on the opposite, the acid content decline.

The present study did not detect any trend in precipitation amount during the growing period, in agreement with the results of the local regional analysis (ARPA, 2020) and no significant relationship between harvest timing and rainfall. Nevertheless, beyond the rainfall amount, rainfall temporal distribution affects greatly the grape development and yield (Schultze *et al.*, 2016). Given a similar amount of precipitation during the growing period, variations of temporal rainfall distribution can affect water availability for the crop when water demand is greater, for example in spring, as was detected by Camps and Ramos (2012) in Spain, with significant consequences on the grape development. During the last 2 decades, in Piedmont, very often cumulated precipitation in spring was lower than the reference average over 1971-2000 (ARPA, 2020). Furthermore, temporal rainfall distribution and rainfall characteristics (intensity and duration of rainfall events) play also a relevant role in determining water and soil losses in sloping vineyards of Monferrato (Biddoccu *et al.*, 2017; Bagagiolo *et al.*, 2018), that can result in the decrease of water input, thus in even lower water availability for plant development, and soil degradation. Further investigation is needed to evaluate the effects of variation in precipitation distribution along the year on the water availability and then on crop growth and phenological phases, grape quality and yields in the Monferrato area. Such research will help address vineyard management choices, including adequate soil and water conservation strategies, to achieve more sustainability in vineyards in the current climate change scenario.

5. CONCLUSIONS

This study contributed to understand how climate change and, in particular, the increasing trends of temperatures observed in the last decades are affecting the harvest period of grapevine in the Basso Monferrato wine-growing area. Indeed, mainly the analysis based on the two long-term homogeneous meteorological series of Vezzolano (1962-2004) and Moncalieri (1961-2019), besides confirming a significant, clear, increasing trend of local temperatures, demonstrated a strong relationship between warming temperatures and the anticipation of grapevine development and harvest dates. The beginning harvest dates showed a significant decreasing trend from 11.6 to 34.2 days in 58 years, in line with several previous studies. Furthermore, the results indicated in the most recent 15 years a tendency to anticipate the harvest by 11-13 days for each increase equal to 1 °C in minimum temperature. These findings show clearly the

effects of climate warming on grapevine phenology in a district with a long tradition of wine production.

Further studies will apply the proposed analysis to the evolution of grapevine phenological events and other areas and varieties, with regard to temperatures and related bio-climatic indices, and precipitation. In the present analysis, the amount of total precipitation did not show a significant trend. Still, it could be relevant to investigate the effects of temporal rainfall distribution on crop development and production and evaluate water availability in different phenological phases in a region where vineyards are traditionally rainfed. As a final note, the present work highlighted that under a climate change scenario, the availability of continuous and homogenous datasets is crucial to properly assess the impact of climate inter-annual variability on crop management.

FUNDING

This study was funded with the contribution of Fondazione CRT-Cassa di Risparmio di Torino (research project "Recupero e valorizzazione delle serie storiche di dati agro-meteorologici di Vezzolano"). Part of this research was carried out within the framework of the WATER4EVER Project (WaterJPI/0010/2016), which is funded under the WaterWorks 2015 Call, with the contribution of European Commission and Italian Ministry of Education University an Research (MIUR).

ACKNOWLEDGMENTS:

The authors very much appreciate the support by the "Cantina Sociale del Freisa – Terre dei Santi" of Castelnuovo Don Bosco and his Director Dr. Paolo Aiassa for providing their grape harvest data. The content of this article reflects only the authors' views and the WaterWorks 2015 Consortium is not liable for any use that may be made of the information contained therein.

CONFLICTS OF INTEREST

The authors declare no conflict of interest. The funders had no role in the design of the study; in the collection, analyses, or interpretation of data; in the writing of the manuscript, or in the decision to publish the results.

REFERENCES

Alikadic A., Pertot I., Eccel E., Dolci C., Zarbo C., Caffarra A., De Filippi R., Furlanello C, 2019. The impact of climate change on grapevine phenology and the influence of altitude: A regional study. Agric. For. Meteorol., 271: 73–82.

Andreoli V., Cassardo C., Iacona T. La, Spanna F. Description and preliminary simulations with the Italian vineyard integrated numerical model for estimating physiological values (IVINE), 2019. Agronomy, 9: 1–5.

ARPA Piemonte Clima - Confronti Storici - Analisi lungo periodo Available online: https://www.arpa.piemonte.it/rischinaturali/tematismi/clima/confronti-storici/analisi-lungo.html (accessed on Jun 22, 2020).

Bagagiolo G., Biddoccu M., Rabino D., Cavallo E, 2018. Effects of rows arrangement, soil management, and rainfall characteristics on water and soil losses in Italian sloping vineyards. Environ. Res., 166: 690–704.

Bertiglia F., Lopardo G., Merlone A., Roggero G., Cat Berro D., Mercalli L., Gilabert A., Brunet M, 2015. Traceability of Ground-Based Air-Temperature Measurements: A Case Study on the Meteorological Observatory of Moncalieri (Italy). Int. J. Thermophys., 36: 589–601.

Biddoccu, M.; Ferraris, S.; Pitacco, A.; Cavallo, E. Temporal variability of soil management effects on soil hydrological properties, runoff and erosion at the field scale in a hillslope vineyard, North-West Italy. *Soil Tillage Res.* **2017**, *165*, 46–58.

Bock A., Sparks T., Estrella N., Menzel A, 2011. Changes in the phenology and composition of wine from Franconia, Germany. Clim. Res., 50: 69–81.

Camps J.O. and Ramos M.C., 2012. Grape harvest and yield responses to inter-annual changes in temperature and precipitation in an area of north-east Spain with a Mediterranean climate. Int. J. Biometeorol., 56: 853–864.

Cat Berro, D.C.; Napoli, G. Di; Mercalli, L., 2015. Moncalieri (Torino), anche l'osservatorio meteorologico compie un secolo e mezzo: aggiornamento della serie di dati 1864-2015. *Nimbus 74*: 16–54.

Dalla Marta A., Grifoni D., Mancini M., Storchi P., Zipoli G., Orlandini S., 2010. Analysis of the relationships between climate variability and grapevine phenology in the Nobile di Montepulciano wine production area. J. Agric. Sci., 148: 657–666.

Duchêne E. and Schneider C, 2005. Grapevine and climatic changes: a glance at the situation in Alsace. Agron. Sustain. Dev., 24: 93–99.

Fraga H., De Cortázar Atauri I.G., Malheiro A.C., Moutinho-Pereira J., Santos J.A., 2017. Viticulture

in Portugal: A review of recent trends and climate change projections. Oeno One, 51: 61–69.

Ganichot, B. Evolution de la date des vendanges dans les Côtes du Rhône méridionales. In Proceedings of the 6th Rencontres rhodaniennes; Orange, France, 2002; pp. 38–41.

Hamed K.H, 2009. Enhancing the effectiveness of prewhitening in trend analysis of hydrologic data. J. Hydrol., 368: 143–155.

IPCC, 2014. Climate Change 2014: Synthesis Report. Contribution of Working Groups I, II and III to the Fifth Assessment Report of the Intergovernmental Panel on Climate Change [Core Writing Team, R.K. Pachauri and L.A. Meyer (eds.)]. IPCC, Geneva, Switzerland, 151 pp.

IPCC, 2018. Global Warming of 1.5°C. An IPCC Special Report on the impacts of global warming of 1.5°C above pre-industrial levels and related global greenhouse gas emission pathways, in the context of strengthening the global response to the threat of climate change, sustainable development, and efforts to eradicate poverty [Masson-Delmotte, V., P. Zhai, H.-O. Pörtner, D. Roberts, J. Skea, P.R. Shukla, A. Pirani, W. Moufouma-Okia, C. Péan, R. Pidcock, S. Connors, J.B.R. Matthews, Y. Chen, X. Zhou, M.I. Gomis, E. Lonnoy, T. Maycock, M. Tignor, and T. Waterfield (eds.)]. In Press.

ISTAT. L'andamento dell'economia agricola Available online: https://www.istat.it/ (accessed on Jun 22, 2020).

Jarvis C., Barlow E., Darbyshire R., Eckard R., Goodwin I, 2017. Relationship between viticultural climatic indices and grape maturity in Australia. Int. J. Biometeorol., 61: 1849–1862.

Jones G.V., 2007. Climate change: observations, projections, and general implications for viticulture and wine production. Working Paper n°7, Whitman College – Economics Department, 15 pp.

Jones G.V. and Davis R.E., 2000. Climate Influences on Grapevine Phenology, Grape Composition, and Wine Production and Quality for Bordeaux, France. Am. J. Enol. Vitic., 51: 249–261.

Jones G.V., Duchene E., Tomasi D., Yuste J., Braslavka O., Schultz H., Martinez C., Boso S., Langellier F., Perruchot C., et al., 2005. Change in European Winegrape Phenology and Relationship with Climate. Atti GESCO Geisenheim, Germania. In: Proceedings of the XIV GESCO Symposium 2005, Geisenheim, Germany, 2005.

Jones G.V., White M.A., Cooper O.R., Storchmann K., 2005. Climate Change and Global Wine Quality. Clim. Change, 73: 319–343.

Kendall, M.G., 1975. *Rank Correlation Methods*. Griffin, Ed., London, UK, 1975.

Koch E., Maurer C., Hammerl C., Hammerl T., Pokorny E. 2009. BACCHUS grape harvest days and temperature reconstruction for Vienna from the 16th to the 18th century. In: Proceedings of the 18th World IMACS Congress and MODSIM International Congress on Modelling and Simulation, Cairns, Australia: 2632– 2638.

Kociper D., Vintar Mally K., Kajfež Bogataj L., 2019. Climate vulnerability of agriculture in statistical regions of Slovenia. Ital. J. Agrometeorol.: 2, 35–48. doi: 10.13128/ijam-651.

Laget F., Tondut J.L., Deloire A., Kelly M.T., 2008. Climate trends in a specific Mediterranean viticultural area between 1950 and 2006. J. Int. des Sci. la Vigne du Vin, 42: 113–123.

Leolini L., Moriondo M., Romboli Y., Gardiman M., Costafreda-Aumedes S., Costafreda-Aumedes S., Bindi M., Granchi L., Brilli L., 2019. Modelling sugar and acid content in Sangiovese grapes under future climates: an Italian case study. Clim. Res., 78: 211–224.

Lisa L. and Spanna F., 2003. Indici meteorologici idonei per la viticoltura. Analisi dei dati rilevati a Vezzolano dal 1964 al 2003. Rapporto interno 03.21. CNR-IMAMOTER, Torino, Italy, 21 pp.

Mariani L., Parisi S., Failla O., Cola G., Zoia G., Bonardi L., 2009. Tirano (1624-1930): A long time series of harvest dates for grapevine. Ital. J. Agrometeorol., 16: 7–16.

Moriondo, M. and Bindi, M., 2007. Impact of climate change on the phenology of typical mediterranean crops. Ital. J. Agrometeorol. 2007, 3: 5–12.

Mullins M.G., Bouquet A., Williams L.E., 1992. Biology of the grapevine. Cambridge University Press, Cambridge, UK, 1992, 252 pp.

Nigrelli G., 1998. Indagine ambientale di una unità di paesaggio collinare del Monferrato Settentrionale, Università degli Studi di Torino, 1998.

Organisation Internationale de la Vigne et du Vin (OIV) State of the World Vitiviniculture Sector in 2019 – April 2020 Available online: http://www.oiv.int/en/technical-standards-anddocuments/statistical-analysis/state-of-vitiviniculture (accessed on Jun 22, 2020).

Piana F., Fioraso G., Irace A., Mosca P., D'Atri A., Barale L., Falletti P., Monegato G., Morelli M., Tallone S., et al., 2017. Geology of Piemonte region (NW Italy, Alps–Apennines interference zone). *J. Maps*, *13*: 395–405.

Pollock M.D., O'Donnell G., Dutton M., Black A., Wilkinson M.E., Colli M., Stagnaro M., Lanza L.G., Lewis E., Kilsby C.G., O'Connell P.E., 2018. Quanti-

fying and Mitigating Wind-Induced Undercatch in Rainfall Measurements. Water. Resour. Res., 54(6), 3863-3875. https://doi.org/10.1029/2017WR022421.

R Core Team R: A language and environment for statistical computing Available online: https://www.r-project.org/ (accessed on Jun 22, 2020).

Ramos M.C., Jones G.V., Martínez-Casasnovas J., 2008. Structure and trends in climate parameters affecting winegrape production in northeast Spain. Clim. Res., 38: 1–15.

Ramos M.C., 2017. Projection of phenology response to climate change in rainfed vineyards in north-east Spain. Agric. For. Meteorol., 247: 104–115.

Ramos M.C., Jones G.V, Yuste J., 2016. Variability of Tempranillo grape quality within the Ribera del Duero DO (Spain) and relationships with climatic characteristics. 11th Int. Terroir Congr.: 15–22.

Regione Piemonte La rete agrometeorologica del Piemonte (RAM) Available online: https://www.regione.piemonte.it/web/temi/agricoltura/agroambiente-meteo-suoli/rete-agrometeorologica-piemonte-ram (accessed on Jun 22, 2020).

Schultze S.R., Sabbatini P., Luo L. 2016. Effects of a warming trend on cool climate viticulture in Michigan, USA. *Springerplus*, *5*: 1119.

Sen P.K., 1968. Estimates of the Regression Coefficient Based on Kendall's Tau. J. Am. Stat. Assoc., 63: 1379–1389.

Soil Survey Staff, 2010. Keys to soil taxonomy. USDA-Natural Resources Conservation Service, Ed.; 11th ed.; Washington, DC, 2010.

Spanna F. and Lovisetto M., 2000. Caratterizzazione delle produzioni vitivinicole nell'area del Barolo - Aspetti climatici. In Barolo, supplemento al n. 24. Quaderni della Regione Piemonte Agricoltura, 24: 35-53.

Tomasi D., Jones G.V., Giust M., Lovat L., Gaiotti F., 2011. Grapevine Phenology and Climate Change: Relationships and Trends in the Veneto Region of Italy for 1964-2009. Am. J. Enol. Vitic., 62: 329–339.

Tonietto J. and Carbonneau A., 2004. A multicriteria climatic classification system for grape-growing regions worldwide. Agric. For. Meteorol., 124: 81–97.

UNESCO Vineyard Landscape of Piedmont: Langhe-Roero and Monferrato Available online: http://whc.unesco.org/en/list/1390 (accessed on Jun 22, 2020).

World Meteorological Organization Centennial Observing Stations Available online: https://public.wmo.int/en/our-mandate/what-we-do/observations/centennial-observing-stations (accessed on Jun 22, 2020).

Italian Journal of Agrometeorology
Rivista Italiana di Agrometeorologia

Firenze University Press
www.fupress.com/ijam

Citation: S.Z. Todorović, S.M. Ivanović, N.Lj. Bogdanov (2021) The influence of extreme weather events on farm economic performance – a case study from Serbia. *Italian Journal of Agrometeorology* (1): 51-62. doi: 10.36253/ijam-1073

Received: September 6, 2020

Accepted: June 4, 2021

Published: August 9, 2021

Data Availability Statement: All relevant data are within the paper and its Supporting Information files.

Competing Interests: The Author(s) declare(s) no conflict of interest.

The influence of extreme weather events on farm economic performance – a case study from Serbia

Saša Z. Todorović, Sanjin M. Ivanović*, Natalija Lj. Bogdanov

University of Belgrade, Faculty of Agriculture, Nemanjina 6, 11080 Belgrade, Zemun, Republic of Serbia
*Corresponding author. E-mail: sanjinivanovic@agrif.bg.ac.rs

Abstract. Western Balkan region, particularly Serbia, is faced with an increased frequency of extreme weather events, as a consequence of global climate change. However, there is still no enough research on how the effects of extreme weather events could be measured on the farm level. More importantly, there is no standard international methodology that is used regularly to address the issue. Therefore, the aim of this research was to evaluate the effects of extreme weather events on business performances of two the most common farm types in Serbia. To achieve this goal, the authors performed a financial loss assessment on a farm level. Panel models and R software environment were used to perform a multiple regression analysis allowing to indicate determinants of financial loss indicator depending on the farm's production type. The results indicated that performance of both farm types is more influenced by drought than by floods. The regression analysis revealed that for both farm types financial stress is the most important independent variable.

Keywords: flood, drought, climate change, type of farming, regression analysis.

INTRODUCTION

Irrespective of the fact that there is a considerable amount of scientific evidence on denying climate change (Dunlap, 2013; Björnberg et al., 2017; Karlsson and Gilek, 2020), there is a widespread agreement that the climate changes (Pachauri et al., 2014) and that humans seem to be responsible for it (Cook et al., 2016). It significantly impacts agriculture and food systems (Gornall et al., 2010; FAO 2016) as the effects become more pronounced (McCallum et al., 2013).

In the Europe, the climate changes have already caused a shift of agroclimatic zones to the north, prolonged growing season and increased active temperature accumulation (Peltonen-Sainio et al., 2009; EEA, 2019). The predictions are that these processes will continue by the end of century, resulting in an increase in drought frequency and intensity in the Mediterranean area, western Europe and northern Scandinavia (under the climate scenario RCP 4.5), and/or more intense droughts all over Europe (under the worst-

case climate scenario RCP 8.5) (Spinoni et al., 2018). Yet, the effects of climate change vary by regions, as well as predictions of future scenarios and seasonal patterns. The predictions are that in southern Europe agriculture sector will be adversely affected by an increase of the heat wave intensity (high confidence) (Kovats et al., 2014; IPCC, 2019); that the migration of agro-climatic zones in eastern Europe will be twice as fast as that recorded during the period 1975-2016 (EEA, 2019); and that extreme precipitation in northern Europe will increase (Kovats et al., 2014; Zampieri et al., 2017).

The impact assessments of climate changes on agriculture sector have been extensively examined, at a multiple scales and in a variety of contexts (Moore and Lobell, 2014; Olsen and Bindi, 2002), yet without considering the complex interdependencies within human and environmental systems (Harrison et al., 2015). However, various scenarios of future change in climate variables impacting the productivity of agriculture sector, predict similar patterns of changes in crop yields for the EU 2080s: southern Europe would experience yield decreases (25% under 5.4°C scenario), central Europe regions would have moderate yield changes, whereas the northern Europe regions would benefit from growing yields (Ciscar et al., 2009; Iglesias et al., 2012; Knox et al., 2016).

According to Zurovec et al. (2015) on the territory of Western Balkan drought is "frequent adverse climatic event over the last decade". In Serbia, there is an increase in average annual temperatures of about 0.6°C/100 years, with a higher trend in the northern and mountainous parts of the country (MAEP, 2015). Nonetheless, compared to the second half of the twentieth century, Serbia has been exposed to more frequent extreme weather occurrences and natural catastrophes in the recent two decades. As per relevant studies, there were 2,000 natural disasters in Serbia between 1980 and 1990, with 2,800 instances documented throughout the 1990s (Kovačević et al., 2012; Lukić et al., 2013; Anđelković and Kovač, 2016). Within the first two decades of the twenty-first century, these patterns remained as the severity and frequency of natural disasters grew and became more extreme. Serbia was affected by severe floods in 1999, 2002, 2005, 2006, and 2014, with most of them taking place during the growing period (April–June) (FAO, 2020).

At the same period of time (1999 – 2019), Serbia experienced above-average temperatures followed by drought in 2003, 2007, 2012, 2015, and 2017. Additionally, the 2012 and 2017 years were among the driest, with record-low rainfall, severely impacting Serbia's agricultural output (FAO, 2020). Temperatures surpassed 35°C for more than 50 days in a row in 2012, resulting in a loss of crop output of over one million hectares and damage caused of more than $141 million (USAID, 2017).

The results of the temperature forecast show an increase in temperature between 0.5°C and 2°C in the next fifty years. The recent regional climate models indicate that in the near future can be expected surplus rainfall in summer and early autumn period (which is in line with current trends), as well as the significant drop in precipitation in the distant future. Regional Climate Model (RCM) also suggests for Serbia an average annual decrease in precipitation, ranging from 0% to 25% / 100 years (MAEP, 2015).

Considering the high importance of agriculture sector for Serbian economy (forming of about 7% of Gross domestic products (GDP)), and livelihood of rural dwellers (40% of total population), the economic losses and damages caused by climate changes can have a profound effects. Despite the large number of studies examining the effects of climate change on individual sectors (Stričević et al., 2020), crop yields (Jančić, 2013), and regions (Lalić et al., 2011; Armenski et al., 2014), the impact on farmers income has not been systematically assessed, mostly due to the lack of data at the level of individual farms or smaller territorial units. Hence, both agricultural producers and policy makers are deprived of the number of important inputs relevant for decision making.

This paper aims to fulfil the gap in understanding the economic effects of climate change on dominant types of farms in Serbia. To determine this, we conducted analysis of selected financial indicators of farm performances in the 14 districts of Serbia which were, in two consecutive years, affected by both floods (2014) and drought (2015). In 2014 heavy rainfall and flooding severely affected many parts of Serbia's territory. According to estimations provided by different sources, in total, 1.6 million people, and 34,500 family holdings were affected by flood and related disasters (WB, 2015; FAO, 2015). The following year (2015) was characterized by extreme drought which affected majority of Serbian territory causing significant drop in most crop yields. In addition to these two years, the analysis also included 2016, during which the weather conditions were stable.

A wide variety of approaches have been used in the different countries/regions to determine the damage caused by extreme weather events. Most of the methods used for economic evaluation of flood damage in agriculture are limited to the national level, while "little research is carried out on the transferability of local methodologies" (Brémond et al., 2013). Research con-

ducted by Cogato et al. (2019) revealed that the relations between extreme weather events, food security and economic loss are of major interest within scientific community. Nevertheless, authors noticed "low level of international collaboration of the vulnerable countries" related to research of extreme weather events, while "developing countries have only more recently been approached through international research". Similarly, Jongman et al. (2012) emphasized the need to develop models for flood damage assessment not only on European but also on global level. Merz et al. (2010) discussed that attention is usually paid to flood hazard assessment, while flood damage assessment "is frequently seen as some kind of appendix within the risk analysis". The authors also noticed that methodology for damage assessment related to other natural disasters (such as storms or droughts) is even less developed. Similarly, Parisse at al. (2020) stated that in future research it is necessary to "consider indicators for events such as hail and strong wind".

Messeri et al. (2015) discussed relations between weather types in Italy and frequency of floods and landslides. Considering each weather type, specific risk indexes for entire country as well as for specific Italian regions were determined (applicable on seasonal and annual level). Such approach could help in appropriate planning, prevention and reduction of damages caused by unfavourable weather events. Vallorani et al. (2018) discussed relations between large-scale circulation and local climate because they "could be useful to evaluate the weather and climate risk on a regional scale linked to extreme weather conditions such as heavy precipitation, flood or drought events and heat waves or cold spells". In such a way it is possible to develop adequate tools (applications) which are "related to water and energy resources management, agronomy, severe weather risk prevention and seasonal forecasts".

Generally, approaches used in assessing the effects of natural hazards may be summarized within the two main concepts – economic loss assessment and financial loss assessment (Penning-Rowsell et al., 2013):

- An economic loss assessment is usually performed on a macro-scale level (i.e. for the entire country or region, usually larger than the affected area) by macroeconomic variables, such as changes in GDP, changes in the output volume and the trade balance, employment etc.
- A financial loss assessment is performed on a micro-scale level (farm) or at the meso-level (of a local community), while the crop damage is usually used as a simplistic proxy of the total damage.

When assessing financial loss in agriculture, various economic indicators are used in the existing literature. According to comprehensive review conducted by Brémond et al. (2013) the most frequently used indicators for estimation of financial loss in plant production are the Gross product and Gross margin adjusted with variable costs. Similarly, Thieken et al. (2008) used percentile deduction of average revenues to calculate crop loss related to flood damage, while Jega (2018) analyzed changes in income of smallholder farmers to evaluate effects of flood disasters. Antolini et al. (2020) used HAZUS-MH estimation model to evaluate crop loss by multiplying damage to crops by crop prices. In the same way Shrestha et al. (2018) performed flood damage assessment by estimation of yield loss and its multiplication by the value of farm gate price. Torrente (2012) explained post disaster losses in agriculture as forgone output (income) as a result of disaster as well as higher production costs.

Vega-Serratos et al. (2018) estimated the damage caused by floods on the basis of production costs of the crop (depending on the phase in its production). Analyzing performance of farms affected by drought, Lawes and Kingwell (2012) used indicators such as return on capital, business equity, the debt-to-income ratio and operating profit per hectare, while Kingwell and Xayavong (2017) also used retained profit per hectare.

MATERIALS AND METHODS

A vast amount of data from both primary and secondary sources needs to be considered in performing analysis of financial loss assessments caused by extreme weather events. The key challenge of data collection relates to the availability of data at lower territorial units from official public sources (statistics, registers, state agencies), while economic data on the farm level is often scarce and may lack accuracy and reliability due to the different methods of data collection and aggregation. Therefore, data on economic and structural characteristics of farms in 14 affected districts (107 farms, out of which 70 farms with mixed crop and livestock production and 37 farms specialized for crop production) was used as a base for panel models. The study area was selected to cover the municipalities which in two consecutive years were affected by both floods (2014) and drought (2015) (Figure 1).

The study area has a continental climate, warm and humid from June through September and cold and dry from December through February. Precipitation occurs throughout the year, but there is a peak in May through July (one third of the annual precipitation). However, climate projections show that these districts in the future

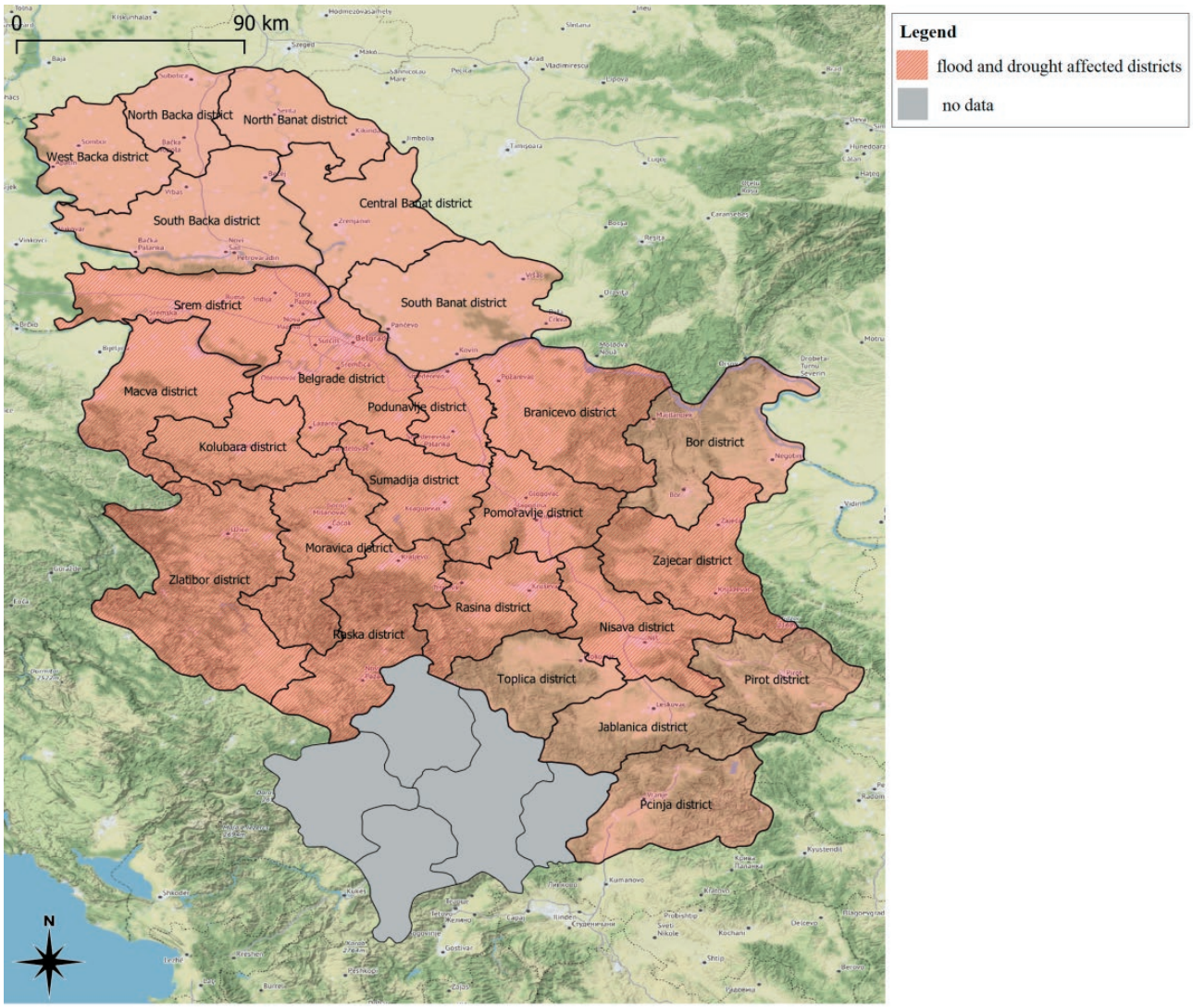

Figure 1. Districts of Serbia which were, in two consecutive years, affected by both floods (2014) and drought (2015). Since the data for the territory of Autonomous Province of Kosovo and Metohija have not been available for the analyzed period, all data and estimates refer to Serbia but without this province.

will experience decrease in precipitation and increase in temperature, especially in summer, compared to an average precipitation and temperature for the period 1979-2013 (Figure 2) and increasing risk of extreme rainfall days and river floods (Alfieri et al., 2017).

Primary data set (which has not been initially collected for the purposes of assessing influence of extreme weather events on farm economic performance) was formed of the database created as a result of an annual survey on a representative sample of farms in these districts. The data were verified through focus groups discussions with farmers in affected districts. To gain a more detailed insight into the support measures and types of assistance to farms in the years with extreme weather events (that could significantly influence the farm business results) semi-structured interviews with institutions and government line agencies were also conducted.

Due to the lack of the official data on economic results of farms within the time period covered by this analysis, the described approach can be considered as sufficiently reliable. A retrospective questionnaire on the selected sample would be less reliable because it would be necessary to collect a large number of economic indicators for previous years (prices, yields, and production costs) based on (unreliable) recollection of the farmers.

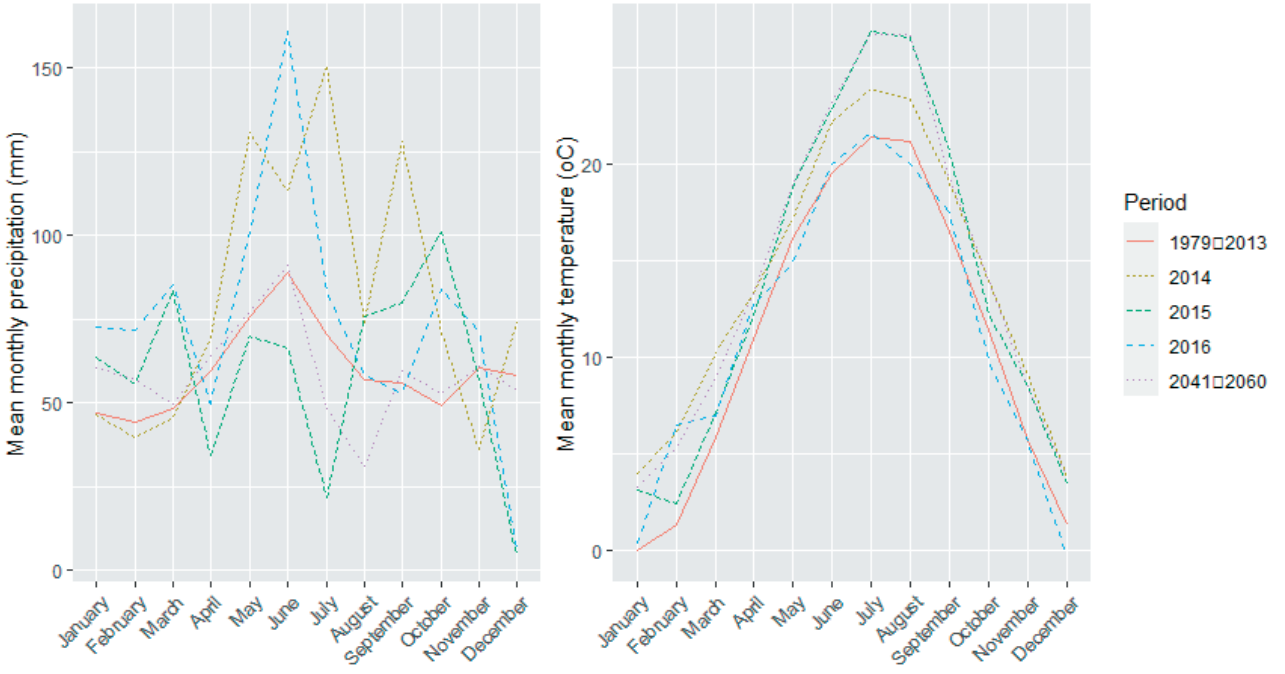

Figure 2. Mean monthly precipitation (mm) and temperature (°C) in study area. (Source: Authors calculations based on TerraClimate dataset, climatic variables 2014-2016, 4 km spatial resolution and CHELSA database, climatic variables 1979-2013, 1 km spatial resolution with future projections, under the climate scenario RCP 8.5). [TerraClimate is a dataset of monthly climate and climatic water balance for global terrestrial surfaces from 1958-2015 (Abatzoglou et al., 2015). CHELSA (Climatologies at high resolution for the earth's land surface areas) is a high resolution (30 arc sec) climate data set for the earth land surface areas currently hosted by the Swiss Federal Institute for Forest, Snow and Landscape Research WSL (Karger et al., 2017a, 2017b)].

In this analysis, as indicators for financial loss assessment, Gross product (GP) and Gross margin adjusted with variable costs (GMAVC) were used. The GP represents the total value of all the products and services produced at a particular farm in a particular year (regardless of whether the products were sold, stored at the end of the year, or used in the household or on the farm). The GP comprises of the crop production, livestock production and other products and services (such as contracted work for others, rural tourism etc.), and is calculated in the following way:

$$\text{Gross product} = \text{Total value of crop production} + \text{Total value of livestock production} + \text{Value of other products and services related to the farm}$$

As already mentioned, majority of authors directly used the variation in the GP as a proxy for crop damage. However, this approximation overlooks variation in production costs due to extreme weather events, so this indicator does not reflect the real changes in the results of the farm business operations caused by the floods or droughts. Therefore, in addition to the GP, the other indictor - the gross margin adjusted with variable costs is also used:

$$\text{Gross margin adjusted with variable costs} = \text{Gross product} + \text{Total subsidies (excl. subsidies on investments)} - \text{Adjusted variable costs}$$

Contrary to the GP, the GMAVC takes into account some variable production costs, which are usually caused by the floods or droughts. These variable costs include, for example, seed costs, plant protection products and fertilizers costs, feed costs and the like (which are expected to be higher if the farm production is renewed/restored in the same year). On the other hand, some costs can decrease, for example harvesting costs related to drought affected crops. In this way, GMAVC allows better determining of the impacts of extreme weather events on the changes in farm economic performance.

In this paper, Gross products and Gross margin adjusted with variable costs were determined for the flood year (2014), for year with extreme drought (2015),

as well as for the following year (2016) which was characterised by average climatic conditions.

Considering that GMAVC provides better understanding of farms performance, the effort is made to obtain the panel models. These models characterize the determinants of the GMAVC according to the farm's type of production. Balanced panel data set consisting of 107 farms (70 farms with mixed crop and livestock production and 37 farms specialized for crop production) was used as a base for panel models, while R software environment for statistical computing and graphics was used to perform a multiple regression analysis allowing to indicate determinants of GMAVC depending on the farm's production type.

The most general formulation of a panel data model may be expressed as the following equation (Baltagi, 2005):

$$yi,t = \alpha i + X'i,t\,\beta + ui,t + \varepsilon i,t \quad (1)$$

with i (i = 1,..., N) denoting individuals, t (t = 1,..., T) denoting time periods, and $X'i,t$ denoting the observation of K explanatory variables in farm i and time t.

It should be noted that αi is time invariant and accounts for any individual-specific effect not included in the regression equation. Two different interpretations may be given to the αi, and, consequently, two different basic models may be distinguished. If the αi's are assumed to be fixed parameters to be estimated, the model expressed in the equation (1) is fixed effect panel data model (FEM). Conversely, if the αi's are assumed to be random, the random effect panel data model (REM) is generated (Arbia and Piras, 2005). Fixed effect model is particularly suitable when the regression analysis is limited to a precise set of individuals, farms or regions; random effect, instead, is an appropriate specification if a certain number of individuals are drawn randomly from a large population of reference (Arbia and Piras, 2005).

In order to choose between REM and FEM approach, the Hausman test is used. The null and alternative hypotheses of Hausman test are (Adkins, 2014):

$Ho : Cov(xi; ei) = 0$, against $Ha : Cov(xi; ei) \neq 0$.

In order to estimate the model, a set of variables describing characteristics of the farm, human capital and technology employed is used (Table 1).

Table 1. Dependant and independent variables used in panel models.

Variable	Description
y Gross margin adjusted with variable costs (EUR)	*Gross product (EUR) + Total subsidies excluding subsidies on investments (EUR) - Adjusted variable costs (EUR)*
x1 Age of farm manager (years)	
x2 Share of rented land (%)	*Rented Utilised Agricultural Area (ha) / Total Utilised Agricultural Area (ha)*
x3 Share of hired labour (%)	*Paid labour input (AWU) / Total labour input (AWU)*
x4 Capital to land ratio (EUR / ha)	*(Depreciation (EUR) + Interest paid (EUR)) / Total Utilised Agricultural Area (ha)*
x5 Capital to labour ratio (EUR / hours)	*(Depreciation (EUR) + Interest paid (EUR)) / Total labour input (hours)*
x6 Labour to land ratio (hours / ha)	*Total labour input (hours) / Total Utilised Agricultural Area (ha)*
x7 Financial stress	*(Rent paid (EUR) + Interest paid (EUR)) / Total output crops & crop production (EUR)*
x8 Marketability of production (%)	*(Total Output (EUR) – Farmhouse Consumption (EUR) - Farm use (EUR)) / Total Output (EUR)*
x9 Percentage of costs of external factors (%)	*Total external factors (wages, rent and interest paid) (EUR) / Family Farm Income (EUR)*
x10 Number of crops grown on farms	

Source: The variables were derived from database of the research team.

RESULTS AND DISCUSSION

A financial loss assessment was conducted on the sample of farms representing the dominant farm types in the affected districts. Farm types were determined based on the share of different lines of production in the gross product of a particular farm. Two types of farms-mixed farms for crop and livestock production, as well as farms specialized for crop production were selected for further analysis because these farm types are dominant in the analyzed districts. According to the data of Farm structure survey conducted in Serbia in 2018, these farm types represent 34.24% (mixed farms for crop and livestock production) and 14.93% (farms specialized for crop production) of total number of farms in analysed districts (SORS, 2019). The key structural characteristics of selected farms are presented in Table 2.

The results indicated that extreme weather events had a different impact on analyzed farm types (Table 3). The GP of farms with mixed crop and livestock production was particularly affected in flood year (2014). It rose in the following year (2015) characterized with drought, and continued to increase in the year with regular weather conditions (2016). On the other hand, the 2015 drought caused a significant decrease in GP of

Table 2. Descriptive statistics of the sample by farm types.

Indicators / Variables	Unit	2014		2015	
		Mean	Standard Deviation	Mean	Standard Deviation
Mixed farms for crop and livestock production (70 farms)					
Structural characteristics					
Farm size	ha	17.54	15.14	16.96	13.42
Livestock units	LU[1)]	9.18	7.46	12.02	10.43
Total labour input	AWU[2)]	2.61	1.14	2.53	1.10
Panel model					
Age of manager	years	45.81	11.80	46.76	11.83
Share of rented land	%	32.00%	30.51%	31.19%	29.43%
Share of hired labour	%	9.50%	13.40%	7.90%	13.61%
Capital to land ratio	EUR per ha	156.73	137.81	229.55	187.81
Capital to labour ratio	EUR per hours	0.64	0.88	0.81	0.79
Labour to land ratio	hours per ha	415.49	304.18	397.93	266.51
Financial stress		0.03	0.05	0.03	0.05
Marketability of production	%	69.41%	22.08%	65.32%	27.35%
Percentage of costs of external factors	%	8.64%	134.08%	16.22%	82.17%
Number of crops grown on farms		2.83	1.05	2.87	1.20
Farms specialized for crop production (37 farms)					
Structural characteristics					
Farm size	ha	62.45	80.45	64.29	82.05
Livestock units	LU	1.51	2.67	1.26	2.53
Total labour input	AWU	2.29	1.26	2.14	1.00
Panel model					
Age of manager	years	47.59	11.27	47.81	11.46
Share of rented land	%	49.11%	32.06%	53.80%	28.47%
Share of hired labour	%	15.42%	19.09%	10.47%	17.82%
Capital to land ratio	EUR per ha	183.94	194.76	184.58	103.91
Capital to labour ratio	EUR per hours	3.22	5.10	3.74	6.17
Labour to land ratio	hours per ha	318.62	593.91	220.97	360.13
Financial stress		0.06	0.05	0.08	0.06
Marketability of production	%	93.33%	12.05%	96.24%	6.74%
Percentage of costs of external factors	%	21.39%	102.71%	15.04%	135.25%
Number of crops grown on farms		2.89	1.26	2.76	1.21

[1] Livestock unit.
[2] Annual work unit is the full-time equivalent employment, i.e. the total hours worked divided by the average annual hours worked in full-time jobs (1,800 hours).
Source: authors' calculations.

farms specialized for crop production (comparing with the year characterized with floods). These indicate that GP of mixed farms is more vulnerable to floods than to drought. On the other hand, GP of specialised crop farms is more affected by drought, because the damage caused by floods could be compensated to some extent by resowing the part of the flooded land.

Analysing values of GMAVC for the observed farm types and weather conditions, it was determined that both farm types were more influenced by drought than by floods, while negative effect of drought on GMAVC was more important for specialized crop farms.

The results indicate that the changes in both the GP and GMAVC for specialized crop farms are similar, which is not the case with mixed crop – livestock farms. The results of the analysis also confirm that the mixed crop–livestock farming systems, with diversified sources of income, made GP and GMAVC of these farms less risky and less dependent on extreme weather events over the observed period.

Table 3. The changes of GP and GMAVC by type of farms in case study regions.

Years	Mixed farms for crop and livestock production Basic indices (2016=100)		Specialised farms for crop production Basic indices (2016=100)	
	Gross product	Gross margin adjusted with variable costs	Gross product	Gross margin adjusted with variable costs
2014 (year of floods)	91.82%	90.17%	98.41%	92.96%
2015 (year of drought)	94.31%	88.22%	89.91%	81.64%
2016 (usual production conditions)	100.00%	100.00%	100.00%	100.00%

Source: authors' calculations.

To extend the understanding of the problem, multiple regression analysis is performed resulting in the random effect models (REM) for GMAVC. In other words, based on the Hausman test, REM proved to be more appropriate than FEM approach for evaluation of GMAVC indicator. The results of the estimation of its parameters according to the type of production are presented in Table 4.

The impact of independent variables on GMAVC depends on the type of production. For the specialized crop farms the share of rented land and capital to labour ratio are the most important (level of significance $p<0.01$). On the other hand, for the mixed crop and livestock farms number of important independent variables at the same level of significance is much higher (the share of rented land, share of hired labour, capital to labour ratio, labour to land ratio, financial stress and marketability of production). At the same time, estimation of regression equation is better for mixed crop and livestock farms.

In the obtained models, one independent variable - financial stress has negative statistically significant influence on dependent variable GMAVC of both types of farms. Besides, the same effect could be noticed for capital to land ratio and labour to land ratio in a model describing mixed crop and livestock farms.

On the other hand, there are two independent variables (share of rented land and capital to labour ratio) which have positive statistically significant influence on dependent variable GMAVC of both types of farms. The highest positive influence on GMAVC is exerted by the share of rented land (for specialized crop farms) and marketability of production (for mixed crop and livestock farms).

Table 4. Panel models for GMAVC by the type of production.

Dependent variable in the models:	Gross margin adjusted with variable costs	
	Specialized crop farms	Mixed crop and livestock farms
Hausman Test	$\chi^2(10) = 6.7649$ (0.7474)	$\chi^2(10) = 13.437$ (0.2002)
Model's type	REM	REM
Independent variables in the models:		
Constant	1,110.472	-6,895.491
	(48,716.070)	(8,150.715)
X1 Age of manager (years)	-654.450	3.805
	(427.502)	(109.137)
X2 Share of rented land (%)	53,259.920***	16,172.320***
	(20,616.470)	(5,149.191)
X3 Share of hired labour (%)	31,906.610	*29,735.810***
	(22,676.150)	(9,331.109)
X4 Capital to land ratio (EUR / ha)	6.401	*-22.481***
	(31.573)	(9.046)
X5 Capital to labour ratio (EUR / hours)	4,794.260***	11,532.420***
	(893.845)	(2,476.407)
X6 Labour to land ratio (hours / ha)	4.950	*-15.527****
	(12.107)	(5.386)
X7 Financial stress	-199,869.900**	-178,593.000***
	(100,673.400)	(38,130.930)
X8 Marketability of production (%)	2,563.432	*34,943.620****
	(38,256.420)	(4,722.506)
X9 Percentage of costs of external factors (%)	-85.142	-375.230
	(2,131.955)	(1,019.573)
X10 Number of crops grown on farms	*8,296.196***	-129.755
	(3,502.391)	(1,163.260)
Observations	74	140
R^2	0.481	0.552
Adjusted R^2	0.398	0.517

Levels of significance: *p<0.1; **p<0.05; ***p<0.01
Note: REM - Random-effects model; Standard error of the coefficients estimates are shown in round brackets.
Source: Authors' calculations.

CONCLUSIONS

There is a growing concern among policy makers about the effect of climate change on food security and

farmers' income. Considering the already observed climate change trends and projections, climate conditions will affect agricultural sector in Serbia in many ways. Therefore, it is important to research and understand the potential impacts of extreme weather events on changes in farmers' income of different farm types.

In this research we examined the impact of extreme weather events on business performances of the two most common farm types in Serbia, by applying a farm-scale approach. Panel models and R software environment were used to perform a multiple regression analysis to indicate determinants of financial loss indicator for both farm types. The results of GMAVC indicator (which considers not only variations of GP but also changes in the appropriate variable costs) indicate that performances of both farm types are more sensitive to drought than to floods. It is also determined that specialized crop farms are more vulnerable to extreme weather events comparing to mixed farms for crop and livestock production.

The results of panel models reveal that financial stress is the variable which dominantly negatively impacts GMAVC for both farm types. This indicated the high relevance of rent and interest costs on economic performance of farms in years characterized with extreme weather events. On the other hand, an increase of share of rented land has positive impact on GMAVC. Therefore, keeping rent paid per hectare at a low level as well as finding ways to decrease interest cost (primarily using loans subsidized by the state) is the key for reducing financial stress of the farms in the years to follow.

The obtained results confirm previous findings indicating the great influence of drought on the decrease of farm economic performance. Therefore, increasing frequency of droughts creates significant risk not only for livelihood of farm households, but also for an overall stability and growth of agricultural sector.

Incentives for adaptation and mitigation of climate change are available to Serbian farmers. Such incentives include investment subsidies for purchase of agricultural machinery, equipment and buildings in plant and livestock production (including anti hail nets, covering materials for frost protection, shade nets and irrigation systems for frost protection) as well as subsidies aiming to reduce risk related to climate change (subsidized insurance premiums).

Nevertheless, agricultural extension services in cooperation with scientific institutions are the key actors in dissemination of knowledge and information concerning climate change and mitigation measures. However, their capacity to play that role are rather limited because they are in charge of number of other tasks, they have the lack of human resources as well as limited technical possibilities.

There is not enough knowledge on effects of extreme weather events on production and economic results of agriculture. There is even less research regarding its influence on certain farm types, agricultural sectors, regions or agricultural products. The existing models and simulations of climate changes do not include economic variables (especially not on the level lower than the national one). Our findings could provide a useful contribution to evidence-based policy making, i.e. to the improvement of the set of mitigation measures provided by national agricultural policy.

ACKNOWLEDGEMENTS

This paper is a result of the research funded by the Ministry of Education, Science and Technological Development of the Republic of Serbia based on the agreement between the Ministry and the Faculty of Agriculture, University of Belgrade (Contract No. 451-03-9/2021-14/200116), on the realisation and financing of scientific research in 2021.

REFERENCES

Abatzoglou J. T., Dobrowski S. Z., Parks S. A., Hegewisch K. C., 2018. Terraclimate, a high-resolution global dataset of monthly climate and climatic water balance from 1958-2015. *Scientific Data*, 5: 170191. https://doi.org/10.1038/sdata.2017.191

Adkins L. C., 2014. *Using GRETL for Principles of Econometrics*. 4th Edition Version 1.041, Oklahoma State University, Oklahoma.

Alfieri L., Bisselink B., Dottori F., Naumann G., De Roo A., Salamon P., Wyser K., Feyen L., 2017. Global projections of river flood risk in a warmer world. *Earth's Future*, 5: 171-182. https://doi.org/10.1002/2016EF000485

Anđelković B., Kovač M., 2016. *Human Development Report - Serbia 2016; Social Capital: The Invisible Face of Resilience*. UNDP Serbia. ISBN 978-86-7728-238-7

Antolini F., Tate E., Dalzell B., Young N., Johnson K., Hawthorne P. L., 2020. Flood Risk Reduction from Agricultural Best Management Practices. *Journal of the American Water Resources Association*, 56(1): 161–179. https://doi.org/10.1111/1752-1688.12812

Arbia G., Piras G., 2005. *Convergence in per-capita GDP across European regions using panel data models extended to spatial autocorrelation effects*. Istituto di Studi e Analisi Economica (ISAE), Roma,

Working Paper. No. 51. https://doi.org/10.2139/SSRN.936327

Armenski T., Stankov U., Dolinaj D., Mesaroš M., Jovanović M., Pantelić M., Pavić D., Popov S., Popović L., Frank A., Ćosić Đ., 2014. Social and economic impact of drought on stakeholders in agriculture. *Geographica Pannonica*, 18(2): 34-42.

Baltagi B. H., 2005. *Econometric Analysis of Panel Data*. 3rd Edition, John Wiley & Sons Ltd., Chichester.

Björnberg K. E., Karlsson M., Gilek M., Hansson S. O., 2017. Climate and environmental science denial: a review of the scientific literature published in 1990–2015. *Journal of Cleaner Production*, 167: 229–241. https://doi.org/10.1016/j.jclepro.2017.08.066

Brémond P., Grelot F., Agenais A. L., 2013. Economic evaluation of flood damage to agriculture – review and analysis of existing methods. *Nat. Hazards Earth Syst. Sci.*, 13: 2493–2512. https://doi.org/10.5194/nhess-13-2493-2013

Ciscar J. C., Soria A., Goodess C. M., Christensen O. B., Iglesias A., Garrote L., Moneo M., Quiroga S., Feyen L., Dankers R., Nicholls R., Richards J., 2009. *Climate change impacts in Europe*. Final report of the PESETA research project, JRC working papers JRC55391, Joint Research Centre, Seville. https://doi.org/10.2791/32500

Cogato A., Meggio F., De Antoni Migliorati M., Marinello F., 2019. Extreme Weather Events in Agriculture: A Systematic Review. *Sustainability*, *11*: 2547. https://doi.org/10.3390/su11092547

Cook J., Oreskes N., Doran P. T., Anderegg W. R. L., Verheggen B., Maibach E. W., Carlton J. S., Lewandowsky S., Skuce A. G., Green S. A., Nuccitelli D., Jacobs P., Richardson M., Winkler B., Painting R., Rice K., 2016. Consensus on consensus: a synthesis of consensus estimates on human-caused global warming. *Environmental Research Letters*, 11(4): 048002. https://doi.org/10.1088/1748-9326/11/4/048002

Dunlap R. E., 2013. Climate change skepticism and denial: An Introduction. *American Behavioral Scientist*, 57(6): 691–698. https://doi.org/10.1177/0002764213477097

EEA, 2019. *Climate change adaptation in the agriculture sector in Europe*. European environment agency report 04/2019, Publications Office of the European Union, Luxembourg. doi:10.2800/537176

FAO, 2015. *Restoring farmers' livelihoods after severe floods in Serbia*. Food and agriculture organization of the United Nations, Rome, http://www.fao.org/in-action/restoring-farmers-livelihoods-after-severe-floods-in-serbia/en/ (10.04.2020).

FAO, 2016. *Climate change and food security: risks and responses*. FAO no 1/2016, Food and agriculture organization of the United Nations, Rome. ISBN 978-92-5-108998-9

FAO, 2020. *Smallholders and family farms in Serbia. Country study report 2019*. Budapest. https://doi.org/10.4060/ca7449en

Gornall J., Betts R., Burke E., Clark R., Camp J., Willett K., Wiltshire A., 2010. Implications of climate change for agricultural productivity in the early twenty-first century. *Philosophical Transactions of the Royal Society B: Biological Sciences*, 365(1554): 2973–2989. https://doi.org/10.1098/rstb.2010.0158

Harrison P. A., Holman I. P., Berry P. M., 2015. Assessing cross-sectoral climate change impacts, vulnerability and adaptation: an introduction to the climsave project. *Climatic Change*, 128(3–4): 153–167. https://doi.org/10.1007/s10584-015-1324-3

Iglesias A., Garrote L., Quiroga S., Moneo M., 2012. A regional comparison of the effects of climate change on agricultural crops in Europe. *Climatic Change*, 112(1): 29–46. https://doi.org/10.1007/s10584-011-0338-8

IPCC, 2019. *Climate Change and Land: an IPCC special report on climate change, desertification, land degradation, sustainable land management, food security, and greenhouse gas fluxes in terrestrial ecosystems*. Shukla P.R., Skea J., Calvo Buendia E., Masson-Delmotte V., Pörtner H-O; Roberts D.C., Zhai P., Slade R., Connors S., Van Diemen R., Ferrat M., Haughey E., Luz S., Neogi S., Pathak M., Petzold J., Portugal Pereira J., Vyas P., Huntley E., Kissick K., Belkacemi M., Malley J. (Eds.). The Intergovernmental Panel on Climate Change.

Jančić M., 2013. Climate Change Impact on Maize Yield in the Region of Novi Sad (Vojvodina). *Ratarstvo i povrtarstvo*, 50(3): 22-28.

Jega A. A., 2018. *Economic effects of flood disaster among smallholder farmers in Kelantan, Malaysia*. Ph.D. Thessis, University Putra Malaysia.

Jongman B., Kreibich H., Apel H., Barredo J. I., Bates P. D., Feyen L., Gericke A., Neal J., Aerts J. C. J. H., Ward P. J., 2012. Comparative flood damage model assessment: towards a European approach. *Natural Hazards and Earth System Sciences,* 12(12): 3733-3752. https://doi.org/10.5194/nhess-12-3733-2012

Karger D. N., Conrad O., Böhner J., Kawohl T., Kreft H., Soria-Auza R. W., Zimmermann N. E., Linder H. P., Kessler M., 2017a. Data from: *Climatologies at high resolution for the earth's land surface areas*. Dryad Digital Repository. https://doi.org/10.5061/dryad.kd1d4

Karger D.N., Conrad O., Böhner J., Kawohl T., Kreft H., Soria-Auza R.W., Zimmermann N. E., Linder H. P.,

Kessler M., 2017b. Climatologies at high resolution for the earth's land surface areas. *Scientific Data*, 4 170122: 1-20. https://doi.org/10.1038/sdata.2017.122

Karlsson M., Gilek M., 2020. Mind the gap: coping with delay in environmental governance. *Ambio*, 49(5): 1067–1075. https://doi.org/10.1007/s13280-019-01265-z

Kingwell R. S., Xayavong V., 2017. How drought affects the financial characteristics of Australian farm businesses. *Australian Journal of Agricultural and Resource Economics*, 61(3): 344-366. https://doi.org/10.1111/1467-8489.12195

Knox J., Daccache A., Hess T., Haro D., 2016. Meta-analysis of climate impacts and uncertainty on crop yields in Europe. *Environmental Research Letters*, 11(11): 113004. https://doi.org/10.1088/1748-9326/11/11/113004

Kovačević D., Oljača S., Dolijanović Z., Milić V., 2012. *Climate changes: Ecological and agronomic options for mitigating the consequences of drought in Serbia*. Third International Scientific Symposium „Agrosym 2012" Jahorina, November 15-17, Faculty of Agriculture, University of East Sarajevo, Republic of Srpska, Bosnia and Hercegovina.

Kovats R.S., Valentini R., Bouwer L.M., Georgopoulou E., Jacob D., Martin E., Rounsevell M., Soussana J.-F., 2014. *Europe*. In: Climate Change 2014: Impacts, Adaptation, and Vulnerability. Part B: Regional Aspects. Contribution of Working Group II to the Fifth Assessment Report of the Intergovernmental Panel on Climate Change (Barros V.R., Field C.B., Dokken D.J., Mastrandrea M.D., Mach K.J., Bilir T.E., Chatterjee M., Ebi K.L., Estrada Y.O., Genova R.C., Girma B., Kissel E.S., Levy A.N., MacCracken S., Mastrandrea P.R., White L.L. (Eds.). Cambridge University Press, Cambridge, United Kingdom and New York, NY, USA, pp. 1267-1326.

Lalić B., Mihailović D. T., Podraščanin Z., 2011. Future State of Climate in Vojvodina and Expected Effects on Crop Production. *Ratarstvo i povrtarstvo*, 48(2): 403-418.

Lawes R. A., Kingwell R. S., 2012. A longitudinal examination of business performance indicators for drought-affected farms. *Agricultural Systems*, 106(1): 94–101. https://doi.org/10.1016/j.agsy.2011.10.006

Lukic T., Gavrilov M., Markovic S., Komac B., Zorn M., Mladjan D., Djordjevic J., Milanovic M., Vasiljevic DJ., Vujicic M., Kuzmanovic B., Prentovic R., 2013. Classification of natural disasters between the legislation and application: experience of the Republic of Serbia. *Acta Geographica Slovenica*, 53(1): 150-164. https://doi.org/10.3986/AGS53301

MAEP, 2015. *Water Management Strategy of the Territory of the Republic of Serbia*. The "Jaroslav Černi" Water Management Institute of Belgrade, Belgrade, Serbia.

Mccallum S., Dworak T., Prutsch A., Kent N., Mysiak J., Bosello F., Klostermann J., Dlugolecki, A., Williams E., König M., Leitner M., Miller K., Harley M., Smithers R., Berglund M., Glas N., Romanovska L., Van de Sandt K., Bachschmidt R., Völler S., Horrocks L., 2013. *Support to the development of the EU strategy for adaptation to climate change: background report to the impact assessment, part I – problem definition, policy context and assessment of policy options*. Environment Agency Austria, Vienna.

Merz B., Kreibich H., Schwarze R., Thieken A., 2010. Assessment of economic flood damage. *Natural Hazards and Earth System Sciences*, 10(8): 1697-1724. doi:10.5194/nhess-10-1697-2010

Messeri A., Morabito M., Messeri G., Brandani G., Petralli M., Natali F., Grifoni D., Crisci A., Gensini G., Orlandini S., 2015. Weather-Related Flood and Landslide Damage: A Risk Index for Italian Regions. *PLoS ONE*, 10(12): e0144468. https://doi.org/10.1371/journal.pone.0144468

Moore F. C., Lobell D. B., 2014. Adaptation potential of European agriculture in response to climate change. *Nature Climate Change*, 4(7): 610–614. https://doi.org/10.1038/nclimate2228

Olesen J. E., Bindi M., 2002. Consequences of climate change for European agricultural productivity, land use and policy. European Journal of Agronomy, 16(4): 239–262. https://doi.org/10.1016/s1161-0301(02)00004-7

Pachauri R. K., Allen M. R., Barros V. R., Broome J., Cramer W., Christ R., Church J. A., Clarke L., Dahe Q., Dasgupta P., Dubash N. K., Edenhofer O., Elgizouli I., Field C. B., Forster P., Friedlingstein P., Fuglestvedt J., Gomez-Echeverri L., Hallegatte S., Hegerl G., Howden M., Jiang K., Jimenez Cisneroz B., Kattsov V., Lee H., Mach K. J., Marotzke J., Mastrandrea M. D., Meyer L., Minx J., Mulugetta Y., O'brien K., Oppenheimer M., Pereira J. J., Pichs-Madruga R., Plattner G. K., Pörtner H. O., Power S. B., Preston B., Ravindranath N. H., Reisinger A., Riahi K., Rusticucci M., Scholes R., Seyboth K., Sokona Y., Stavins R., Stocker T. F., Tschakert P., Van Vuuren D., Van Ypserle J. P., 2014. *Climate change 2014: synthesis report. Contribution of working groups I, II and III to the fifth assessment report of the intergovernmental panel on climate change*. In: R. Pachauri and L. Meyer (Eds.), p. 151, IPCC, Geneva, Switzerland. ISBN 978-92-9169-143-2

Parisse B., Pontrandolfi A., Epifani C., Alilla R., De Natale F., 2020. An agrometeorological analysis of

weather extremes supporting decisions for the agricultural policies in Italy. *Italian Journal of Agrometeorology*, 1: 15-30. https://doi.org/10.13128/ijam-790

Peltonen-Sainio P., Jauhiainen L., Hakala K., 2009. Climate change and prolongation of growing season: changes in regional potential for field crop production in Finland. *Agricultural and Food science*, 18(3–4): 171-190. https://doi.org/10.2137/145960609790059479

Penning-Rowsell E. C., Priest S., Parker D., Morris J., Tunstall S., Viavattene C., Chatterton J., Owen D., 2013. *Flood and Coastal Erosion Risk Management: a Manual for Economic Appraisal*, Routledge. ISBN 9780415815154

Shrestha B. B., Sawano H., Ohara M., Yamazaki Y., Tokunaga Y., 2018. *Methodology for agricultural flood damage assessment*. In: Recent Advances in Flood Risk Management, IntechOpen, p. 1-19. https://doi.org/10.5772/intechopen.81011

SORS, 2019. *Farm Structure Survey (FSS) 2018*. Statistical office of the Republic of Serbia, Belgrade, Serbia. https://data.stat.gov.rs/ (15.04.2020).

Spinoni J., Vogt J. V., Naumann G., Barbosa P., Dosio A., 2018. Will drought events become more frequent and severe in Europe? *International Journal of Climatology*, 38(4): 1718-1736. https://doi.org/10.1002/joc.5291

Stričević R. J., Lipovac A. D., Prodanović S. A., Ristovski M. A., Petrović-Obradović O. T., Đurović N. L., Đurović D. B., 2020. Vulnerability of agriculture to climate change in Serbia – farmers' assessment of impacts and damages. *Journal of Agricultural Sciences (Belgrade)*, 65(3): 263-281. https://doi.org/10.2298/JAS2003263S

Thieken A. H., Ackermann V., Elmer F., Kreibich H., Kuhlmann B., Kunert U., Maiwald H., Merz B., Müller M., Piroth K., Schwarz J., Schwarze R., Seifert I., Seifert J., 2008. *Methods for the evaluation of direct and indirect flood losses*. 4th International Symposium on Flood Defense: Managing Flood Risk, Reliability and Vulnerability, Toronto, Ontario, Canada, May 6-8. Institute for Catastrophic Loss Reduction.

Torrente E. C., 2012. *Post Disaster Damage, Loss and Needs Assessment in Agriculture*. Guidance note. FAO, Sub-regional office for the Pacific islands.

USAID, 2017. *Climate Risk Profile: Serbia.* United States Agency for International Development, https://www.climatelinks.org/sites/default/files/asset/document/2017_USAID_Climate%20Change%20Risk%20Profile_Serbia.pdf (10.04.2020).

Vallorani R., Bartolini G., Betti G., Crisci A., Gozzini B., Grifoni D., Maracchi G., 2018. Circulation type classifications for temperature and precipitation stratification in Italy. *International Journal of Climatology*, 38(2): 915-931. https://doi.org/10.1002/joc.5219

Vega-Serratos B. E., Domínguez-Mora R., Posada-Vanegas G., 2018. Seasonal flood risk assessment in agricultural areas. *Tecnología y Ciencias del Agua*, 9(3): 91-127. https://doi.org/10.24850/j-tyca-2018-03-04

WB, 2015. *Floods Emergency Recovery Project (P152018)*. World Bank Report No.: PIDA12087, http://documents1.worldbank.org/curated/en/390211468294331189/pdf/PID-Appraisal-Print-P152018-09-04-2014-1409835763732.pdf (10.04.2020).

Zampieri M., Ceglar A., Dentener F., Toreti A., 2017. Wheat yield loss attributable to heat waves, drought and water excess at the global, national and subnational scales. *Environ Res Lett*, 12(6): 064008. https://doi.org/10.1088/1748-9326/aa723b

Zurovec O., Vedeld P.O., Sitaula B.K., 2015. Agricultural Sector of Bosnia and Herzegovina and Climate Change - Challenges and Opportunities. *Agriculture, 5(2)*: 245-266. https://doi.org/10.3390/agriculture5020245

Italian Journal of Agrometeorology
Rivista Italiana di Agrometeorologia

Firenze University Press
www.fupress.com/ijam

OPEN ACCESS

Citation: E.E. Başakın, Ö. Ekmekcİoğlu, M. Özger, N. Altınbaş, L. Şaylan (2021) Estimation of measured evapotranspiration using data-driven methods with limited meteorological variables. *Italian Journal of Agrometeorology* (1): 63-80. doi: 10.36253/ijam-1055

Received: August 18, 2020

Accepted: March 21, 2021

Published: August 9, 2021

Data Availability Statement: All relevant data are within the paper and its Supporting Information files.

Competing Interests: The Author(s) declare(s) no conflict of interest.

Estimation of measured evapotranspiration using data-driven methods with limited meteorological variables

Eyyup Ensar Başakın[1,*], Ömer Ekmekcİoğlu[1], Mehmet Özger[1], Nilcan Altınbaş[2], Levent Şaylan[2]

[1] *Hydraulics Division, Civil Engineering Department, Istanbul Technical University, Maslak 34469, Istanbul, Turkey*
[2] *Department of Meteorological Engineering, Faculty of Aeronautics and Astronautics, Istanbul Technical University, Maslak 34469, Istanbul, Turkey*
*Corresponding author. E-mail: basakin@itu.edu.tr

Abstract. Determination of surface energy balance depends on the energy exchange between land and atmosphere. Thus, crop, soil and meteorological factors are crucial, particularly in agricultural fields. Evapotranspiration is derived from latent heat component of surface energy balance and is a key factor to clarify the energy transfer mechanism. Development of the methods and technologies for the aim of determining and measuring of evapotranspiration have been one of the main focus points for researchers. However, the direct measurement systems are not common because of economic reasons. This situation causes that different methods are used to estimate evapotranspiration, particularly in locations where no measurements are made. Thus, in this study, non-linear techniques were applied to make accurate estimations of evapotranspiration over the winter wheat canopy located in the field of Atatürk Soil Water and Agricultural Meteorology Research Institute Directorate, Kırklareli, Turkey. This is the first attempt in the literature which consist of the comparison of different machine learning methods in the evapotranspiration values obtained by the Bowen Ratio Energy Balance system. In order to accomplish this aim, support-vector machine, Adaptive neuro fuzzy inference system and Artificial neural network models have been evaluated for different input combinations. The results revealed that even with only global solar radiation data taken as an input, a high prediction accuracy can be achieved. These results are particularly advantageous in cases where the measurement of meteorological variables is limited. With the results of this study, progress can be made in the efficient use and management of water resources based on the input parameters of evapotranspiration especially for regions with limited data.

Keywords: bowen ratio energy balance, artificial neural network, adaptive neuro fuzzy inference system, winter wheat.

1. INTRODUCTION

Investigation of the relocation of water with events such as precipitation, surface flow, evapotranspiration and infiltration are of great importance for

the management of water resources. Throughout the world, clean water resources are gradually decreasing due to climate change and, most importantly, inadequate management of water resources in agriculture. Sustainable use of water resources is only possible through accurate monitoring of all hydrological cycle elements and utilizing this information for decision support in water resources management. Evapotranspiration (ET) is one of the most important components in hydrological cycle among the others which are precipitation, infiltration, surface and groundwater flow. Evapotranspiration can be described as the change of phase of water in the soil, plants, rivers, lakes and seas with the effect of atmospheric conditions and movement towards the atmosphere. It consists of two factors: evaporation and transpiration. Evaporation represents the conveyance of water from the water surface to the atmosphere, while transpiration accounts for the transmission of water from land to the atmosphere through plants. Evapotranspiration calculations are performed either by direct measurement or indirect methods as well as estimation methods. In this study, the Bowen Ratio Energy Balance (BREB) method was used to measure actual ET and mathematical models have been proposed using the data obtained from the measurements.

Artificial Neural Network (ANN) and Adaptive Neuro Fuzzy Inference System (ANFIS), which are frequently used in many areas in recent years, are also widely used in ET calculations (Wu *et al*., 2019; Ferreira *et al*., 2019; Maroufpoor *et al*., 2020). In addition, new machine learning techniques have been introduced such as support vector machine (SVM), gene expression programming (GEP), extreme learning machine (ELM) and the methods that enable to predict ET have been diversified. Abdullah *et al*. (2015) predicted the reference ET (ET_0) values by using ELM and feedforward backpropagation (FFBP), then compared the results with the values obtained from Penman & Monteith equation (Allen *et al*., 1998). Besides, they conducted sensitivity analysis with five variables (maximum and minimum air temperature, sunshine hours, relative humidity and wind speed) for 3 different locations. It was pointed out that the sensitivity of the variables was changed according to the location. Estimations were made with different input variations and ELM performance was found to be higher than the FFBP model with higher coefficient of determination (R^2=0.991 for ELM and R^2=0.985 for FFBP) as well as lower computation time. It has been shown that the solution in the ELM model is almost twice as fast as in the FFBP model. In addition, compared to the estimates made with all inputs, the predictions made with four inputs (without net radiation) are more successful, albeit with a slight difference.

Gocic *et al*. (2016) calculated monthly reference evapotranspiration by using ELM and compared their results with different empirical equations for a 31-year period. Minimum and maximum air temperatures, actual vapor pressure, wind speed and sunshine duration were used as inputs while the empirical equation results as the output. The outputs obtained by three different empirical equations, namely Hargreaves, Priestley–Taylor and Turc, were subjected to correlation analysis with the results of FAO Penman & Monteith equation (FPM). It is stated that the results of the three above mentioned equations have high correlations with FPM. The prediction models were established by separating the dataset as 50% training and 50% testing sets. The model performances were evaluated on the basis of empirical equations and they concluded that the Hargreaves model outperforms to models obtained by with other two equations.

Wen *et al*. (2015) predicted daily evapotranspiration using support vector machines. Predictions were conducted with limited data and the results compared with the values obtained from FAO Penman & Monteith equation. Similar to previous studies in the literature, the model with predominant maximum temperature (T_{max}) and minimum temperature (T_{min}) parameters was also evaluated by comparing with different empirical calculation methods as well as ANN results. In order to avoid dimensional differences in models, normalization was performed on each data set. As a result of the model evaluation, it was stated that SVM model showed superior performance even when the different model structures of ANN were considered. However, although the dominant parameters were expressed as T_{max} and T_{min}, it was found that the predictions made by these two inputs (R^2=0.772) performed rather poorly than the predictions made by all inputs (R^2=0.95). Similarly, Antonopoulos and Antonopoulos (2017) made predictions with ANN by using limited meteorological variables and compared the results with different empirical methods. Optimum input combination was determined with different input variations. As a result of the normalization of daily data for five years, the results of ANN model and other deterministic models were evaluated by considering the results of the widely accepted Penman & Monteith method. The most appropriate ANN structure (4-6-1) was obtained for the predictions and it was concluded that better predictions can be achieved with a smaller number of variables, e.g. temperature and solar radiation.

With the daily data obtained from the 13 different meteorological stations, Yassin *et al*. (2016) evaluated the performance of ANN and GEP. Reference ET was predicted by using maximum, minimum and mean air

temperatures; maximum, minimum and mean relative humidity, wind speed and global solar radiation. They aimed to improve model performance by using validation set and the calculated ET values by means of Penman & Monteith equation was used as a target value. Furthermore, the ANN model was found to be slightly more successful than the GEP. Nevertheless, GEP can be used in ET calculations in terms of less time consuming, since it gives algebraic equations. In the study, in which the validation phase was also considered during the data set separation, in order to increase the reliability of the model results, Banda *et al*. (2017), predicted reference evapotranspiration by dividing the data set into three as train, validation and test. In their evaluation it is pointed out that multi-layer perceptron (5-5-1) has the highest accuracy, although there is not a big difference between the applied neuro computing techniques. The small difference between the model performances may be due to the normalization process.

In the study comparing tree algorithms, which are one of another machine learning techniques, with SVM results, Fan *et al*. (2018) stated that SVM has higher accuracy than the tree algorithms for different climate conditions, particularly with the limited meteorological data. Ferreira *et al*. (2019) drew attention to regional models rather than local predictions in the calculation of ET_0. They used the temperature and relative humidity data of 203 stations representing the entire Brazil. For ANN, the previous 2-day and 4-day data were shown to be the best options for generalization capacity in temperature-based and temperature-and relative humidity-based models, respectively. Additionally, the ANN approach was applied to estimate the surface soil temperature by Lazzus (2014) and to determine the harvestable water from air humidity data by Khaledi (2019). Furthermore, Şaylan *et al*. (2017) used ANN and adaptive neuro-fuzzy inference system for modeling of soil water content. Şaylan *et al*. (2019) modeled the surface conductance parameter in Penman & Monteith equation over a crop by ANN. Following the widespread use of mathematical models in the prediction of hydrological parameters, ensemble models are also frequently used in the literature. Ensemble models are used for precipitation (Xu *et al*., 2020; Ahmed *et al*., 2020), flood (Tiwari and Chatterjee, 2010; Liu et al. 2017) and water quality (Partalas *et al*. 2008; Elkiran *et al*. 2019) predictions. For reference evapotranspiration, Nourani *et al*. 2019 has established both empirical ensemble and artificial intelligence ensemble models with 2 different strategies. They used Feed Forward Neural Network (FFNN), Adaptive Neuro Fuzzy Inference System (ANFIS), Support Vector Regression (SVR) methods for artificial intelligence ensemble, while Hargreaves and Samani (HS), Modified Hargreaves and Samani (MHS), Makkink (MK) and Ritchie (RT) equations were utilized for the empirical ensembles. They established models to predict reference evapotranspiration with meteorological variables obtained from five different regions, including Turkey. It was concluded that ensemble models have higher accuracy than stand-alone models. In addition, it has been pointed out that artificial intelligence-based ensemble performs better than empirical ensemble models.

As seen above, in many studies, daily total reference evapotranspiration was modeled with nonlinear approaches using daily meteorological data. The difference of this study from other studies is that instead of reference ET, the actual evapotranspiration measured by the BREB method with short time intervals (30-min) is determined for the first time in the literature using data-driven models with a limited number of meteorological variables measured in the same time interval.

Main aim of this study was to estimate the 30-min actual evapotranspiration of winter wheat measured by BREB method as a function of limited number of meteorological variables such as 30-min average air temperature (T), relative humidity (RH), global solar radiation (R_S), vapor pressure deficit (VPD) using data-driven models (SVM, ANFIS and ANN) at the experiment field of Atatürk Soil Water an Agricultural Meteorology Research Institute in the Kırklareli city, locates in the north-west part of Turkey.

2. MATERIALS AND METHODS

2.1. Study area and data

Study area covering 8 ha is located in the field of Atatürk Soil Water and Agricultural Meteorology Research Institute Directorate (41°41'53" N, 27°12'37" E, 171 m asl), in Kırklareli which is one of three provinces located in the Thrace Region, Turkey (Fig. 1). The surface water potential of Kırklareli constitutes 1.2% of the Turkey's surface water, while the amount of economically irrigable land in the province is 112013 ha (Ekmekyapar and Cebi, 2017). Thus, Kırklareli has a suitable area to observe the agricultural activities. In this study, the observations were taken during the 2009-2010 winter wheat growing period from this area.

The evapotranspiration (obtained from latent heat flux) values were calculated by using Bowen Ratio Energy Balance method by using the following equations (Bowen, 1926).

$$\beta = \gamma \left(\frac{\Delta T}{\Delta e}\right) = \frac{H}{LE} \quad (1)$$

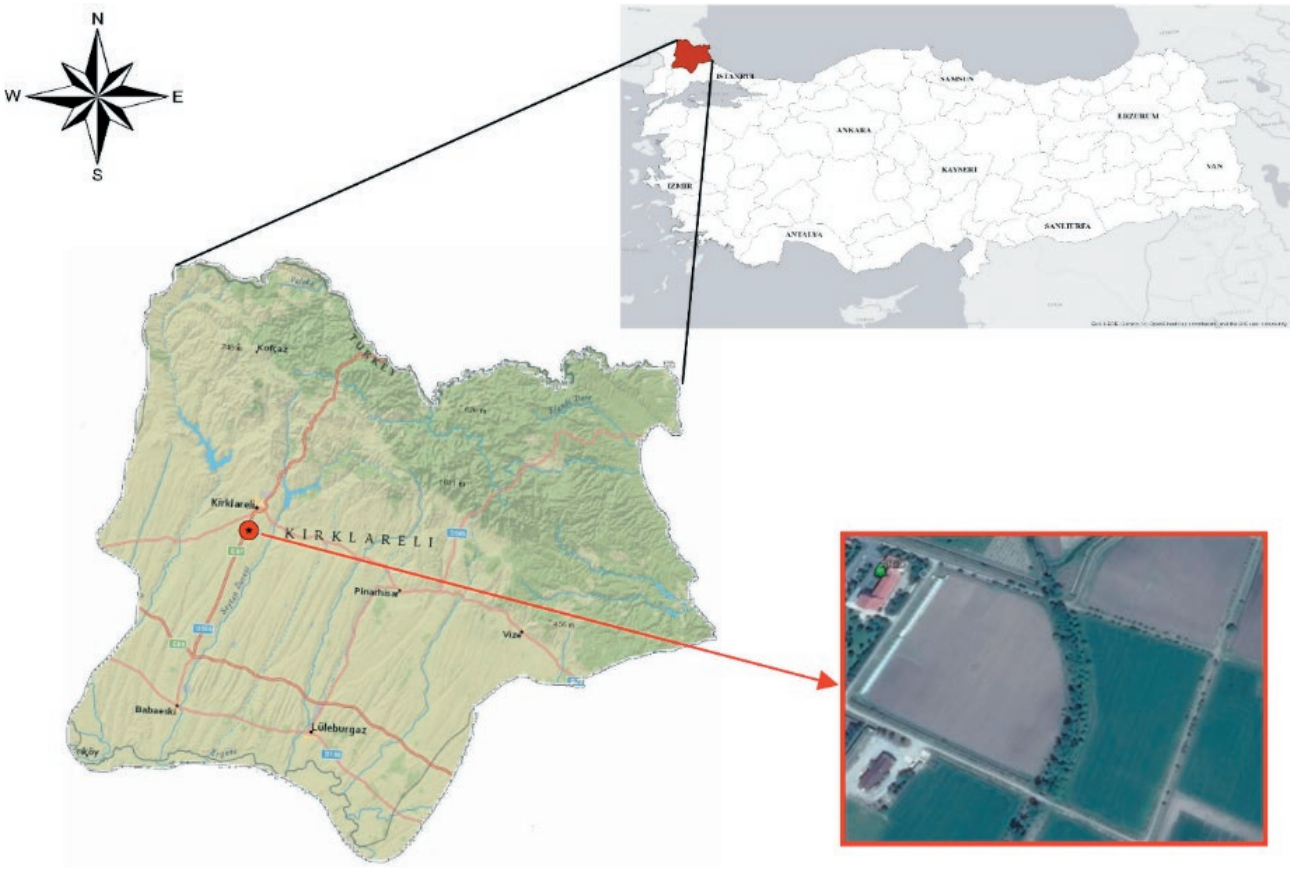

Fig. 1. Study area.

$$R_n\text{-}G\text{-}LE\text{-}H=0 \quad (2)$$

$$LE = \frac{R_n - G}{(1+\beta)} \quad (3)$$

where, β is Bowen ratio, is psychrometric constant (kPa $^{\circ}C^{-1}$), R_n is net radiation (Wm^{-2}); G is soil heat flux (Wm^{-2}); LE is latent heat flux (Wm^{-2}); H is sensible heat flux (Wm^{-2}); ΔT is the temperature gradient (^{o}C) and Δe is the vapor pressure gradient (kPa) over the height interval above canopy surface.

BREB system is built on a 10 m measurement mast. The sensors found in the BREB measurement system and their measurement heights are given in Tab. 1.

Meteorological variables were measured in an interval of 1 s and recorded as an average of 30 minute. In this study, the raw BREB data recorded in every 30-min were used to estimate evapotranspiration. One of the most difficulties in using the BREB method is that the temperature and vapor pressure differences used in calculation of the bowen ratio generally approach -1 near dawn and dusk. Apart from this, the temperature and vapor pressure gradients should be controlled in the relationships between H and LE. Therefore, data were checked according to the criteria of Ohmura (1982) and Perez *et al.* (1999) to avoid suspicious data situations. Then, incorrect data were eleminated and miss-

Tab. 1. BREB measurement system components and the measurement heights.

Sensor	Model	Measurement height/ depth
Data Logger	Campbell Scientific, CR1000	-
Temperature and Relative Humidity	Vaisala, HMP	2 m and 3m
Wind speed and direction	NRG, RNRG	0.5 m, 1 m, 2 m, 5 m, 10 m
Precipitation	Campbell Scientific, TE	1 m
Global solar radiation	Kipp&Zonen, NR	2 m
Net radiation	Kipp&Zonen, NR	2 m
Soil heat flux	Hukseflux, HFP	8 cm

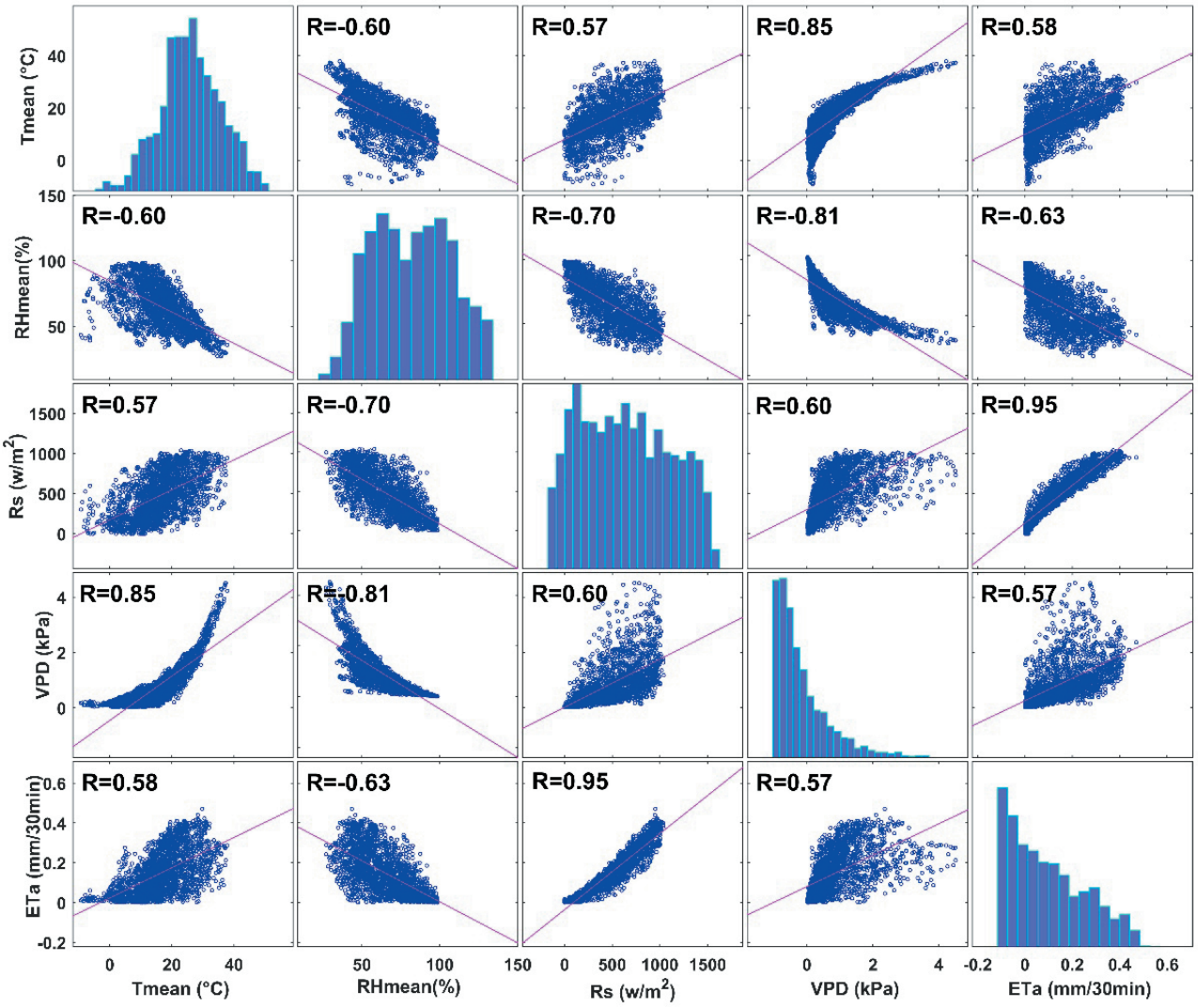

Fig. 2. Correlation matrix.

ing data were completed by considering criteria. During the measurement, various meteorological factors such as global solar radiation, net radiation, humidity and temperature etc. were measured and recorded. However, each measured variable is not included in the models as an input in data driven techniques to ensure the usability of the proposed methods. For instance, net radiation was not included in the model, even though it has considerably high correlation with the actual ET, since it is already calculated by using solar radiation. Additionally, net radiation is not continuously measured data in the world. Therefore, it is considered sufficient to include only global solar radiation in the model to pay regard to easy use of the models. As a result, using these variables, latent heat flux was calculated with the help of Equation 1 to Equation 3 and it is converted from the latent heat flux to the actual evapotranspiration (ET_a). Thus, mean temperature (T), relative humidity (R_H), global solar radiation (R_S) and vapor pressure deficit (VPD) were used as inputs, while actual evapotranspiration was used as the output for the proposed models. The correlation matrix is introduced in Fig. 2. The time-series of the input variables and output are also given in Fig. 3.

As can be seen from the correlation matrix in Figure 2, global solar radiation has the highest correlation with the ET_a among the other input variables. It is followed by relative humidity, which has the negative correlation, mean temperature and vapor pressure deficit, respectively. Considering that global solar radiation shows such a high correlation (R=0.95), it is possible that high accu-

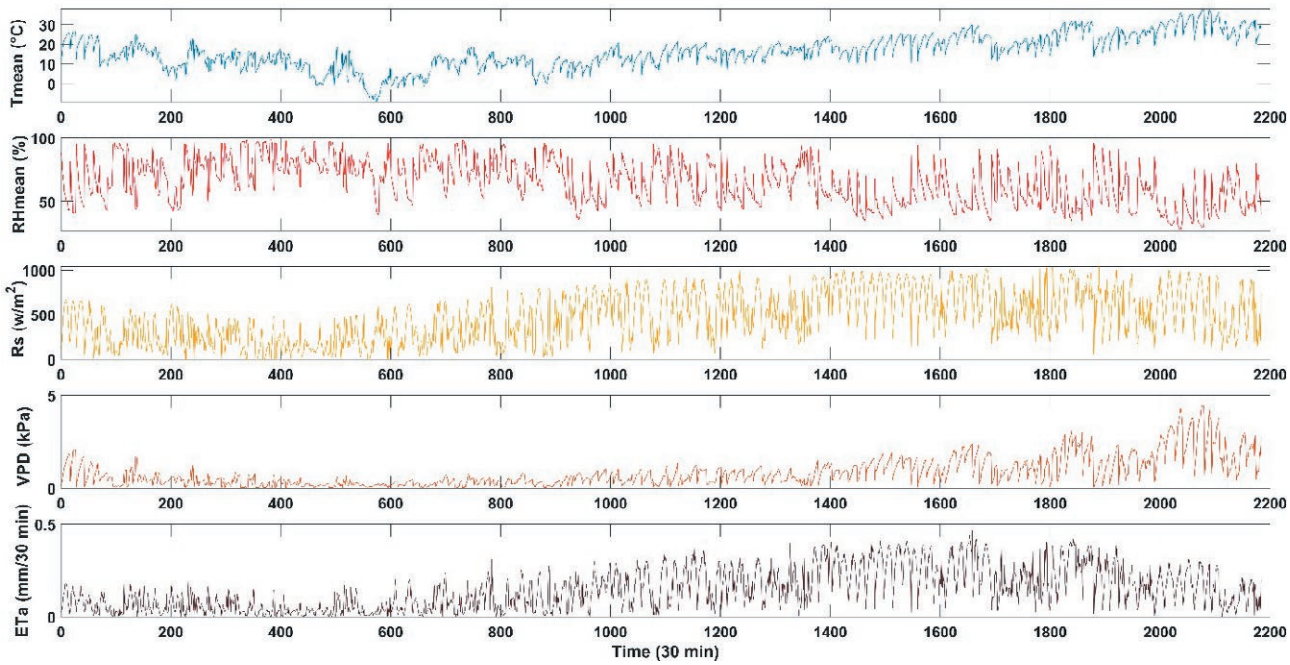

Fig. 3. Time series of the calculated variables with BREB.

Tab. 2. Basic statistical properties of the measured 30-min average meteorological and calculated variables with BREB.

Variables	Min	Max	Median	Average	Std. Deviation
T (°C)	-9.27	37.86	16.19	16.38	8.39
R_{Hmean} (%)	27.04	98.49	65.34	65.16	16.72
VPD (kPa)	0.02	4.51	0.60	0.85	0.79
R_S (W/m^2)	0	1039	464.1	478.5	273.4
ET_a (mm)	0	0.47	0.12	0.14	0.11

racy models can be obtained even by using only global solar radiation as the input.

The statistical features of the observed parameters used in this study are given in Tab. 2.

2.2 Support vector machine

Support vector machine (SVM) is a data-driven machine learning approach based on statistical learning theory. Although SVM was initially used to best distinguish between two classes of data, it was later developed with multiple classification studies for data requiring more than two classes. This separation is expected to be made as optimal as possible. To make the most appropriate classification, a linear decision surface, i.e. the hyperplane, is constructed (Cortes and Vapnik, 1995). The hyperplane established in the space, maximizes the distance between the data of both classes. This distance is called a margin and maximizing margin is essential to minimize error. Besides, in determining the hyper-plane that separates the instance space linearly, only the marginal values have an effect, while changing the remaining samples does not have an effect on hyper-plane. The support vector machines model is implemented by moving the input vectors nonlinearly to a high dimensional space. The kernel functions are used for this process. For the nonlinear data, kernel functions greatly increase learning performance.

The structure of the support vector machines is shown in Fig. 4. In this method, the SVM has no information about the distribution of input data set. The attribute value of each input data, along with the value of a given coordinate, is plotted as a support vector in n-dimensional space. Decision planes are created for classification using these support vectors as training data and thereafter, it is able to classify input data sets with support vector machines separating the two classes. With this method, learning process is performed on input data and prediction is made.

Let $[(x_1,y_1),(x_2,y_2),(x_3,y_3),\ldots,(x_n,y_n)]$ be a training set, where n denotes the number of training data set, x_i and y_i represent input and output vectors, respectively. The best function for the support vector regression as follows:

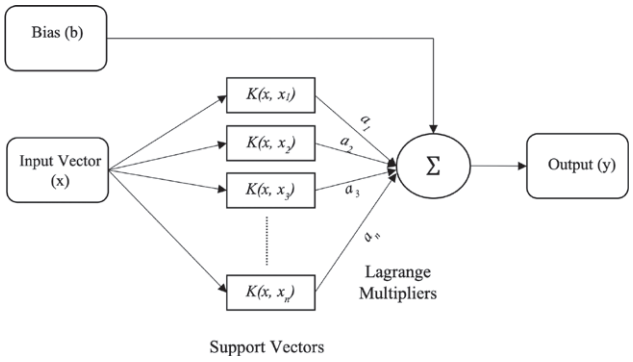

Fig. 4. Schematic view of the SVM structure.

$$f(x)=w\cdot\varphi(x)+b \tag{4}$$

in which, w represents the normal vector, b and $\varphi(x)$ are the bias term and the non-linear function, respectively. The objective function is the minimum of the $\varphi(x)$ as following:

$$\min\frac{1}{2}\|w\|^2+C\sum_{i=1}^{n}(\xi_i+\xi_i^*) \tag{5}$$

Constraints:

$$\begin{aligned} &y_i-w\cdot\varphi(x)-b\le\varepsilon_i+\xi_i\\ &w\cdot\varphi(x)+b-y_i\le\varepsilon_i+\xi_i^*\\ &\xi_i,\xi_i^*\ge 0\ ;i=1,2,\ldots,n \end{aligned} \tag{6}$$

C is the penalty parameter which provides stability to maximize margin range and minimize misclassification. ε is the insensitive loss function, ξ and ξ^* are slack variables denotes the upper and lower constraints on the system output, respectively. The insensitive loss function is a function that ignores the error at a certain distance from the target value. By using the Lagrange theory, the function can be expressed as:

$$f(x)=sign\left[\sum_{i=1}^{n}(a_i-a_i^*)\,K(x_i,x)+b\right] \tag{7}$$

where $K(x_i,x)$ is the Kernel function and a, a^* represents the Lagrange multipliers. Kernel function can be expressed as generally:

$$K(x,y)=\langle\varphi(x)\ .\varphi(y)\rangle \tag{8}$$

In this study, the radial basis function (RBF) was used as kernel and the equation of RBF as follows:

$$K(x,y)=exp\left(-\frac{\|x-y\|^2}{2\sigma^2}\right) \tag{9}$$

where σ denotes the radial basis function width. The parameters of SVM, C, ε and σ are selected by trial-error method.

2.3. Adaptive neuro fuzzy inference system

Fuzzy logic is an approach introduced by Zadeh (1965). It is based on expressing an object or phenomenon in a fuzzier manner, without sharp boundaries, rather than being expressed with precise values. This form of expression is called fuzzification. The fuzzified values are then processed in accordance with the rules set by the user and the desired modeling is performed. The process of converting model outputs to actual values is called defuzzification, and there are two commonly used types in the literature. The first inference type is Mamdani (1974) which can work with the help of verbal expressions and graphical operations. The second and the most widely used inference in engineering field is Takagi-Sugeno (1985) type inference system. This method is suitable for use with numerical values and clarifies fuzzy expressions with the help of a constant or linear equation. Today, the most commonly used structure of Takagi-Sugeno inference system is ANFIS. ANFIS can be described as the combination of fuzzy logic approach and artificial neural network learning algorithms (Jang 1993). The ANFIS algorithm is described in Fig. 5.

Layer 1: The data set values are fuzzified. For instance, "Less" and "Very" were used to express the input values divided into two sets. Therefore, the membership degree for the input value is determined as follows:

$$\mu_{A_i}(I_i)=\exp\left[-\left(\frac{I-c_i}{\sigma_i}\right)^2\right] \tag{10}$$

in which; I_i denotes the two fuzzy sets named as "Less" and "Very". c_i and σ_i refer to the parameters of the mem-

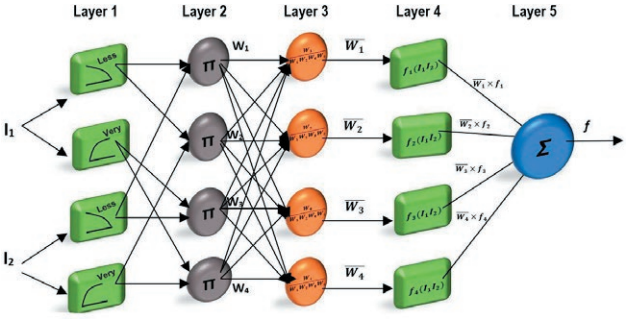

Fig. 5. Architecture of ANFIS model.

bership function, which will be optimized later, called the premise parameters.

Layer 2: By multiplying the membership degrees calculated in Layer 1, the output value of each node is obtained. The result will be named as firing strength:

$$w_i=\mu_{Ai}(I_1)\times\mu_{Bi}(I_2) \qquad i=1,2,\ldots \tag{11}$$

Layer 3: Using the input values of Layer 2, the normalized firing strength is calculated as follows:

$$\overline{w}_i=\frac{w_i}{\sum w_i} \qquad i=1,2,\ldots \tag{12}$$

Layer 4: Using the firing strength value from Layer 3, the correct equations representing the relationships are obtained. The so-called consequence parameters are calculated in Layer 4:

$$\overline{w}_i f_i=\overline{w}_i(p_i I_1+q_i I_2+r_i) \qquad i=1,2,\ldots \tag{13}$$

where p_i, q_i and $r_i^{'}$ are the consequence parameters.

Layer 5: In the fifth layer, the final output value is obtained by summing all the values from the previous step. Besides, there is only one node in this layer.

$$f=\sum \overline{w}_i f_i \qquad i=1,2,\ldots \tag{14}$$

2.4. Artificial neural network

The application of ANN has continued to increase over the last few decades (Aghelpour *et al.*, 2019). Research in this area revealed that ANN plays a vital role in the modeling of parameters which have nonlinear behavior with low error. Firstly, in the 1940s, engineering studies were carried out (McCulloch and Pitts, 1943). When it comes to the 1960s, rapidly developing artificial neural network model studies entered the period of stagnation since the networks that can be used easily in solving linear problems could not solve nonlinear problems. Following the 1970s, there was a great explosion in the studies carried out in this field, starting with the comprehension of the abilities of ANN about solving non-linear problems (Rumelhart *et al.*, 1986). Today, artificial neural networks focused on the concept of "deep learning" (LeCun *et al.*, 2015). Considerable progress has been made in several fields of study, such as image processing (Indraswari *et al.*, 2019) and object recognition (Mhalla *et al.*, 2019). Complex structures can be solved very quickly, particularly with the increasing

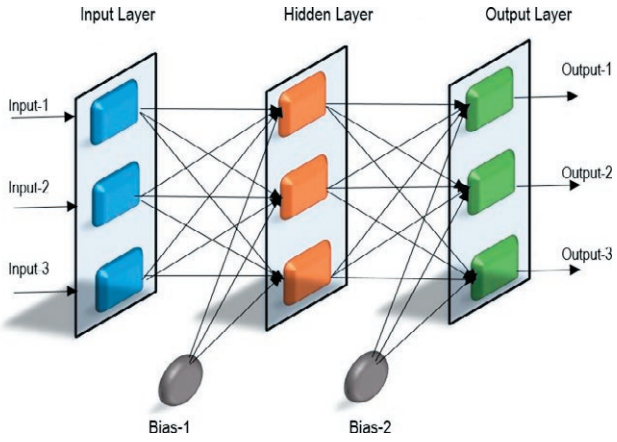

Fig. 6. Structure of the multi-layer perceptron.

of computer processor speeds. For the solution of nonlinear problems, Rumhelard (1986) developed multilayer artificial neural networks. Similar to the working principle of single-layer networks, multi-layer networks undergo a learning process by comparing the given input samples with the outputs. In the learning process, weights are obtained to minimize the difference between output and expected values.

Multilayer artificial neural networks consist of 3 layers, named as input layer, hidden layer, and output layer (Fig. 6).

Multilayer artificial neural networks work with the principle of supervised learning. In multi-layer perceptron (MLP), inputs and expected outputs should be given for the learning of the network and the network intends to compare the model output values with the expected output values in order to minimize the difference. MLP, performs this purpose with two types of calculation: (1) Feed Forward and (2) Back Propagation. The calculation steps are as follows:

1. The net input value obtained by multiplying the weights by the input values:

$$Net=\sum_i^n I_i W_i \tag{15}$$

2. The net input value is converted into the following equation via the activation function:

$$F(Net)=\frac{1}{1+e^{-Net}} \tag{16}$$

where I and W represent input value and weights, respectively.

3. The output of the activation function from the hidden layer is re-weighted and the final output value is

reached by a linear transfer function in the output layer.

4. The final output value is compared with the expected values identified to the network. The comparison is performed by taking the difference between the expected value and the output generated by the network. At this stage, it is desired that the error sum of squares be zero. If it is far from zero, the weights must be re-updated in order to approach zero.

$$E = \frac{1}{2}\sum_{i}^{n}(E_i - O_i)^2 \quad (17)$$

where E_i and O_i denote expected and output values, respectively. From this step, backpropagation is carried out.

5. The gradient of the "E" value representing the error is taken to update the network weights. In each iteration, new values of weights are found and subtracted from the previous weight values.
6. If the change in the weight of the neuron connecting the *i*th element in the hidden layer to *n*th element in the output layer is A, the change in weight at time *t* is calculated as follows:

$$\Delta A_{in}^{a} = \lambda \delta_n Ç_i^a + \alpha \Delta A_{in}^{a}(t-1) \quad (18)$$

where λ and α represent the learning coefficient and momentum coefficient, respectively. The momentum coefficient ensures that the amount of change is added to the next change at a constant rate, while preventing the network from getting stuck to the local minimum during the learning process. The learning coefficient determines how much change required to be in weights. δ_n is the error of the output and calculated as follows:

$$\delta_n = f'(Net)E \quad (19)$$

7. After determining the amount of change in weight, the value in th iteration is calculated with the help of the Equation 6.

$$A_{in}^{a}(t) = A_{in}^{a}(t-1) + \Delta A_{in}^{a}(t) \quad (20)$$

8. Updating the weights of the threshold values also be carried out with the aid of Equation 20.

2.6. Performance evaluation criteria

In data driven models, a number of metrics are used to evaluate model performances. With the help of these metrics, statistical comparisons are made and it is concluded whether the model results are statistically significant or not. In this study, mean absolute error (MAE), mean squared error (MSE), Nash-Sutcliffe Efficiency (NSE), Performance index (PI) and Willmott's refined index of agreement (WI) were employed in the model evaluation (Nash and Sutcliffe, 1970). All the metrics used have different ability to measure the closeness of model results and observations. Therefore, a fair comparison can be achieved by using those metrics.

Nash-Sutcliffe Efficiency (NSE) varies between -∞ and 1. If the efficiency value is 1, then it means that the model has a perfect match with observations.

$$NSE = 1 - \frac{\sum_{i=1}^{n}(D_{oi} - D_{pi})^2}{\sum_{i=1}^{n}(D_{oi} - \overline{D_o})^2} \quad (21)$$

Where D_o is observed values, D_p is predicted values and $\overline{D_o}$ is the average of observed values. Performance Index (PI) varies between 0 and ∞. If the PI values are close to zero, then the model has high accuracy (Gandomi and Roke 2015).

$$PI = \frac{RMSE/\overline{D_o}}{1 + \frac{\sum_{i=1}^{n}\left[(D_{oi} - \overline{D_o})(D_{pi} - \overline{D_p})\right]}{\sqrt{\sum_{i=1}^{n}(D_{oi} - \overline{D_o})^2 \sum_{i=1}^{n}(D_{pi} - \overline{D_p})^2}}} \quad (22)$$

Willmott's refined index of agreement (WI) varies between -1 and 1. Likewise NSE, the model can be defining as successful if the WI value approaches to 1. If the WI value is -1, model interpretation should be performed carefully (Willmott *et al.* 2012).

$$WI = 1 - \frac{\sum_{i=1}^{n}|D_{pi} - D_{oi}|}{c \times \sum_{i=1}^{n}|D_{oi} - \overline{D_o}|}, \text{ when}$$

$$\sum_{i=1}^{n}|D_{pi} - D_{oi}| \leq c \times \sum_{i=1}^{n}|D_{oi} - \overline{D_o}| \text{ ; (with } c=2) \quad (23a)$$

$$WI = 1 - \frac{c \times \sum_{i=1}^{n}|D_{oi} - \overline{D_o}|}{\sum_{i=1}^{n}|D_{pi} - D_{oi}|} - 1, \text{ when}$$

$$\sum_{i=1}^{n}|D_{pi} - D_{oi}| > c \times \sum_{i=1}^{n}|D_{oi} - \overline{D_o}| \text{ ; (with } c=2) \quad (23b)$$

Coefficient of determination (R^2) value varies between -1 and 1, just the same way as WI. Positive values indicate that two variables are directly proportional, while negative values represent the inverse relationship. Approaching to -1 or 1 increases the strength of the relationship, whereas in the case of zero, it means that there is no relationship between the variables. MSE and MAE

are both expected to be close to zero and the equations are given as follows:

$$MSE = \frac{1}{n}\sum_{i=1}^{n}(D_{pi} - D_{oi})^2 \quad (24)$$

$$MAE = \frac{1}{n}\sum_{i=1}^{n}\left|D_{pi} - D_{oi}\right| \quad (25)$$

3. RESULTS AND DISCUSSION

In this study, three different data-driven methods, named as support vector machines, adaptive-network-based fuzzy inference system and artificial neural networks were used to estimate 30-min actual evapotranspiration values. In this context, the field measurement of various climatic variables that are used in the calculation of evapotranspiration has been carried out, and estimationss have been made depending on these parameters. Thus, global solar radiation, relative humidity, mean temperature and vapor pressure deficit were used as input variables to the proposed models, while actual ET as the output. To achieve the parsimonious selection of the most effective inputs, first of all single input-output models were tried by taking each variable separately as an input (Tab. 3). Then the accuracy of the multiple input – single output models were compared with the results of the single input – single output models by increasing the number of inputs to the proposed models in each time. Additionally, the separation of the data set, which is one of the most influencing factors on the model accuracy, was performed as 70% training set and 30% test set.

3.1. SVM results

In the training phase of models that use SVM method, data were transformed to a different space to perform linear separation due to the nonlinear nature of the data. For this process, there are four different kernel functions used in the literature: (1) linear, (2) polynomial, (3) sigmoid, and (4) radial based function (RBF). The choice of the kernel functions depends on user's preferences, as well as the data structure. The structure of natural phenomena is generally non-linear and contains chaotic behavior. For this reason, the RBF is the most preferred function by researchers since it has ability to generalize the bounds on the probability of classification error. Therefore, RBF was used in the present study. There are three parameters that need to be optimized for Radial Basis Function (RBF) kernel SVM. Those parameters are called as gamma, penalty parameter (C) and epsilon. Here, the parameters were optimized using-trial error method.

First, single input – single output models were obtained as reference models, then multiple input – single output models were built. The abbreviations SVM1, SVM2, SVM3 and SVM4 represent the models built by using mean temperature, relative humidity, vapor pressure deficit and solar radiation as an input, respectively. The results obtained by the SVM models revealed that the SVM4 model which uses the solar radiation variable as a single input has the highest accuracy among all single input-single output models. The SVM4 model has the determination coefficient as R^2=0.909, while the rest of the models have lower than the R^2=0.5. The model performance started to improve as the number of inputs increase in the model setup. For instance, SVM5 and SVM6 models perform better (NSE_{SVM5}= 0.9387, NSE_{SVM6} =0.9163), and SVM7 model that uses all of the four input variables, shows highest prediction performance (NSE_{SVM7}= 0.9398). It is observed that multiple input - single output SVM models deviate slightly from the perfect model line (Fig. 7). The SVM4 model performance is considered to be quite satisfactory when compared to the SVM7 model event if its error criteria is slightly less than the SVM7. The evaluation of the SVM models with

Tab. 3. Models identities and corresponding input variables.

	Methods			INPUTS	OUTPUT
	SVM	**ANFIS**	**ANN**		
Model IDs	SVM1	ANFIS1	ANN1	T	ET_a
	SVM2	ANFIS2	ANN2	R_H	ET_a
	SVM3	ANFIS3	ANN3	VPD	ET_a
	SVM4	ANFIS4	ANN4	R_S	ET_a
	SVM5	ANFIS5	ANN5	T, R_S	ET_a
	SVM6	ANFIS6	ANN6	T, R_H, R_S	ET_a
	SVM7	ANFIS7	ANN7	T, R_H, R_S, VPD	ET_a

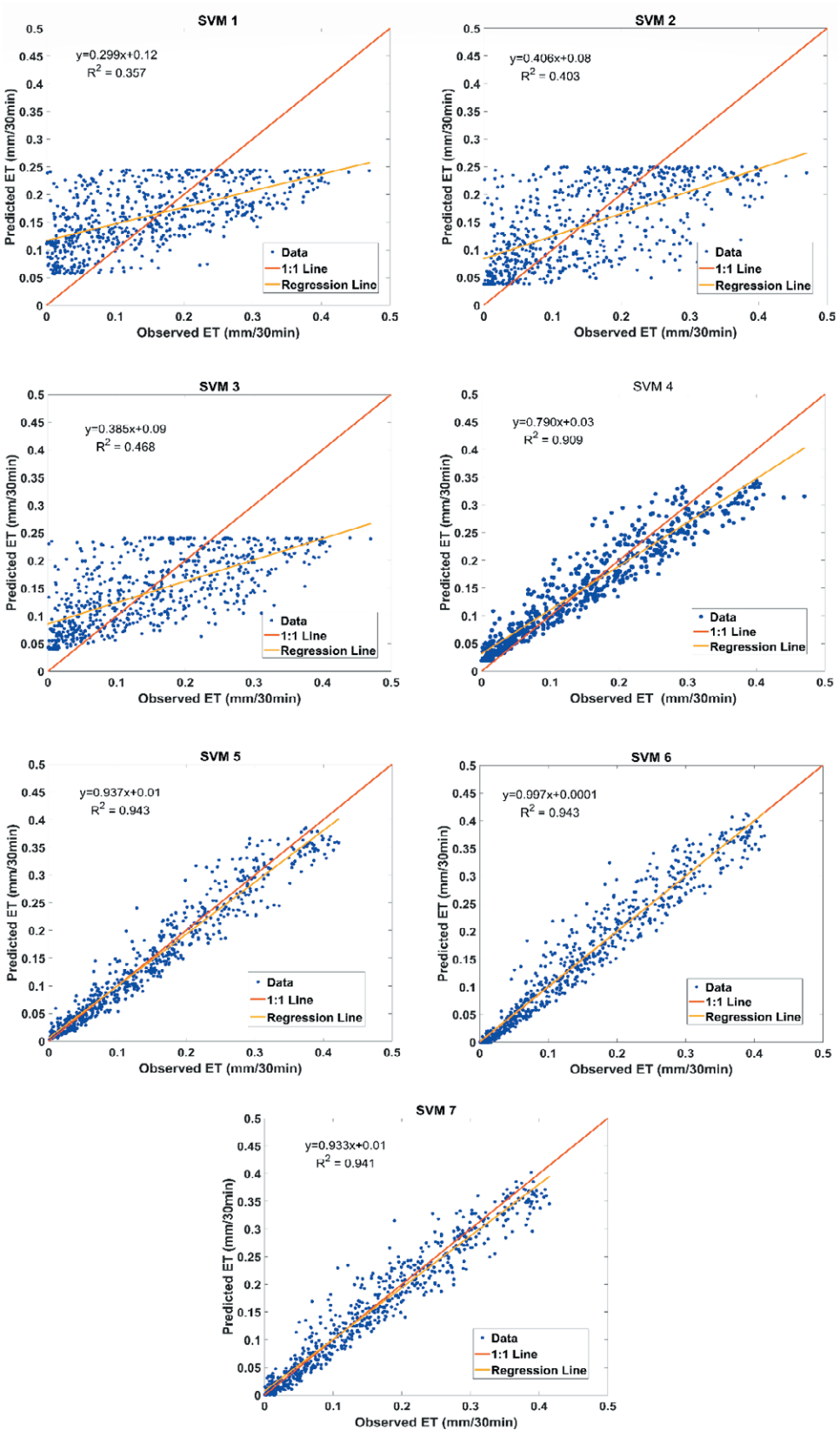

Fig. 7. Scatter plots of SVM models for testing data.

respect to different performance indicators is given in the Tab. 4.

3.2. ANFIS results

ANFIS models were built by using fuzzy logic toolbox found in MATLAB software. Triangle, trapezoidal and gaussian type membership functions were used for the different model setups. Using trial and error method, it is found that the models with gaussian type membership function has the lowest training error. Therefore, gaussian type member function was employed for the ANFIS model to predict the ET_a values in testing part. The number of fuzzy sets, which is selected based on expert opinion, is another parameter encountered during the training phase. In this study, the number of fuzzy sets which can be between 2 and 5 was determined by trial and error method. Although a training error decreases as the number of fuzzy sets increase, it may cause over-learning to select too many membership functions. Since overlearning would reduce the generalization ability of the models, generally upper limit is taken as five membership functions depending on time series length. Three fuzzy sets were found to be adequate to achieve the best ANFIS model performances in training part.

In the Sugeno inference type, the output values can be in the form of either a constant number or a linear equation. This option is selected by the user and does not have any significant impact on our current results. So, it is decided to use linear equations for a better generalization. The parameters of linear equation were calculated with least squares method, the membership function parameters were obtained by back propagation algorithm. These training methods readily built in Matlab ANFIS editor under the "hybrid" option. ANFIS7 model, which has 4 inputs, gave the best prediction accuracy for the testing data set, among the models established by ANFIS. On the other hand, the single input-single output models, except ANFIS4 model, yield lower prediction performance (NSE_{ANFIS1}=0.308, MAE_{ANFIS1}=0.075; NSE_{ANFIS2}=0.392, MAE_{ANFIS2}=0.067; NSE_{ANFIS3}=0.4658, MAE_{ANFIS3}=0.061) compared to multiple input-single output models (NSE_{ANFIS5}=0.928, MAE_{ANFIS5}=0.022; NSE_{ANFIS6}=0.935, MAE_{ANFIS6}=0.021; NSE_{ANFIS7}=0.941, MAE_{ANFIS7}=0.0198). Also, ANFIS4 model gave considerably successful results according to the performance metrics, such as MAE, MSE, NSE, WI and PI with 0.025, 0.001, 0.907, 0.866 and 0.113 respectively. Even tough, the accuracy of multiple input-single output models is better than the ANFIS4 model, the results are considered to be close to each other and successful predictions can be made with solar radiation (R_S), particularly in the cases where limited data exists.

The results show that the ANFIS model that has the same input combination gives very close NSE and MSE values to the SVM model. In other words, the actual ET values predictions were achieved with a high accuracy using a single input solar radiation both in the SVM and ANFIS model. The NSE, MSE, WI and PI values of each ANFIS model are given in Table 4. Moreover, the scatter plot of the models created with only solar radiation revealed a good scattering which can be considered as useful (Fig. 8).

3.3. ANN results

Multilayer perceptron (MLP) have been used in the application of ANN. As a first step, input and output data were normalized. The normalization is the de-unitization process, which enables the use of data in different scales within the same model. Normalization was performed by dividing all values by the time series' maximum values, which can be called also as idealization. Thus, values for all data set are reduced between 0 and 1. The neural network architecture consists of three layers which are (1) input layer, (2) hidden layer and (3) output layer. Sigmoid, tangent-hyperbolic and step functions, which are not only mostly used for the solution of the non-linear problems but also the most common transfer functions in the literature, were evaluated to use in the hidden layer. The tangent-hyperbolic function (THF) was chosen, because of its best performance results. The number of hidden neurons was evaluated in the range of 3 to 5 by trial and error method. Since the number of neurons 15 and/or above 15 is thought to lead to overlearning and will result in complex model structure, the number of hidden neurons is restricted to 15. Backpropagation was chosen as the training algorithm and learning coefficient and momentum coefficients were selected as 0.001 and 0.5, respectively. Considering the evaluations carried out according to different performance metrics, it is concluded that the ANN5 (the model with 2 inputs, named as T_{mean} and R_S) has the highest accuracy with NSE = 0.946 and MSE = 7E-4. Besides, with a slight difference between each other, ANN6 and ANN7 models were obtained as the second and third best models, respectively (NSE_{ANN6}=0.942, MSE_{ANN6}=8E-4; NSE_{ANN7}=0.941, MSE_{ANN7}=8E-4).

On the other hand, ANN4 model, which was generated by using only R_S as an input, has the best estimation performance among the single input single output models with NSE = 0.91 and MSE = 11E-4. Considering that there is not much difference between the results according

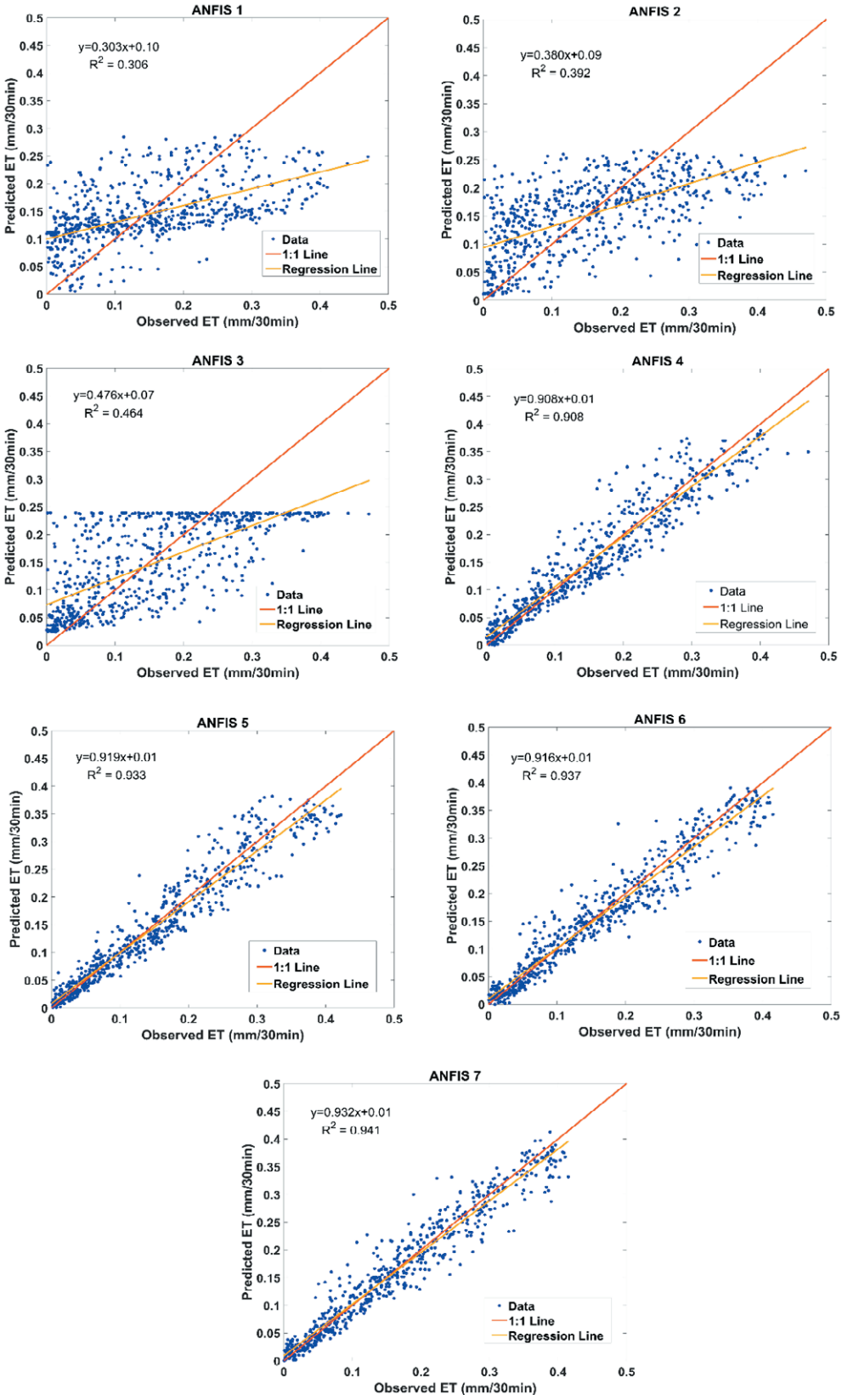

Fig. 8. Scatter plots of ANFIS models for testing data.

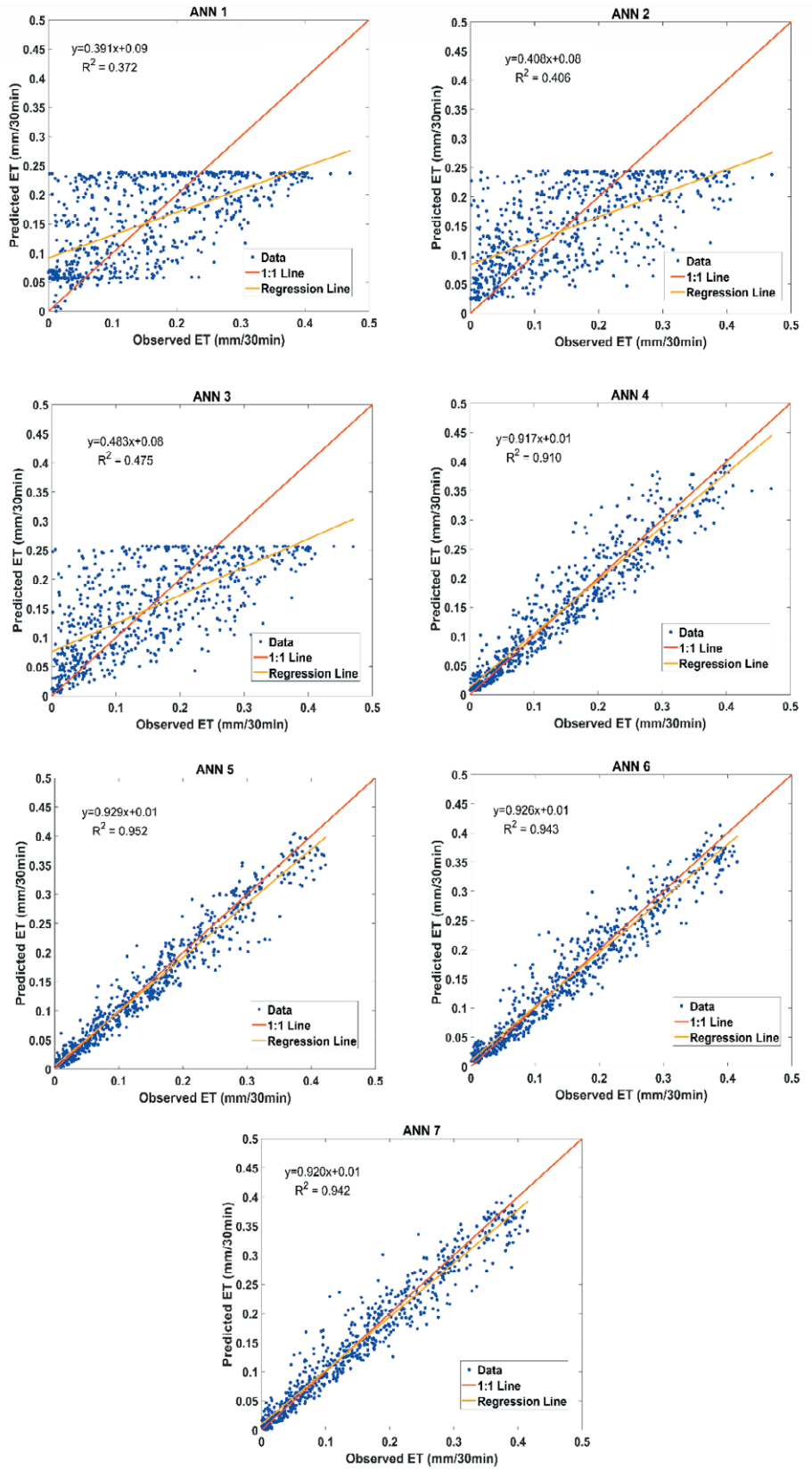

Fig. 9. Scatter plots of ANN models for testing data.

to the performance indicators, the actual ET values can be estimated at high success rate by using solely measured R_S with the help of ANN4. Model structures and prediction performances of ANN are also given in Table 4.

The scattering plots of the models established with ANN are shown in Fig. 9. ANN4, ANN5, ANN6 and ANN7 models distributed on a 1:1 perfect model line, while ANN1, ANN2 and ANN3 deviate highly from the perfect model line. Also, it indicates that the ANN4 model is not underestimated or overestimated and can be preferred in prediction of ET_a values as an alternative for the multiple input - single output models with a slight difference in the model accuracies.

As can be seen from the box plot diagrams given in Fig. 10, error distribution range for single input - single output data-driven models, except the models which only solar radiation was used as an input, can be considered as high, in comparison to the multiple input - single output data-driven models' error distributions. There are extreme error values for single input - single output data-driven models, while weights of negative and positive values tend to be relatively equal in the distribution of error values for the multiple input - single output data-driven models, as well as the models which only solar radiation was used as an input. The box plots also present that the errors of the data-driven models are distributed as close to zero. Consequently, it can be said that although multiple input - single output models provide relatively better performances, the model with global solar radiation as an input appears to be considerably successful in terms of practical use with that requires only one variable.

4. CONCLUSION

Today, with inadequate clean water resources, the large amount of water used in agricultural irrigation and the increasing evaporation rate, ET calculations have gained importance for the effective use of water resources. In this article, data-based models were used to evaluate ET_a values measured by BREB method. Throughout the study, the prediction of the measured ET_a values with different and limited meteorological variables, which are temperature, relative humidity, global solar radiation and vapor pressure difference, was performed. According to the obtained results of the study, the prediction performances of the models which are created using only global solar radiation (R_S) as an input were very close to the performance of the multiple input-single output models created using all other meteorological inputs. The main findings of the study are as follows:

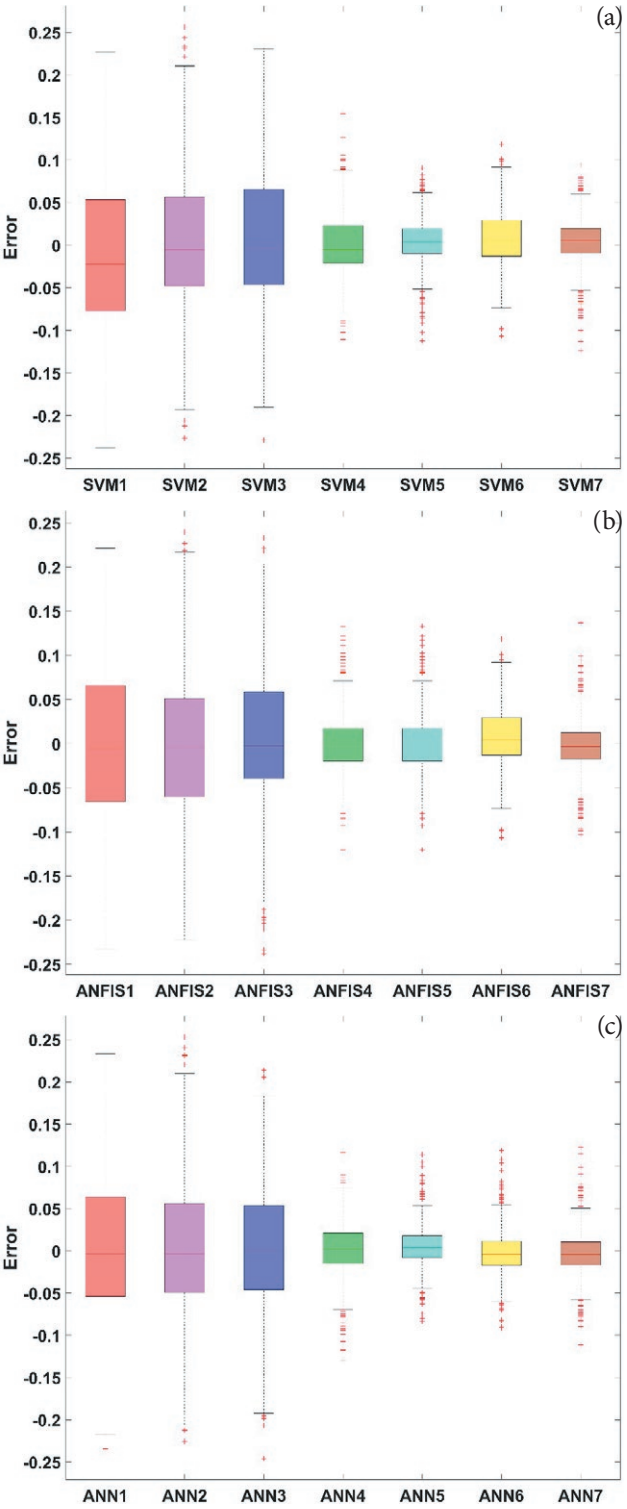

Fig. 10. Box plots of the models' error values for testing data. (a) SVM models (b) ANFIS models (c) ANN models.

Tab. 4. Performances of All Models.

Method	Model	Inputs	Output	TRAIN					TEST				
				MAE	MSE	NSE	WI	PI	MAE	MSE	NSE	WI	PI
SVM	1	T	ET_a	0.0749	0.0079	0.346	0.598	0.381	0.0741	0.0078	0.3407	0.6009	0.3686
	2	R_H	ET_a	0.0678	0.0073	0.399	0.636	0.359	0.0066	0.0071	0.4012	0.6426	0.3435
	3	VPD	ET_a	0.0640	0.0065	0.468	0.656	0.325	0.0645	0.0065	0.4527	0.6523	0.3187
	4	R_S	ET_a	0.0272	0.0013	0.8971	0.8539	0.1243	0.0277	0.0013	0.8938	0.8508	0.1213
	5	T, R_S	ET_a	0.0211	0.0008	0.9297	0.8864	0.1013	0.0204	0.0008	0.9387	0.8908	0.0936
	6	T, R_H, R_S	ET_a	0.0240	0.0010	0.9169	0.8686	0.1114	0.0251	0.0011	0.9163	0.8704	0.1062
	7	T, R_H, R_S, VPD	ET_a	0.0202	0.0008	0.9341	0.8896	0.0991	0.0207	0.0008	0.9398	0.8930	0.0900
ANFIS	1	T	ET_a	0.0753	0.0084	0.3059	0.5956	0.4062	0.0749	0.0082	0.3081	0.5962	0.3884
	2	R_H	ET_a	0.0695	0.0075	0.3797	0.6269	0.3690	0.0674	0.0072	0.3923	0.6367	0.3485
	3	VPD	ET_a	0.0602	0.0061	0.5012	0.6766	0.3132	0.0615	0.0063	0.4658	0.6685	0.3155
	4	R_S	ET_a	0.0241	0.0010	0.9142	0.8706	0.1134	0.0249	0.0011	0.9073	0.8659	0.1134
	5	T, R_S	ET_a	0.0222	0.0009	0.9253	0.8803	0.1045	0.0222	0.0009	0.9277	0.8814	0.1019
	6	T, R_H, R_S	ET_a	0.0203	0.0008	0.9328	0.8888	0.1001	0.0209	0.0008	0.9359	0.8920	0.0929
	7	T, R_H, R_S, VPD	ET_a	0.0180	0.0006	0.9450	0.9016	0.0903	0.0198	0.0008	0.9410	0.8974	0.0890
ANN	1	T	ET_a	0.0701	0.0075	0.3847	0.6237	0.3667	0.0694	0.00746	0.3762	0.6260	0.3559
	2	R_H	ET_a	0.0672	0.0073	0.4025	0.6390	0.3583	0.0660	0.0071	0.4044	0.6444	0.3426
	3	VPD	ET_a	0.0604	0.0061	0.4975	0.6760	0.3150	0.6094	0.0062	0.4794	0.6717	0.3100
	4	R_S	ET_a	0.0236	0.0010	0.9157	0.8735	0.1125	0.0240	0.0011	0.9096	0.8710	0.1119
	5	T, R_S	ET_a	0.0194	0.0007	0.9383	0.8956	0.0946	0.0185	0.0007	0.9459	0.9011	0.0877
	6	T, R_H, R_S	ET_a	0.0199	0.0008	0.9351	0.8909	0.0983	0.0203	0.0008	0.9422	0.8952	0.0881
	7	T, R_H, R_S, VPD	ET_a	0.0197	0.0007	0.9369	0.8922	0.0969	0.0201	0.0008	0.9409	0.8960	0.0891

- The application of data-driven models such as SVM, ANFIS and ANN models showed that data-driven mathematical methods can yield easier and faster solutions in ET predictions.
- It is concluded that in cases of limited facilities in the measurement of climatic variables, it is possible to make accurate ET_a calculations by using only global solar radiation.

In addition, unlike the other studies that a few performance metrics were employed to measure their model accuracies, a variety of performance metrics were used in this paper. This led to a fairer evaluation of model performances. Also, the accuracy of the models established using limited meteorological variables was highlighted, while well accepted predictions were obtained using only global solar radiation as an input.

ACKNOWLEDGEMENTS

The data used in this study was obtained from the project (109R006) supported by the Scientific and Technological Research Council of Turkey (TÜBİTAK). Therefore, we would like to thank TÜBİTAK for financial support of the project. In addition, special thanks to Dr. Fatih Bakanoğulları and the technicians who helped us during the experimental studies at Atatürk Soil Water and Agricultural Meteorology Research Institute for their contributions.

REFERENCES

Abdullah, S.S., Malek, M.A., Abdullah, N.S., Kisi, O., Yap, K.S. 2015. Extreme Learning Machines: A new approach for prediction of reference evapotranspiration. *Journal of Hydrology,* https://doi.org/10.1016/j.jhydrol.2015.04.073

Aghelpour, P., Mohammadi, B., Biazar, S.M. 2019. Long-term monthly average temperature forecasting in some climate types of Iran, using the models SARIMA, SVR, and SVR-FA. *Theoretical and Applied Climatology,* https://doi.org/10.1007/s00704-019-02905-w

Ahmed, K., Sachindra, D.A., Shahid, S., Iqbal, Z., Nawaz, N., Khan, N. 2020. Multi-model ensemble predictions of precipitation and temperature using machine learning algorithms. *Atmospheric Research.,* https://doi.org/10.1016/j.atmosres.2019.104806

Allen, R.G., Pereira, L.S., Raes, D., Smith, M. 1998. Crop evapotranspiration —guidelines for computing crop water requirements. FAO Irrigation and drainage paper 56. Food and Agriculture Organization, Rome.

Antonopoulos, V.Z., Antonopoulos, A. V. 2017. Daily reference evapotranspiration estimates by artificial neural networks technique and empirical equations using limited input climate variables *Computers and Electronics in Agriculture*, https://doi.org/10.1016/j.compag.2016.11.011

Banda, P., Cemek, B., Küçüktopcu, E. 2018. Estimation of daily reference evapotranspiration by neuro computing techniques using limited data in a semi-arid environment. *Archives of Agronomy and Soil Science*, https://doi.org/10.1080/03650340.2017.1414196

Bowen, I.S. 1926. The ratio of heat losses by conduction and by evaporation from any water surface. *Physical Review.* 27, 779-787.

Cortes, C., Vapnik, V. 1995. Support-Vector Networks. *Machine Learning* https://doi.org/10.1023/A:1022627411411

Ekmekyapar, F., Cebi, U.K. 2017. An investigation of inorganic chemicals and heavy metals in Kırklareli dam water, thrace region. *Desalination and Water Treatment*, https://doi.org/10.5004/dwt.2017.21316

Elkiran, G., Nourani, V., Abba, S.I. 2019. Multi-step ahead modelling of river water quality parameters using ensemble artificial intelligence-based approach. *Journal of Hydrology,* https://doi.org/10.1016/j.jhydrol.2019.123962

Fan, J., Yue, W., Wu, L., Zhang, F., Cai, H., Wang, X., Lu, X., Xiang, Y. 2018. Evaluation of SVM, ELM and four tree-based ensemble models for predicting daily reference evapotranspiration using limited meteorological data in different climates of China. *Agricultural and Forest Meteorology*, https://doi.org/10.1016/j.agrformet.2018.08.019

Ferreira, L.B., da Cunha, F.F., de Oliveira, R.A., Fernandes Filho, E.I. 2019. Estimation of reference evapotranspiration in Brazil with limited meteorological data using ANN and SVM – A new approach. *Journal of Hydrology,* https://doi.org/10.1016/j.jhydrol.2019.03.028

Gandomi, A.H., Roke, D.A. 2015. Assessment of artificial neural network and genetic programming as predictive tools. *Advances in Engineering Software,* https://doi.org/10.1016/j.advengsoft.2015.05.007

Gocic, M., Petković, D., Shamshirband, S., Kamsin, A. 2016. Comparative analysis of reference evapotranspiration equations modelling by extreme learning machine. *Computers and Electronics in Agriculture,* https://doi.org/10.1016/j.compag.2016.05.017

Indraswari, R., Kurita, T., Arifin, A.Z., Suciati, N., Astuti, E.R. 2019. Multi-projection deep learning network for segmentation of 3D medical images. *Pattern Recognition Letters,* https://doi.org/10.1016/j.patrec.2019.08.003

Jang, J.R. 1993. ANFIS: adaptive-network-based fuzzy inference system. *IEEE Transactions on Systems, Man, and Cybernetics: Systems,* https://doi.org/10.1109/21.256541.

Khaledi, C.K.A. 2019. Projection of harvestable water from air humidity using artificial neural network (Case study: Chabahar Port). *Italian Journal of Agrometeorology*. 24 (1), 3-11.

Lazzus, J. A. 2014. Estimation of surface soil temperature based on neural network modeling. *Italian Journal of Agrometeorology.* 19 (2), 5-12.

LeCun, Y., Bengio, Y., Hinton, G. 2015 Deep learning. *Nature* https://doi.org/10.1038/nature14539

Liu, L., Gao, C., Xuan, W., Xu, Y.P. 2017. Evaluation of medium-range ensemble flood forecasting based on calibration strategies and ensemble methods in Lanjiang Basin, Southeast China. *Journal of Hydrology,* https://doi.org/10.1016/j.jhydrol.2017.08.032

Mamdani, E.H. 1974. Application of Fuzzy Algorithms for Control of Simple Dynamic Plant. *Proceedings of the Institution of Electrical Engineers,* https://doi.org/10.1049/piee.1974.0328

Maroufpoor S., Bozorg-Haddad O., Maroufpoor E. 2020. Reference evapotranspiration estimating based on optimal input combination and hybrid artificial intelligent model: Hybridization of artificial neural network with grey wolf optimizer algorithm. *Journal of Hydrology* 588:125060. https://doi.org/10.1016/j.jhydrol.2020.125060

McCulloch, W.S., Pitts, W. 1943. A logical calculus of the ideas immanent in nervous activity. *Bulletin of Mathematical Biophysics*, https://doi.org/10.1007/BF02478259

Mhalla, A., Chateau, T., Amara, N.E. Ben. 2019. Spatio-temporal object detection by deep learning: Video-interlacing to improve multi-object tracking. *Image and Vision Computing* https://doi.org/10.1016/j.imavis.2019.03.002

Nash, J.E. and Sutcliffe, J.V. 1970. River Flow Forecasting through Conceptual Model. Part 1—A Discussion of Principles. *Journal of Hydrology*, http://dx.doi.org/10.1016/0022-1694(70)90255-6

Nourani, V., Elkiran, G., Abdullahi, J. 2019. Multi-station artificial intelligence based ensemble modeling of reference evapotranspiration using pan evaporation measurements. *Journal of Hydrology,* https://doi.org/10.1016/j.jhydrol.2019.123958

Ohmura, A. 1982. Objective criteria for rejecting data for Bowen ratio flux. *Journal of Applied Meteorology and Climatology.* 21, 595-583 598.

Partalas, I., Tsoumakas, G., Hatzikos, E. V., Vlahavas, I. 2008. Greedy regression ensemble selection: Theory and an application to water quality prediction. *Information Sciences* https://doi.org/10.1016/j.ins.2008.05.025

Penman, H.L. 1948. Natural Evaporation from Open Water, Bare Soil and Grass. *Proceedings of the Royal Society of London*, https://doi.org/10.1098/rspa.1948.0037

Perez, P.J. Castellvi, F., Ibañez, M., Rosell, J.I. 1999. Assessment of reliability of Bowen ratio method for partitioning fluxes. *Agricultural and Forest Meteorology*, 97, 141-150.

Rumelhart, D.E., Hinton, G.E., Williams, R.J. (1986) Learning representations by back-propagating errors. *Nature*, https://doi.org/10.1038/323533a0

Şaylan, L., Kimura, R., Çaldağ, B., Akataş, N. 2017. Modeling of soil water content for vegetated surface by artificial neural network and adaptive neuro-fuzzy inference system. *Italian Journal of Agrometeorology*. 22 (3), 37-44.

Şaylan, L., Kimura, R. Altınbas, N., Çaldağ, B., Bakanoğulları, F. 2019. Modeling of Surface Conductance over Sunn Hemp by Artificial Neural Network, *Italian Journal of Agrometeorology*, 24, 3, 37-48.

Takagi, T., Sugeno, M. 1985. Fuzzy Identification of Systems and Its Applications to Modeling and Control. *IEEE Transactions on Systems, Man, and Cybernetics: Systems*. https://doi.org/10.1109/TSMC.1985.6313399

Tiwari, M.K., Chatterjee, C. 2010. Uncertainty assessment and ensemble flood forecasting using bootstrap based artificial neural networks (BANNs). *Journal of Hydrology,* https://doi.org/10.1016/j.jhydrol.2009.12.013

Turc, L. 1961. Water requirements assessment of irrigation, potential evapotranspiration: Simplified and updated climatic formula. *Annales Agronomiques*, 12, 13-49.

Wen, X., Si, J., He, Z., Wu, J., Shao, H., Yu, H. 2015. Support-Vector-Machine-Based Models for Modeling Daily Reference Evapotranspiration with Limited Climatic Data in Extreme Arid Regions*Water Resources Management,* https://doi.org/10.1007/s11269-015-0990-2

Willmott, C.J., Robeson, S.M., Matsuura, K. 2012. A refined index of model performance. *International Journal of Climatology,* https://doi.org/10.1002/joc.2419

Wu, L., Zhou, H., Ma, X., Junliang, F., Zhang., F. 2019. Daily reference evapotranspiration prediction based on hybridized extreme learning machine model with bio-inspired optimization algorithms: Application in contrasting climates of China. *Journal of Hydrology*. 577:123960. https://doi.org/10.1016/j.jhydrol.2019.123960

Xu, L., Chen, N., Zhang, X., Chen, Z. 2020. A data-driven multi-model ensemble for deterministic and probabilistic precipitation forecasting at seasonal scale. *Climate Dynamics*. https://doi.org/10.1007/s00382-020-05173-x

Yassin, M.A., Alazba, A.A., Mattar, M.A. 2016. Artificial neural networks versus gene expression programming for estimating reference evapotranspiration in arid climate. *Agricultural Water Management*. https://doi.org/10.1016/j.agwat.2015.09.009

Zadeh, L.A. 1965. Fuzzy Sets. *Information and Control,* 8, 338–353.

Italian Journal of Agrometeorology
Rivista Italiana di Agrometeorologia

Firenze University Press
www.fupress.com/ijam

Citation: F. Orlandi, A. Ranfa, L. Ruga, C. Proietti, M. Fornaciari (2021) Meteorological and *Salix* species (*S. acutifolia*, *S. smithiana*, *S. viminalis*) phenological trends in central Italy. *Italian Journal of Agrometeorology* (1): 81-88. doi: 10.36253/ijam-822

Received: January 15, 2020

Accepted: January 17, 2021

Published: August 9, 2021

Data Availability Statement: All relevant data are within the paper and its Supporting Information files.

Competing Interests: The Author(s) declare(s) no conflict of interest.

Meteorological and *Salix* species (*S. acutifolia, S. smithiana, S. viminalis*) phenological trends in central Italy

Fabio Orlandi*, Aldo Ranfa, Luigia Ruga, Chiara Proietti, Marco Fornaciari

Department of Civil and Environmental Engineering, University of Perugia, Borgo XX Giugno 74, 06121 Perugia, Italy
*Corresponding author: fabio.orlandi@unipg.it; ORCID: 0000-0003-4021-8664

Abstract. Plant phenology, through opportune observing and interpreting techniques can be useful to interpret the eventual plant vegetative and reproductive adaptation to climate changes. Some plants of *Salix acutifolia Willd., S. smithiana Willd.* and *S. viminalis L.* were considered in a phenological garden in central Italy for analysing their phenological growth stages according to the International gardens network indications during a 10-year period (2008-2017) which allowed us to realize some preliminary trend analyses. The 3 Salix species showed different behaviours in the same cultivation area. *S. acutifolia* manifested no trend for spring and autumnal phases, *S. viminalis* presented low significant trends while *S. Smithiana* was that with the more evident tendencies for all the considered vegetative phases during the study period. The reproductive phase (BBCH 65) showed no significant trend for any *Salix* species during the study period not being influenced by the different meteorological variables and suggesting that photoperiod in this case may play an important role. The more evident phenological trends were represented for 2 *Salix* species by the advance of the leaf development during spring and by the progressive delay of the senescence during the last part of the summer, with the fallen leaves phase that was recorded averagely 2 weeks later during the last years of the study period.

Keywords: phenological stages, *Salix* species, climate.

INTRODUCTION

Phenological monitoring of the vegetative and reproductive plant developments recorded during the annual cycle of different species utilized as biomonitors in sampling campaigns allow to interpret the relationships between the principal environmental factors and biological response of spontaneous and agricultural plants (Menzel et al. 2006; Orlandi et al. 2007).

Plant phenology, which refers to the growth cycle of plant species in different regions, can be highly affected by climatic changes above all considering focal development stages such as the start and the end of the growing season or the flowering (Kramer 1994; Bergant et al. 2002; Schleip et al.

2008; Chuine et al. 2010; Gordo and Sanz 2010; Aguilera et al. 2014). In deciduous arboreal species, the flowering and leafing dates at the end of winter-early spring are influenced by the chilling amounts for buds and the successive forcing temperature summations (after break dormancy) as an adaptation for preventing the beginning of vegetative development once frosts during February-march in Mediterranean area may be very dangerous (Larcher 2003).

The purpose of this study was to describe and interpret the phenological vegetative and reproductive growth stages of some clone plants of *Salix spp* in comparison to the climate characteristics recorded in a "Garden" of central Italy included in the International Phenological Gardens network (IPG) and consequently not subjected to invasive agronomic techniques. The garden located near Rieti, central Italy, and managed by personnel of the University of Perugia (UNIPG) contains from 2005 to nowadays some indicator species, common to the IPG network (Schnelle and Volkert 1964; Orlandi et al. 2007) obtained from mother plants received from the German Weather Service, the European coordinator for the distribution of IPG clones.

Usually in these types of Gardens, the principal area is dedicated to the International section where plants common to the large part of the European phenological gardens are present. Other sections are the "National" and the "Local" ones where often plants of economic interest for the cultivation area are present. The principal aim of this study was to show the presence of eventual trends of the main meteorological variables and Willow plants vegetative and reproductive phenological dates during a 10-year period (from 2008 to 2017) monitoring also the current climatic changes and observing potential adaptations of the plants through morphological variations during the different growing seasons.

MATERIALS AND METHODS

The phenological gardens

The first gardens in Italy were planted from'90 in accordance with the common indications established by the phenological gardens pioneers in central Europe some decades in advance (Orlandi et al. 2007, 2014). The first 2 gardens representing Italy in IPG network were those of S.Pietro Capofiume (near the city of Bologna) and Perugia (Umbria Region, central Italy) hosting national plants and some indicator species common to all IPGs in an area of Mediterranean climate with a subcontinental influence. The Perugia garden is managed by the University of Perugia that during 2005 planted other 3 gardens in Rieti area (Lazio Region) at different altitudes (about 350m, 1100m and 1700m a.s.l.). The garden considered in the present investigation is that located in the Rieti plain (Lat: N 42°25'30"; Long: E 12°49'45"; Alt. about 350m a.s.l.) in an area of about 2,000 m^2.

In the cited garden, since first cultivation period, 5 Willow trees of different Salix species (*S. acutifolia* Willd., *S. smithiana* Willd. and *S. viminalis* L.) were planted considering their importance as guide plants in north-central European gardens.

Climate data

The meteorological data essential to realize consistent statistical interpretation of biological responses to environmental variables were available directly from a meteorological station located nearby the same garden. In the Rieti plain, the meteorological station was managed by the "Apennines Centre of Terminillo Mountain" of the University of Perugia (http://www.cat.unipg.it). The variables considered were: Maximum and minimum Temperature (Tmax-Tmin in °C), Precipitation (Rain in mm), Relative Humidity (RH %), Solar Radiation (SR in cal/cm^2). The daily data of the 10-year considered period (2008-2017) were elaborated to obtain weekly summations to be used in the trend analysis.

Phenological methodology

The international phenological key of interpretation (BBCH) was utilized to obtain comparable values from the observations made in the monitored garden (Chmielewski and Rötzer, 2001; Saska & Kuzovkina 2010). The following phenological phases were considered for the vegetative cycle of the Salix species: BBCH02, beginning of bud swelling; BBCH11, first true leaf; BBCH95, the leaves are mostly fallen (50% of leaves fallen). Moreover, the flowering phase was observed monitoring the BBCH65 phase (full flowering). In each garden, the observations were conducted on three individuals of the five present plants for each *Salix* species, to limit random variability and the mean date for the onset of each phenophase was calculated as an average considering contemporarily the three plants. Two principal periods "First leaf development-FLD" and "Leave presence period-LPP", were calculated and evaluated during the study years in the two areas. FLD was calculated as the weeks number between BBCH 02 and BBCH 11, while LPP as the weeks between BBCH 11 and 95.

Relationships between meteorological requirements and the phenological phases

To evaluate the potential meteorological tendencies of the last decade in the study area, the weekly summations of the principal meteorological variables (Tmax, Tmin, Rain, RH, SR) were calculated year by year during the "FLD" and "LPP" periods. Statistical analyses were realized between the phenological periods and the meteorological variables amounts considering the 10 years of the study.

A correlation analysis was realized considering the length of the two periods "FLD" and "LPP" and the amounts of the weekly values of the principal meteorological variables during the same periods. The more significant correlated variables were considered to realize a multiple regression analysis between FLD-LPP periods as dependent variables and meteorological data as independent variables. Moreover, a trend analysis was done using nonparametric Mann-Kendall tests, for monotonic positive or negative trends. In particular, positive Z values demonstrate a trend for a delay in the biological data, while negative Z values indicate a trend for anticipation (earlier) of the historical series of each phase. To test the presence of meteorological tendencies, the weekly summations of TMax, Tmin, Rain, RH, SR, were calculated for three different periods determined on the base of the phenological phases recorded. The first period, precedent the beginning of bud swelling, from the 1st of January of each year to the mean date of BBCH 02 (calculated during the 10-year period). The second period, between mean bud swelling date (BBCH02) and first true leaf (mean BBCH 11 date). The third period, between first true leaf and leaves fallen (from the mean dates of BBCH11 to the BBCH95) during the study period. Finally, the trend analysis was also realized for the weekly summations of the meteorological variables (positive Z, increased; negative Z, decreased), for both of the phenological gardens. To estimate the true slope of an existing trend (as change per year), the Sen nonparametric method was used (Sirois 1998). For the significance levels, the following symbols are used: *, trend at $p < 0.05$; **, trend at $p < 0.01$; and ***, trend at $p < 0.001$. The Excel template application MAKESENS version 1.0 (Salmi et al. 2002) was used for the Mann-Kendall trend analysis.

RESULTS

In Fig. 1 the trend analysis of the weekly summations of the solar radiation calculated from 1 January to 2 conventional dates of the year (13th and 39th week) are shown.

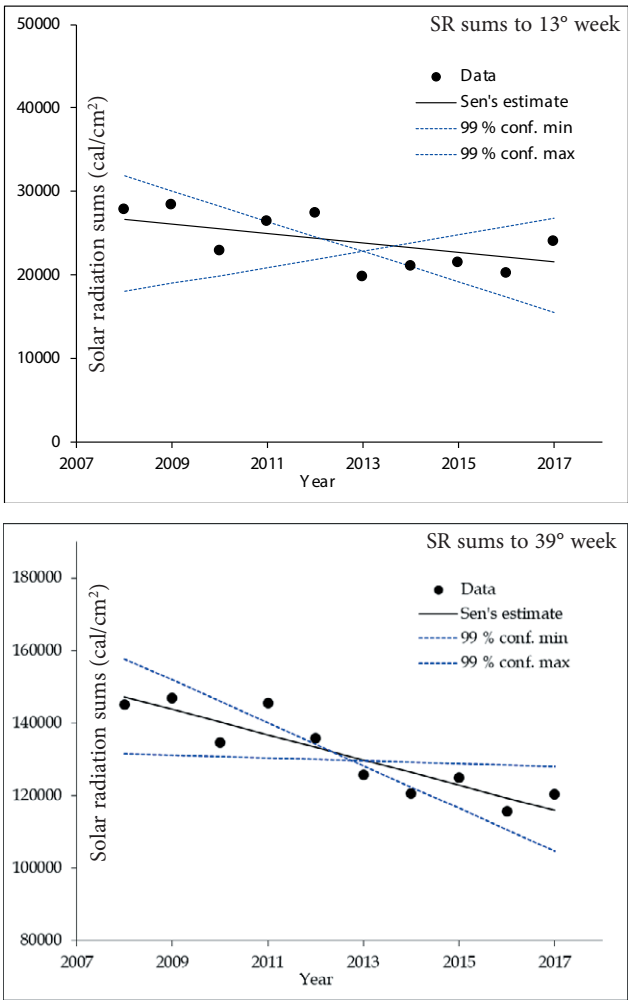

Fig. 1. Trend analysis of the weekly summations of the solar radiation (cal/cm²/day) calculated to 2 conventional dates (13th and 39th week of the year). In the chart the original data points of the time series, the Sen's estimator for a linear trend, the lines for 99% confidence intervals are shown.

The 13th week summations practically corresponded to the average date of BBCH11 phase for all the *Salix* species in the study area while 39th week summation is just precedent to the average BBCH95 phase occurrence. In the 10-year series no trends have been shown by quite all the different meteorological variables. Only the SR summations to the 39th week evidenced a significant negative trend (Test Z -2.50, Significance * $p < 0.01$) indicating a temporary reduction of this variable amounts particularly over the summer periods in the study area. The calculation of the average value of the 2 sub-periods 2008-2012 and 2013-2017 showed a solar radiation reduction of about 14% which determined the trend analysis result although the small size of the sample should do not lead to misleading interpretations.

In Table 1 the trend analyses (Mann-Kendall test Z coefficients) are reported for the considered phenological phases that for the meteorological variable summations recorded to the same phases dates. *S. acutifolia* not presented significance for any phases so neither meteorological amounts were calculated to its development dates.

On the other hand, both *Salix smithiana* that *viminalis* evidenced some valuable results although conditioned by the low number of years considered in the trend analysis and therefore to validate with subsequent analyses.

However, *S. smithiana* presented significant trends during the study period for BBCH 02-11 and 95, also the two calculated periods "First leaf development-FLD" and "Leave presence period-LPP" showed high significance.

In particular, the beginning of bud swelling (BBCH 02) showed a low decreasing significant trend corresponding to a progressive advance, such as the successive phase, BBCH 11, even more evident (Z coefficient -2.68). The senescence phase, BBCH 95, showed an increasing trend related to a progressive delay of the phenological dates with the consequences that FLD trend was significantly decreasing while LPP even more significantly increasing.

Salix viminalis showed the same trends of *S. smithiana* even if with lowest significance values, while BBCH02 presented no trends.

In Table 1 is also possible to evidence that considering *S. smithiana*, Tmin and Rain weekly summations from the first of January to BBCH_11 dates not showed any trends, while Tmax, and above all RH and SR presented significant values. Moreover, RH, Rain and Tmin from 1st January to BBCH95 dates not evidenced any trend during the study period. As regard as *Salix viminalis* BBCH11, above all Tmin and Rain showed no trends but, in this case, also Tmax was not significant. Moreover, for this species the RH and Rain summations to BBCH95 dates showed no trends but also both the temperature variables showed not significant values.

In Table 2 the multiple regression analysis between phenological phases and LPP periods which previously showed significant trend, as dependent variables and meteorological data as independent ones for the *Salix* species were reported. The BBCH11 phase for both the species was better related with Tmin and RH, *S. smithiana* presented also Rain as important independent variable while *S. viminalis* SR. The BBCH95 phase and LPP period showed Tmax and RH as the more important variables to explain their variance during the study year.

Tab. 1. Trend analysis of the phenological phases/periods and meteorological variable amounts for two *Salix* species during the 10-year study period (2008–2017).

Mann-Kendall test Z coefficient

Salix smithiana			*Salix viminalis*		
	Test Z	Signific.		Test Z	Signific.
BBCH_02	-1.73	+			
BBCH_11	-2.68	**	BBCH_11	-2.08	*
BBCH_95	2.11	*	BBCH_95	1.70	+
FLD	-2.02	*	FLD	-1.67	+
LPP	3.26	**	LPP	1.86	+
BBCH11_Tmax	-1.79	+	BBCH11_Tmax	-1.35	
BBCH11_Tmin	-0.18		BBCH11_Tmin	0.18	
BBCH11_Rain	-0.89		BBCH11_Rain	-0.89	
BBCH11_RH	-2.15	*	BBCH11_RH	-1.55	+
BBCH11_SR	-2.50	*	BBCH11_SR	-2.68	**
BBCH95_Tmax	2.33	*	BBCH95_Tmax	0.89	
BBCH95_Tmin	0.89		BBCH95_Tmin	0.18	
BBCH95_Rain	-0.36		BBCH95_Rain	-0.36	
BBCH95_RH	0.18		BBCH95_RH	0.00	
BBCH95_SR	-1.79	+	BBCH95_SR	-1.79	+

+ p< 0.05; * p< 0.01; ** p< 0.001
w1-w7 = period precedent the beginning of bud swelling
w8-w14 = period between bud swelling and first true leaf
w15-w43 = period between first true leaf and leaves fallen

Tab. 2. Multiple regression analysis between Phenological phases, FLD-LPP periods as dependent variables and meteorological data as independent variables for the *Salix* species.

	F	R2	Adj. R2	Variable	Coeff.	t	Sig.
Phenological Phases							
BBCH11 *S. smithiana*	84.84	0.977	0.965	Constant	-2.183	-2.184	0.072
				Tmin	-0.017	-2.947	0.026
				RH	0.017	15.545	0.000
				Rain	-0.005	-3.524	0.012
BBCH95 *S. smithiana*	33.86	0.9063	0.880	Constant	8.204	1.815	0.091
				Tmax	0.035	7.855	0.000
				RH	0.004	4.452	0.003
BBCH11 *S. viminalis*	52.9	0.964	0.945	Constant	2.600	2.126	0.078
				Tmin	-0.014	-2.531	0.045
				RH	0.009	5.978	0.001
				SR	0.000	3.688	0.010
BBCH95 *S. viminalis*	26.83	0.885	0.852	Constant	10.562	2.375	0.049
				Tmax	0.025	5.974	0.001
				RH	0.003	3.770	0.007
Phenological Periods							
LPP *S. smithiana*	91.54	0.963	0.953	Constant	-6.014	-2.052	0.079
				Tmax	0.035	8.397	0.000
				RH	0.005	5.469	0.001
LPP *S. viminalis*	50.82	0.936	0.917	Constant	-7.417	-1.985	0.087
				Tmax	0.036	8.720	0.000
				RH	0.005	4.168	0.004

In Fig. 2 and 3, trend analysis of the BBCH11, BBCH95 and LPP during the 10-year study period for *Salix smithiana* and *viminalis* have been presented. If the BBCH11 dates are similar for the two *Salix* species, BBCH95 dates showed some differences with *S. viminalis* in advance of about 2 weeks.

DISCUSSION AND CONCLUSION

The 3 *Salix* species showed different behaviours in the same cultivation area. *S. acutifolia* manifested no trend for spring and autumnal phases, *S. viminalis* presented low significant trends while *S. Smithiana* was that with the more evident tendencies for all the considered vegetative phases during the study period.

The reproductive phase (BBCH 65, data not published) showed no significant trend for any *Salix* species during the study period not being also influenced by the different meteorological variables. This result validated the hypothesis according to which photoperiod is one of the principals forcing variable to regulate the timing of growth cessation in temperate and boreal regions at the end of the summer and the flower structure maturation when the first leaves have been developed during spring (Johansson and Staiger 2015; Orlandi et al. 2005). The photoperiodic signal controlling seasonal growth in trees appears to be perceived in the leaves even if other environmental variables mostly winter and spring temperatures interact with it determining complex species-specific interactions making difficult to correctly interpret the phenomena (Singh et al. 2017).

In this sense, the photoperiod, mainly determined by a function of latitude and time of year, is insensitive to the climate change, except under very cloudy conditions, not allowing to flowering phenomena to manifest significant tendencies.

Moreover, the graphic interpretation of the trend analysis suggested as the trend of BBCH11 evidenced a narrower 99% confidence interval evidencing less uncertainty about the results in comparison to that of BBCH 95.

In particular, on the base of the obtained results, the shortening trend of the FLD period for the *Salix* species may be attributed to the significant progressive advance during the years of the first true leaf dates (BBCH 11) and to the substantial unchanging (or lowest changing) of the bud swelling beginning (BBCH 02).

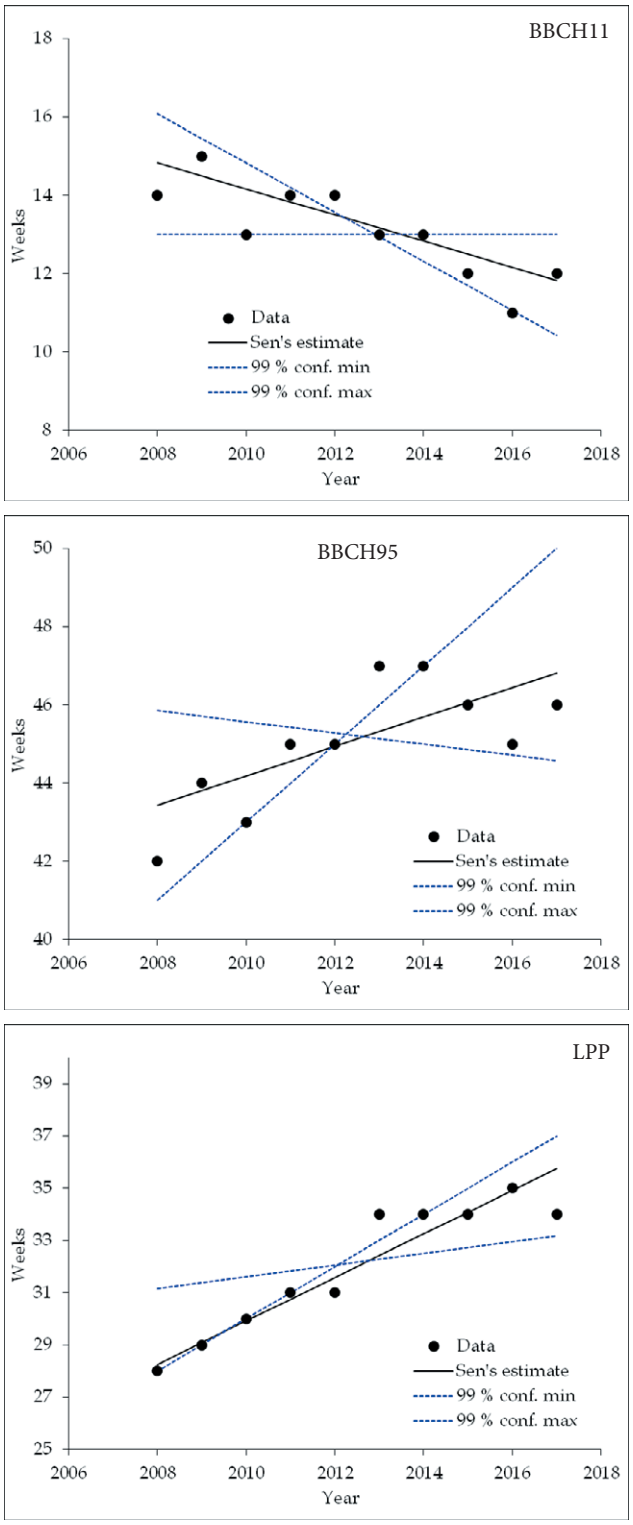

Fig. 2. Trend analysis of the BBCH11, BBCH95 and LPP during the 10-year study period for *Salix smithiana*. In the chart the original data points of the time series, the Sen's estimator for a linear trend, the lines for 99% confidence intervals are shown.

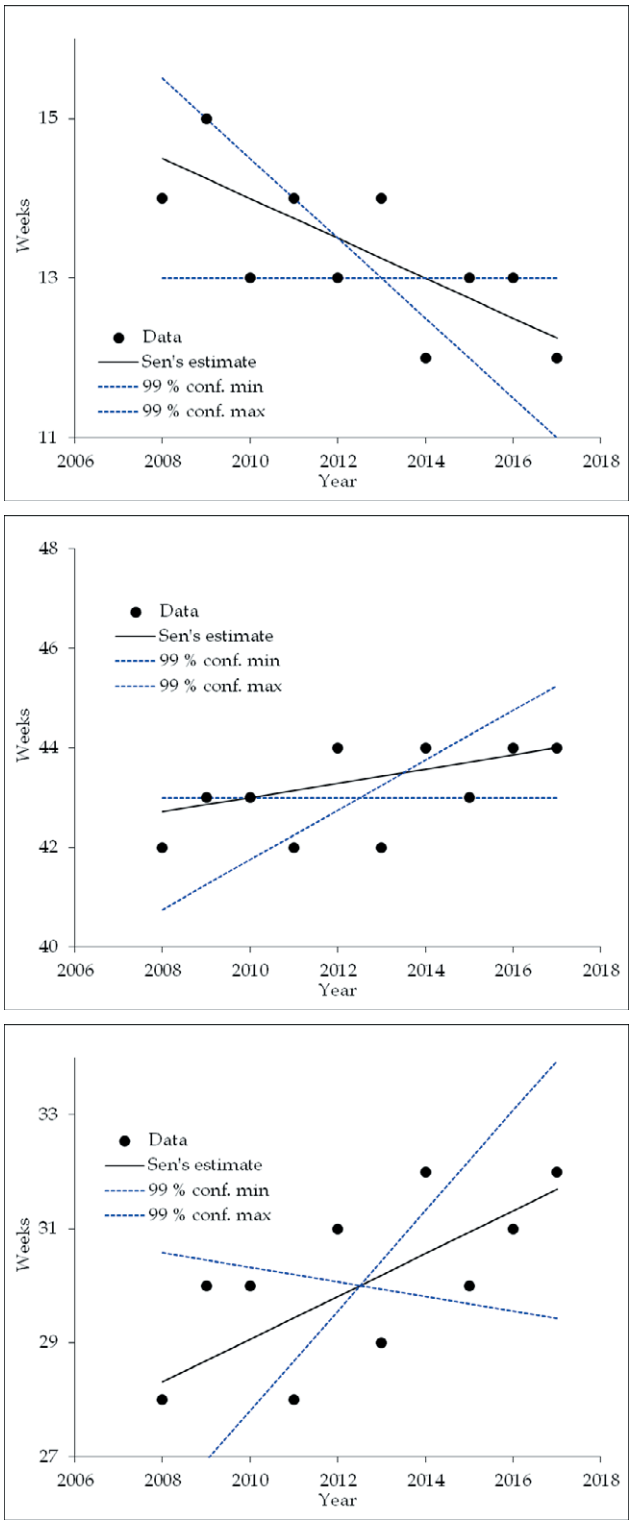

Fig. 3. Trend analysis of the BBCH11, BBCH95 and LPP during the 10-year study period for *Salix viminalis*. In the chart the original data points of the time series, the Sen's estimator for a linear trend, the lines for 99% confidence intervals are shown.

The trend analyses realized for the meteorological variable summations recorded until the BBCH11 showed for *S. smithiana* Tmin and Rain as the variables without a significant trend. Moreover, RH, Rain and Tmin summations to BBCH95 not evidenced any trend.

In this case, we assumed that the no "trendy" meteo-variables for phenological phases with significant trends, were those which recorded "similar" summations year by year and so which more "regularly" influenced the plant development not being affected by the advance or delay of the same dates. In particular, BBCH11 of *S. smithiana* and *viminalis* was more influenced by "similar" chilling (Tmin) sums during the first weeks of the year, while BBCH95 by RH amounts.

Practically, the influence of Tmin but also of RH, Rain and SR permitted to the young leaves to develop in shorter periods reaching in advance a complete development.

On the other hand, the trends of the LPP periods in both the areas were influenced by the simultaneous BBCH11 and 95 dates variation. In this sense, the lengthening of LPP may be related also to the progressive delay of the senescence phase during the years, with the BBCH95 that were recorded averagely 2 weeks later during the last years of the study period. The senescence delay of both *S. smithiana* and *viminalis* can be related to the high significant decreasing trend of SR summations to 39th week, furthermore considering that SR manifested negative trend even if calculated to the BBCH95 dates themselves in progressive delay during the study years. In general, solar radiation have a limited impact on spring phenology compared with temperature and precipitation and its influence is mainly concentrated in August and September. Precedent investigations carried out as insolation sums also influence the phenological process in autumn, although their effects were largely biome dependent (Liu et al. 2016). The decline of August solar radiation may contribute to vegetation activities and accumulation of non-structural carbohydrate (Fu et al., 2014) in such a way that solar radiation reduction can postpone autumn senescence phenological phases.

REFERENCES

Aguilera F., Fornaciari M., Ruiz-Valenzuela L., Galán C., Msallem M., Ben Dhiab A., Díaz de la Guardia C., Trigo MM., Bonofiglio T., Orlandi F., 2014. Phenological models to predict the main flowering phases of olive (Olea europaea L.) along a latitudinal and longitudinal gradient across the Mediterranean region. International Journal of Biometeorology doi:10.1007/s00484-014-0876-7.

Bergant K., Kajfez-Bogataj L., Crepinsek Z., 2002. Statistical downscaling of GCM simulated average monthly air temperature to the beginning of flowering of dandelion (Taraxacum officinale) in Slovenia. International Journal of Biometeorology, 46: 22–32.

Chmielewski FM., Rötzer T., 2001. Response of tree phenology to climate change across Europe. Agriculture Forest and Meteorology, 108: 101-112.

Chuine I., Morin X., Bugmann H., 2010. Warming, photoperiods, and tree phenology. Science, 329: 277–278.

Fu YS., Campioli M., Vitasse Y., De Boeck HJ., Van den Berge J., AbdElgawad H., Janssens IA., 2014. Variation in leaf flushing date influences autumnal senescence and next year's flushing date in two temperate tree species. Proceedings of the National Academy of Sciences, 111(20): 7355-7360.

Gordo O., Sanz JJ., 2010. Impact of climate change on plant phenology in Mediterranean ecosystems. Global Change Biology, 16: 1082-1106.

Johansson M., Staiger D., 2015. Time to flower: interplay between photoperiod and the circadian clock. Journal of Experimental Botany, 66(3,1): 719-730.

Kramer K., 1994. Selecting a model to predict the onset of growth of Fagus sylvatica. Journal of Applied Ecology, 31: 172-181.

Larcher W., 2003. Physiological plant ecology: ecophysiology and stress physiology of functional groups. Biologia Plantarum, 47 (4): 500–513.

Liu Q., Fu YH., Zeng Z., Huang M., Piao S., 2016. Temperature, precipitation, and insolation effects on autumn vegetation phenology in temperate China. Global Change Biology, 22(2): 644-655.

Menzel A., Sparks TH., Estrella N. et al. 2006. European phenological response to climate change matches the warming pattern. Global Change Biology, 12: 1969-1976.

Orlandi F. et al. 2005. Bioclimatic requirements for olive flowering in two mediterranean regions located at the same latitude (Andalucia, Spain, and Sicily, Italy). Annals of Agriculture and Environmental Medicine, 12: 47-52.

Orlandi F., Bonofiglio T., Ruga L., Sgromo C., Romano B., Fornaciari M., 2007. Phenological investigations of different winter-deciduous species growing under Mediterranean conditions. Annals of Forest Science, 64: 557-568.

Orlandi F., Ruga L., Bonofiglio T., Romano B., Fornaciari M., 2014. Fifteen-year phenological plant species and meteorological trends in central Italy. Intenational Journal of Biometeorology, 58: 661-667.

Salmi T., Maatta A., Anttila P., Ruoho-Airola T., Amnell T., 2002. Detecting Trends of Annual Values of Atmospheric Pollutants by the Mann-Kendall Test and Sen's Slope Estimates-The Excel Template Application Makesens". Finnish Meteorological Institute Publications on Air Quality No. 31, Helsinki, Finland.

Saska MM., Kuzovkina YA., 2010. Phenological stages of willow (Salix). Annals of Applied Biology, 156: 431-437.

Schleip C., Rutishauser T., Luterbacher J., Menzel A., 2008. Time series modelling and central European temperature impact assessment of phenological records over the last 250 years, Journal of Geophysical Research, 113: doi:10.1029/2007JG000646.

Schnelle F., Volkert E. 1964. Internationale Phaenologische Garten. Agriculture Meteorology, 1: 22-29.

Singh, R.K., Svystun, T., AlDahmash, B., Jönsson, A.M., Bhalerao, R.P., 2017. Photoperiod- and temperature-mediated control of phenology in trees—A molecular perspective. New Phytol., 213: 511-524.

Sirois A., 1998. A Brief and Biased Overview of Time Series Analysis or How to Find that Evasive Trend. In WMO report No. 133: WMO/EMEP workshop on Advanced Statistical methods and their Application to Air Quality Data sets (Helsinki, 14-18 September 1998).

Italian Journal of Agrometeorology
Rivista Italiana di Agrometeorologia

Firenze University Press
www.fupress.com/ijam

OPEN ACCESS

Citation: S.J. Kadbhane, V.L. Manekar (2021) Development of agro-climatic grape yield model with future prospective. *Italian Journal of Agrometeorology* (1): 89-103. doi: 10.36253/ijam-406

Received: June 28, 2019

Accepted: June 4, 2021

Published: August 9, 2021

Data Availability Statement: All relevant data are within the paper and its Supporting Information files.

Competing Interests: The Author(s) declare(s) no conflict of interest.

Development of agro-climatic grape yield model with future prospective

S.J. Kadbhane[1,*], V.L. Manekar[2]

[1] *Civil Engineering MVPS's KBT College of Engineering Nashik, Maharashtra, India. E-mail: sharad_kadbhane@rediffmail.com*
[2] *Civil Engineering, Sardar Vallabhbhai National Institute of Technology, Surat, Gujarat, India. E-mail: vivek_manekar@yahoo.co.in*
*Corresponding author.

Abstract. Agriculture sector is most vulnerable to climate change. To predict the crop yield in accordance with the changing climate is a need of hour than choice. To know the climate in advance is crucial for grape growing farmers and grape export agencies for its better planning and security of grape industries from climate change perspective. In the present study, the Agro-Climatic Grape Yield (ACGY) model is developed on monthly scale climatic parameters using correlation, significance and multi-regression analysis approach. The developed model is statistically tested for its predictive ability. The discrepancy ratio, the standard deviation of discrepancy ratio, mean percentage error and standard deviation of mean percentage error for the developed model is obtained as 1.03, 0.19, 0.03% and 0.19 respectively. Sensitivity analysis is carried out for the developed ACGY model using the parametric sensitivity method. In order to know the grape yield for future using developed ACGY model, climate scenarios are generated under Canadian Earth System Model (CanESM2) for three emissions Representative Concentration Pathways (RCP) as RCP2.6, RCP4.5, and RCP8.5. Model response variability is carried out to understand the variation of grape yield. It is observed that grape yield is showing adverse variation with the increase in minimum temperature in January and November months, and precipitation in August and November months. Whereas, minimum temperature in April and sum of monthly mean evapotranspiration showing accordance effect on the grape yield. It is recommended the use of ACGY model for grape yield estimations applicable for the present and future climate of the study area based on the predictive capability of developed model.

Keywords: climate change, agro-climatic grape yield models, food security, Grape yield, statistical downscaling.

1. INTRODUCTION

The agriculture sector is a backbone of Indian economy. About 58% of the rural population of India depends on agriculture sector directly or indirectly for the live hood (Srinivastav 2015). As per the *Central Intelligence Agency (CIA) fact-book*, Indian nation's gross domestic product (GDP) of different sector composed in 2017 is as Services (57.9%), Industry (24.2%), and Agriculture

(17.9%) (http://statisticstimes.com). Cumulative agriculture production is $ 366.92 billion. India is the second largest producer of the agriculture product in world. India accounts for 7.68% of total global agricultural output and hence agriculture sector's contribution to the Indian economy is much higher than world's average contribution (6.1%). According to Agriculture Production Development and Economics Authority, India (APDEA 2016), the agriculture sector has 10% contribution in the total export of Indian goods. Table Grape (Vitis vinifera cultivars) is one of the important cash crops of the country, which contributes to the socio-economic development particularly of the rural area. In the year 2016, India exported 1.5 Mt of grapes to European and Arabian countries which cost the amount of 15,513 Million Indian Rupees (INR). There is 2% export contribution of grape among all fruits cultivated in India; out of that 90% grapes are exported only from the Nashik district (Saxena, 2014).

The productivity of grape is highest in India among grape growing countries in the world (FAO 2016). In the country, Maharashtra is a highest grape producing state. Specifically, within Maharashtra state, Nashik district is a highest grape producing. Grape has potential to generate a large amount of employment. On an average, in India, one hectare grape orchard is offering employment to five people throughout the year. Among all districts of India, Nashik is the largest grape producer (APDEA, 2016). The socio-economic growth of the rural area of the Nashik district is mostly due to grape crop and its export potential.

It is well known and accepted fact that agriculture sector is highly impacted by climate change than any other sector. Globally, the effect of climate change is indicating the increase in temperature and decrease in precipitation (IPCC 2013). In Indian subcontinent, large variations are noticed in the occurrences of precipitation. There are chances of meteorological, agricultural, and hydrological drought due to such kind of variations and larger gap in the precipitation occurrences (Bowden and Bormann 1986).

Under such circumstances, it becomes difficult to predict the crop yield. Weather effects and adaptation approaches are increasingly becoming major zones of research on crop production worldwide (Hoogenboom, 2000; Yinhong et al., 2009). A condition where there is an effect of climate can have the theatrical situation and affect the food security of billions of people (Abbaspour, 1994; Droogers, 2004). An understanding of climate impact over the crop quality and quantity is essential in predicting the yield (Adams et al., 2003). The variations in crop yield associated with climatic parameters will probably have key influences on local and universal food production (Abraha and Savage, 2006).

Prediction of climate in advance is crucial to grape growing farmers and grape export agencies for its better planning and security of grape industries from climate change perspective. The estimation of yield is another important issue related to the grape industry. It is revealed from the literature survey that there are many yield estimating models available for crops like wheat, rice, maize, sorghum, sugarcane, etc., but for the estimation of grape yield need to develop new models (Zhang and Shen, 2008). Moreover, models are observed as location specific with limited variables involved in the model. There is no evidence of any model reported in the literature so far for the estimation of grape yield of Indian terrain. Therefore, it is felt that there is an urgent need for such agro-climatic grape yield (ACGY) model which can estimate the yield considering significant parameters together and which can represent the grape yield process in accordance with the climate. It is also revealed from the literature survey that crop yield models are performing better on the local scale than global scale. Hence, the present study is undertaken to develop Agro-Climatic Grape Yield (ACGY) model for the study area as Nashik district with reference to the current and future climate.

2. MATERIALS AND METHODS

In the present study, it is tried to developed ACGY model using parameters mainly from the domain of climate. In the development of ACGY model, the parameters from the climate domain are considered as temperature, precipitation, relative humidity, sunshine hour, and evapotranspiration. Climate data is collected from India Meteorological Department (IMD) India. Soil domain data is collected by field survey, and laboratory testing at National Horticultural Research and Development Foundation (NHRDF) Niphad. All grape plants are of common variety cultivated in the study area, namely Thompson seedless. The planted spacing between rows is 2.4 m and spacing between plants is 1.2 m. A drip irrigation system is used. The training system mostly used is T and Y shape trellis structure, for high yields of grape plant. In the study area from March to May temperature is high, there is no precipitation and low humidity. Whereas from June to October temperature is low, precipitation and humidity are high. From November to February, there is low temperature, rare rainfall and low humidity. Based on the recommended ranges of the various properties of the soil, it is found that the soil of the study area is of good quality for yielding grape. Study area has good characteristics and climatic conditions for production of grape.

2.1 Location details of study area

The location of the Nashik district is $18^0$19'48" to $20^0$31'48" N latitude and $73^0$09'36" to $75^0$09'17" E longitude at the North-West part of Maharashtra state, at 565-meter altitude. Nashik district is having total fifteen talukas, namely Nashik, Surgana, Trimbak, Peint, Igatpuri, Niphad, Sinnar, Dindori, Kalwan, Yeola, Nandgaon, Chandwad, Satana, Deola, and Malegaon. According to the census report 2011, the district includes 1931 villages (https://nashik.nic.in).

2.2 Phenological stages and climatic associations of grape plant

The phenological cycle of the grape plant in the tropical and subtropical region includes phases of dormancy, active vegetation, reproductive development, and growth. The grape plant has mainly six phenological stages i.e. bud breaking, flowering, berry set, berry growth, veraison and harvest. In the study area grape plant is broadly having two pruning cycles such as foundation pruning (April to September) and fruit pruning (October to March). Near about 90% of grape orchards are following this schedule except color varieties and vineyards located in the Northern region of Nashik district. The evolution of the phenological phases or the particular monthly variation in the climate plays a vital role in the grape production (Adsule, 2013). Fruit pruning takes place in the first week of October. In this particular stage, due to decrease in temperature or increase in humidity or decrease in evapotranspiration or occurrence of rainfall, either all or any one of these parameters affecting the bud break and lead to induce fungal disease. If rainfall occurs in the month of October, then there are major chances of having the fungal disease which also disturb the vegetative growth. In the month of November, most of the grape orchards are under the phenological stage of flowering. The flowering stage is found to be very sensitive towers humidity and rainfall. If rainfall occurs during the flowering stage, grape clusters get heavily damage and flowers are not able to convert into the berry. The berry growth phenological stage is observed in the month of December and January andthe temperature affects the growth of the berry.

2.3 Pearson correlation and regression coefficient

Correlations and regressions aim at defining the relationship among parameters. The aim of this method is to investigate the significant correlation between one or more dependent and independent variables (Gupta, 1981). A sample correlation coefficient between the X and Y variables can be found using Pearson correlation coefficient (r) and defined as given in Eq.(1).

$$r = \frac{cov(X,Y)}{SD_X . SD_Y} = \frac{\frac{1}{n}\sum_{i=1}^{n}(x_i - M_X)(y_i - M_Y)}{\sqrt{\frac{1}{n}\sum_{i=1}^{n}(x_i - M_X)^2}\sqrt{\frac{1}{n}\sum_{i=1}^{n}(y_i - M_Y)^2}} \quad (1)$$

Where, cov (X, Y) is the covariance among X and Y, SD_X and SD_Y are the standard deviations of the series of variables, X and Y are the series of variables, M_X and M_Y are mean of the series of variables, and x_i is independent variable and y_i dependent variable. Pearson correlation coefficient (r) can be calculated using the original values of X and Y. Essentially, *r* is $-1 \leq r \leq 1$ showing negative and positive values of *r* indicating linear correlation between X and Y, both associates with large values. If r is zero, then there is no linear correlation.

2.4 Multi-regression analysis

The prediction capability of any model is dependent on the model parameters representing that model. Selection of model parameters, if selected, based on their level of significance improves the model performance. It also depends upon the total number of model parameters involved in the model. Therefore, the selection of model parameters is a crucial stage in the model development. It is revealed from the literature survey that climatic conditions during the phenological stages of grape plant plays an important role in deciding the yield. Hence, to develop ACGY model, the most significant climatic parameters at the phenological stages should be selected after carrying out the separate regression analysis for each of the selected parameters. The climatic parameter such as temperature and precipitation always shows the non-monotonic effect on the crop yield. Model variables from the domain of climate, soil, and irrigation practices are seem to be most significant for the grape yield. In the development of such models, which need the involvement of multi-parameters, it is found that multi-regression analysis technique is the most appropriate technique due to the advantage of getting freedom in selecting multi parameters (Gupta, 1981). Hence, in the development of ACGY model, selection of variable based on statistical relationship and grape phenology is used in its development. The parameters from the domain of climate, soil, and irrigation practices are considered in the development of the agro-climatic grape yield (ACGY) model using the multi-regression analysis. The basic form of the multi-regression model is indicated below in Eq. (2).

$$Y = C + \alpha_1 X_1 + \alpha_2 X_2 + \alpha_2 X_3 + \alpha_n X_n \quad (2)$$

Where Y is a dependent parameter, C is the value of y when all the independent variables are zero, α_1, $\alpha_{2.....}$ α_n are regression coefficients and X_1, X_2, X_3, ….X_n are independent parameters. The regression coefficients are estimated using. Eq.(3).

$$\alpha = \left(\frac{r_{y\,xj} - r_{y\,xi} r_{xi,xj}}{1-(r_{xi,xj})^2}\right)\left(\frac{SD_y}{SD_{xj}}\right) \quad (3)$$

Where α is the regression coefficients, *r* is the correlation coefficient, *SD* is the standard deviation, i and j are the sample parameters from the series x and y.

2.5 Comparison of data samples using t-test

The objective of t-test is to equate two unpaired sets of data and apply to non-continuous or continuous data (Gupta, 1981). The t-statistics can be calculated by estimating the pooled variance. Initially, the estimation of unbiased pooled variance is carried out using Eq. (4).

$$V = \frac{V_A(N_A-1)+V_B(N_B-1)}{V_A+V_B-2} \quad (4)$$

Where, V is unbiased pooled variance, N_A and N_B are the number of data point in group A and B and V_A and V_B are variances of groups A and B.

The standard error using unbiased pool variance is calculated using Eq. (5).

$$SE = \sqrt{V\left(\frac{1}{N_A}+\frac{1}{N_B}\right)} \quad (5)$$

The t-statistics are calculated as the ratio of using difference of the means and the standard error as shown below in Eq. (6).

$$t = \frac{M_A - M_B}{SE} \quad (6)$$

Where M_A and M_B are mean of group A and B respectively.

2.6 p-values

Once the t-statistics value and degree of freedom are determined then p-value is determined by using t-statistics table. Once hypotheses, H_0 (data samples created from the similar parameter data set), and H_1, (most data sample created from different parameter data set) is true then p-value (<0.05) is an approximate value adapted as significant value (Gupta, 1981). It is indicated that there should be 5% possibility of incorrectly identifying the significant change (p-value < 0.05) i.e. 5% significance level, it means 95% confidence interval.

2.7 Parametric and component sensitivity method

Any system is cover under three functions such as the output functions, transfer function, and input functions. The transfer function converts the input function into the output function. Hence, this function could be the probability distribution function which depends on one or more variables.

The sensitivity analysis of the mathematical model is to find out the parametric variation on the output. The parametric sensitivity is algebraically expressed as given in Eq. (7).

$$S_{pi} = \frac{\partial O}{\partial P_i} = \frac{f(P_i+\Delta P_j; P_{jlj\neq i}) - f(P_1, P_2 \ldots\ldots, P_n)}{\Delta P_i} \quad (7)$$

Here, O is output functions and Pi represent response function parameter. In general, crop yield models are more complex, so it is difficult to compute the parametric sensitivity. Hence, by considering the input and output function, sensitivity can be defined. Therefore, component sensitivity is found using input function on the output function O as shown in the Eq. (8).

$$\frac{\partial O}{\partial I} \quad (8)$$

The relative sensitivity value (RSV) of the input can be computed. Here, the mean values, the relative sensitivity of output parameters O_i and O_j to the input Pi and Pj would be estimated using Eq. (9 and 10)

$$R_{si} = \frac{\partial Oi}{\partial P_i}\left(\frac{\bar{P_i}}{\bar{O}_i}\right) \quad (9)$$

$$R_{sj} = \frac{\partial O_j}{\partial P_j}\left(\frac{\bar{P_j}}{\bar{O}_j}\right) \quad (10)$$

Where, R_{si} and R_{sj} are the relative sensitivity values, $(\partial O_i/\partial P_i)$ and $(\partial O_j/\partial P_j)$ are the coefficient of input parameters $\overline{P_i}$ and $\overline{P_j}$ (the mean of input parameters) and $\overline{O_i}$ and $\overline{O_j}$ the mean of the output parameter. The higher value of relative sensitivity R_{si} and R_{sj} indicates greater the impact of the input parameter on output parameters.

2.8 Forecasting of climate

Several climate predicting models are reported in the literature. General circulation models (GCMs) are reported to acquire climate data on the global scale or large scale. Due to coarser resolution, it becomes essential to downscale this data to regional or local scale. Large numbers of such models are available, which explore the relationship between large scales to local scale data. In this study statistical downscaling model (SDSM) is used for predicting future climate. Using SDSM, different climate scenarios under different climatic conditions are possible to generate (Wilby et al., 2002). Ocean element has 40 vertical layers, 10 m approximately resolution and 1.410° N x 0.940° E horizontal resolution (Hoskin, 1980). The CanESM2 is organized for Coupled Model Inter-comparison Project Phase 5 (CMIP5), (Taylor et al., 2012) and this is mainly the involvement for IPCC Fifth Assessment Report (AR5) (Arora and Boer, 2014). Different scenarios are used at various stages of time in climate research according to IPCC's first SRES (Special Report on Emissions and Scenarios) used in the third and fourth report of assessment. During 2013-14, IPCC 5th Assessment Report (AR5) was published. The results are the basis of new scenarios set that replaced the SRES. The Representative Concentration Pathways (RCPs) are new scenarios and it is the latest iteration of the scenario process. These are four pathways such as RCP 2.6. 4.5, 6, and 8.5. The RCPs are developed using the combined efforts of the researchers from different disciplines involved in climate research (Van Vuuren et al., 2011). They are named at the end of the 21st century based on the radiative forcing target 2.6. 4.5, 6, and 8.5 W/m^2. In this study mainly RCP 2.6, 4.5, and 8.5 are considered for forecasting the future climate.

3. RESULTS AND DISCUSSIONS

3.1 Selection of model parameters

It is tried to cover up the maximum and significant parameters in the model development which represents the entire phenomenon of the grape yield significantly. In order to develop a meaningful relationship between the dependent and independent variables of the yield process, functionally grape yield can be written as shown below in Eq. (11);

$$Y = f(T, P, S_h, R_h, ETo) \quad (11)$$

Where, Y is a Grape yield (ton/ ha); T is Temperature (the monthly minimum, maximum, average in °C); P is Precipitation (monthly total mm); S_h is Sunshine hours (hr); R_h is Relative humidity (%), and ET_o is reference evapotranspiration (mm day^{-1}).

3.2 Correlation analysis for yield with climatic parameters

Climatic parameters are shown the effect on crop yield throughout the phenological stages of the grape crop. It is difficult to find out the relationship between yield and climatic parameters due to its scale of variability from day to day and month to month. To check the correlation of these climatic parameters, correlation analysis is carried out for the dependent parameter and independent parameter using 70% data i.e. during the period 1991-2008. Temperatures are observed on daily scale as minimum, maximum, and average. Correlation analysis is carried out for monthly mean minimum temperature, monthly mean maximum temperature, and monthly mean average temperature with the grape yield. Whereas, precipitation considered as monthly total precipitation. Relative humidity (%) and Sunshine hours (hr) are considered as monthly mean values. Evapotranspiration ET_o (mm/day) is the important parameter of the crop yield model which essentially exists throughout the year. Therefore ET_o is considered on the annual scale. Correlation coefficient value ranges between +1 to -1. The results of correlation analysis are shown below in Table 1.

Based on the obtained results, as shown in Table 1, the value of correlation coefficient equal to or greater than ±0.3 is considered as a correlated variable, and there is exists a correlation between independent variables and dependent variables (Nikolić et al., 2012). Accordingly, there exists a correlation between yield and i) monthly mean average temperature in the month of June and September, ii) monthly mean maximum temperature in the month of May, July, and February, iii) monthly mean minimum temperature in the month of April, November, and January, iv) monthly precipitation in the month of August, September and November, v) relative humidity in the month of August, September, and November and vi) sunshine hours in the month of April, October, November, and January; vii)

Table 1. Results of correlation analysis between monthly climatic parameters and grape yield.

Months → Monthly ↓	Apr	May	Jun	Jul	Aug	Sep	Oct	Nov	Dec	Jan	Feb	Mar
Mean Avr. Temperature (Tav °C)	0.12	-0.07	**0.30**	0.18	0.20	**0.30**	0.12	-0.13	0.13	-0.01	-0.05	0.09
Mean Max. Temperature (Tmax °C)	-0.01	**0.40**	-0.07	**0.54**	-0.21	0.24	0.17	0.19	0.08	-0.13	**-0.67**	-0.10
Mean Min. Temperature (Tmin °C)	**0.35**	-0.24	0.00	0.09	-0.02	0.09	-0.28	**-0.55**	0.02	**-0.54**	-0.28	-0.13
Precipitation (P mm)	-0.09	0.04	-0.20	-0.11	**-0.30**	**0.32**	0.12	**-0.79**	-0.22	0.14	-0.05	0.15
R. Humidity (Rh %)	-0.18	-0.14	0.09	-0.06	**-0.40**	**-0.34**	0.05	**-0.35**	-0.22	0.01	0.06	-0.10
Sunshine hours (Sh hr)	**0.53**	-0.29	0.24	0.23	0.11	-0.07	**0.45**	**-0.54**	0.09	**0.39**	-0.02	0.09
ETo (mm/day)	**0.53**	**-0.67**	-0.23	0.11	-0.21	-0.11	-0.07	**0.73**	**0.49**	0.24	0.21	**-0.33**

ETo in the month of April, May, November, December and March. Evapotranspiration is observed to be significant in the phenological cycle of the grape plant. The evapotranspiration of plants significantly influences the yield of grapes in all phenological phases (Netzer et al., 2009) and consequently in the further analysis the unit for evapotranspiration is considered as monthly average mm. Thereafter, all these independent variables which are highly correlated with the grape yield are considered in the further analysis.

3.3 Significance analysis using t-stat and p-test

The above mentioned variables which are showing correlation are considered for their significance testing. The t-stat and p-test are carried out using Microsoft-Excel 2010 data analysis tool to check the significance of the variables. If the p-value of the variable is found to be less than 0.05, then it is considered as significant and considered further in the construction of the model. The t-stat and p-value results are shown below in Table 2.

It is observed from the obtained results of t-stat and p-value that results, there is no significant relationship among yield and the climatic parameters such as monthly mean average, monthly mean maximum temperature, relative humidity and sunshine hours as p-value are observed to be greater than 0.05 and hence the monthly mean average, monthly mean maximum temperature, relative humidity and sunshine hours are discarded from the consideration of parameters in the model development. It is observed that P-value showing less than 0.05 for the monthly mean minimum temperature in the month of January, April and November, precipitation in the month of August and the November and sum of monthly mean evapotranspiration as shown in Table 2. Hence, these parameters are considered to be statistically significant and are considered as the model parameters in the development of ACGY model.

Table 2. Results of t-stat and p-value of model parameters.

Parameters	Month	t-stat	p-value	Parameters	Month	t-stat	p-value
Monthly Mean Avr. Temp (°C)	Jun	-0.03	0.976	Relative Humidity (%)	May	-0.608	0.586
	Sep	0.96	0.349		Jun	-0.468	0.672
Monthly Mean Max. Temperature (°C)	Feb	-0.44	0.670		Aug	0.468	0.672
	Apr	0.95	0.380	Sunshine hour (hr)	Apr	-0.511	0.631
	Nov	-1.56	0.170		May	-0.036	0.973
Monthly Mean Min. Temperature (°C)	Jan	-3.35	**0.000**		Jun	0.573	0.591
	Apr	2.35	**0.030**		Aug	-0.252	0.811
	Nov	-2.17	**0.040**		Nov	-1.730	0.144
Monthly Precipitation (mm)	Aug	-2.48	**0.023**		Dec	-0.095	0.928
	Sep	0.79	0.438	ETo (mm)	Annual	2.02	**0.040**
	Nov	-5.48	**0.000**				

As per the phenological study of grape plant, August and November month precipitation is highly sensitive towards grape yield. Physically, during the month of August if heavy rainfall occurs, the roots of the vine go into asphyxiation and significantly affect growth. Also, during the month of November, 80% of vineyards are in the phenological stage known as flowering in the study area. On receiving precipitation during this stage, the berry setting cycle get disturbed and it shows the adverse effect on the grape production. It is also noticed from the literature that crop production is most delicate to precipitation than temperature (Popova et al. 2005; Akpalu et al.2008). Hence, the relationship between grape yield and minimum temperature in the month of January, April, and November, precipitation in the month of August and November and sum of monthly mean evapotranspiration is obtain using multi-regression approach. Selection of parameters is the crucial stage in model development. Based on the grape yield phenological stages and weather effects model parameters are selected.

3.4 Agro-climatic grape yield model

Correlation analysis is carried out for screening the most correlated climatic parameters with yield. The ACGY model is developed by using the approach of multi-regression analysis. In the process of model development, grape yield is considered as dependent parameter and climatic parameters as independent parameters. Accordingly, coefficients for the model parameters are obtained from the multi-regression analysis and estimated model coefficients are summarized as shown below in Table 3.

It is observed from Table 3, that the model intercept is -44.67, the coefficient for the monthly mean minimum temperature for January month (T_{ja}) is -1.60, the coefficient for the monthly mean minimum temperature for April month (T_{ap}) is 1.33, the coefficient for monthly mean minimum temperature for November month (T_n) is -0.49, the coefficient of total monthly precipitation for August month (P_{au}) is -0.01, the coefficient of total monthly precipitation for November (P_n) month is -0.15, and the coefficient for the sum of monthly mean evapotranspiration (ETo) is 0.94. Hence using intercept and coefficient value of parameters as shown in Table 3 the model is formed as shown below Eq. (13).

$$Y= (-44.67-1.60T_{ja}+1.33T_{ap}-0.49T_n-0.01P_{au} -0.15P_n+0.94\ ETo) \quad (13)$$

Where, Y= Grape yield (ton ha^{-1}); T_{ja} = Monthly mean minimum temperature in the month of January (°C); T_{ap} = Monthly mean minimum temperature in the month of April (°C); T_n = Monthly mean minimum temperature in month of November (°C); P_{au} = total monthly precipitation in the month of August (mm); P_n = Total monthly precipitation in the month of November (mm); ET_o = Sum of monthly mean evapotranspiration (mm).

3.5 The validation of developed ACGY model (Eq. 13)

Recommendation for applicability of the developed ACGY model (Eq.13) is based on its validation performance. The independent datasets are used for the purpose of validation (2009-2016) which is other than the data used in the development of the model (Eq.13). For validation of the above ACGY model, 30% independent data set of climatic parameter and yield during the years 2009 to 2016 is used. Using independent data set and the developed ACGY model (Eq.13), the grape yield is estimated and compared with the observed grape yield. A plot between the observed and predicted grape yield is shown below in Figure 1.

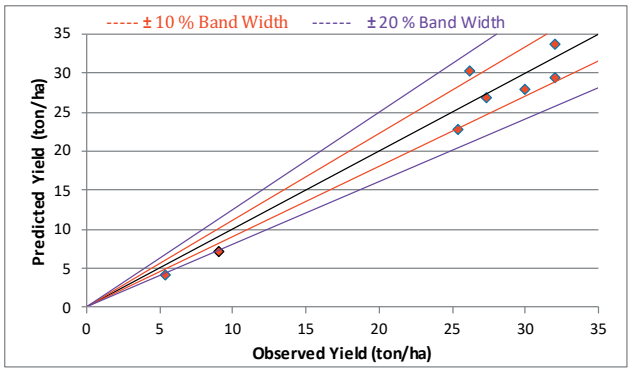

Fig. 1. Validation plot of the developed ACGY model Eq. 13 (2009-2016).

Table 3. Coefficient for model parameters.

	Intercept	Tmin. Jan. (T_{ja})	Tmin. Apr. ((T_{ap})	Tmin. Nov. (T_n)	Pre. Aug. (P_{au})	Pre. Nov. (P_n)	ET_o
Coefficients	-44.67	-1.60	1.33	-0.49	-0.01	-0.15	0.94

From the validation plot, as shown in Figure 1, it is observed that 62.5 % of data points fall within ±10% bandwidth and remaining 37.5 % data point fall within 20 % bandwidth. This confirms the predictive capability of the developed model (Eq. 13).

Further, the sensitivity analysis is carried out to understand the most sensitive agro-climatic parameters of the developed ACGY model (Eq.13) which affect the model output more with small variation within them. Sensitivity analysis is carried out as described below.

3.6 Sensitivity Analysis

It is revealed from the literature survey that parametric and component sensitivity analysis method is found more appropriate to carry out the sensitivity analysis of grape yield model (Hamby 1994). Using parametric and component sensitivity method Eq. (10) the relative sensitivity values are obtained for each parameter of the developed model. Eq. (10) is use to calculate the relative sensitivity value (RSV) which require the component like $\bar{O}_i$, $\bar{P}_i$ and ($\partial P_i/\partial O_i$). The value of mean output parameter ($\bar{O}_i$) (mean of grape yield 1991 to 2016) is 22.49 t/ha and the values of mean of input (independent) parameters $\bar{P}_i$, coefficient estimated using multi-regression analysis ($\partial P_i/\partial O_i$), as shown in Table 3 and RSV are summaries in Table 4.

The parameters obtain the higher value of relative sensitivity (RSV) indicating a higher sensitivity of that parameter. From the obtained results, sum mean monthly evapotranspiration (ETo) is found to be most sensitive as it has highest relative sensitivity value (RSV) as 3.24. Whereas, monthly total precipitation in August (P_{au}) is having lowest value of relative RSV as -0.08, indicates less sensitivity of the parameter. This helps in understanding the parametric variations on the model output. Now the developed agro-climatic grape yield (ACGY) model is tested for its statistical performance as described below.

Table 5. Statistical performance of the developed ACGY model (Eq.13).

Statistical tests	Developed ACGY model (Eq.13) (ton/ ha)
Discrepancy ratio (r)	1.03
Standard Deviation of r	0.19
Mean Percentage Error (MPE)	0.03
Standard Deviation of MPE	0.19

3.7 The statistical performance of developed agro-climatic grape yield (ACGY) model

It is revealed from the literature review that there is no evidence of having any agro-climatic grape yield model for Indian Terrain. The statistical fitness of the developed ACGY model (Eq.13) is tested using statistical tests such as discrepancy ratio (r), the standard deviation of r, mean percentage error (MPE) and standard deviation of MPE. The discrepancy ratio (r) is the ratio of simulated grape yield and observed grape yield. The ideal value of the discrepancy ratio should be one. The mean percentage error (MPE) is calculated as the difference of simulated grape yield and observed grape yield divided by observed crop yield in percentage. The obtained results of the statistical performance carried out for developed ACGY model Eq. (13) is shown below in Table 5.

It is observed from the Table 5 that the discrepancy ratio for developed model (Eq.13) is 1.03 which is very close to its ideal value of one. Mean percentage error of developed model is 0.03 %. The standard deviation of discrepancy ratio and mean percentage error is observed as 0.19. From the obtained results of the statistical performance, it is observed that the developed model (Eq.13) is performing satisfactory. Besides this, results of model yield and actual yield are compared by considering the data during 1992 to 2016 which shown in Figure 2.

Table 4. Results of sensitivity analysis.

Climatic parameters	Mean ($\bar{P}_i$)	Coefficient ($\partial P_i/\partial O_i$)	RSV
Monthly mean min. temperature in January (T_{ja})	14.36	-1.60	-1.02
Monthly mean min. temperature in April (T_{ap})	23.19	1.33	1.37
Monthly mean min. temperature in November (T_n)	17.83	-0.49	-0.39
Monthly total precipitation in August (P_{au})	181.28	-0.01	-0.08
Monthly total precipitation in November (P_n)	18.07	-0.15	-0.12
Sum of monthly mean Evapotranspiration (ET_o)	77.63	0.94	3.24

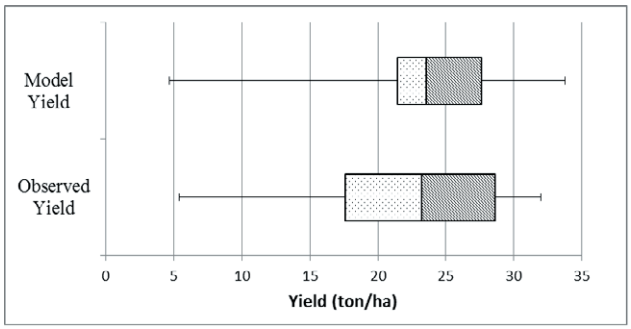

Figure 2. Comparison between observed yield and model yield (Eq. 13) (1992-2016).

Figure 2 shows the box plot of observed yield and model yield (Eq. 13). Accordingly, it is observed that median of developed ACGY model is 23.5 (ton/ha) and that observed data is 23.2 (ton/ha). The upper quartile and lower quartile values are close to the median value of model yield as compared to observed yield. Hence, it is recommended that the developed ACGY model is found suitable to predict the grape yield for the study area.

3.8 Climate plot between ACGY model estimated grape yield and climate variables under three RCPs during 2021-2050

It is more interesting to see the variations of the model yield with climate variables for all the 30 years (2021-2050). Hence, the climate plot between ACGY model estimated grape yield and climate variables under RCP 2.6, 4.5 and 8.5 during 2021-2050 is plotted and shown below in Figures 3, 4, 5, 6, 7 and 8.

It has been noticed from the plot shown in Figures 3 and 4 that the lowest crop yield is observed as 18.63 ton/ha in the year 2049 wherein November precipitation is predicted as 72.36 mm which is the highest precipitation during the years 2021-2050. The maximum crop yield is observed in the year 2047 as 28.64 ton/ha for which the sum of monthly average evapotranspiration in this year is observed highest as 77.55 mm among all years under RCP2.6. Hence from the Figures 3 and 4 it is observed that evapotranspiration and temperature in April show a positive impact on yield, whereas, the temperature in January, November, precipitation in August and November shows a negative impact on yield Similarly, the climate variables generated under RCP4.5 are comparing with the predicted grape yield during 2021-2050. Climate plot is shown in Figure 5 and 6.

It has been noticed from the plot shown in Figures 5 and 6 that the lowest crop yield is observed as 19.31 ton/ha in the year 2024 wherein November precipitation is 57.73 mm and August precipitation is 96.12 mm which is the highest precipitation during the years 2021-2050 under the RCP4.5 scenario. The highest crop yield is observed in the year 2039 as 30.0 ton/ha for which precipitation in the month of November is 17.09 mm which is near to lowest value and minimum temperature in the month of April 20.15 is highest among all years under RCP4.5. Similarly, the climate variables generated under RCP8.5 are comparing with the predicted grape yield

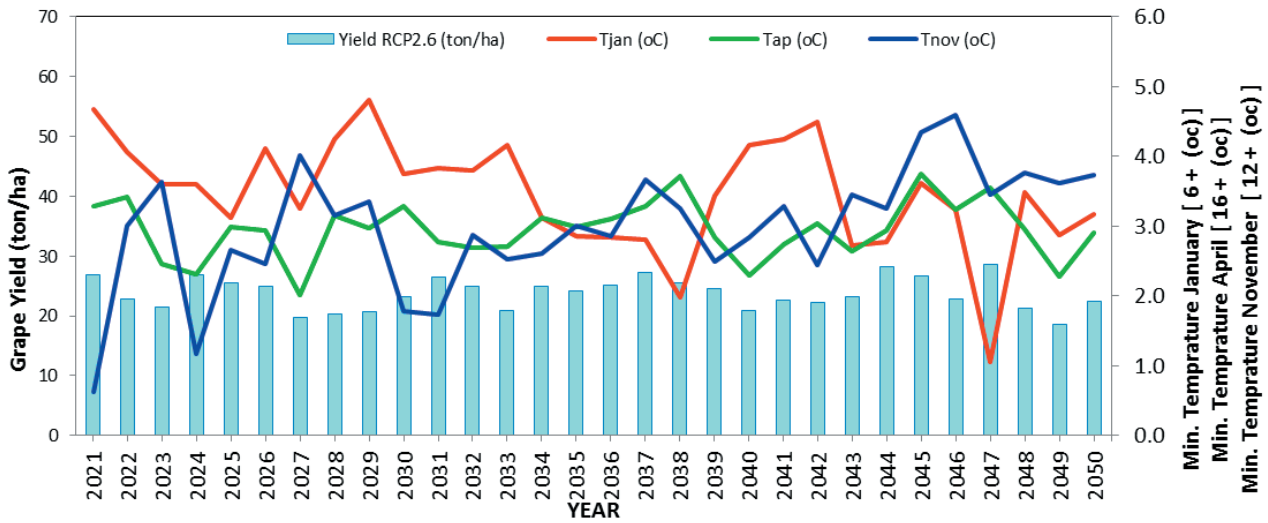

Figure 3. Climate plot between the model crop yield and minimum temperature in January, April, and November under RCP2.6 scenario (2021-2050).

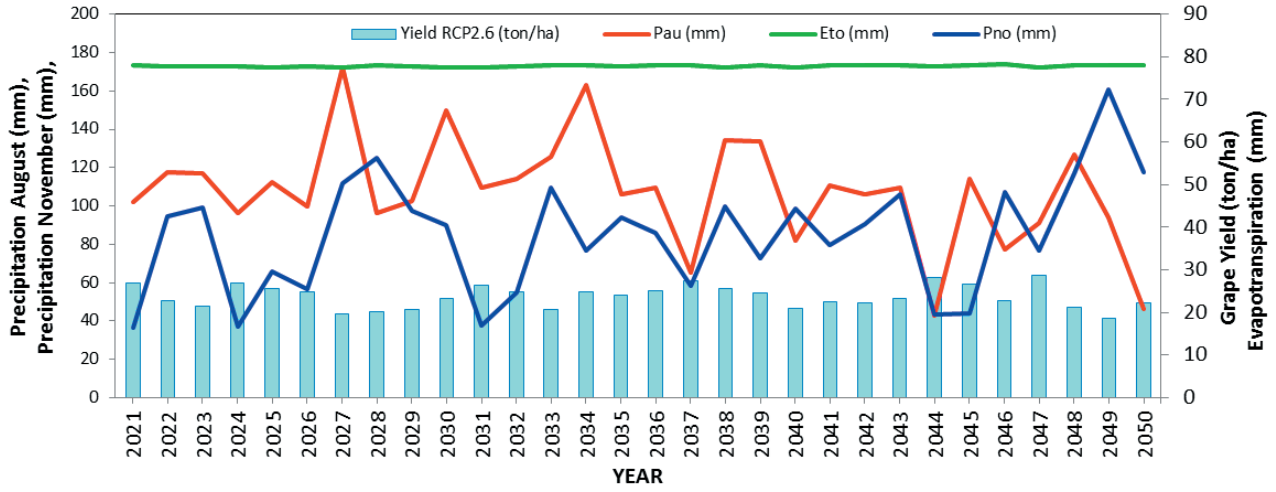

Figure 4. Climate plot between the model crop yield and evapotranspiration, precipitation in August and November under RCP2.6 scenario (2021-2050).

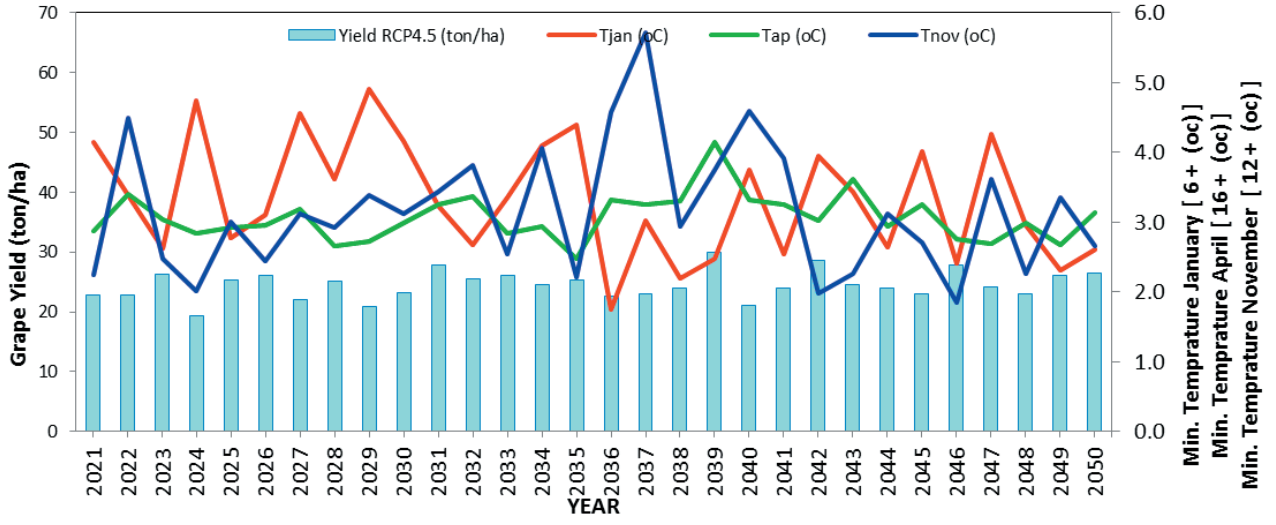

Figure 5. Climate plot between the model crop yield and minimum temperature in January, April, and November under RCP4.5 scenario (2021-2050).

during 2021-2050. Climate plot is shown below in Figure 7 and 8.

It has been noticed from the plot shown in Figures 7 and 8 that the lowest crop yield is observed as 18.50 ton/ha in the year 2019 wherein January lowest value of minimum temperature as 10.71 °C. The maximum crop yield is observed in the year 2039 as 30.40 ton/ha for which November precipitation is 6.44 mm which is lowest among all year under RCP 8.5.

3.9 Model response variability

A comparative study is carried out to find model yield responses in terms of current and future climate. The developed model (Eq. 13) is considered to estimate grape yields in context to the current climate and future climate under three future climate scenarios such as RCP2.6, RCP4.5, and RCP8.5. The current climate is considered during the period of 1991-2016 taken same as considered in the previous analysis. The future climate is derived using SDSM for the period of 2021-2050. Devel-

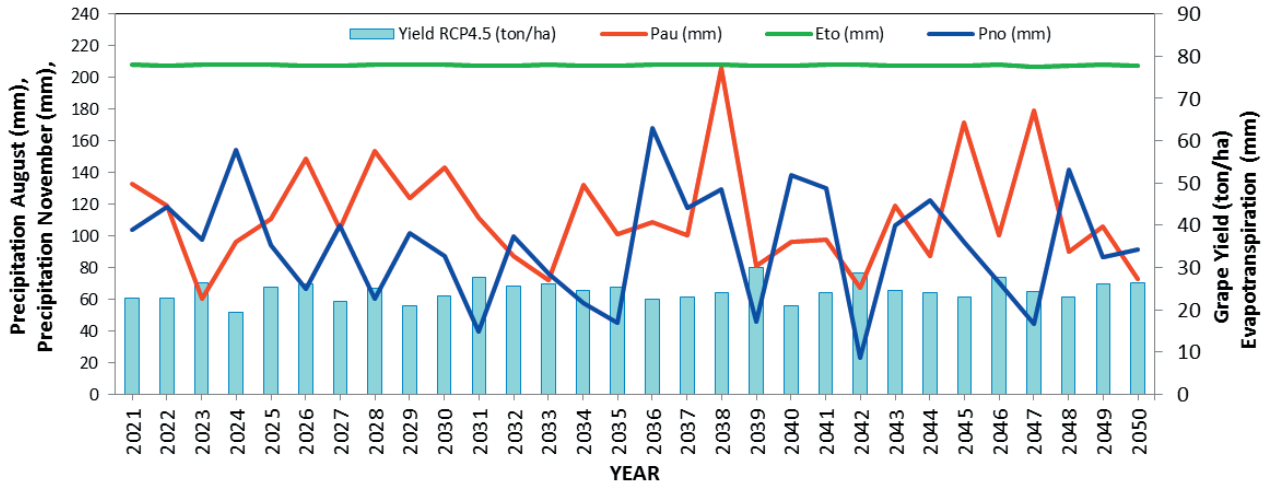

Figure 6. Climate plot between the model crop yield and evapotranspiration, precipitation in August and November under RCP4.5 scenario (2021-2050).

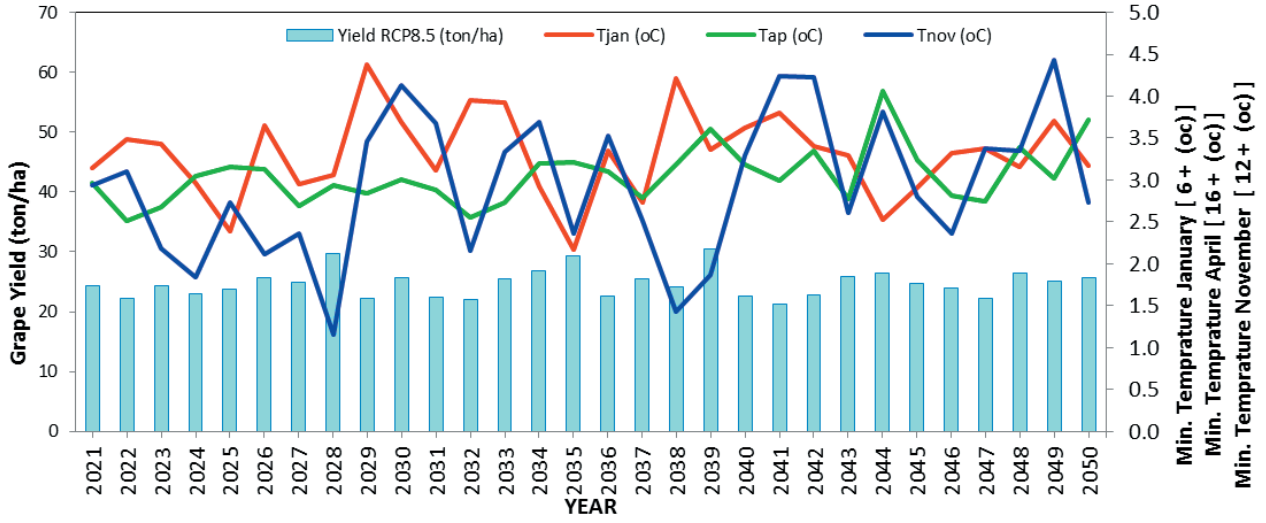

Figure 7. Climate plot between the model crop yield and minimum temperature in January, April, and November under RCP8.5 scenario (2021-2050).

oped ACGY model (Eq. 13) is used to estimate grape yields for the current and future climate. The future climate is considered under the generated climate scenarios as RCP2.6, 4.5 and 8.5 derived from SDSM under CIMIP5 experiments. The estimated crop yield is then compared in box and whisker plot to understand the model response variability with the current and future climate as shown in Figure 9.

It is observed from the Figure 9 that the median yield is observed as 23.2 t/ha for the current climate and lower and upper quartile values are observed to be away from median values as compare to all RCPs yield values. Upper and lower fence values are also away from median values as compare to all RCP yield values. Whereas, future climate median yields are observes as 24.1 t/ha under RCP 2.6, 24.52 t/ha and 24.72 ton/ha under RCP4.5 and RCP8.5 scenarios respectively. The lower and upper quartile values of RCP2.6, 4.5 and 8.5 are observed near to their median values as compared to yield values obtained for current climate. Under RCP2.6 minimum yield (lower fence) is 18.63 ton/ha and maximum yield (upper fence) is 28.64 ton/ha which

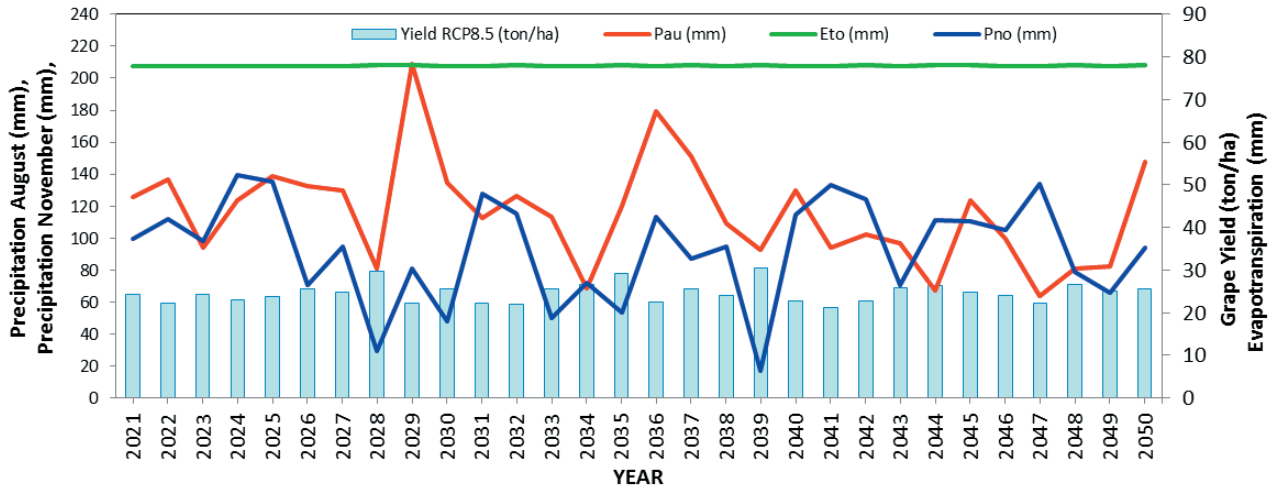

Figure 8. Climate plot between the model crop yield and evapotranspiration, precipitation in August and November under RCP8.5 scenario (2021-2050).

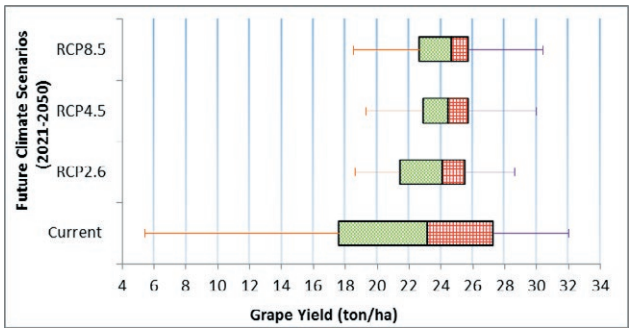

Figure 9. Box plot of model response variability with reference to current and future climate.

are near to median yield 24.12 t/ha as compare to the current climate values. RCP4.5 shows 19.31 t/ha lower fence and 30.00 ton/ha upper fence which are nearer to median yield 24.52 t/ha as compare to current yield and also RCP8.5 shows 18.50 t/ha lower fence and 30.40 t/ha upper fence yields are near to median yield 24.72 t/ha as compare current yield values. It is observed from the model response variability that the grape yield of the future climate is showing the increase in yield as compared to the current climate.

3.10 Future grape yield scenario

In order to develop the grape yield scenarios, projected climate obtained from SDSM is used. Future yield scenarios are developed during the years 2021 to 2050 using ACGY model Eq. (13). All model parameters are obtained up to the year 2050 under RCP2.6, RCP4.5, and RCP8.5. The crop yield scenario is generated by considering the existing field management practices like irrigation as drip irrigation, soil type as clay base soil (black cotton soil), fertilizers as per soil nutrient value, pesticides, and tillage are considered as common practices adopted in the study area. Using developed ACGY model Eq.(13) and projected climate scenario under RCP2.6, 4.5 and 8.5, grape yield scenario is generated. The obtained grape yield scenario under three RCPs during the year 2021 to 2050 is shown below in Figure 10.

It is observed from the Figure 10 that under RCP2.6 the lowest crop yield of 18.63 ton/ha is observed in the year 2049. This is due to the fact that precipitation occurred in the month of November of 72 mm which is the highest rainfall predicted in half a century. The maximum crop yield is found in the year 2047 as 28.64 t/ha due to the fact that August precipitation is observed as 91.01 mm and November precipitation as 34.53 mm which are observed near to the lowest values of precipitation. Under RCP4.5, it is observed that the lowest crop yield of 19.31 t/ha in the year 2024 is predicted with November precipitation as 57.73 mm and August precipitation 96.12 mm which are nearer to its highest value. The highest crop yield is observed in the year 2039 as 30.00 t/ha for which November precipitation is 17.09 mm and August precipitation 80.75 mm which are observed near to lowest values. According to the RCP8.5 scenario, it is indicated that the lowest crop yield of 21.01 t/ha in the year 2041 is indicated with November precipitation of 125.25 mm and August precipitation 100.02 mm which are nearer to their highest values. The

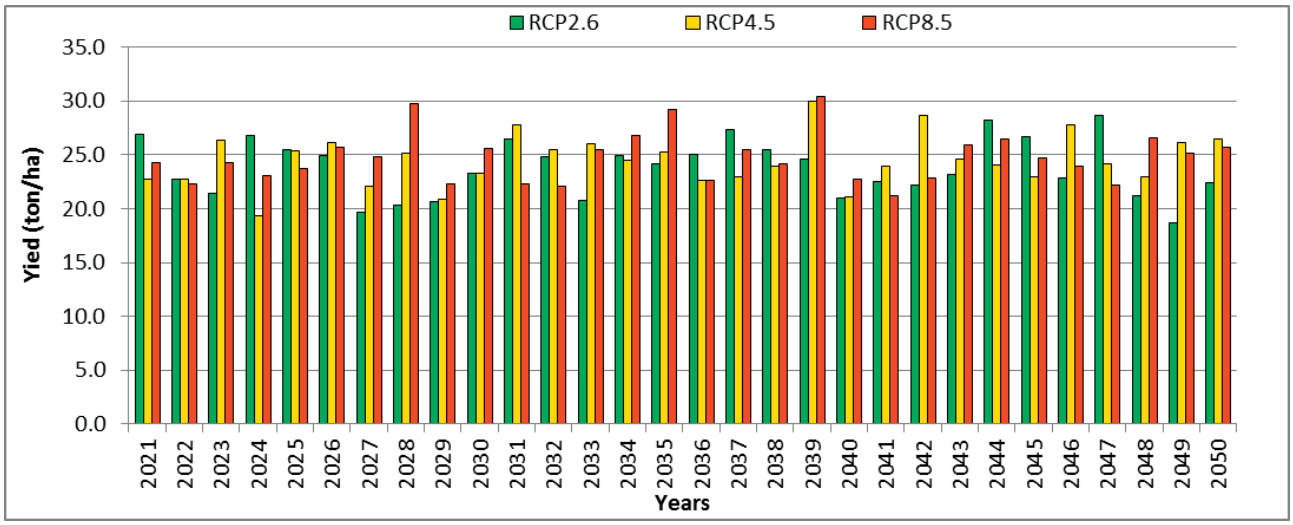

Figure 10. Grape yield scenario under RCP2.6, 4.5 and 8.5 using developed ACGY model (Eq. 13) (2021-2050).

highest crop yield is found in the year 2039 as 30.40 t/ha for which November precipitation is 6.44 mm and August precipitation 92.97 mm which are observed nearer to their lowest values.

3.11 Statistical performance of developed ACGY model (Eq.13)

The predicted climate data is considered during the year 2011 to 2016. Using this predicted data under three RCPs and developed ACGY model Eq. (13) the yield is estimated during the year 2011-2016. The statistical fitness of the developed ACGY model (Eq.13) over the projected data for the duration of 2011-16 is checked using statistical tests as discrepancy ratio (r), standard deviation of the discrepancy ratio (r), mean percentage error (MPE) and standard deviation of MPE. The tests are already discussed in detail in section 5.11. Obtained results of all tests are shown in the Table 6.

It is observed that developed ACGY model (Eq.13) found performing most satisfactorily under RCP2.6. From the obtained results of statistical performance, it is observed that the developed ACGY model (Eq.13) is overall performing satisfactorily for the projected climate data obtained under different climate scenarios as RCP 2.6, 4.5 and 8.5. The following section discussed the projected grape yield using proposed irrigation methods using developed ACGY model and projected climate data.

CONCLUSIONS

The multi-regression analysis is carried out to obtain the final form of the ACGY model. The developed agro-climatic grape yield (ACGY) model (Eq.13) is statistically tested for its fitness. The discrepancy ratio, the standard deviation of discrepancy ratio, mean percentage error and standard deviation of mean percentage error for the developed model is obtained as 1.03, 0.19, 0.03% and 0.19 respectively. Sensitivity analysis is carried out for the developed ACGY model using the parametric sensitivity method. Based on the obtained results of the statistical tests the developed ACGY model (Eq.13) is recommended for its use to estimate the grape yield. To understand

Table 6. Results of the statistical performance of the developed ACGY model Eq.(13) (2011-2016).

Statistical Test	RCP2.6		RCP4.5		RCP8.5	
	Discrepancy Ratio (r)	Mean % Error (MPE)	Discrepancy Ratio (r)	Mean % Error (MPE)	Discrepancy Ratio (r)	Mean % Error (MPE)
mean	1.08	8 %	1.16	16 %	1.22	22 %
SD	0.58	0.58	0.65	0.65	0.80	0.80

the most sensitive parameters of the ACGY model Eq. (13), sensitivity analysis is carried out using the methods of parametric and component sensitivity method. From the obtained results of sensitivity analysis, it is found that sum of monthly mean evapotranspiration, the monthly mean minimum temperature in April and precipitation in August parameters found to be more sensitive. It is recommended that the developed ACGY model Eq. (13) can be used for the estimation of grape yield of the study area. It is observed from the sensitivity analysis that the grape is found highly sensitive to climatic parameters. Therefore, in order to know the grape yield in advance, it is necessary to know the future climate. By knowing future climate it is possible to generate the grape yield scenarios using developed agro-climatic grape (ACGY) model (Eq. 13).

Grape yield projections are generated using future predicted climate data. According to the analysis carried out grape crop showing increasing yield in the future i.e. up to 2050 as compared to current yield. The analysis of grape yield shows that annual evapotranspiration and minimum temperature in the month of April shows in accordance impact on the yield, whereas, the minimum temperature in January and November, precipitation in August and November shows an adverse impact on the yield. From the obtained results of statistical performance of the developed model, it is observed that model is performing better for future yield predictions under three RCP scenarios.

REFERENCES

Abbaspour K.C., (1994). "Bayesian risk methodology for crop insurance decisions." Agri. Forest Meteorol., 71:297-314.

Abraha M.G., Savage M.J.,(2006)."Potential impacts of climate change on the grain yield of maize for the midlands of KwaZulu-Natal, South Africa."Agric. Ecosyst. Environ.,115, 150–60.

Adams R.M., Wu J., and Houston L., (2003). "Climate Change and California, Appendix IX: The effects of climate change on yields and water use of major California crops." California Energy Commission, Public Interest Energy Research (PIER), Sacramento, 21-32.

Adsule P.G., (2013). "Good agriculture practices for production of quality table grapes." report of a national research center for grapes, Manjari, Pune, 1-83.

Akpalu W., Hassan R.M., Ringler C., (2008). "Climate variability and maize yield in South Africa: results from GME and MELE methods." Environment and production technology division IFPRI discussion paper; 1–12.

APDEA (2016) Agriculture production development and Economics authority India, Export of Agro. Food Products Report, 20-32.

Arora V.K., and Boer G.J,.(2014). "Terrestrial ecosystems response to future changes in climate and atmospheric CO_2 concentration." Bio geosciences, 11(15), 4157-4171.

Bowden, W. B., Bormann F. H., (1986). "Transport and loss of nitrous oxide in soil water after forest clear-cutting." Science 233, 867- 869.

Droogers P., (2004). "Adaptation to climate change to enhance food security and preserve environmental quality: an example for southern Sri Lanka." Agr. Water Manag., 66:15–33.

FAO (2016). "FAO-OIV FOCUS 2016 Table and dried grape" 32-33

Gupta S.G., (1981). "Fundamental of statistics, Himalaya publishing house." 7, 27.1-27.31.

Hamby D.M. (1994). "A review of techniques for parameter sensitivity analysis of environmental models." Environmental monitoring and assessment 32: 135-154.

Hoogenboom G. (2000). "Contribution of agrometeorology to the simulation of crop production and its applications." Agric. Forest Meteorol, 103:137–57.

Hoskins Brian J. (1980). "Representation of earth topography using spherical harmonics" notes and correspondence of American metrological society, 111-115.

IPCC, (2013). "Climate Change 2013, the physical science basis, contribution of working group 1 to 5 assessment report of the Intergovernmental Panel on Climate Change." Cambridge, United Kingdom and New York, USA, Cambridge University Press, Cambridge.

Netzer, Y., Yao, C.R., Shenker, M., Bravdo, B.A., Schwartz A., (2009). "Water use and the development of seasonal crop coefficients for Superior Seedless grapevines trained to an open-gable trellis system." Irrigation Science, 27, 109-120.

Nikolić, D., Muresan R.C., Feng, W., Singer W., (2012). "Scaled correlation analysis: a better way to compute a cross-correlogram." European Journal of Neuroscience, 1–21.

Popova Z., Kercheva M., (2005). "CERES model application for increasing preparedness to climate variability in agricultural planning-risk analyses." Phys. Chem. Earth., 30:17–24.

Saxena Mamta, (2014). "Handbook on horticulture statistics 2014." Government of India Ministry of Agriculture Department of Agriculture and Cooperation New Delhi, 25-26.

Srinivastav A.K. (2015). "Agriculture statistics system in India." NSSO (FOD), 1-2.

Taylor K.E., Stouffer R.J., and Meehl G.A., (2012). "An overview of CMIP5 and the experiment design." Bulletin of the American Meteorological Society, 93(4), 485-498.

Van Vuuren D.P., Edmonds, J.A., Kainumaa M., Riahi K., and Weyant, J., (2011). "A special issue on the RCPs." Climate Change, 109 (1), 1-4.

Wilby R.L., Dawson C.W., Barrow E.M. (2002). "SDSM — a decision support tool for the assessment of regional climate change impacts." Environmental Modelling & Software 17, 147–159.

Yinhong K., Shahbaz K., Xiaoyi M., (2009). "Climate change impacts on crop yield, crop water productivity, and food security – A review" Progress in Natural Science 19, 1665–1674.

Zhang R., and Shen X., (2008). "On the development of the GRAPES—A new generation of the national operational NWP system in China." Chinese Science Bulletin, 53(22):3429-3432.

Finito di stampare da
Logo s.r.l. – Borgoricco (PD) – Italia

RIGOROUS PEER REVIEW
Each submission to IJAm is subject to a rigorous quality control and peer-review evaluation process before receiving a decision. The initial in-house quality control check deals with issues such as competing interests; ethical requirements for studies involving human participants or animals; financial disclosures; full compliance with IJAm's data availability policy, etc.
Submissions may be returned to authors for queries, and will not be seen by our Editorial Board or peer reviewers until they pass this quality control check.
Each paper is subjected to critical evaluation and review by Field Editors with specific expertise in the different areas of interest and by the members of the international Editorial Board.

OPEN ACCESS POLICY
The Italian Journal of Agrometeorology provides immediate open access to its content. Our publisher, Firenze University Press at the University of Florence, complies with the Budapest Open Access Initiative definition of Open Access: By "open access", we mean the free availability on the public internet, the permission for all users to read, download, copy, distribute, print, search, or link to the full text of the articles, crawl them for indexing, pass them as data to software, or use them for any other lawful purpose, without financial, legal, or technical barriers other than those inseparable from gaining access to the internet itself. The only constraint on reproduction and distribution, and the only role for copyright in this domain is to guarantee the original authors with control over the integrity of their work and the right to be properly acknowledged and cited. We support a greater global exchange of knowledge by making the research published in our journal open to the public and reusable under the terms of a Creative Commons Attribution 4.0 International Public License (CC-BY-4.0). Furthermore, we encourage authors to post their pre-publication manuscript in institutional repositories or on their websites prior to and during the submission process and to post the Publisher's final formatted PDF version after publication without embargo. These practices benefit authors with productive exchanges as well as earlier and greater citation of published work.

COPYRIGHT NOTICE
Authors who publish with IJAm agree to the following terms:
Authors retain the copyright and grant the journal right of first publication with the work simultaneously licensed under a Creative Commons Attribution 4.0 International Public License (CC-BY-4.0) that allows others to share the work with an acknowledgment of the work's authorship and initial publication in IJAm.
Authors are able to enter into separate, additional contractual arrangements for the non-exclusive distribution of the journal's published version of the work (e.g., post it to an institutional repository or publish it in a book), with an acknowledgment of its initial publication in this journal.
Authors are allowed and encouraged to post their work online (e.g., in institutional repositories or on their website) prior to and during the submission process, as it can lead to productive exchanges, as well as earlier and greater citation of published work (See The Effect of Open Access).

PUBLICATION FEES
Unlike many open-access journals, the Italian Journal of Agrometeorology does not charge any publication fee.

WAIVER INFORMATION
Fee waivers do not apply at Firenze University Press because our funding does not rely on author charges.

PUBLICATION ETHICS
Responsibilities of IJAm's editors, reviewers, and authors concerning publication ethics and publication malpractice are described in IJAm's Guidelines on Publication Ethics.

CORRECTIONS AND RETRACTIONS
In accordance with the generally accepted standards of scholarly publishing, IJAm does not alter articles after publication: "Articles that have been published should remain extant, exact and unaltered to the maximum extent possible". In cases of serious errors or (suspected) misconduct IJAm publishes corrections and retractions (expressions of concern).

Corrections
In cases of serious errors that affect or significantly impair the reader's understanding or evaluation of the article, IJAm publishes a correction note that is linked to the published article. The published article will be left unchanged.

Retractions
In accordance with the "Retraction Guidelines" by the Committee on Publication Ethics (COPE) IJAm will retract a published article if:
- there is clear evidence that the findings are unreliable, either as a result of misconduct (e.g. data fabrication) or honest error (e.g. miscalculation)
- the findings have previously been published elsewhere without proper crossreferencing, permission or justification (i.e. cases of redundant publication)
- it turns out to be an act of plagiarism
- it reports unethical research.
- An article is retracted by publishing a retraction notice that is linked to or replaces the retracted article. IJAm will make any effort to clearly identify a retracted article as such.

If an investigation is underway that might result in the retraction of an article IJAm may choose to alert readers by publishing an expression of concern.

ARCHIVING
IJAm and Firenze University Press are experimenting a National legal deposition and long-term digital preservation service.

SUBMITTING TO IJAm
Submissions to IJAm are made using FUP website. Registration and access are available at: https://riviste.fupress.net/index.php/IJAm/submission
For more information about the journal and guidance on how to submit, please see https://riviste.fupress.net/index.php/IJAm/index

Principal Contact
Simone Orlandini, University of Florence
simone.orlandini@unifi.it

Support Contact
Alessandro Pierno, Firenze University Press
alessandro.pierno@unifi.it

GUIDE FOR AUTHORS
1. Manuscript should refer to original researches, not yet published except in strictly preliminary form.
2. Articles of original researches findings are published in Italian Journal of Agrometeorology (IJAm), subsequent to critical review and approval by the Editorial Board. External referees could be engaged for particular topics.
3. Three types of paper can be submitted: original paper, review, technical note. Manuscript must be written in English. All pages and lines of the manuscript should be numbered.
4. First Name, Last Name, position, affiliation, mail address, telephone and fax number of all the Co-Authors are required. Corresponding Authors should be clearly identified.
5. The abstract should be no longer than 12 typed lines.
6. Full stop, not comma, must be used as decimal mark (e.g. 4.33 and not 4,33).
7. Figures, tables, graphs, photos and relative captions should be attached in separate files. All images must be vector or at least 300 effective ppi/dpi to ensure quality reproduction.
8. Captions should be written as: Fig. x – Caption title, Tab. x – Caption title. Images should be referred to in the text as (Fig. x), (Tab. x).
9. Proof of the paper (formatted according to the Journal style) will be sent to the Corresponding Author for proof reading just one time. Corrections can be made only to typographical errors.
10. All the references in the text must be reported in the "References" section and vice-versa. In the text, only the Author(s) last name must be present, without the name or the first letter of the name (e.g. "Rossi, 2003" and not "Federico Rossi, 2003" or "F. Rossi, 2003"). If two authors are present, refer to them as: "Bianchi and Rossi, 2003" in the text (do not use "&" between the surnames). If more than two Authors are present, refer to them as: "Bianchi et al., 2003" in the text.
For journals, references must be in the following form:
Bianchi R., Colombo B., Ferretti N., 2003. Title. Journal name, number: pages.
For books:
Bianchi R., Colombo B., Ferretti N., 2003. Book title. Publisher, publishing location, total number of pages pp.
Manuscripts "in press" can be cited.

BECOME A REVIEWER
Peer review is an integral part of the scholarly publishing process. By registering as a reviewer, you are supporting the academic community by providing constructive feedback on new research, helping to ensure both the quality and integrity of published work in your field. Once registered, you may be asked to undertake reviews of scholarly articles that match your research interests. Reviewers always have the option to decline an invitation to review and we take care not to overburden our reviewers with excessive requests.
You must login before you can become a reviewer.
If you don't want to be a reviewer anymore, you can change your roles by editing your profile.

COMPETING INTERESTS
You should not accept a review assignment if you have a potential competing interest, including the following:
- Prior or current collaborations with the author(s)
- You are a direct competitor
- You may have a known history of antipathy with the author(s)
- You might profit financially from the work

Please inform the editors or journal staff and recuse yourself if you feel that you are unable to offer an impartial review.
When submitting your review, you must indicate whether or not you have any competing interests.

Italian Journal of Agrometeorology

Rivista Italiana di Agrometeorologia

n. 1 – 2021

Table of contents